PURIFICATION AND STRUCTURAL ANALYSIS OF THE CANNABINOID RECEPTOR CB_1:

INSIGHTS INTO ALLOSTERIC REGULATION OF A GPCR.

By

Jonathan Firoze Fay

A dissertation

Presented to the Department of Biochemistry & Molecular Biology

and the Oregon Health & Science University

School of Medicine

in partial fulfillment of

the requirements for the degree of

Doctor of Philosophy

August 2012

School of Medicine

Oregon Health & Science University

CERTIFICATE OF APPROVAL

This is to certify that the PhD dissertation thesis of

Jonathan Firoze Fay

has been approved

Dr. David Farrens Mentor/Advisor

Dr. Kim Neve, Committee Chair

Dr Ujwal Shinde, Committee Member

Dr. Francis Valiyaveetil, Committee Member

Dr. John Williams, Committee Member

TABLE OF CONTENTS

LIST OF TABLES

LIST OF FIGURES

LIST OF ABBREVIATIONS

1D4	Mouse monoclonal anti-rhodopsin antibody. Specifically binds to the C-terminal epitope TETSQVAPA-COOH of rhodopsin.
2AG	2-arachidonylglycerol
A2AR	adenosine A2A receptor
Adenosine A3	Adenosine receptor subtype A3
AEA	Anandamide
AM251	1-(2,4-dichlorophenyl)-5-(4-iodophenyl)-4-methyl-N-(1-piperidyl)pyrazole-3-carboxamide
AM281	1-(2,4-Dichlorophenyl)-5-(4-iodophenyl)-4-methyl-N-4-morpholinyl-1H-pyrazole-3-carboxamide
AM630	6-Iodo-2-methyl-1-[2-(4-morpholinyl)ethyl]-1H-indol-3-yl](4-methoxyphenyl)methanone
ANKTM1	Transient receptor potential cation channel, subfamily A, member 1
B1AR	beta-1 adrenergic receptor
B2AR	beta-2 adrenergic receptor
BAR	beta adrenergic receptor
BSA	Bovine serum albumin
C11	see shCB1-C11
Cannabigerol	2-[(2E)-3,7-dimethylocta-2,6-dienyl]-5-pentyl-benzene-1,3-

	diol
catechol	Benzene-1,2-diol
CB_1	Cannabinoid Type-1 Receptor
CB_1a	Cannabinoid Type-1 Receptor Isoform a
CB_1b	Cannabinoid Type-1 Receptor Isoform b
CB_2	Cannabinoid Type-2 Receptor
CBD	Cannabidiol
CBN	Cannabinol
CCD	0.06% CHAPS, 0.01% DM, 0.01% CHS
CHAPS	3-[(3-Cholamidopropyl)dimethylammonio]-1-propanesulfonate
CHS	Cholesterol hemisuccinate
CMC	critical micelle concentration
CNS	central nervous system
CP55940	(-)-cis-3-[2-Hydroxy-4-(1,1-dimethylheptyl)phenyl]-trans-4-(3-hydroxypropyl)cyclohexanol
CTM	cubic ternary complex model
CXCR4	C-X-C chemokine receptor type 4
Δ^8THC	delta-8-tetrahydrocannabinol
Δ^9THC	delta-9-tetrahydrocannabinol or (−)-(6aR,10aR)-6,6,9-trimethyl-3-pentyl-6a,7,8,10a-tetrahydro-6H-benzo[c]chromen-1-ol
DALN	desacetylnantradol or (6S,6aR,9R,10aR)-6-methyl-3-[(2R)-5-

	phenylpentan-2-yl]oxy-5,6,6a,7,8,9,10,10a-octahydrophenanthridine-1,9-diol
Δ417	C-terminal CB_1 truncation mutant at residue 417
ΔIL3	mutant CB1 receptors lacking iL3 (residues 307-326) in θ background
DM	n-Dodecyl-β-D-Maltoside
DMEM	Dulbecco's Modified Eagle Medium
DNA	Deoxyribonucleic acid
Δ103/Δ417	N-terminal CB_1 truncation mutant at residue 103 & C-terminal CB_1 truncation mutant at residue 417
Δ88/Δ417	N-terminal CB_1 truncation mutant at residue 88 & C-terminal CB_1 truncation mutant at residue 417
Δ103	N-terminal CB_1 truncation mutant at residue 103
DPH	Diphenylhexatriene
DTT	Dithiothreitol ((2S,3S)-1,4-bis(sulfanyl)butane-2,3-diol)
E. coli	Escherichia coli
EL	Extracellular loop
EL2	Extracellular loop 2
ELISA	Enzyme-linked immunosorbent assay
ETC	extended ternary complex model
ETMR	Extracellular transmembrane region
EtOH	Ethanol
Fab	Fragment antigen-binding

FSEC	Fluorescence detected size exclusion chromatography
G protein	guanine nucleotide-binding protein
GABA	γ-aminobutyric acid type A
GDP	Guanosine diphosphate
geranyl pyrophosphate	3,7-Dimethyl-2,6-octadiene pyrophosphate
GFP	Green fluorescent protein
GIPs	GPCR interacting proteins
GPCR	G protein-coupled receptor
GTP	Guanosine-5'-triphosphate
GTPγS	Guanosine 5'-[gamma-thio]triphosphate
H8	Helix 8
HIV	Human immunodeficiency virus
HPLC	High-performance liquid chromatography
HU210	(6a*R*,10a*R*)- 9-(Hydroxymethyl)- 6,6-dimethyl- 3-(2-methyloctan-2-yl)- 6a,7,10,10a-tetrahydrobenzo [c]chromen-1-ol
IgG	Immunoglobulin G antibody isotype
IL	Intracellular loop
INAD	Inactivation no afterpotential D
JH-176	E-1-[1-(1-Naphthalenylmethylene)-1H-inden-3-yl]pentane
M2	Muscarinic acetylcholine receptor type 2
MAB	Monoclonal antibodies
mAChr M3	Muscarinic acetylcholine receptor type 3

meAEA	(R)-N-(2-Hydroxy-1-methylethyl)-5Z,8Z,11Z,14Z-eicosatetraenamide
Mevalonic acid	(3R)-3,5-Dihydroxy-3-methylpentanoic acid
Muscarinic M4	Muscarinic acetylcholine receptor type 4
NAPE	N-arachidonoyl-phosphatidylethanolamide
NESS 0327	N-piperidinyl-[8-chloro-1-(2,4-dichlorophenyl)-1,4,5,6-tetrahydrobenzo [6,7]cyclohepta[1,2-c]pyrazole-3-carboxamide]
NIDA-41020	1-(2,4-Dichlorophenyl)-5-(4-methoxyphenyl)-4-methyl-N-(1-piperidinyl)-1H-pyrazole-3-carboxamide
NMDA	N-Methyl-D-aspartic
NMR	Nuclear magnetic resonance
Nt2/C2	Minimal cys CB_1 construct D88-D417 containing only C98,C107, C257, & C264
O-1057	3-(5'-cyano-1',1'-dimethylpentyl)-1-(4-N-morpholinobutyryloxy)-Δ8-tetrahydrocannabinol
Olivetol	5-Pentyl-1,3-benzenediol
Org 27759	(3-ethyl-5-fluoro-1H-indole-2-carboxylic acid [2-94-dimethylamino-phenyl)-ethyl]-amide
Org 29647	5-chloro-3-ethyl-1H-indole-2-carboxylic acid (1-benzyl-pyrrolidin-3-yl)-amide, 2-enedioic acid salt
Org 27569	5-chloro-3-ethyl-1H-indole-2-carboxylic acid[2-(4-piperidin-1-yl-phenyl)ethyl]amide

OxyR	*Escherichia coli* transcription factor that activates the expression of antioxidant defensive
P. pastoris	*Pichia pastoris*
PDT-bimane	2,3,6-Trimethyl-5-[(2-pyridinyldithio)methyl]-1H,7H-pyrazolo[1,2-a]pyrazole-1,7-dione
PMSF	phenylmethanesulfonyl fluoride
PSNCBAM-1	1-(4-Chlorophenyl)-3-[3-(6-pyrrolidin-1-ylpyridin-2-yl)phenyl]
ROS	Rod outer segment
RTI-371	3β-(4-methylphenyl)-2β-[3-(4-chlorophenyl)isoxazol-5-yl]tropane
S1P1	Sphingosine 1 phosphate receptor
Salbutamol	(RS)-4-[2-(tert-butylamino)-1-hydroxyethyl]-2-(hydroxymethyl)phenol
SAR	Structure-activity relationship
SDFL	site-directed fluorescent labeling
SDS	Sodium dodecyl sulfate
SDS-PAGE	sodium dodecyl sulfate polyacrylamide gel electrophoresis
S.E.M.	Standard error of the mean
shCB1	synthetic human CB_1 receptor
shCB1-C11 (C11)	synthetic human CB_1 receptor containing 11 cysteine residues (C98A and C107A) - and last 8 amino acids replaced with last nine of rhodopsin

shCB1-C13	synthetic human CB_1 receptor containing 13 cysteine residues – and last 8 amino acids replaced with last nine of rhodopsin
shCB1-C2	synthetic human CB_1 receptor containing 2 cysteine residues (C257 & C264) –and last 8 amino acids replaced with last nine of rhodopsin
shCB1-C4 (C4)-386A	CB_1 receptor containing C257,C264,C355,& C382
Sf	Spodoptera frugiperda (Army worm)
SR141716A	5-(4-Chloro-phenyl)-1-(2,4-dichloro-phenyl)-4-methyl-1H-pyrazole-3-carboxylic acid piperidin-1-ylamide hydrochloride
θ	Minimal cys CB_1 construct Δ88/Δ417 containing only C257 & C264
TCA	Trichloroacetic acid
TCEP	tris(2-carboxyethyl)phosphine
THC	tetrahydrocannabinol
THF	Tetrahydrofuran
TM	Transmembrane
TM1	Transmembrane Helix 1
TM2	Transmembrane Helix 2
TM3	Transmembrane Helix 3
TM4	Transmembrane Helix 4
TM5	Transmembrane Helix 5
TM6	Transmembrane Helix 6

TM7	Transmembrane Helix 7
TrIQ-Bimane	Tryptophan-induced-quenching of bimane
TRPV1	Transient receptor potential cation channel subfamily V member 1
VCHR	5-(4-chlorophenyl)-3-[(E)-2-cyclohexylethenyl]-1-(2,4-dichlorophenyl)-4-methyl-1H-pyrazole
WIN55212-2	(R)-(+)-[2,3-Dihydro-5-methyl-3-(4-morpholinylmethyl)pyrrolo[1,2,3-de]-1,4-benzoxazin-6-yl]-1-naphthalenylmethanone mesylate

Nomenclature used for shCB1 mutants in this Thesis.

Mutant	Cys residues retained in mutant	Modification(s)
shCB1-C13 (wt)	All 13 cysteines retained	1D4 tag C-term
shCB1-C11	11 cysteines retained (C98 and C107 are absent)	1D4 tag C-term
shCB1-C2	C257 and C264	1D4 tag C-term
shCB1-C0	All 13 cysteines changed to alanine	1D4 tag C-term
shCB1-C4-386A	C257, C264, C355, and C382	1D4 tag C-term
CB1-I	All 13 cysteines retained	GFP tag C-term
Δ103-I	12 cysteines retained C98 is lost due to N-terminal truncation	N-terminal truncation 103 GFP tag C-term
Δ 417-I	11 cysteines retained C431 and C449 are lost due to C-terminal truncation	C-terminal truncation 417 GFP tag C-term
Δ 103/Δ417-I	11 cysteines retained C98 is lost due to N-terminal truncation C431 and C449 are lost due to C-terminal truncation	N-terminal truncation 103 C-terminal truncation 417 GFP tag C-term
Δ 417-II	C257, C264, C355, and C382	C-terminal truncation 417 GFP tag C-term 1D4 tag C-term
Δ 88/Δ417-II	C257, C264, C355, and C382	N-terminal truncation 88 C-terminal truncation 417 GFP tag C-term 1D4 tag C-term
Δ 88/Δ 417-III	C257, C264, C355, and C382	N-terminal truncation 88 C-terminal

		truncation 417 1D4 tag C-term
θ	C257 and C264	N-terminal truncation 88 C-terminal truncation 417 1D4 tag C-term
A342C/θ	C257, C264, and A342C	N-terminal truncation 88 C-terminal truncation 417 1D4 tag C-term
C2 (θ) – Chapter 4	C257 and C264	N-terminal truncation 88 C-terminal truncation 417 1D4 tag C-term
Nt2/C2	C98, C107, C257, and C264	N-terminal truncation 88 C-terminal truncation 417 1D4 tag C-term
ΔIL3	C257 and C264	N-terminal truncation 88 IL3 truncation 307-326 C-terminal truncation 417 1D4 tag C-term
CB1a	All 13 cysteines retained	N-terminus of CB1a added to shCB1-C13 1D4 tag C-term

Note: That the residue number of cysteines and truncations are referred to as their original sequence number in full length wild-type CB_1

Acknowledgements

I would like to acknowledge my mentor, Dr. David Farrens, whom has played a major role in shaping me as a scientist, writer, and person. Additionally, I would like to thank members of my thesis committee Dr. Kim Neve, Dr. Ujwal Shinde, Dr. Francis Valiyaveetil, Dr. John Williams and formerly Dr. Svetlana Lutsenko.

I would also like to thank members of the Farrens' lab, past and present for making the lab environment social and productive: Dr. Biran Nauert, Dr. Jay Janz, Dr. Martha Sommer, Dr. Tom Dunham, Dr. Abhinav Sinha, Mark DeWitt, Emily Weimer, Lauren Brown, Alex Diezmann, Chris Schafer, Amber Jones and Emily Lorenzen.

I would also like to thank friends, family and colleagues for their support and love.

"The best moments, when everything comes together are few and fleeting, but you will never get to the next great moment if you don't keep going."

Overview of Thesis

G protein-coupled receptors (GPCRs) serve as conduits for dissemination of information across the cell membrane. Many pharmaceutical drugs act through these receptors to produce their therapeutic effects. Understanding how drugs can manipulate these bio-machines has been one of my long-standing passions.

The overarching goal of this dissertation is to explore receptor mechanisms of activation using reductionist approaches. In pursuing this goal, I established new ways to work with the receptor. These techniques included purifying the receptor (Chapter 2) and studying dynamic structural changes using fluorescence spectroscopic approaches, with special emphasis on understanding how an intriguing allosteric ligand affects CB_1 (Chapter 3). In Chapter 4, I cover my investigation of the structure and role of the long N-terminus. Finally, using the purified CB_1 receptor as an antigen, I created and characterized several novel CB_1 specific antibodies, one of which is conformationally sensitive and shows an allosteric effect on the receptor (Chapter 5).

This introductory review will encompass many wide aspects of GPCR research, with a focus on pharmacological probes, structure, and the cannabinoid receptor system. I will begin with the initial discovery of cannabinoid receptors, and then focus on the neuronal cannabinoid receptor, CB_1. I have provided an overview of some of the commonly used ligands that bind to CB_1 and briefly describe some general physiological roles of this receptor in the body. I will then highlight some aspects of GPCR structure/function, and finally conclude with a discussion of allosteric modulation and biased signaling in GPCRs. In an effort to keep the introduction concise, I have provided more in-depth mathematical analyses of allosteric models in the appendix.

Chapter 1

Introduction

1.1: Cannabinoid Receptors

Overview: In this section, I detail some major phytocannabinoids and their role in the discovery of proteins with which they interact, as well as sites of distribution of some of these proteins.

1.1.1: Cannabinoid Receptors: *Phytocannabinoids*

The *Cannabis* plant contains a class of compounds known as phytocannabinoids. These compounds are produced through the mevalonic acid pathway and extruded as a viscous resin through the cell membrane, via glandular hairs (trichomes) [1]. At least seventy distinct cannabinoids have been identified in *Cannabis sativa* [2]. All classes are derived from cannabigerol and produced through the condensation of two substrates (geranyl pyrophosphate and olivetol) by olivetolate geranyltransferase [3-5]. The major active components and most abundant natural cannabinoids are tetrahydrocannabinol (THC), cannabidiol (CBD) and cannabinol (CBN) (Figure 1.1) [6].

Both Δ^9THC and Δ^8THC are psychoactive cannabinoids in marijuana, however, due to the lower amount of Δ^8THC in *C. sativa* it is generally agreed that Δ^9THC is the major psychoactive constituent [7]. THC is often an acid, carboxylated at the 2 and 4 position of the phenol ring and these carboxy groups are released by gastric acid or by combustion (see Figure 1.1) [1, 7]. Hence, inhalation and oral digestion are the primary delivery routes used by cannabis consumers. Decarboxylation can also occur though the drying (or curing) process and/or storage of plant material [5]. CBN is found as the product of

THC degradation and is thought to be only mildly psychoactive. While CBD is not psychoactive, it can moderate the euphoric effects of THC. This is due to the well-known ability of CBD to interfere with drug metabolism. There is evidence that CBD can inactivate cytochrome P450 enzymes (CYP2C11 and 3A), which are responsible for the majority of THC metabolism; in addition CBD can be biotransformed into THC derivative by mammalian systems [8, 9]. Interestingly, phytocannabinoids have been identified in plants other than *Cannabis* (for a review see [10]).

1.1.2: Cannabinoid Receptors: *Identification of different cannabinoid receptors*

By definition, cannabinoid receptors are proteins that bind cannabinoids and are responsible for their pharmacological effects. Due to the diverse nature of these compounds (as discussed above), initial research focused on Δ^9THC, the principle psychoactive phytocannabinoid. Identification of Δ^9THC as the major psychoactive constituent in marijuana led to the synthesis of various high-affinity analogs [11-13].

One such derivative, CP 55940, facilitated the discovery of an enantioselective cannabinoid receptor in rat brain tissue [12]. Additionally, a 'nonhydrolyzable' guanosine-5'-triphosphate (GTP) analogue decreased tritium labeled CP 55940 binding. Combined with previous evidence that THC inhibited adenylate cyclase activity [14, 15], this observation indicated that these cannabinoid receptors were likely members of the guanine nucleotide binding protein-coupled receptor (GPCR) family.

Subsequently, the gene encoding the rat cannabinoid receptor was cloned in 1990, and

termed CB_1 [16]. A year later, Gerard et al. (1991) isolated a cDNA encoding a cannabinoid receptor from a human brainstem cDNA library [17]. The amino acid sequence encoded a protein of 472 residues which shared 97.3% identity with the rat cannabinoid receptor cloned by Matsuda et al. (1990). Additionally, they provided evidence for the existence of an identical cannabinoid receptor expressed in human testes.

A second GPCR cannabinoid receptor, termed CB_2, was identified within immune cells two years later [18]. Human CB_1 and CB_2 receptors possess approximately 44% amino acid similarity. Cannabinoid receptors have since been identified in mammals, birds, fish, and amphibians, thereby indicating a potentially conserved evolutionary role.

Alternative human splice variants of CB_1 that result in amino-terminal variants have also been identified and termed CB_1a and CB_1b [19, 20]. Other cannabinoid GPCRs have also been identified. GPR55, an orphan GPCR first described in 1999, contains ~14% amino acid sequence homology with CB_1 and CB_2 [21]. Two patents from GlaxoSmithKline and AstraZenneca allege GPR55 can be activated by cannabinoids [22, 23]. More recently, GPR18 has also been reported as a cannabinoid receptor (19.3% identity to CB_1) [24]. See Figure 1.2 for a sequence alignment of these various cannabinoid GPCRs.

Of note, other non-GPCR targets for cannabinoids have been identified. The ion channels TRPV1 and ANKTM1 have been shown to be modulated by cannabinoids [25, 26]. There is even evidence that nuclear receptor transcription factors can bind cannabinoids. The complexity of the pharmacological landscape of cannabinoid

receptors continues to grow. For the remainder of this document I will focus mainly on the CB_1 cannabinoid receptor. Ion channels and nuclear receptor transcription factors modulated by cannabinoids will not be discussed (for review, see [27] and [28]).

1.1.3: Cannabinoid Receptors: *Distribution and relative amounts*

CB_1 is often referred to as the neuronal cannabinoid receptor, as it is abundant in the brain and found in the neocortex, hippocampus, hypothalamus, amygdala, basal ganglia, and cerebellum [29-31]. In fact, CB_1 receptors are one of the most ubiquitously expressed GPCRs in the brain, at levels 10 times that of *mu* opioid receptors [32]. The CB_1 receptors are mainly localized on presynaptic nerve terminals and thought to modulate synaptic transmission [33].

The mRNAs for two human CB_1 isoforms, CB_1a and CB_1b, have been detected in a number of tissues, although in much lower abundance than CB_1 [19, 20]. Interestingly, these two isoforms have truncated N-terminal regions. Deletions in the amino terminus of CB_1 have been shown to enhance cell surface expression [34]. This may result in more efficient cell surface production of the CB_1 isoforms. Also of note, 2-arachidonoyl-glycerol has been shown to function as an inverse agonist on CB_1a and CB_1b [20] whereas it typically is an agonist for CB_1. It has not been confirmed, however, that CB_1a and CB_1b are actually expressed proteins. Development of selective antibodies directed at these isoforms may prove invaluable to determine what functional role these receptor isoforms may play.

In contrast to CB_1, CB_2 receptors are found predominantly in the immune system (spleen and white blood cells) [18], and it is thought that the ability of cannabinoids to suppress the immune system occur through a CB_2 mediated pathway. In support of this claim, cannabinoids have been shown to (1) decrease resistance to bacterial infection, (2) decrease T-cell proliferation, (3) reduce natural killer cells, (4) suppress macrophage function, (5) inhibit antibody production, and (6) reduce cytokine release [35-40]. There is also evidence of cannabinoid receptors in the uterus, ovary, testis, bone marrow, thymus, tonsils, adrenal gland, lung, prostate, vas deferens, small intestine, urinary bladder, and sympathetic nerve terminals to the heart [8, 41].

Interestingly, mouse GPR55 mRNA is expressed throughout the CNS, although at significantly lower levels than those for CB_1, except for the brain stem, striatum, and hypothalamus, which are at comparable levels [42]. GPR55 has some divergent pharmacology that differs from CB_1; notably, CBD (which doesn't appear to bind CB_1) functions as an antagonist and the CB_1 antagonist SR141716A may function as an agonist [43]. Also of note, evidence of actual protein localization of GPR55 has not yet been determined.

1.2: Brief overview of orthosteric CB_1 Ligands (cannabinoids)

1.2.1: Definition of pharmacological terms: *orthosteric, affinity, efficacy, potency, partial agonist, full agonist, antagonist and inverse agonist*

Before a discussion of CB_1 ligands begins, it is prudent to first briefly define some of the

pharmacological terms. The orthosteric site is defined as the traditional binding site on the receptor that binds endogenous agonists, classical antagonists and inverse agonists in a competitive fashion. Determination of ligand affinity usually consists of binding isotherm measurements using a radiolabeled ligand. These experiments predict a dissociation constant for the ligand (K_d), or an inhibitory constant (K_I) when the radioligand differs from the compound being analyzed.

On the other hand, efficacy refers to the ability to measure downstream biological response upon ligand binding to the receptor. Ligand efficacy can be divided into two classes, agonists and antagonist. Orthosteric ligand (that are competitive towards each other) efficacies can differ dramatically. Agonists activate the receptor to varying degrees and with relative potencies – creating a spectrum of full agonist or partial agonists with varying degrees of potency. In contrast, true antagonists display no efficacy – by definition.

Many alleged 'antagonists' have been found later to impart negative efficacy (in recombinant systems) and such ligands are now being referred to as inverse agonists. This phenomena is thought to be due to residual constitutive activity of the receptor in the absence of ligands (however, this may be more complicated for the cannabinoid system – see Summary). To help clarify this redefinition, some antagonist are termed neutral antagonist (which is technically redundant). To summarize, the efficacy of a full agonist is by definition 100%, partial agonists are a fractional value of 100%, a neutral antagonist is 0%, and an inverse agonist has an efficacy less than 0%. These concepts are further

illustrated in Figure 1.3, which shows a few choice examples of the broad pharmacological dimensions that can be imparted upon a receptor by various ligands.

1.2.2: Overview of orthosteric CB_1 Ligands

Here I will briefly discuss some of the well-known synthetic analogs and briefly touch on some of the pharmacophore that have been identified through various chemical analogues. Much of this body of literature has been instrumental in developing various orthosteric cannabinoid ligands. Although considerable effort has been contributed to making CB_2 selective ligands, here I will focus mainly on ligands that bind to the orthosteric site of CB_1.

All of these compounds discussed in this section are competitive for the traditional (orthosteric) binding site and while structurally heterogeneous, they do share one common attribute; they are all extremely lipophilic (Figure 1.4 and Table 1.1). Thus employing these compounds using classical biochemical approaches to determine ligand affinity faces some practical difficulties. For example, cannabinoid receptor studies are often troubled with high non-specific binding (~60%) due to the lipophilicity of these molecules [44]. Interestingly, one compound called O-1057 (3-(5'-cyano-1',1'-dimethylpentyl)-1-(4-N-morpholinobutyryloxy)-Δ8-tetrahydrocannabinol) synthesized in the laboratory of Dr. Razdan [1]has been shown to bind CB_1 receptors with high affinity and is reported to be soluble in water up to about 40 mM [45].

[1] Department of Pharmacology and Toxicology, Medical College of Virginia, Virginia Commonwealth University, Richmond Virginia

1.2.2: Further examination of Natural/Classical cannabinoid agonist

Identification of the psychoactive phytocannabinoid present in *Cannabis* as Δ^9THC (and the more stable nearly equally active isomer Δ^8THC) has led to numerous structure–activity relationship studies (SAR), resulting in a "three tier" hypothesis proposed for the action of THC. The groups that are thought to be responsible for high-affinity binding are (1) the phenolic hyrdoxyl at C1, (2) the hydrophobic pentyl side chain at C3, and (3) the C11 position (see Figure 1.5A) [46].

The phenolic hydroxyl is an important moiety for interaction with the cannabinoid receptor, and when replaced (with an amine, carboxyl, acetylation, glycosylation or methylation) reduces or abrogates the ability of respective THC analogues to confer biological response [47]. These results suggests this hydroxyl may be hydrogen bonding with the receptor. Studies in which the alkyl side chain has been systematically altered have found that dimethylheptyl (DMH) is the most potent modification [48]. Alkyl side chains of less than 5 carbons decreases potency and removal of this side chain is more detrimental to biological response than removal of the phenolic hydroxyl [49]. Optimal activity occurs with a length of around seven to eight carbons, suggesting a steric restriction of the alkyl side chain.

Interestingly, the first liver metabolite of Δ^9-THC is 11-OH-Δ^9-THC which is approximately three times more potent than Δ^9-THC [8]. Dr. Mechoulam[2] created a

[2] Institute for Drug Research, Hebrew University, Medical Faculty Jerusalem Israel

dimethylheptyl analog of 11-hydroxy- Δ^8- tetrahydrocannabinol, termed HU210, that was determined to be at least 100 times more potent than THC. This compound is widely used in the literature as a full classical cannabinoid agonist and is one of the most potent known cannabinoid receptor agonists [11]. By comparison, THC is less potent and a partial agonist (affinity in the 100's of nM K_d range) [41].

1.2.3: High-affinity synthetic "classical" and "non-classical" cannabinoid agonists

Bicyclic cannabinoid compounds (analogues of THC that lack a pyran ring) were developed by Pfizer. Once such prominent ligand, CP 55940, is arguably the most widely used non-classical cannabinoid ligand. It possesses nanomolar affinity and is a full agonist like HU210. SAR studies have shown that rigid positioning of the hydroxyproply moiety by a ring enhances CP 55940 binding [49].

Another group at Sterling Winthrop discovered a completely different class of cannabinoid ligands – the so-called aminoalkylindoles (AAI) based cannabinoid agonist. Original interest in these compounds was due to their anti-inflammatory actions, but they were later were found to also bind cannabinoid receptors. The archetype AAI is WIN55212-2. The parent compound pravadoline (a non-acid analogue of the non-steroidal anti-inflammatory indomethacin) exhibits prostoglandin synthatase inhibition and a series of analogues were designed that had analgesia independent of prostoglandin synthase inhibition. Restraining the amide side chain was responsible for attenuation of its inhibitory actions on prostoglandin synthatase and increased CB_1 receptor activity [50].

WIN55212-2 binds CB_1 receptors in the nanomolar range, and while it is structurally different than classical, non-classical or eicosanoid cannabinoids, WIN55212-2 is fully competitive for the orthosteric binding site. Like CP 55940 and HU210, WIN55212-2 is also thought to be a full agonist. Although, in contrast to classical cannabinoid-like analogues, it is thought to bind to the receptor with minimal contribution of hydrogen bonding, thus a possible aromatic stacking model has been proposed for its mechanism of binding [51].

The most definitive demonstration that hydrogen bonding was not required for binding of AAI ligands was established by the synthesis and testing of the hydrocarbon JH-176 [52]. This AAI analogue (containing no heteroatoms) is incapable of hydrogen bonding. It was found to be a high-affinity cannabinoid agonist and as such its ability to bind to CB_1 supports an aromatic stacking mechanism as being the predominate mechanism of binding.

Due to the competition of WIN55212-2 for classical cannabinoids it is clear that these compounds show an overlapping (orthosteric) binding site. Thus, an alignment of WIN55212-2 with classical cannabinoids was proposed that places the morpholine group in line with the alkyl side chain of classical cannabinoids, and the napthyl ring in line with the B and C rings (see Figure 1.5B) [53]. In support of this alignment, replacement of the morpholine with alkyl side chains of 1-7 carbons found the best binding with a butyl and pentyl replacement, and anything above hexyl greatly attenuated affinity [54]. Additionally, substitution of the napthyl ring with a phenyl or substituted phenyl

substantially attenuates receptor affinity [54]. Finally, of note is the 2-position of the indole; a small substituent is preferred for retaining high-affinity binding [55].

1.2.4: High-affinity synthetic cannabinoid antagonists

The general term 'antagonist' is used in this section as opposed to inverse agonist.

An aminoalkylindole based cannabinoid antagonist, AM630 (iodopravadoline) was identified and appears to act as neutral antagonist against WIN5521-2 [56]. However, the most widely employed cannabinoid receptor antagonist was discovered (in 1994) by researches from Sanofi-Synthelabo, and called SR141716A or Rimonabant [57]. This compound was later determined to be an inverse agonist. It is probably the most widely used CB_1 antagonist, and at one point widely considered as a promising weight loss drug [58] until complaints forced it to be pulled from the market.

Many other analogues of SR141716A have been subsequently created. Dr. Makriyannis[3] has developed structural analogues of SR141716A, of note, AM251 (where the monochloro phenyl substituent is replaced with a para iodophenyl group) and AM281 (also containing the p-iodo substitution in addition to a morpholine replacement of the piperidine ring). Also, reduced lipophilicity variants like NIDA-41020, containing methoxy substitutions have also been created (soluble to 100 mM in EtOH) [59]. Interestingly, O-1269, an analog where the piperidine ring is replaced by a pentyl carbon chain, has demonstrated some partial agonism *in vivo* [60].

[3] Center for Drug Discovery and Department of Chemistry and Chemical Biology and Barnett Institute of Chemical and Biological Analysis, Northeastern University , Boston, Massachusetts

From these analogues a general pharmacophore model can be summarized (see Figure 1.5C). The pyrazole ring (green Figure 1.5C) acts as a central scaffold and requires two aromatic moieties X and Y. Amusingly, the pyrazole scaffold has been substituted (in part due to promising clinical results of Rimonabrant) with different five and six membered rings (as well as purine) arguably to circumvent patents [61]. The X moiety is the 2,4-dichloro-phenyl ring at the pyrazole 1-posistion and Y is the 4-chlorophenyl ring at the pyrazole 5-position [62]. A single chloro group at the 4′-position on the X ring has reduced binding [62]. On the Y ring para is favorable over ortho substitutions, with NH_2>NO_2>Br>Cl>I for Ki values versus SR141716A [62]. At the pyrazole 3-position a hydrogen bonding partner is favorable like the carboxamide linker; and after the carboxamide linker hydroxyethyl <N-heterocyclic substituted < pyrrolidinyl = piperidine. Lipophilic carbon chains tentatively impart agonist like properties [62].

1.2.5: Putative neutral antagonists

Two compounds have been reported to behave as 'neutral' antagonist (i.e., true antagonists) and both are structural analogues of SR141716A. These compounds are NESS 0327 and VCHR [63, 64]. VCHR lacks the carboxamide hydrogen bonding partner and NESS 0327 has reduced flexibility on the mono-chloro ring due to introduction of a seven-membered ring. Both are truly neutral antagonists, as they bind and inhibit agonist activity and by themselves exhibit no efficacy. Also of note, another constrained SR141716A analogue is produced via a photocyclization of SR141716A. Where the X and Y rings are locked together, the authors report that this compound while

possessing reasonable affinities towards CB_1 receptor had no efficacy, and thus may represent another neutral antagonist [65].

1.2.6: Endogenously produced Endocannabinoids (Eicosanoids) Ligands

Since the discovery of the CB_1 receptor through lipophilic phytocannabinoid derivatives, it was suspected that the endogenous ligand(s) would also have similar properties. In 1992 Devane and colleagues isolated lyophilic compounds from water-insoluble porcine brain fractions that bound to cannabinoid receptors [66]. The identity was further confirmed by NMR and total synthesis. The compound identified, N-arachidonoylethanolamide (ethanolamine amide of arachidonic acid), was named Anandamide (AEA) – a combination of the Sanskrit word ananda, which means "bliss," and amide. In 1997 Stella and colleagues isolated another endogenous cannabinoid (or endocannabinoid) *sn*-2 arachidonylglycerol (2AG) from rat brains [67]. Both of the structures of these prototypic and widely investigated endocannabinoids are shown in Figure 1.4.

Both AEA and 2AG are fatty acid phospholipid-derived poly unsaturated eicosanoid (20 carbon) ligands. AEA is a partial agonist and 2AG is a full agonists towards CB_1 [68, 69]. Both ligands are thought to be produced on demand from lipid precursors by actions of a phospholipase [67, 70, 71]. Their biosynthesis is mediated by elevations of intracellular calcium [33]. The first step in AEA biosynthesis is cleavage from a membrane phospholipid precursor, N-arachidonoyl-phosphatidylethanolamide (NAPE) that is found in the brain in a concentration around 20-40 pmoles/g [33]. The levels of

2AG are ~200 fold higher in the brain than that of AEA [33]. 2AG is formed mainly by hydrolysis of phospholipid precursors including phosphatidylinositol and arachidonoyl-*sn*-glycero-phosphocholine [72]. Both AEA and 2AG are deactivated by hydrolytic enzymes –AEA mainly by fatty acid amid hydrolase (FAAH), and 2AG mainly by monoacylglycerol lipase [33]. Other bioactive lipids have been extracted from animal tissues that may be endocannabinoids [33]. Interestingly, the effects of AEA and 2AG appear to be enhanced through what has been termed the "entourage effect" – the co-release of other endogenous fatty acid derivatives that potentiate the effects of the prototypic endocannabinoids [73].

Working with endocannabinoids presents some technical challenges. AEA can be rapidly degraded into arachidonic acid and ethanolamine by amino peptidases. One variant of AEA that can help alleviate this potential issue is Methanandamide (mAEA). It contains a methyl group on the first carbon in the ethanolamine moiety – that substantially reduces the susceptibility of the amide bond to hydrolysis by amino peptidases, and thus this compound is sometimes preferable for cell-based studies. It has a higher affinity to CB_1 than AEA and has enhanced metabolic stability [74]. Interestingly, most eicosanoids do not have any chiral centers, however methanandamide does and its R-(+)-isomer is 9 times more potent than the S-(-)-isomer .

2AG possesses a different technical issue that is not always appreciated in the literature. It can rapidly and readily undergo acyl migration in solution to form 1-arachidonylglycerol. The half-life for 2AG in solution is only about 10 min, and this is

brought down to about 2 min in the presence of serum – which is often used as a carrier for pharmacological assays [75]. Another important consideration is that many experimental models may contain endocannabinoid agonists that may enhance exogenously added endocannabinoids and/or increase the basal activity of the system [76]. Accurately determining the affinity and efficacy of endocannabinoids is thus problematic and can complicate their SAR studies.

1.2.7: Orthosteric Ligand Summary

The outline above describes some of the major cannabinoid ligands used as pharmacological tools to activate and inhibit the receptor, from the plant-derived phytocannabinoids and their synthetic analogues to high-affinity agonist, antagonist and neutral antagonists. In summary, pharmacophore actions have been elucidated through the use of various structural variants for some of these molecules. Two key endocannabinoids have also been described, as well as the obstacles pertaining to their use. While I have gone into some discussion of neutral agonists, this topic can be complicated by the presence of endocannabinoids in an experimental system that may activate the receptor. These compounds can only be acknowledged as neutral antagonists if CB_1 is constitutively active. If elevated basal activity is due to endocannabinoids then these 'neutral antagonists' are merely permissive to endocannabinoid tone. Finally, it should be pointed out that the rank order of potency towards CB_1 for these various cannabinoid ligands is as follows: HU210 > CP 55940 > WIN55212-2 > THC > AEA > 2AG – although this is not always the case, and this topic will be re-addressed in the biased signaling section of this chapter.

1.3: G protein-coupled receptors: A brief overview

As mentioned earlier, CB_1 is a member of the G protein-coupled receptor (GPCR) family. They are the largest family of membrane surface receptors comprising roughly 3% of human genome (note that this percentage doesn't account for various splice variants) [77]. Based on sequence similarity (excluding the N-termini), human GPCRs can be clustered into 5 families: the rhodopsin family (or Class A, the largest family with ~700 members), the adhesion family, the frizzled/taste family, the glutamate family, and the secretin family [78].

As indicated by their diversity, GPCRs can mediate transmembrane signaling in a wide variety of cells, for a wide range of diverse molecules. They exist as important and pharmacologically exploitable conduits for transmission of information from outside the cell to inside, and act when stimuli-induced changes in receptor conformation instigate downstream protein-protein interactions and subsequent signal amplification.

The classical role for this superfamily of proteins, as their name implies, is to interact with heterotrimeric GTP binding proteins (or G proteins). The G protein complex is composed of 3 distinct polypeptide chains: an α (39-52 kDa), β (35-36 kDa) and γ subunit (7-8 kDa). There are about 21 different α subunits, 6 β subunits and 12 γ subunits [79], highlighting further combinatorial complexity of GPCR signaling, however, not all permutations of subunits occur [80]. The $\beta\gamma$ heterodimer are not

covalently bound together but an interaction between two of their α-helices is very strong, and they can only be dissociated under denaturing conditions [81]. Functionally, a key role of the βγ dimer is to act as a guanine nucleotide dissociation inhibitor, preventing GDP release. Post-translational modifications that help tether the subunits to the membrane include isoprenylation at the C-termini of γ subunits, and (usually) palmitoylation of the Gα subunits at the N-terminus [82].

The signaling cascade initiated by these seven transmembrane spanning receptors is called the G protein cycle (Figure 1.6). In brief, this involves the receptor binding to an extracellular signal (classically an agonist ligand, denoted as L), which then causes conformational changes in the receptor (denoted R) that lead to activating a cognate G protein.

"Activation" involves the G protein exchanging GDP for GTP, then dissociating into its respective α and βγ subunits [82]. This process exposes interacting surfaces on the faces of α and βγ, which then initiates a second step in the signal transduction cascade by activating or inhibiting various downstream effector proteins. The latter typically are involved in the generation of cellular molecules, called second messengers, which go on to further modulate downstream cellular machinery in a second round of stimulated receptor amplification. Finally, after sufficient time, the system "resets" itself when the intrinsic GTPase activity of the α subunit hydrolyzes bound GTP back to GDP, thus inactivating the α subunit and enabling it to recombine with βγ subunits, forming a re-associated heterotrimer that can then associate with a GPCR to repeat the cycle.

GPCRs exhibit a wide array of responses that extend beyond the classical activation of G proteins. They can internalize and desensitize, and even interact with other membrane associated proteins that are not G proteins. Moreover, GPCRs can form homodimers, heterodimers, and higher-order oligomers [83, 84]. Given this enhanced repertoire of interaction, one can envisage the entire surface of a GPCR having the potential to be modulated by drugs, proteins [85], membrane lipids [86] and even voltage [87, 88]. This inherent ability of a GPCR to be modulated at distinct sites are the hallmarks of an allosteric protein [89] and this aspect of CB_1 and other GPCRs will be discussed more fully in a subsequent allosteric section of this chapter.

1.4: CB_1 receptor signaling

CB_1 has been shown to mediate neurotransmitter release in presynaptic terminals through the action of endogenous cannabinoid ligands [90-92]. The modulation of neurotransmission is consistent with the CB_1 receptor signal transduction pathway. Cannabinoid receptors couple to G_i or G_o proteins and inhibit adenylate cyclase [17], N- and P/Q-type calcium channels [93], and activate A-type inwardly rectifying potassium channels [94]. These modulations have been shown to in turn modulate the amplitude or frequency of neurotransmission. CB_1 activation also causes short or long-term changes in the efficacy of synaptic transmission through retrograde signaling, a process where the postsynaptic cell feeds back on the presynaptic cell to attenuate neurotransmitter release.

Moreover, other CB_1 mediated signaling paradigms have emerged that involve other

accessory and effector protein modulation or even different signaling pathways. For example cannabinoids and endocannabinoids can increase intracellular free calcium, activate p42/p44 mitogen-activated protein kinases, Jun N-terminal kinases, nitric oxide production, become phosphoralated (by either protein kinase C and/or G protein receptor kinases) and associate with β-arrestin 2 and other GPCR interacting proteins [95-97].

1.5: GPCR structure/function

Overview: In this section I will compare and contrast GPCRs of known structure. I will also review the mechanism of activation with a focus on spectroscopic/biophysical approaches.

1.5.1: Overview of GPCR structures

Structurally, all GPCRs share a characteristic architecture that consists of seven transmembrane-spanning (TM) domains connected by three extracellular and intracellular loops (IL or EL) (see Figure 1.7A). These receptor helices associate with the membrane to form a helical bundle that contains a ligand-binding site (see Figure 1.7B). Apparently, this common architecture can accommodate a structurally varied set of stimuli that lead to signal transduction.

Until relatively recently, the precise 3D structures of GPCRs were unknown. However, significant advancements have been developed for GPCR crystallization[4] and the days of

[4] Some of these advancements include: truncation of flexible termini, T4 lysozyme fusion chimaeras, use of camelid antibody fragments ('nanobody'), thermostabilized receptor mutants and/or high-affinity ligand thermostabilization.

low resolution cryo-electron microscopy homology models are now long gone. When I began my research project as a graduate student, there were only a handful of GPCR structures, and all were of the visual receptor rhodopsin. However, since 2007, when the first non-visual GPCR was crystallized [98], the field of GPCR structures has exploded and we are currently in an exciting time for GPCR research – a GPCR renaissance, if you will. At the time of writing this manuscript there are over 50 GPCR structures (in the PDB database) for 9 different general types of ligand binding receptors (see Appendix: An Incomplete List of GPCRs of Known Structure – preemptively named as it is soon to be out of date).

1.5.2: Structural comparison of GPCR structures

Extracellular regions

Figure 1.8 shows the A chain for some of the highest resolution structures for nine different GPCRs. Upon examining these models, it is immediately apparent that the general seven transmembrane architecture is conserved, and differences among receptors lie primarily in the extracellular regions. For instance, the extracellular loop two (EL2) (Figure 1.8 – EL2 is colored blue) exhibits clear structural heterogeneity between receptors. The EL2 of rhodopsin, CXCR4, and opioid receptors all have an antiparallel beta hairpin. In contrast, EL2 in the β2-adrenergic receptor (B2AR) has a striking 2.5 Å turn alpha helix, and adenosine A_{2A} (A2A) and muscarinic acetylcholine receptor M2 (M2) also have helical EL2s (albeit shorter). The EL2 in the A2A receptor also forms a β-strand that makes contacts with a β-strand on extracellular loop 1.

A highly conserved feature of Class A GPCRs is a disulfide bond between EL2 and TM3. This bond serves to stabilize EL2 and position it appropriately within the helical core. Although CB_1, lacks this conserved disulfide, it does contain an intra-loop disulfide. Interestingly, the BAR EL2 also contains an intra-loop disulfide bond, and the EL2 of A2A has three disulfide bonds that are important for maintaining the structure of this vital region.

The variable conformations of EL2 and its position at the ligand entrance suggest it may play a key role in regulating the entry and exit of ligands. In fact, numerous mutational and structural studies within this region further support the possibility that the role of EL2 is to act as a 'gatekeeper' in the binding of ligands [99-108]. In examination of GPCRs of known structure, EL2 appears to forms a 'lid' that extends (at least partially) into the interior of the transmembrane helical bundle. This 'lid' is less dramatic in the opioid structures, but is very dramatic in rhodopsin. While EL2 may not act as a 'gatekeeper' in the binding of ligands for all GPCRs it clearly contributes to ligand specificity at least for some. For instance, in some GPCRs the structures exhibit contacts between residues in EL2 and their bound ligands, implicating EL2 forms part of the orthosteric binding site.

Orthosteric binding site

Almost all GPCR structures show solvent accessible binding pockets (see Figure 1.9). With the large exposed vestibule of the opioid receptor being the most conspicuous example. The exceptions are rhodopsin and sphingosine 1 phosphate receptor (S1P1),

which are both GPCRs that bind hydrophobic ligands. Rhodopsin and S1P1 both have their N-terminus resolved (or partially), and both show significant occlusion of the binding pocket, and thus limited solvent access. Furthermore, in both cases the N-terminus and EL2 appear to stack upon each other, forming a 'hand-over-hand' like lid over the ligand pocket – although this is more pronounced in rhodopsin than S1P1. These observations highlight the concept that the N-terminus may confer domain coupling to EL2 (an idea that is expanded upon further in Chapter 4). CXCR4 is the only other GPCR with a partially resolved N-terminus, and it also appears to lie over the binding pocket. The N-terminus in CXCR4 also forms a disulfide with EL3, which may help tether transmembrane helix one (TM1) to the helix bundle and thus serve as an important structural role in maintaining ligand binding site.

Interestingly, all of the structures I examined for this review show the ligands binding in close proximity to a highly conserved tryptophan in a conserved motif (CWxP) in TM6 (with the exception of CXCR4). This is of interest because this region has been proposed to undergo structural repacking upon agonist binding in a way that ultimately leads to receptor activation [109, 110]. Additionally, structural waters clustered near key conserved residues in GPCRs are thought to rearrange upon activation and serve to link the orthosteric site to the intracellular domain [111] (also see Figure 1.7B).

Intracellular regions

Recent analysis indicates structural and sequence inequality between extracellular transmembrane regions (ETMR) and intracellular regions of GPCRs of known structure.

For instance, only 6% of ETMR amino acids are exactly conserved and the structures show ~2.7Å RMSD [112]. In contrast to the variability of the ETMR, the intracellular transmembrane region of GPCRs shows 28% exact amino acid conservation and only a ~1.5 Å RMSD [112]. Some of the conserved features (for class A GPCRs) in the intracellular TM region include a "DRY" motif in TM3, a tyrosine in helix 5 (5.58) and a "NPxxY" motif in helix 7 that form important contacts upon receptor activation.

Given the well-conserved sequence motifs between many GPCRs and the disproportionate amount of structural and sequence conservation between the two halves of the transmembrane domains, it not surprising that a similar mechanism of activation has been proposed. This reinforces the notion that extracellular variance enables selection of a broad range of stimuli that couple to similar intracellular proteins. Moreover, these observations imply that not only the binding pocket but also the diverse extracellular surface of GPCRs may be unique druggable targets – with potential for subtype-selectivity.

One intriguing exception to the conserved architecture is the observation that the cytoplasmic end of TM5 appears to exist in different positions between crystalized receptors. Moreover, the differences appear to cluster into groups that correlate with G protein-coupling specificity (i.e., $G_{i/o}$, G_t, G_q and G_s) [113]. I have performed a similar analysis on the 4 very recently published opioid receptors and find similar clustering with $G_{i/o}$ specificity (Figure 1.10). One caveat, however, is that this analysis may be biased by the stabilization approaches used to facilitate crystallogenesis.

Not included in the above TM analysis are the intracellular loops. The backbone architecture of IL1 and the amphipathic helix 8 (H8) are conserved (again CXCR4 is the exception having a disordered H8). Although, IL2 appears to present itself in an ~2.5 α-helix existing parallel to the membrane, extended or even disordered conformations have been observed. This loop contains key residues that mutational analysis has revealed to be important for G protein interaction. For example, when a conserved leucine is mutated to an aspartic acid in IL2 of CB_1, G protein activation is inhibited; even with the G protein is tethered to the receptor (Fay – unpublished data). Swapping IL2 with different receptors can even alter the G protein-coupling specificity [114].

IL3, the 'loop' that connects TM5 to TM6, (these TM domains will be discussed in more detail below) is well known to play a role in G protein-coupling. IL3 also has a high degree of sequence divergence (and length) between GPCRs and even between subtypes, and thus IL3 is thought to be a key player in G protein subtype specificity. Intriguingly, IL3 generally has α-helical propensity. For instance, NMR studies on peptides of IL3 of CB_1 [115] and homology/structure prediction models I have generated point towards an extremely helical character for this region (Figure 1.7). Moreover, studies of intact rhodopsin and β1-adrenergic receptor (which do not replace IL3 with a stabilizing fusion protein) find IL3 is elongated to the ends of TM5 and 6 [116, 117]. The ends of IL3 extend far into the cytoplasm, as was also observed initially in squid rhodopsin [118]. Curiously, in squid rhodopsin the distal C-terminus extends into the TM5 and TM6 region, and also makes contacts with IL2. This factor may be important for modulating

recognition by intracellular effectors or may even play in role receptor oligomerization (linking promoters of rhodopsin together by C-terminal interaction with an adjacent receptor's extracellular face). This IL3 region (that extends cytoplamic ends of TM5 & 6) is highly mobile [119, 120] and until recently, was often unresolved (or replaced) in many GPCR crystal models. In Chapter 5, I will give examples of how an antibody directed at this region can alter the conformational landscape of the receptor.

1.5.3: Structural Models of GPCR activation

How is ligand binding transferred to structural changes in intracellular components that enable coupling with effector molecules? Some of the first experimental insights into the mechanisms of activation were established by site-directed spin labeling studies of rhodopsin, which showed that spectroscopic probes attached to cysteines on the inner surface of TM6 had increased mobility upon receptor photoactivation [121, 122]. Less dramatic structural rearmaments at the cytoplasmic end of TM1 and TM7 have also been observed [123]. Interestingly, disulfide linkages between TM6 and TM3 were shown to block activation of G protein by the receptor [121]. Around the same time, comparable studies in Kobilka[5]'s laboratory postulated a similar interpretation in B2AR [124, 125]. Structural changes in TM6 are also proposed to occur in parapinopsin upon activation, although the amount of changes appear to be less than what is observed in rhodopsin, leading to the proposal that the magnitude of TM6 movement could explain greater efficiency of rhodopsin for activating G protein than parapinopsin [126].

[5] Department of Molecular and Cellular Physiology, Stanford University School of Medicine, Stanford, California

In Chapter 3, I will discuss similar site-directed fluorescence labeling that I applied on the CB_1 receptor to test if this mechanism of action is conserved, and to address the nature of how an allosteric ligand can alter receptor conformation.

Interestingly, early studies on the B2AR suggest the receptor may actually exist in a number of conformational states – as indicated by the observation of different ligand dependent fluorescence lifetime distributions [127, 128]. Interpretations of these results suggest that full agonist and partial agonist exist in two states (intermediate and active), in contrast to a neutral antagonist which stabilized a state that was similar to the unliganded (or apo) receptor state.

Moreover, the binding of an agonist and subsequent formation of an active receptor seems to proceed through a series of conformational intermediates [127-129]. These interpretations are consistent with observations in rhodopsin – it also proceeds through several spectrally distinct conformational changes during the conversion of the inactive state to fully activated receptor [130, 131]. Interestingly, in B2AR, fluorescent studies showed that salbutamol (a non-catechol partial agonist) induced a slow monophasic fluorescence change at a probe on the cytoplasmic end of TM6 and this change was potentiated by a weak partial agonist (catechol). This result suggested that salbutamol occupies a non-overlapping binding site (compared to catechol) and the active state induced by salbutamol is different than that of catecholamine agonists. Further investigation using a tryptophan-induced-quenching of bimane (TrIQ-bimane) fluorescence method [132, 133] found that breaking a highly conserved salt-bridge between TM3 and TM6 is ligand dependent [134]. Intriguingly, salbutamol by itself was

fully able to elicit this spectral change – what is interpreted to be disruption of the ionic lock. This indicates differential modes of agonist activation. Of note, it has been proposed that multiple ligand specific conformational states exist and can even be exploited to induce (or stabilize) specific signaling states [135] – (this is reviewed in further detail in functional selectivity section). Intriguingly, more recent structural/dynamic evidence points towards receptor mediated non-G protein signaling pathways that involve structural changes at or around TM7 [136-138].

TM6 movement – G protein-coupling & activation

The "reason" for TM6 movement in GPCR activation was established by early spectroscopic work on rhodopsin. These studies found a peptide corresponding to the C-terminus of the G protein α subunit (Gα Cterm) binds to a cleft that is exposed upon TM6 movement. Moreover, a key part of the binding appears to involve interaction with hydrophobic residues that become exposed on the inner faces TM5 by TM6 movement [139]. The C-terminus of the G protein fused to B2AR was also shown to be almost completely responsible for forming the high-affinity agonist binding site (discussed in further detail below). In crystallographic models the Gα subunit's C-terminus is often unresolved. This helix is connected directly to a loop that forms the nucleotide binding pocket. It has been suggested that desolvating this region is important for forming an extended alpha helix structure that acts to distort this loop [140].

Subsequent crystallographic models of opsin and active rhodopsin bound to a Gα Cterm peptide confirmed this role for TM6 movement [141-144]. In addition, these structures

show substantial rearrangements in TM5 and TM6 consistent with earlier spectroscopic studies. These movements have also been observed crystallographically in B2AR and (to a lesser extent) in A2A [109, 145].

Through extensive stabilization techniques, a crystallographic model of B2AR bound to its G protein (Gs) has been determined [109]. The model provides an insight into a guanine nucleotide free ternary complex (receptor, ligand & G protein). Interestingly, in this model the G protein exists in an open conformation and hydrogen-deuterium-exchange mass spectrometry (DXMS) hints at a mechanism of activation [146]. Based on their evidence Chung et al. propose the N-terminal helix of the α subunit of Gs destabilizes an adjoining highly conserved β-strand that perturbs the guanine nucleotide binding pocket. This facilitates opening of the G protein where two independent folding domains are splayed. This domain rearrangement in the Gα subunit has also been observed in rhodopsin ternary complex by site-directed spin labeling studies, and moreover, cross-linking the two G protein domains together resulted in impaired rates of guanine nucleotide exchange [147]. While the structural basis for increase in agonist affinity by G protein is speculative at the moment, it appears that the extracellular region may contract and thereby provide an increase in affinity of the ligand to the receptor. This has been observed for agonist bound A2A [148], and my own comparisons of other A2A and B2AR models.

In a recent talk by Dr. Sunahara here at OHSU, the mechanism for the G protein activation process was described by the following eloquent analogy: “The G protein is like a chainsaw that the receptor is holding. The C-terminus of the G protein is the

handle. To ‘start the motor,’ the receptor IL2 grabs the ‘starter rope’ (N-terminus) and gives it a yank.”

1.6: Allosteric Modulation of GPCRs

Overview: In this section I will describe allosteric modulation of GPCRs. I will briefly give context to how an allosteric model was first used to describe receptor coupling to the G protein. I will then highlight some general points of small molecule allosteric ligands and briefly review some of the mathematical models used to describe their behavior.

1.6.1: Allosteric Modulation of GPCRs: To describe G protein activation

Allosteric proteins were first conceptualized by Monod, Wyman, Jacob and Changeux over half a century ago [149]. Allosteric modulation allows for the activity at one site on a protein to alter the function at another spatially distinct site. As mentioned earlier in this chapter, GPCRs can be thought of as intrinsically allosteric proteins due to the their ability to recognize and bind molecules at one site, which then leads to structural rearrangements on another site. For example, binding of a ligand in the orthosteric site causes changes in the intracellular surface that allows the receptor to bind and interact with cytoplasmic proteins.

As mentioned in the previous section, agonist binding is thought to stabilize (or induce) an opening out of helices on the cytoplasmic surface, specifically TM5 and TM6 that

creates a cavity into which the C-terminus of the Gα protein can bind. An early observation for this phenomenon was the decrease in agonist affinity upon addition of a 'non-hydrolysable' GTP analogue. This led to the ternary complex model, first published by De Lean, Stadel and Lefkowitz over 30 years ago [150] to describe the binding of ligands to the B2AR. This model is the first allosteric model to describe GPCR function. Amusingly, it was unknown at the time that drug-binding receptors coupled to a G protein, and hence this unidentified membrane component was termed "X" [151]. The ternary complex model (shown in Figure 1.11A) describes a model for a bound G protein leading to a high-affinity agonist binding site in the receptor that is then lost when the G protein is activated and released. More recently this model has been recapitulated with purified components and this high-affinity agonist binding site has been localized to specifically involve binding of the G protein C-terminus (or even a G protein mimetic) to a site exposed by TM6 movement in the receptor [109, 152].

Other models have emerged to include and describe other phenomena (such as constitutive GPCR activity), for example the extended ternary complex model (ETC) [153] and the cubic ternary complex model (CTM) [154]. For an excellent review on these models please see reference: [155].

1.6.2: Allosteric Modulation of GPCRs: by small molecules

Drug discovery has typically involved optimization and modification of natural compounds that were initially observed to bind to a "classic" agonist binding site. For

instance, for CB_1, modifying the compound THC led to the development of high-affinity agonists like HU210 and CP 55940. Many molecules have been developed and selected based on their ability to bind to a spatially overlapping region (or orthosteric binding pocket) on the receptor. Such an approach has led to the discovery of agonists, neutral antagonists and inverse agonists for various GPCRs, and enhanced our ability to pharmacologically probe different receptor states. However, there is no requirement that a drug must bind to a "traditional" orthosteric binding site. For instance, arguably the most used (and abused) allosteric drug on the market today is ethanol, which acts on the ligand-gated ion channels GABA and NMDA. It is now becoming increasingly common to find GPCRs that also contain small molecule binding sites that are topographically distinct from the orthosteric site. These "other" sites can bind drugs (allosteric modulators) and further alter receptor states.

The potential for new small molecule allosteric binding sites provides some possible advantages in pharmacotherapy. Since an allosteric ligand can be conformationally linked to the orthosteric site, and 'action at a distance' allows communication between these linked sites, an allosteric ligand can for example only shift the affinity for an endogenous ligand and thus alter the responsiveness of a receptor. In doing so, the receptor can continue to respond to endogenous signals in a physiological relevant fashion – but with an altered receptor 'set point.'

By contrast, orthosteric agonists provide broad receptor activation which can be associated with toxicity, receptor desensitization and long-term changes in receptor homeostasis – due to persistent receptor occupancy. On the other hand, allosteric ligands

can theoretically have no direct effect by themselves on a receptor, and thus have the potential to avoid such effects. Another interesting property of allosteric ligands is that they can be permissive and thus be exploited to combat HIV infection – changing the shape of the receptor to inhibit viral entry while allowing endogenous signaling at the receptor [156]. Allosteric modulators also have a limit to their effects (described in more detail below), allowing larger doses to be administered that can extend their duration without causing an overreaction. Another important characteristic of allostery is the phenomenon of 'probe-dependence,' whereby allosteric modulators can have a variable effect on different orthosteric ligands [157].

Allosteric ligands have been shown to exhibit exquisite receptor subtype selectivity – as has been observed for muscarinic M4 and adenosine A3 receptors [158, 159]. This is thought to occur due to less evolutionary constraints toward an allosteric site (between subtypes), in contrast to an orthosteric site [160]. Other exciting avenues are being explored and envisioned, including bitopic ligands that can functionally couple allosteric and orthosteric sites, thus yielding subtype selectivity and enhanced affinity [161].

The concepts of differential effects of allosteric ligands on affinity vs efficacy, saturability, and stimulus-bias are discussed further below.

1.6.3: Allosteric Modulation of orthosteric ligand binding

The simplest model to describe an allosteric ligand binding to the receptor and modulating an orthosteric ligand's affinity is the allosteric ternary complex (Figure 1.11B) [162]. This model is formally identical to the ternary complex model described

earlier. However, here K_A and K_B are the equilibrium dissociation constants for orthosteric ligand A and allosteric ligand B. The cooperativity factor, α, governs the magnitude by which one ligand can alter the affinity for the other when they form a ternary complex. Values of α greater than 1 denote positive cooperativity (increased affinity), and values less than one denote negative cooperativity (decreased affinity).

Interestingly, the model predicts value of α equal to 1 denoting neutral cooperativity – a condition where ligand affinity is not altered. Another interesting condition predicted by this model is extreme negative cooperativity (when alpha approaches 0); the model essentially reduces to an orthosteric competition-like behavior.

Allosteric Saturability

Figure 1.12 illustrates the binding orthosteric ligand in the presence of increasing concentration of an allosteric modulator for α values that deviate from 1 (this is reviewed in more detail in the Allosteric Appendix). This Figure also shows a classical orthosteric competition where ligands A and B compete for binding to the same site on the receptor. Notably, there is a near limitless right shift in affinity for this type of scenario. In contrast, allosteric ligands saturate when the allosteric site is fully occupied, and this maximal effect is determined by the cooperativity factor.

Another way to visualize and measure the cooperativity imparted by an allosteric ligand is to plot the modulation of binding to a fixed concentration of orthosteric ligand in the presence of increasing concentrations of allosteric modulator. This is illustrated in Figure 1.13. Notably, this type of analysis can be especially useful for allosteric ligands with cooperativity factors that do not significantly deviate from 1. This style of assay can be

just as useful for determining the cooperativity factor and has the advantage of requiring fewer data points.

1.6.4: Allosteric Modulation of orthosteric ligand efficacy

Using a model described in Figure 1.14 (middle panel) one can further define cooperativiy factors for efficacy. Allosteric modulation of an effect can thus be quantified by two cooperativity factors α (as described above) and β, where β denotes the effect the modulator has on efficacy. Efficacy is defined as the signal imparted on the receptor system by orthosteric ligand A (S_A). For a case where modulators do not have direct effect on receptor efficacy, the model predicts 8 main types of combined effects (see Figure 1.14 and Allosteric Appendix for more detail).

Shaded in gray are the conditions outlined previously (in Figure 1.12) where $\beta = 1$ and accordingly the allosteric ligand imparts no cooperativity to efficacy and only to binding. Shaded in orange are the conditions there is no cooperativity with respect to <u>binding</u> ($\alpha = 1$) but there is positive ($\beta > 1$) and negative cooperativity ($\beta < 1$) with respect to <u>efficacy</u>. Consequently, the alteration in efficacy results in an increase potency and efficacy for $\beta > 1$ and decrease in potency and efficacy for $\beta < 1$.

Differential effects on affinity vs efficacy

Illustrated top left of Figure 1.14 are simulated conditions were α and β are both positive thus there are additive effects. Also illustrated top right and bottom left are simulations where these effects are opposite. (For instance, where the allosteric modulator has negative cooperativity for efficacy and positive cooperativity for binding and the

converse.) Interestingly, a CB_1 specific allosteric compound Org 27569 exhibits opposite effects (similar to top right, Figure 1.14).

1.6.5: Allosteric Modulators of CB_1

Other CB_1 allosteric ligands have also been described. The structures of these modulators are shown in Figure 1.15. Price and colleagues' original report described 3 allosteric compounds (Org 27569, Org 27759 and Org 29647) that enhanced agonist binding, decreased antagonist binding, and inhibited G protein dependent pathways [163]. More recently an SAR study has been performed creating two new high-affinity Org analogues (compounds 13 and 21 – see Figure 1.15) [164]. Interestingly, this study finds that carboxamide at the position 2 of the indole is essential for allosteric enhancement of CP 55940 binding. Upon replacement of the carboxamide with an ester resulted in an ~15-20% inhibition of CP 55940 binding.

Another compound PSNCBAM-1that was synthesized behaves in a similar manner to the Org series described by Price and others. While it did not appear to cause any G protein dependent effects on its own in yeast cells expressing CB_1, it did, however, produce an inverse effect on [^{35}S]GTPγS binding in unstimulated HEK293 cells expressing CB_1 [165]. Furthermore, PSNCBAM-1 also blocked the effects of agonists and even antagonist in electrophysiological studies [166].

The dopamine transporter inhibitor, RTI-371, has been suggested to act as an allosteric

CB_1 modulator, though, the binding data is lacking and warrants further investigation [167]. Other allosteric modulators that inhibit CB_1 agonist binding have also been identified [168], and the identification of allosteric compounds that enhance CB_1 agonist potency and decreased agonist dissociation have also been reported (AZ-4) [169, 170].

The site of binding for these allosteric ligands is currently unknown. Given their cooperative nature, an interesting point of consideration is whether or not allosteric ligands can bind in different poses in the presence or absence of an orthosteric ligand. Another point of contemplation is that mutational analysis can also reveal 'hits' that are not directly related to binding of an allosteric ligand, but instead are related to the vectoral transfer of information to the orthosteric site (conformational chage). While fascinating, differentiating between potential allosteric poses and/or networks of residues that couple the two sites (orthosteric and allosteric) can complicate data interpretation — I propose the term of allosteric entanglement to encompass these concepts.

One exciting methodology for identifying allosteric ligand binding sites has recently been demonstrated by the Sakmar laboratory. Their approach involves cross-linking a probe to the allosteric binding site by utilizing receptor mutants containing photoactivatable unnatural amino acids [171, 172].

Recent computational studies on the mAChR M3 suggest an orthosteric ligand (with slower dissociation rates toward M3) can bind to an allosteric site [113]. The Org compounds described by Price et al. have been shown to slow the dissociation of CP 55940 from the orthosteric binding site [163]. It is tempting to speculate that Org 27569

may work in a similar manner. However, given the lipophilic nature of cannabinoid ligands this site would presumably be in the egress pathway that connects the orthosteric binding site to the membrane. Interestingly, the lipid binding GPCR S1P1 structure hints at a lipid access channel between TM1 and TM7 [173]. A similar channel may exist in the CB_1 receptor, and may represent an area where allosteric CB_1 ligands bind or allosterically close.

1.6.6: A brief overview of biased signaling (or functional selectivity)

Some ligands can stabilize (or induce) receptor states that are selective for only some of the receptor's spectrum of behaviors. This phenomena (termed biased signaling – also referred to as functional selectivity among other names) has been observed in a number of GPCR systems [174] and represents further ways to design/screen drugs that selectively engage therapeutically relevant pathways while avoiding pathways that lead to undesirable side effects.

The aforementioned model (shown in Figure 1.14) can be utilized to describe a biased signaling model (reviewed in more detail in the Allosteric Appendix). Notably, all of these thermodynamic linkage models describe phenomena where each interacting molecule (with its own set of unique thermodynamic parameters) is capable of capturing a distinct conformation. Thus, they all predict multiple (and theoretically infinite) receptor active states.

Here I will briefly discuss some select aspects of biased signaling that have been observed primarily in the CB_1 system (for cannabinoid specific reviews on this topic please see [170] and [175]). For example, the endogenous cannabinoid 2AG has been shown to act as full agonist in inducing an increase in intracellular free calcium (by a $G\alpha_i/G\alpha_o$ mechanism) in cells of neuronal lineage containing CB_1 [69]. In contrast, WIN55212-2, CP 55940, and HU210 were less efficacious (partial agonists) despite being established as full CB_1 receptor agonists in [^{35}S]-GTPγS binding assays [176].

Another example of functional efficacy includes measuring the ability of different ligands to interact with various $G\alpha_i$ and $G\alpha_o$ G proteins and subtypes. Glass and Northup previously monitored agonist stimulated GTPγS binding for recombinantly expressed CB_1 receptors and purified G proteins from native sources ($G\alpha_i$ subtypes 1,2&3 and $G\alpha_o$) and found HU210 to be a potent full agonist for both $G\alpha_i$ and $G\alpha_o$ [177]. In contrast, WIN55212-2 and AEA were less potent but still full agonists for $G\alpha_i$ yet only partial agonist for $G\alpha_o$. Subsequent co-immunoprecipitation studies further demonstrated variations in interactions for WIN55212-2, mAEA, and desacetyllevonantradol (DALN – a THC like compound) stimulated CB_1 receptors with different G protein subtypes (i.e., $G\alpha_{i1}$, $G\alpha_{i2}$, $G\alpha_{i3}$, $G\alpha_{o1}$, $G\alpha_{o2}$) [178, 179]. These results show there are clearly some subtype selectivity of CB_1 orthosteric ligands toward different G protein subtypes, and these have the potential to culminate in ligand selective mediation of potentially different G protein signaling pathways.

Other examples of functional selectivity by allosteric ligands have been documented. For

instance, the chemoattractant receptor expressed on TH2 cells (CRTH2 receptor) binds prostaglandins D2 (PGD2). A small indole derivative allosterically enhances PGD2 binding, yet has no effect on G protein dependent signaling (in the presence or absence of PGD2). In contrast, the same allosteric compound on its own inhibits interaction of the receptor with arrestin [180]. The ability of an allosteric modulator to alter receptor behavior, independent of exogenous ligands, brings to light that allosteric ligands can sometimes also possess (intrinsic) efficacy by themselves.

Interestingly, recent literature suggests that Org 27569 may act as a functionally selective ligand. The evidence suggests that on its own, Org 27569 can enhance G protein independent pathways, including ERK phosphorylation and receptor internalization (most likely β-arrestin mediated) [181]. Thus, Org 27569 appears to be an allosteric ligand that also possesses intrinsic efficacy. The term ago-allosterism (coined by Schwartz et al. [182]) is also used to describe this behavior (i.e., were there exists agonist properties in the absence of a bound orthosteric ligand) and this concept is reviewed further in the Allosteric Appendix.

Ago-allosteric modulators can contain overlapping binding sites with orthosteric ligands [183], and this may indeed be the case for Org 27569 (Reggio personal communication). How can one reconcile this possibility given the fact that these ligands are allosteric and by definition bind at a topographically distinct site? Schwarts has proposed three different explanations for this discrepancy: 1) ago-allosteric ligands can have multiple binding poses, 2) receptor dimers – where an allosteric ligands may impart their ‘action

at a distance' by binding to one protomer altering the other orthostericly bound protomer, and 3) bias efficacy and potency can occur by modulating the dynamic transitions between inactive and active receptor conformations [182].

In Chapter 3, I explore the mechanism of Org 27569's allosteric effects on CB_1 in more detail using purified CB_1 receptor and a site-directed labeling approach. While our data does not rule out the first two possibilities listed above, they do suggest the third as a major player in the actions of Org 27569. Based on our findings we propose that Org 27569 may trap the receptor in an intermediate conformation on the pathway to an activated receptor (Chapter 3). Indeed, recent work by Kendall's laboratory that was published while our work was under review suggests that a constitutively active mutant does not appear to be altered by Org 27569 [181]. This observation is consistent with our hypothesis – as one would expect, reducing the energy barrier towards an activated receptor species (by making a constitutively active receptor – with respect to G protein dependent pathways) would be commensurate with diminished actions of Org 27569 modulation.

1.7: Dissertation overview

The goal of this chapter was to give a brief but informative introduction to GPCRs and the CB_1 system, and to describe some aspects of allosterism in the broad context of GPCR signaling. Further information can be found in the appendix chapter relating to allosteric models. In the following chapters, I will address purification of CB_1 (Chapter

2) then proceed to site-directed labeling experiments to address allosteric mediated conformational changes in CB_1 (Chapter 3), followed by our discovery for an allosteric role of the CB_1 N-terminus (Chapter 4), then a discussion of novel CB_1 specific allosteric antibodies (Chapter 5), and finally a conclusion and summary chapter.

Classification	Ligand	CB_1 Ki values (nM)	Log $P_{o/w}$
Classical	(-)-Δ^9-THC	5.05 - 80.3	6.47 ± 1.02
	HU210	0.06 - 0.73	6.73 ± 1.20
Non-classical	CP 55940	0.5 - 5.0	6.14 ± 1.05
Aminoalkylindole	WIN55212-2	1.89 - 123	4.25 ± 0.58
Endocannabinoids	Anandamide	61 - 543	5.59 ± 0.79
(***Eicosanoids)***	2-Arachidonylglycerol	58.3 - 472	5.56 ± 0.91
Antagonist/Inverse Agonist	SR141716A	2 - 12	5.58 ± 0.81

Table 1.1: Pharmacological properties of cannabinoid receptor agonists. Shown are their respective K_i values (for the *in vitro* displacement of [^{3}H]CP 55940) and octonal water partition coefficients ($P_{o/w}$). The $P_{o/w}$ values were calculated using ALOGPS 2.1 (http://www.vcclab.org/lab/alogps/start.html) [184]. K_i values ranges were retrieved from Dr. Pertwee's review (http://www.tocris.com/scientificReviews.php).

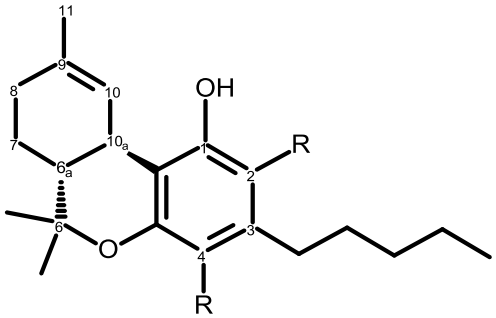

Delta-9-tetrahydrocannabinol

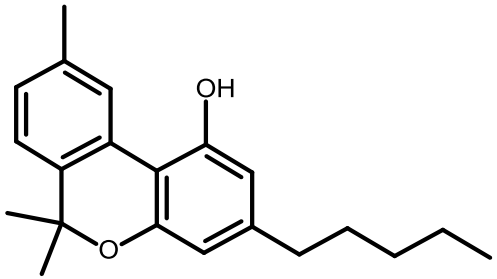

Cannabinol

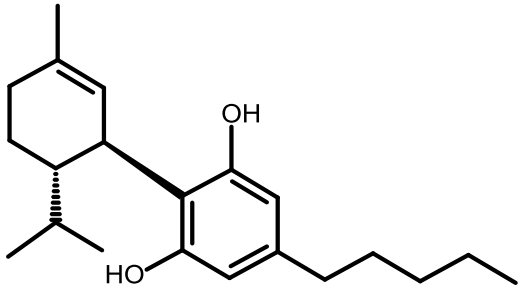

Cannabidiol

Figure 1.1: Chemical structures of cannabinoid ligands found in marijuana. (left) Δ^9-THC with dibenzyopyran numbering system, where R is an indication of 2 and/or 4 position carboxyl groups, (middle) cannabinol (CBN), and (right) cannabidiol (CBD).

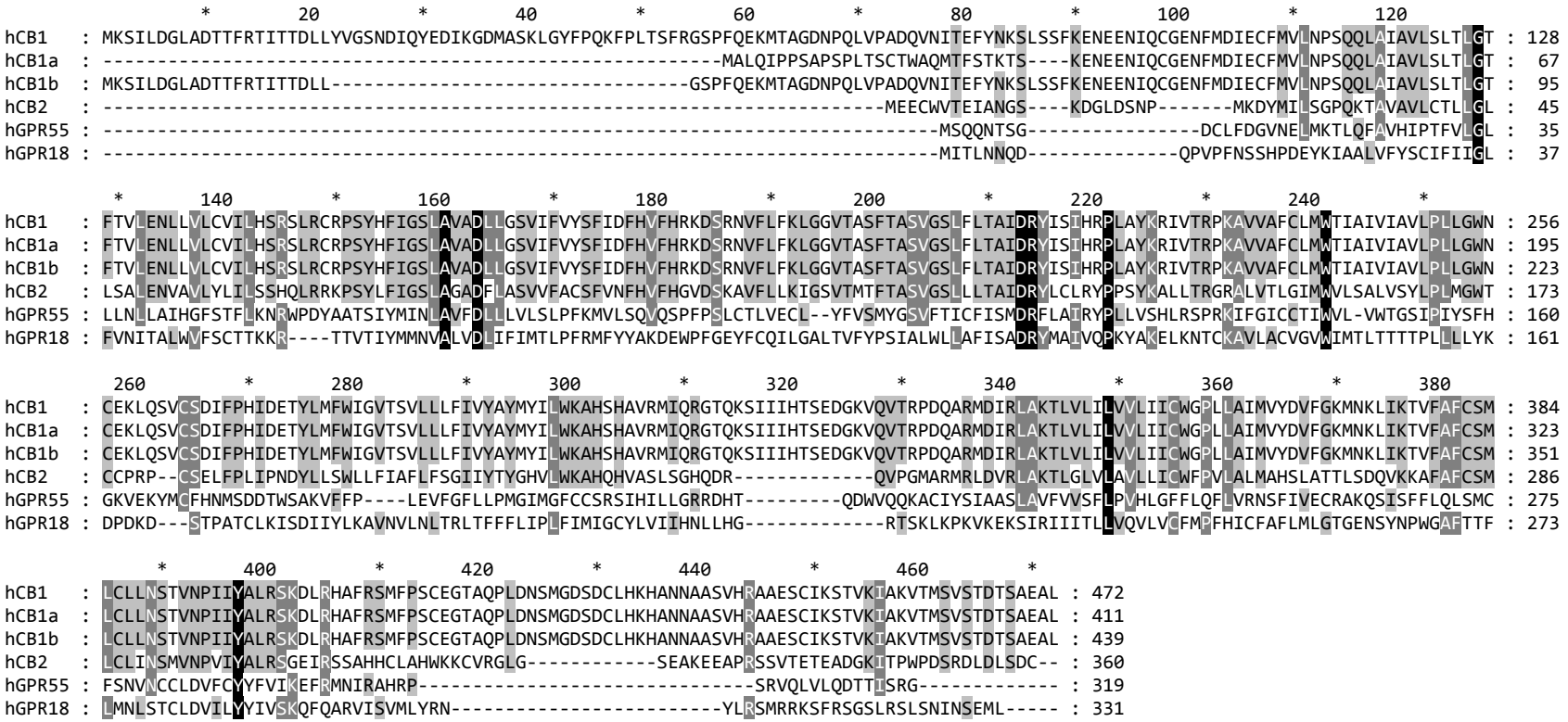
hCB1 : MKSILDGLADTTFRTITTDLLYVGSNDIQYEDIKGDMASKLGYFPQKFPLTSFRGSPFQEKMTAGDNPQLVPADQVNITEFYNKSLSSFKENEENIQCGENFMDIECFMVLNPSQQLAIAVLSLTLGT : 128
hCB1a : ----------MALQIPPSAPSPLTSCTWAQMTFSTKTS----KENEENIQCGENFMDIECFMVLNPSQQLAIAVLSLTLGT : 67
hCB1b : MKSILDGLADTTFRTITTDLL----------GSPFQEKMTAGDNPQLVPADQVNITEFYNKSLSSFKENEENIQCGENFMDIECFMVLNPSQQLAIAVLSLTLGT : 95
hCB2 : ----------MEECWVTEIANGS----KDGLDSNP-------MKDYMILSGPQKTAVAVLCTLLGL : 45
hGPR55 : ----------MSQQNTSG----------DCLFDGVNELMKTLQFAVHIPTFVLGL : 35
hGPR18 : ----------MITLNNQD----------QPVPFNSSHPDEYKIAALVFYSCIFIIGL : 37
hCB1 : FTVLENLLVLCVILHSRSLRCRPSYHFIGSLAVADLLGSVIFVYSFIDFHVFHRKDSRNVFLFKLGGVTASFTASVGSLFLTAIDRYISIHRPLAYKRIVTRPKAVVAFCLMWTIAIVIAVLPLLGWN : 256
hCB1a : FTVLENLLVLCVILHSRSLRCRPSYHFIGSLAVADLLGSVIFVYSFIDFHVFHRKDSRNVFLFKLGGVTASFTASVGSLFLTAIDRYISIHRPLAYKRIVTRPKAVVAFCLMWTIAIVIAVLPLLGWN : 195
hCB1b : FTVLENLLVLCVILHSRSLRCRPSYHFIGSLAVADLLGSVIFVYSFIDFHVFHRKDSRNVFLFKLGGVTASFTASVGSLFLTAIDRYISIHRPLAYKRIVTRPKAVVAFCLMWTIAIVIAVLPLLGWN : 223
hCB2 : LSALENVAVLYLILSSHQLRRKPSYLFIGSLAGADFLASVVFACSFVNFHVFHGVDSKAVFLLKIGSVTMTFTASVGSLLLTAIDRYLCLRYPPSYKALLTRGRALVTLGIMWVLSALVSYLPLMGWT : 173
hGPR55 : LLNLLAIHGFSTFLKNRWPDYAATSIYMINLAVFDLLLVLSLPFKMVLSQVQSPFPSLCTLVECL--YFVSMYGSVFTICFISMDRFLAIRYPLLVSHLRSPRKIFGICCTIWVL-VWTGSIPIYSFH : 160
hGPR18 : FVNITALWVFSCTTKKR----TTVTIYMMNVALVDLIFIMTLPFRMFYYAKDEWPFGEYFCQILGALTVFYPSIALWLLAFISADRYMAIVQPKYAKELKNTCKAVLACVGVWIMTLTTTTPLLLYK : 161
hCB1 : CEKLQSVCSDIFPHIDETYLMFWIGVTSVLLLFIVYAYMYILWKAHSHAVRMIQRGTQKSIIIHTSEDGKVQVTRPDQARMDIRLAKTLVLILVVLIICWGPLLAIMVYDVFGKMNKLIKTVFAFCSM : 384
hCB1a : CEKLQSVCSDIFPHIDETYLMFWIGVTSVLLLFIVYAYMYILWKAHSHAVRMIQRGTQKSIIIHTSEDGKVQVTRPDQARMDIRLAKTLVLILVVLIICWGPLLAIMVYDVFGKMNKLIKTVFAFCSM : 323
hCB1b : CEKLQSVCSDIFPHIDETYLMFWIGVTSVLLLFIVYAYMYILWKAHSHAVRMIQRGTQKSIIIHTSEDGKVQVTRPDQARMDIRLAKTLVLILVVLIICWGPLLAIMVYDVFGKMNKLIKTVFAFCSM : 351
hCB2 : CCPRP--CSELFPLIPNDYLLSWLLFIAFLFSGIIYTYGHVLWKAHQHVASLSGHQDR----------QVPGMARMRLDVRLAKTLGLVLAVLLICWFPVLALMAHSLATTLSDQVKKAFAFCSM : 286
hGPR55 : GKVEKYMCFHNMSDDTWSAKVFFP----LEVFGFLLPMGIMGFCCSRSIHILLGRRDHT---------QDWVQQKACIYSIAASLAVFVVSFLPVHLGFFLQFLVRNSFIVECRAKQSISFFLQLSMC : 275
hGPR18 : DPDKD---STPATCLKISDIIYLKAVNVLNLTRLTFFFLIPLFIMIGCYLVIIHNLLHG----------RTSKLKPKVKEKSIRIIITLLVQVLVCFMPFHICFAFLMLGTGENSYNPWGAFTTF : 273
hCB1 : LCLLNSTVNPIIYALRSKDLRHAFRSMFPSCEGTAQPLDNSMGDSDCLHKHANNAASVHRAAESCIKSTVKIAKVTMSVSTDTSAEAL : 472
hCB1a : LCLLNSTVNPIIYALRSKDLRHAFRSMFPSCEGTAQPLDNSMGDSDCLHKHANNAASVHRAAESCIKSTVKIAKVTMSVSTDTSAEAL : 411
hCB1b : LCLLNSTVNPIIYALRSKDLRHAFRSMFPSCEGTAQPLDNSMGDSDCLHKHANNAASVHRAAESCIKSTVKIAKVTMSVSTDTSAEAL : 439
hCB2 : LCLINSMVNPVIYALRSGEIRSSAHHCLAHWKKCVRGLG----------SEAKEEAPRSSVTETEADGKITPWPDSRDLDLSDC-- : 360
hGPR55 : FSNVNCCLDVFCYYFVIKEFRMNIRAHRP----------SRVQLVLQDTTISRG---------- : 319
hGPR18 : LMNLSTCLDVILYYIVSKQFQARVISVMLYRN----------YLRSMRRKSFRSGSLRSLSNINSEML----- : 331

Figure 1.2. Alignment comparison of known and suspected human cannabinoid GPCRs. ClustalW multiple sequence alignment of human (h) CB_1, CB_1a, CB_1b, CB_2, GPR55 and GPR18. Shading is based on the following parameters: 100% sequence identity black box white letters, ≥80% dark gray box, ≥60% light gray box and <60% is not shaded with black letters. Amino acid sequence identity with respect to CB_1 is 93.9% for CB_1a, 99.8% for CB_1b, 42.5% for CB_2, 14.7% for GPR55, and 19.3% for GPR18. Sequence identity was determined using UCSF Chimera multi-sequence alignment view and percent amino acid identity with respect to shorter sequence length.

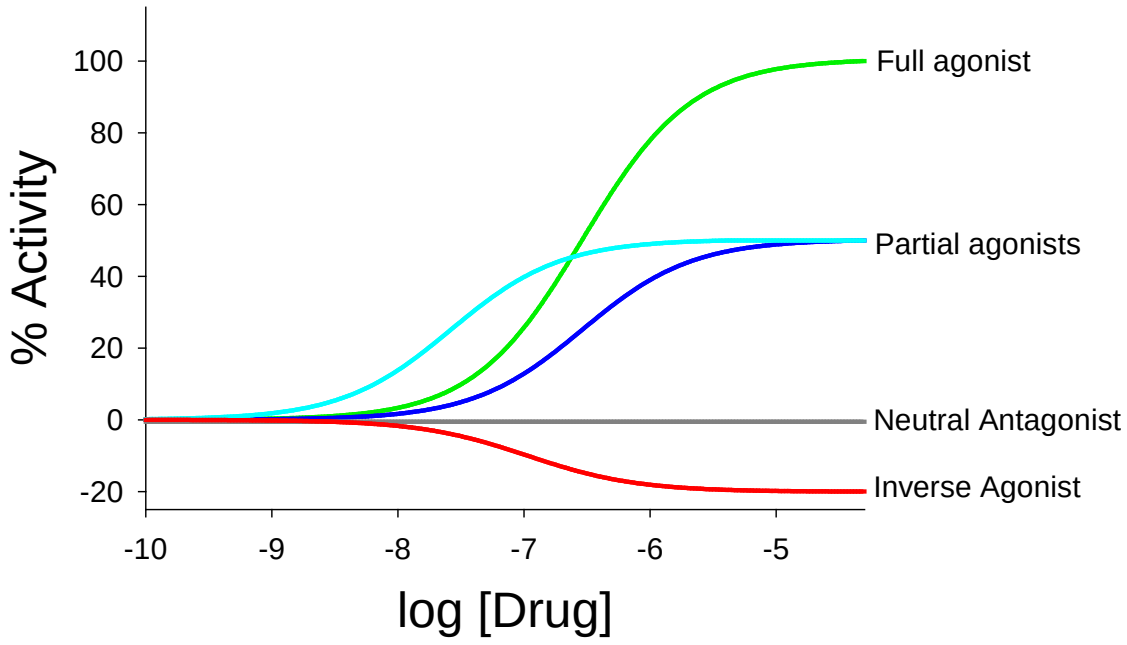
100
80
60
40
20
0
-20
% Activity
-10
-9
-8
-7
-6
-5
log [Drug]
Full agonist
Partial agonists
Neutral Antagonist
Inverse Agonist

Figure 1.3. Cartoon illustration depicting how different ligands/drugs effect response (Y axis). Definitions related to the illustration: **Full Agonist**: a compound that is able to elicit a maximal response following receptor occupation and activation (in green). **Partial Agonists:** compounds that activate receptors but do not elicit the maximal response of the receptor system. Shown above are two partial agonists, one that is equipotent to the full agonist (in blue) and the other which shows a higher degree of potency (in cyan). **Neutral Antagonist:** a compound that binds to the same receptor binding site as an agonist but has no efficacy (in gray). **Inverse agonist**: a molecule that binds to the same receptor binding site as an agonist for that receptor and reverses constitutive activity of receptors. The opposite pharmacological effect of a receptor agonist is imparted by an inverse agonist (in red).

Agonists

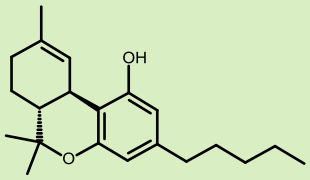

Δ^9-THC

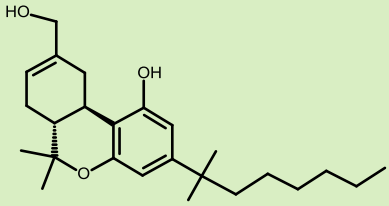

HU210

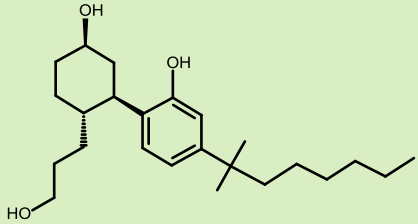

CP 55940

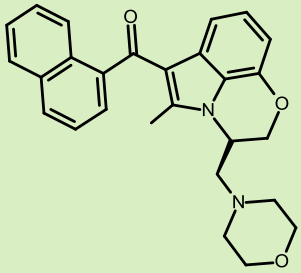

WIN55212-2

Antagonist

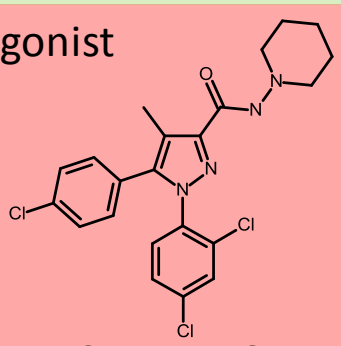

SR141716A

Endocannabinoids

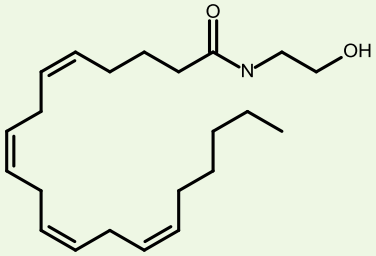

Anandamide

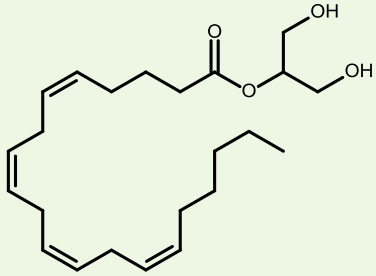

2-Arachidonoylglycerol

Figure 1.4. Structures of commonly used cannabinoid ligands: (top, "classical" cannabinoids) Δ^9THC, HU210, CP 55940, (middle, left) non-classical agonist the amino akyl indole WIN55212-2 (agonist in green shade). (Middle, right) The antagonist (inverse agonist) SR141716A (red shade). (Bottom) The two most prominent endocannabinoids (endogenous cannabinoids — lighter green shade) anandamide (N-arhiconoylethanolamine, AEA), and 2-arachidonoylglycerol (2-AG).

A)

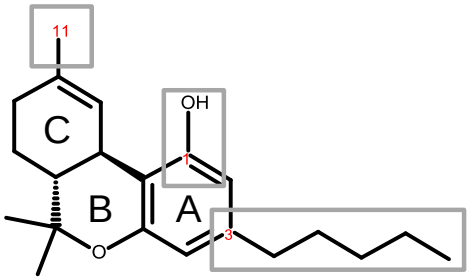

B)

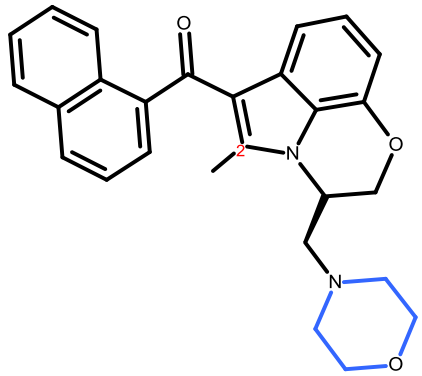

C)

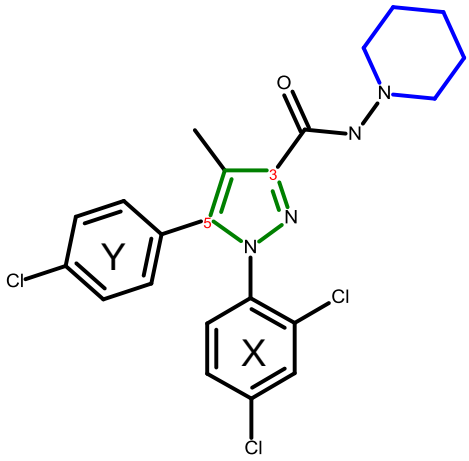

Figure 1.5. Pharmacore models for: A) classical cannabinoids, B) aminoalkyl indoles and C) general inverse agonist pharmacophore. In A), the "three tiers" proposed for the action of THC are: (1) the phenolic hydroxyl at C1, (2) the hydrophobic pentyl side chain at C3, and (3) the C11 position. In B) alignment of napthol with B and C rings and morpholinyl (cyan) with the acyl chain, the 2 position of the idole ring is labeled in red. In C) pyrazole (green) with the 1-position dichlophenyl group labeled X and the 5-position monochlorophenyl group labeled Y. The piperidine ring (blue) is attached to the 3-position via a carboxamide group.

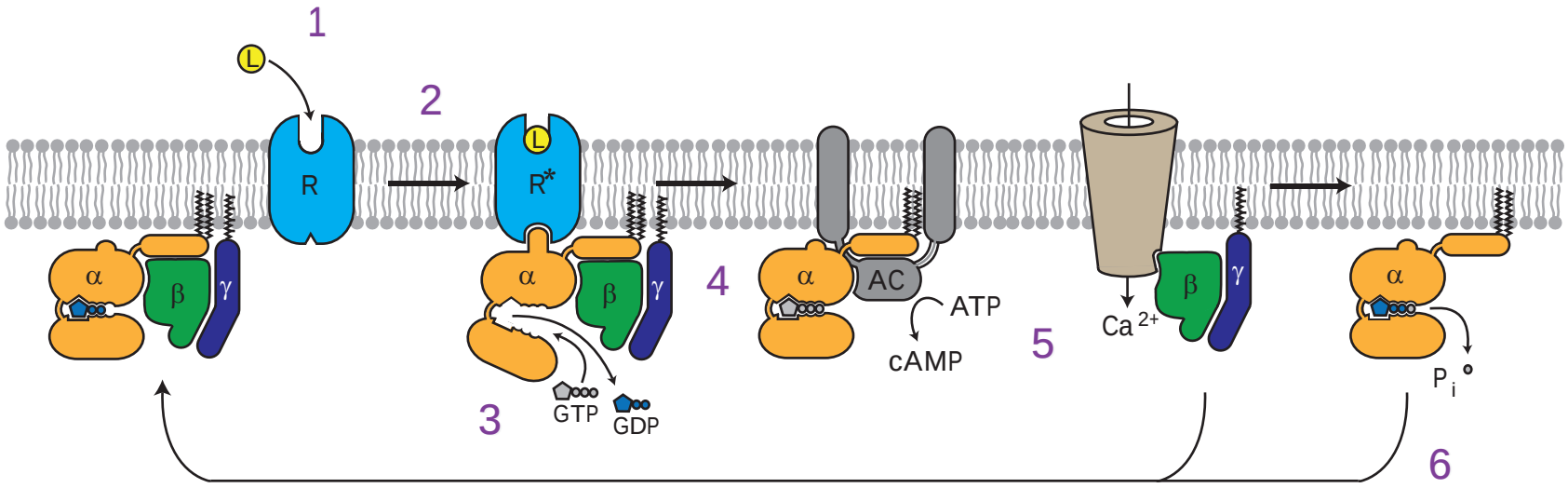

Reassembly of heterotrimeric G protein

Figure 1.6. Cartoon depicting the classical heterotrimeric G protein activation cycle initiated by receptors. **1)** L, agonist ligand binds to the receptor (R) producing an active state (R*). **2)** The activated form of the receptor interacts with its cognate G protein (consisting of an α, β, and γ subunits) that triggers a conformational change in the G protein. **3)** This results in GDP release and subsequent GTP binding. **4)** The activated G protein subunits α and βγ dissociate from the receptor, and then **5)** activate or inhibit effector proteins such as adenylate cyclase and calcium channels (denoted as AC and the calcium channel). **6)** The intrinsic GTPase activity of the α subunit hydrolyzes bound GTP back to GDP and becomes inactive, recombining with βγ subunits to form an inactive G protein that can re-associate with a receptor to repeat the cycle. Figure was adapted from Rasmussen et al. 2011 [152].

A)

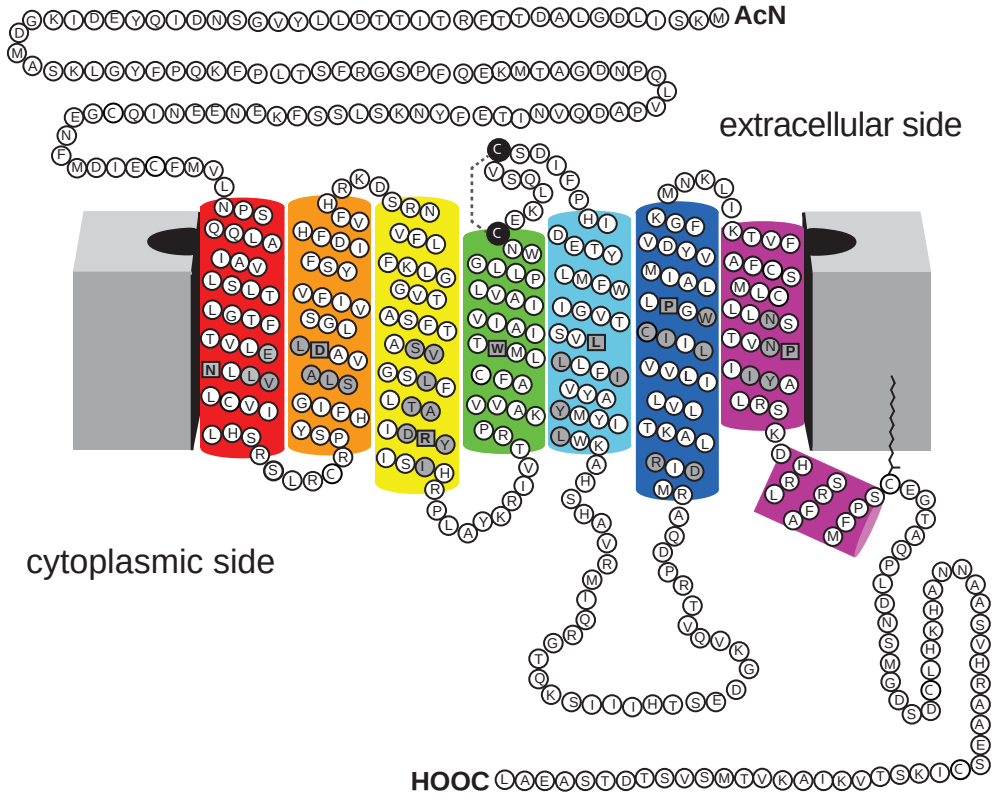

B)

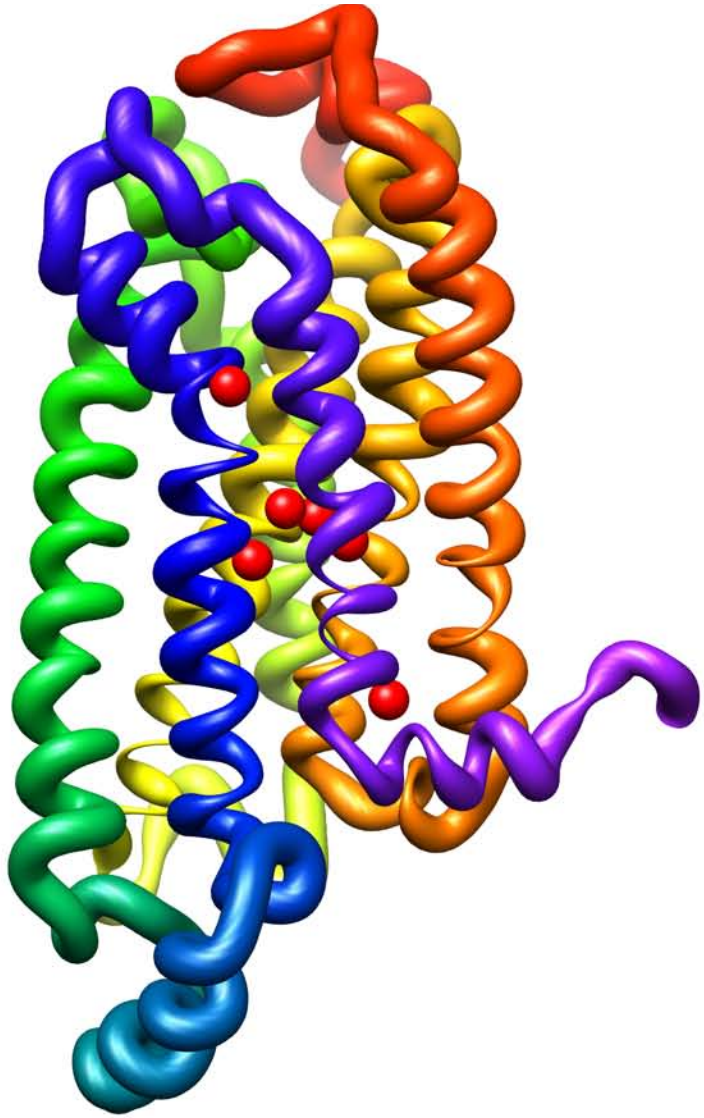

Figure 1.7 Architecture and conserved regions in GPCRs. A) 2D cartoon (snake plot) of CB_1. Highly conserved residues in GPCRs, N134 (1.50), D163 (2.50), R214 (3.50), W241 (4.50), L286 (5.50), P358 (6.50), and P394 (7.50), are depicted with boxes and bold letters. Conserved GPCR residues (shown in panel B) are highlighted in gray. **B)** 3D homology model of CB_1. Model was generated using S1P1 (2V2Y) as a template. 200 GPCRs from http://bioinfolab.unl.edu /emlab/gpcr/ was used to create a multiple sequencing alignment (clustalW) and rendered on the surface of the homology model using chimera. Conserved residues (>60% sequence identity) are mapped to the worm plot as thin 'wires,' in contrast, more divergent residues are represented as bigger diameter tubes. Notably, structural waters (red spheres) from rhodopsin (1GZM) appear to cluster around these conserved regions.

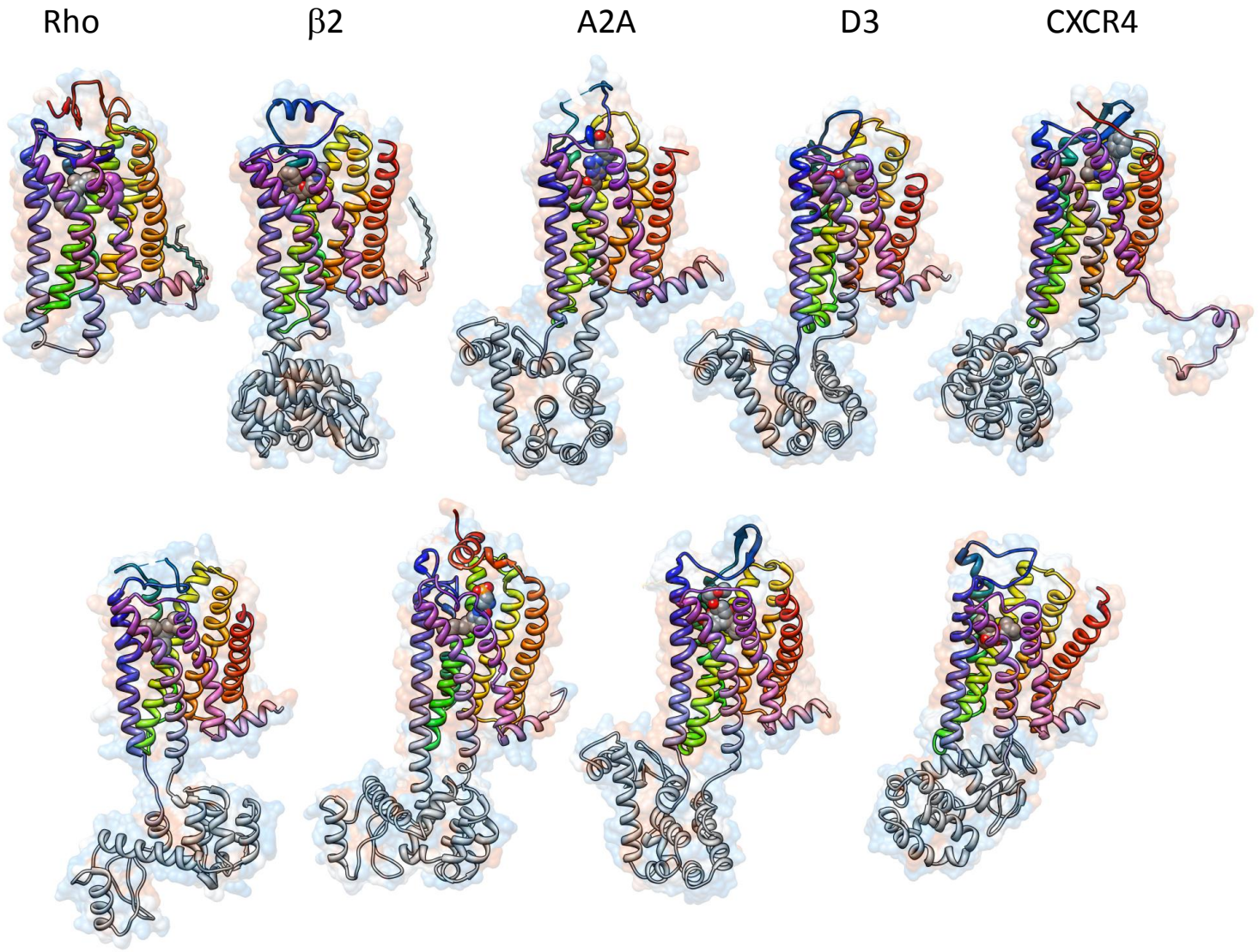
Rho
β2
A2A
D3
CXCR4
H1
S1P1
μ-OR
M2

Figure 1.8 Comparison of crystallographic models for nine different antagonist bound GPCRs. Rhodopsin (1GZM), β2- Adrenergic (2RH1), Adenosine (3EML), D3 Dopamine (3PBL), CXCR4 chemokine (3ODU), H1 Histamine (3RZE), S1P1 (3V2Y), μ-Opioid (4DKL), M2 Muscarinic (3UON). Ribbons are colored in rainbow from N-terminus to C-terminus (red, orange, yellow, green, blue, gray (T4L/Il3), purple and pink). The shadow in each figure is a surface plot, with hydrophobic residues in orange and hydrophilic in light blue.

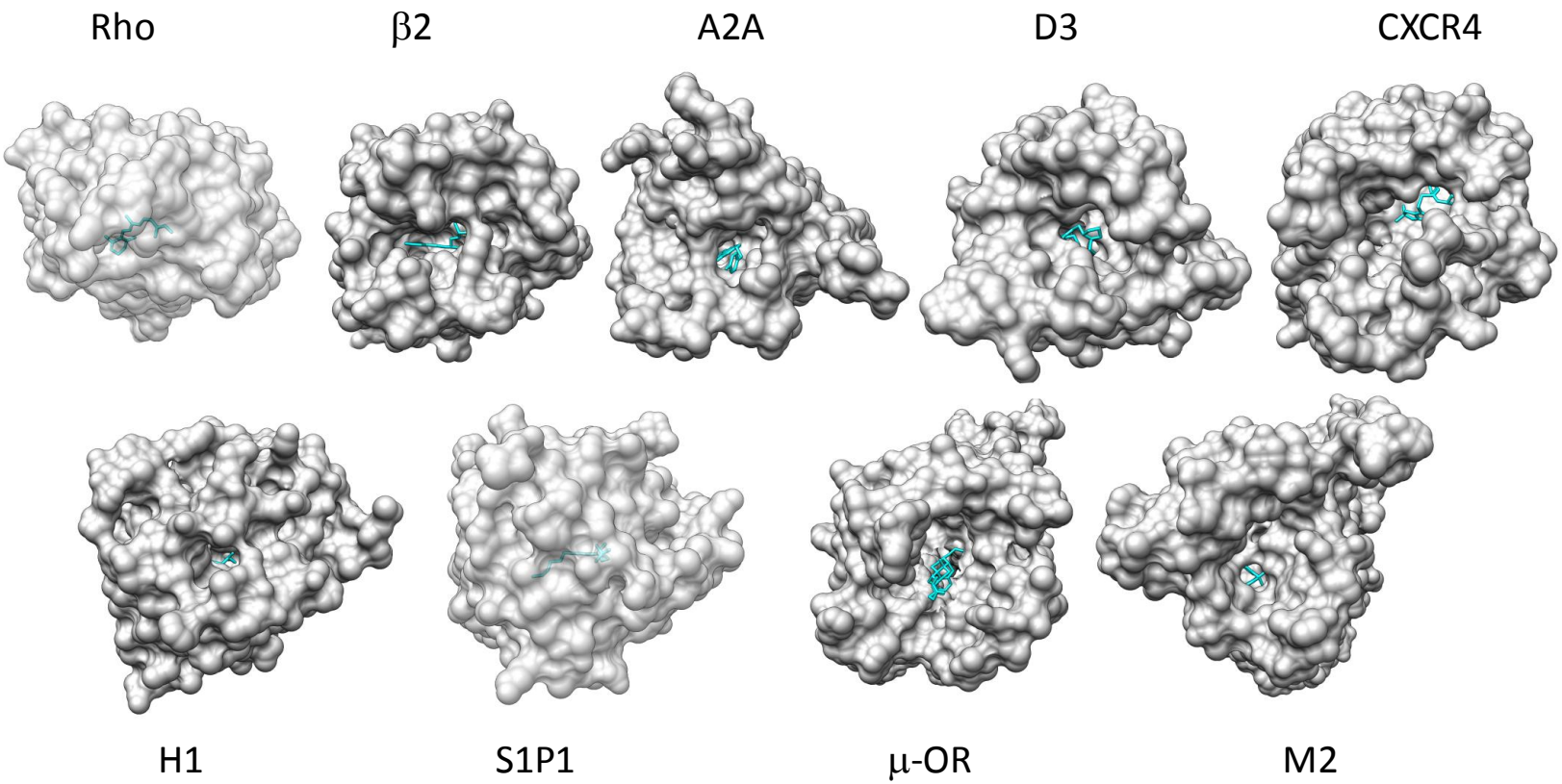
Rho
β2
A2A
D3
CXCR4
H1
S1P1
μ-OR
M2

Figure 1.9 Extracellular view comparing the ligand binding pocket for different antagonist bound GPCR crystallographic models. Surface map is shown in gray and the cognate ligand is depicted in cyan. All three dimensional images appear to have a highly solvent exposed ligand binding pocket, except the lipid binding receptors Rhodopsin and Sphingolipid S1P1, which are shown with semi-transparent surface maps so that the ligand can be seen. Notably, S1P1 does appear to have solvent/membrane access which from this vantage point is obscured. PDB models used for generation of this figure are as follows: Rhodopsin (1GZM), β2- Adrenergic (2RH1), Adenosine (3EML), D3 Dopamine (3PBL), CXCR4 chemokine (3ODU), H1 Histamine (3RZE), S1P1 (3V2Y), μ-Opioid (4DKL), and M2 Muscarinic (3UON). All images were rendered in UCSF Chimera.

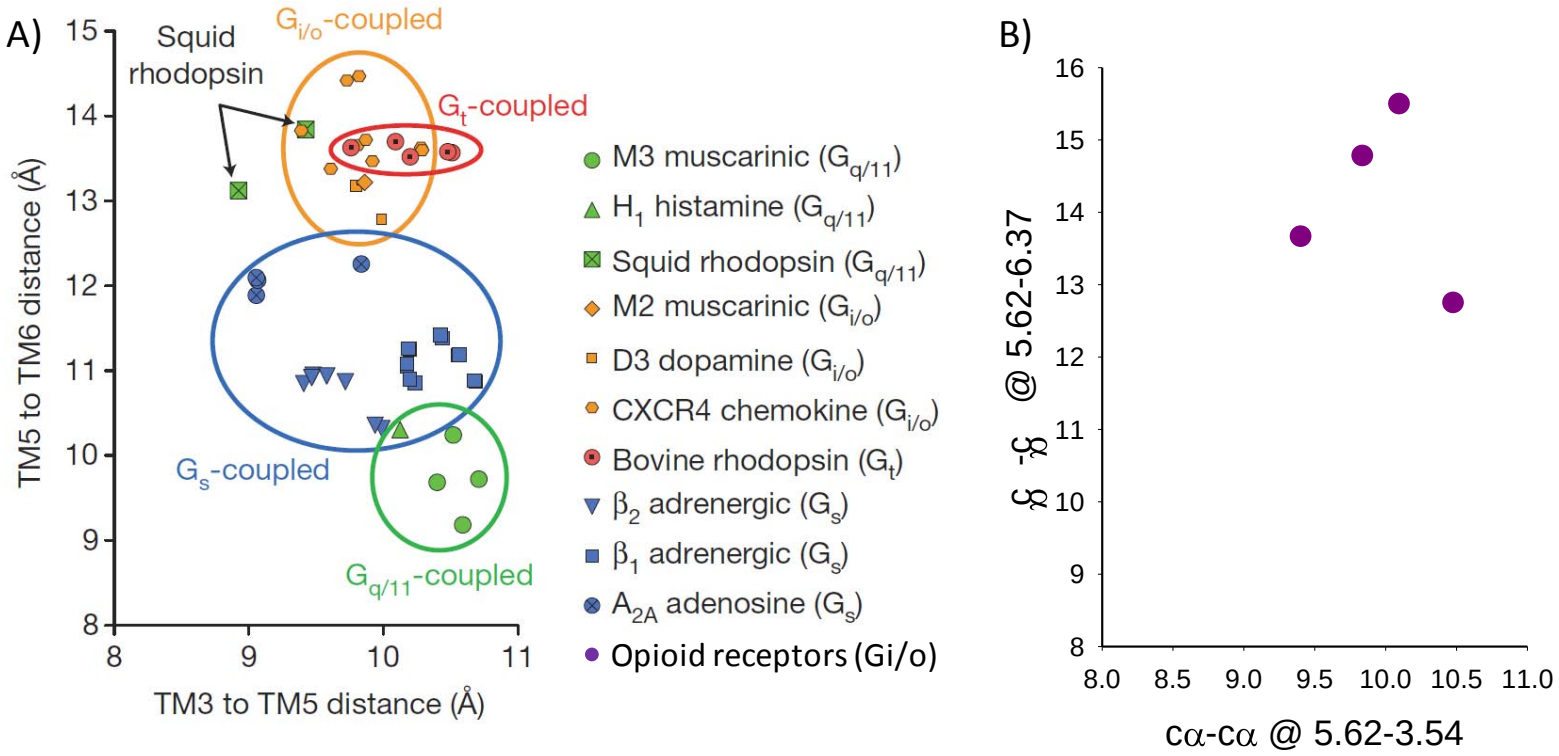
A)
Squid rhodopsin
$G_{i/o}$-coupled
G_t-coupled
G_s-coupled
$G_{q/11}$-coupled
TM5 to TM6 distance (Å)
TM3 to TM5 distance (Å)
M3 muscarinic ($G_{q/11}$)
H_1 histamine ($G_{q/11}$)
Squid rhodopsin ($G_{q/11}$)
M2 muscarinic ($G_{i/o}$)
D3 dopamine ($G_{i/o}$)
CXCR4 chemokine ($G_{i/o}$)
Bovine rhodopsin (G_t)
β_2 adrenergic (G_s)
β_1 adrenergic (G_s)
A_{2A} adenosine (G_s)
Opioid receptors (Gi/o)
B)
cα-cα @ 5.62-6.37
cα-cα @ 5.62-3.54

Figure 1.10. Determinants of G protein-coupling specificity. Where GPCRs cluster by G protein-coupling specificity. **A & B)** Plot of interhelical distances for antagonist bound GPCR structures published to date. Distances were measured between Cα atoms of TM5 residue 5.62 and TM6 residue 6.37 (y-axis) and TM5 residue 5.62 and TM3 residue 3.54 (x-axis). Figure from A is from Kruse et al. 2012 [113]. Figure B distances were calculated in UCSF Chimera at indicated positions using opioid receptor PDB codes, 4DKL, 4EJ4, 4DJH, and 4EA3.

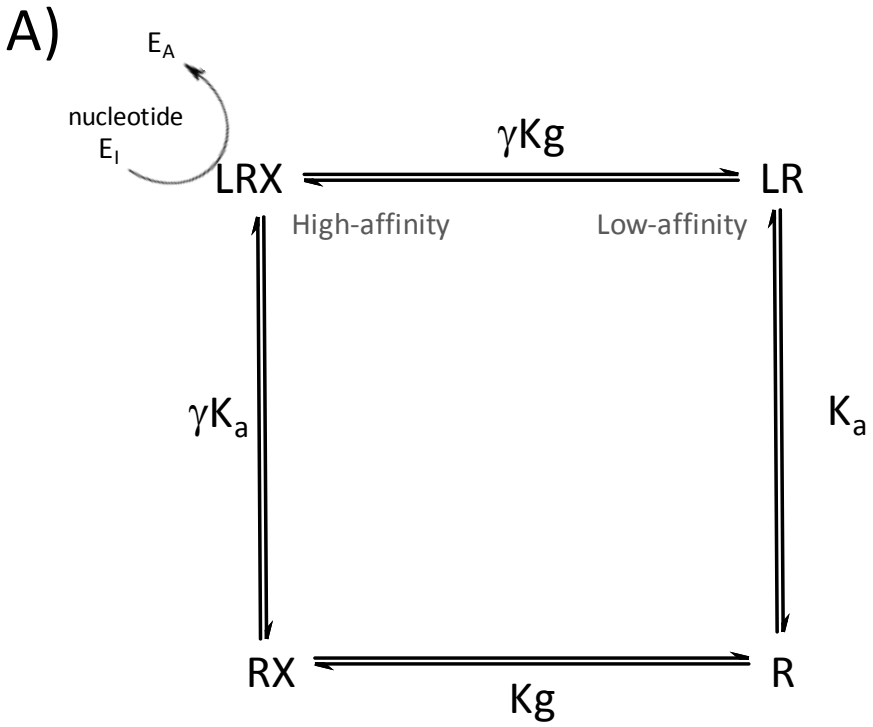
A)
E_A
nucleotide
E_I
LRX
γKg
LR
High-affinity
Low-affinity
γK_a
K_a
RX
Kg
R

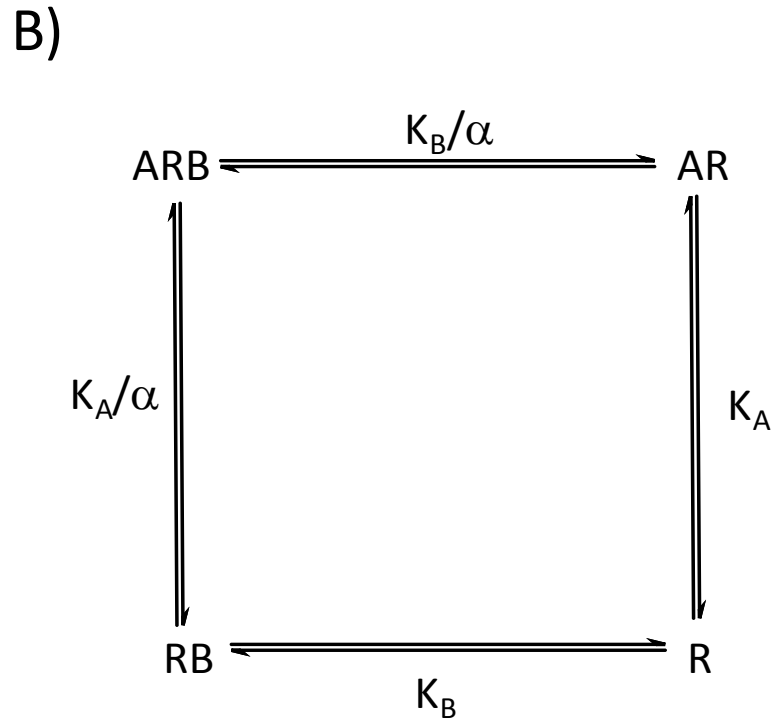
B)
ARB
K_B/α
AR
K_A/α
K_A
RB
K_B
R

Figure 1.11. Allosteric Ternary complex models. A) Classic G protein modulation of agonist affinity [150]. The model describes a receptor (R) that can couple to a G protein (X) in the absence or presence of orthosteric ligand (L). K_a is the equilibrium association constant for ligand binding and K_g is the association constant for G protein binding. This is modified to an extent that is dictated by the cooperativity factor γ. **B)** Allosteric ternary complex model [162], which describes a receptor (R) that can interact with orthosteric ligand (A) or allosteric ligand (B). K_A and K_B are the equilibrium dissociation constants for A and B respectively. The interaction of these two ligands to form a ternary complex is defined by the cooperativity factor α.

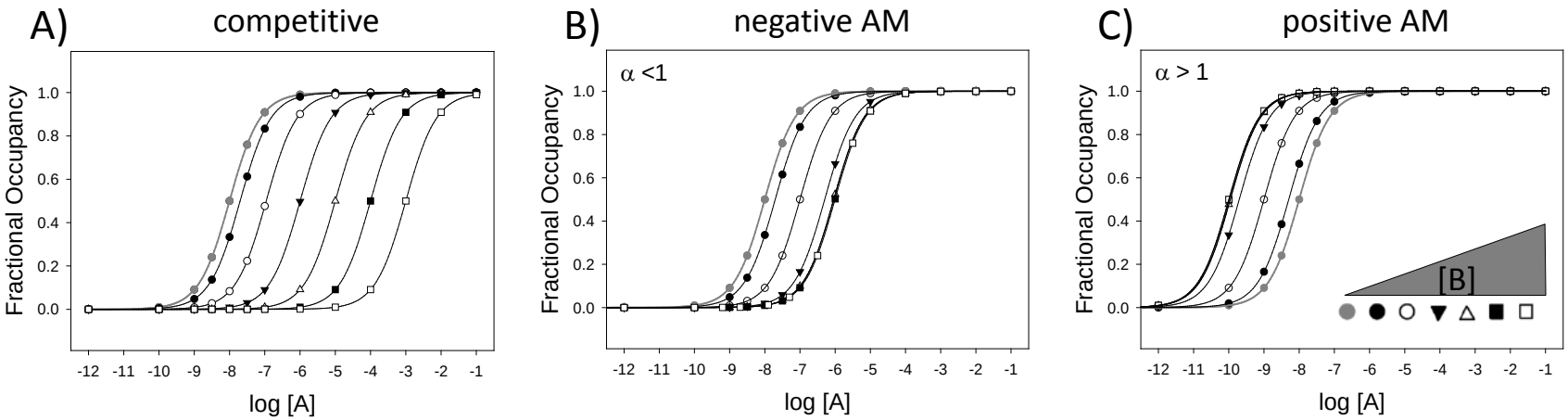
A)
competitive
Fractional Occupancy
1.0
0.8
0.6
0.4
0.2
0.0
-12 -11 -10 -9 -8 -7 -6 -5 -4 -3 -2 -1
log [A]
B)
negative AM
α <1
Fractional Occupancy
1.0
0.8
0.6
0.4
0.2
0.0
-12 -11 -10 -9 -8 -7 -6 -5 -4 -3 -2 -1
log [A]
C)
positive AM
α > 1
Fractional Occupancy
1.0
0.8
0.6
0.4
0.2
0.0
[B]
-12 -11 -10 -9 -8 -7 -6 -5 -4 -3 -2 -1
log [A]

Figure 1.12. Simulations demonstrating the different ligand binding profiles for **(A)** orthosteric competition and allosteric interaction for **(B)** a negative ($\alpha<1$) and **(C)** a positive allosteric modulator (AM) ($\alpha > 1$). Shown are the binding of A in the absence of B (gray circles) and in the presence of increasing concentrations of B (see inset legend). Competitive binding simulations show a limitless displacement of orthosteric ligand occupancy with increasing concentrations of a competitive orthosteric ligand B. In contrast, an allosteric modulator binds to a topographically distinct site from the orthosteric ligand and modifies the orthosteric ligand affinity to a limit defined by α, the cooperativity factor. A more detailed description of this simulation can be found in the Allosteric Appendix.

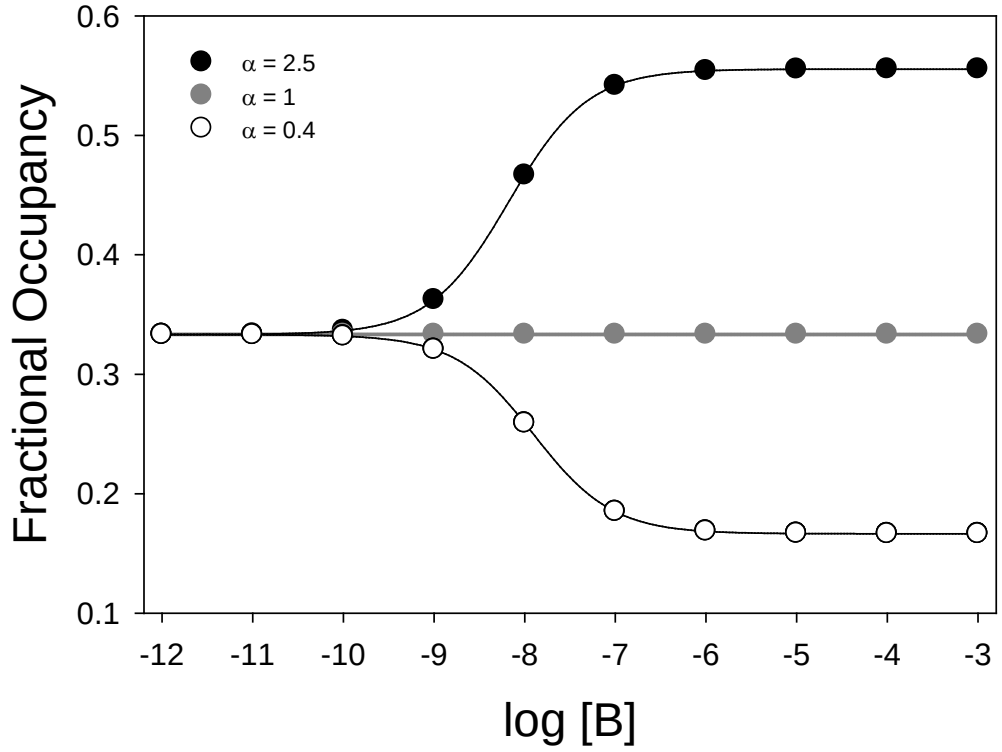
0.6
0.5
0.4
0.3
0.2
0.1
Fractional Occupancy
α = 2.5
α = 1
α = 0.4
-12
-11
-10
-9
-8
-7
-6
-5
-4
-3
log [B]

Figure 1.13. Simulation of the binding of a fixed concentration of orthosteric ligand, A, is altered as a function of allosteric modulator, B. When $\alpha > 1$, there is an increase in orthosteric ligand binding, and when $\alpha < 1$, there is a decrease. When alpha = 1, there is no effect and hence no change. A more detailed description of this simulation can be found in the Allosteric Appendix.

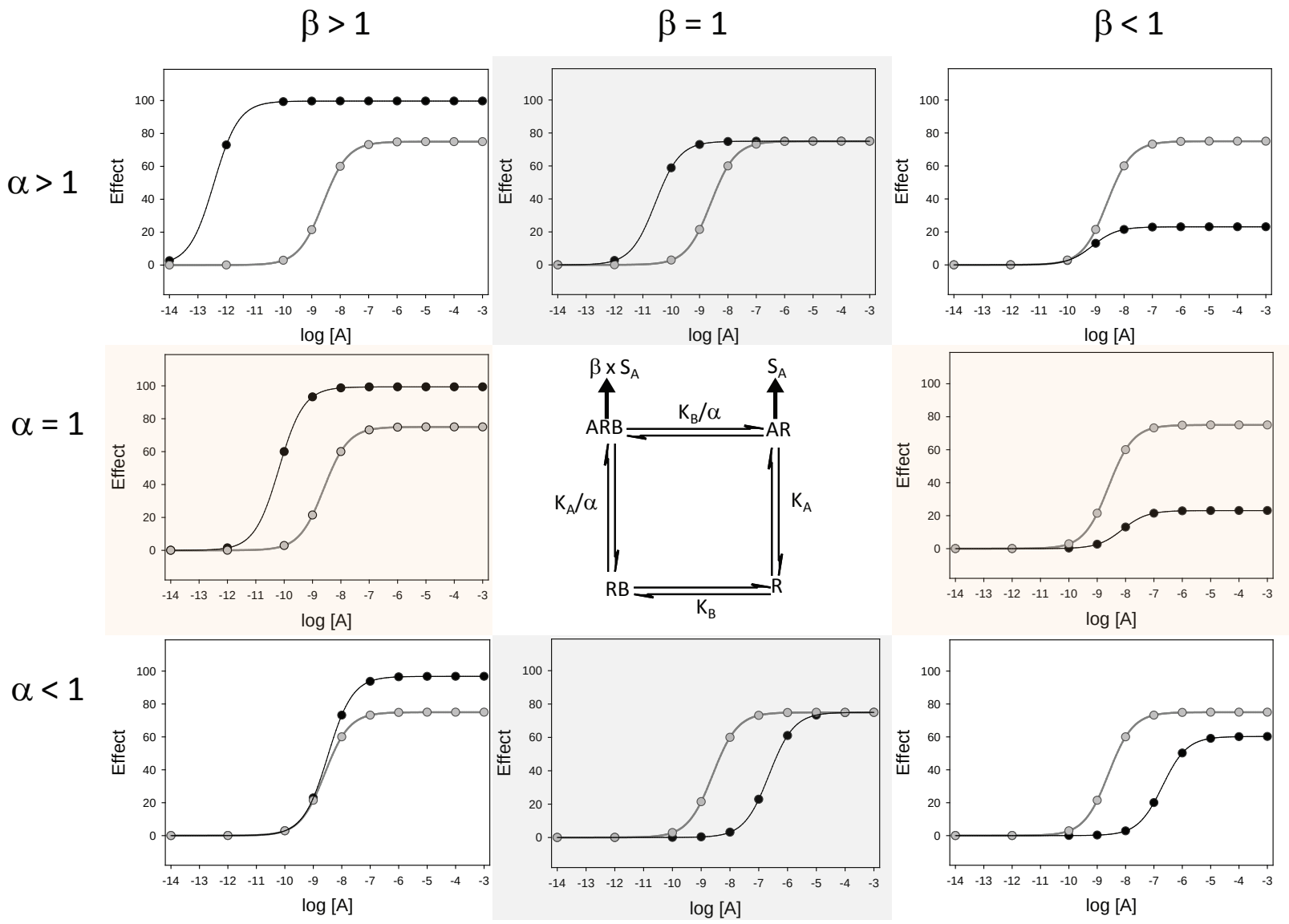
β > 1
β = 1
β < 1
α > 1
α = 1
α < 1
Effect
log [A]
β x S_A
S_A
ARB
AR
RB
R
K_B/α
K_A/α
K_A
K_B

Figure 1.14. Simulations for possible allosteric interaction and modulation of efficacy – for modulators with no intrinsic efficacy. In the middle is a schematic diagram that combines the allosteric ternary complex model (where α quantifies the effect of the modulator B on affinity of the receptor to A), and the term β quantifies the effect the modulator has on the efficacy of A. The effects of A in the absence of B (gray circles) and in the presence of B (black circles) is shown for general possibilities. A qualitative representation for α and β values used for each condition is shown on the top and far left. More detailed and description of these simulation can be found in the Allosteric Appendix (see Figures A1.5 and A1.6).

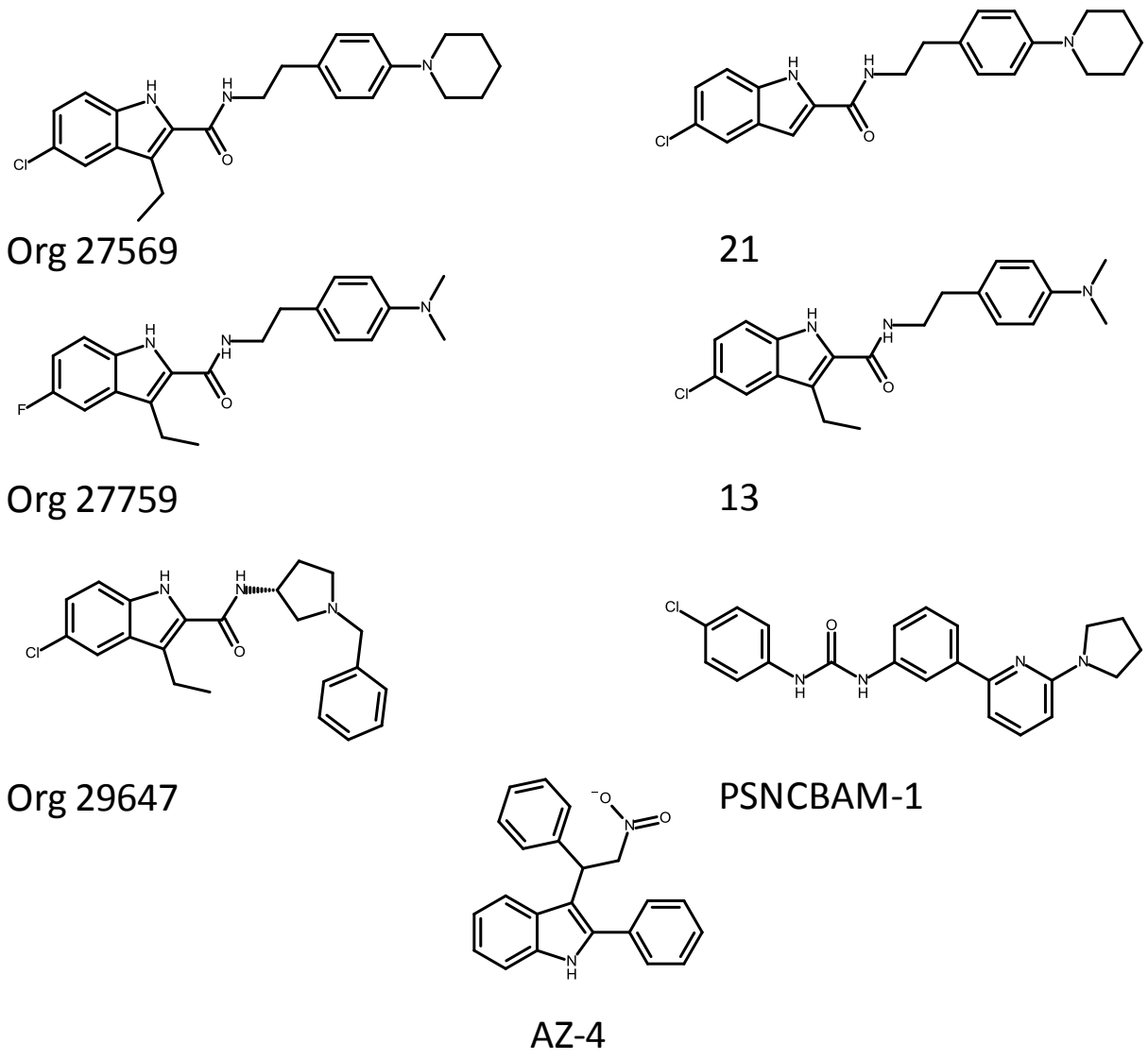

Figures 1.15. Chemical structures of CB_1 allosteric modulators.

Chapter 2

Purification of functional human cannabinoid receptor CB_1 from a mammalian cell expression system

Jonathan F. Fay[1] & David L. Farrens[1]

[1] *Department of Biochemistry and Molecular Biology, Oregon Health and Science University, Portland, Oregon 97239*

2.1: SUMMARY

The human cannabinoid receptor, CB_1, has proven elusive to purification in a functional form. Here we present an approach using a CB_1-green fluorescent protein (GFP) chimera for purification of functional CB_1 from a mammalian expression system. We first identified detergent conditions that retain a functional receptor and developed assay conditions for measuring receptor ligand binding and G protein activation in detergent. We then identified mutant constructs that further increase expression and solubility. Finally, we optimized a single step immunoaffinity purification method to obtain highly purified CB_1. The purified mutant construct appears to be ~85% functional, as assessed by radioligand antagonist binding and it also retains the ability to activate G protein. The approach described here sets the stage for the purification and structural analysis of other CB_1 mutants described in the rest of this thesis.

All experiments and data analysis reported in this chapter were performed by the author of this dissertation, except for the DPH measurements of CMC, which were assisted by Mr. Diezmann, a visiting summer student.

Parts of data presented in this chapter were previously presented at the 2011, Molecular Pharmacology Gordon-Merck Research Seminar. Ventura, CA.

2.2: INTRODUCTION

The cannabinoid receptor, CB_1, is a member of the G protein-coupled receptor (GPCR) family and is ubiquitous throughout the central nervous system (CNS). In fact, CB_1 is one of the most highly expressed GPCRs in the brain [32, 185]. CB_1 produces a wide range of physiological effects when activated, and thus it is thought CB_1 could be a promising target for therapeutic application [186-191]. Additionally, the cannabinoid system has been implicated to be involved in many diseases, including Parkinson's, Alzheimer's, depression, inflammation, neuropathic pain and obesity [185]. However, structural information about CB_1 is limited in part due to the difficulties of obtaining purified functional receptor.

Numerous attempts to overexpress and purify CB_1 are described in the literature, (Table 2.1) but these have been met with limited success. Notably, functional characterization of the purified CB_1 receptor is often not reported. CB_1 has been reported to have no binding in *E. coli*. membranes [192] (although one report indicates that ~30% functional CB_1 can be achieved from *E. coli* [193]); in contrast, the CB_2 receptor seems to be a better candidate for *E. coli* expression, although, initially only 25-35% of the CB_2 purified from this systems appears to be functional [194]. (More recent studies, however, have shown significant improvements, reporting $\geq$ 90% retention of ligand binding for a reconstituted CB_2 in addition to clear agonist-activated receptor G protein activity [195].) Eukaryotic expression systems, such as *P. pastoris*, have not fared much better and have led to no detectable ligand binding of the purified receptor, although binding was detected in yeast membranes [196]. More promising, eukaryotic expression of CB_1 using insect Sf9 cell membranes have demonstrated the expression of ~50 pmoles/mg total

membrane protein, however, no binding data of purified solubilized receptor in detergent were reported in that study [197].

In our work we set out to: (1) purify a functional form of the CB_1 receptor and (2) develop a functional assay for studying purified CB_1 in detergent. Basically, our approach was to first express the protein using a codon optimized CB_1 gene and transient mammalian expression system we previously developed [198, 199], and then use a detergent solubilization and an immunoaffinity approach that has previously been very successfully applied to the GPCR rhodopsin [200] and even used to obtain the first successful crystal structure of a recombinantly expressed GPCR [106]. Our hope was that in employing a similar approach, we would be empowered to carry out future biophysical characterizations of the cannabinoid receptor.

We also employed CB_1-GFP chimeric receptors, in order to rapidly assess expression levels, solubilization conditions, and determination of the relative functionality. The CB_1-GFP chimeras were also analyzed by fluorescence detected size-exclusion chromatography (FSEC) profiles [201], in order to further identify gene constructs and conditions that produced a monodisperse and properly folded protein.

In this way, we were able to identify (1) optimal solubilization/detergent conditions for CB_1 functionality; (2) screen mutant constructs; (3) assess heterogeneity of solubilized CB_1; and (4) quantify the amount of GFP tagged CB_1 present for comparison with the estimates of receptor concentration based on radioligand binding data.

After this initial screening, the best candidates were chosen and tagged with the 1D4 epitope (the last 9 amino acids of rhodopsin) on the C-terminal tail of GFP (or CB_1),

to enable immunoaffinity purification. These samples were immuno affinity purified to homogeneity, yielding 15-20 μg / 15 cm plate.

The function of the purified detergent solubilized CB_1 was measured using an assay we developed to determine the ability of ligands to bind in detergent. This proved a non-trivial measurement due to the difficulty in measuring binding of the extremely hydrophobic cannabinoid ligands to detergent solubilized receptors. Finally, the ability of the purified CB_1 to activate G protein was confirmed.

2.3: EXPERIMENTAL PROCEDURES

2.3.1 Buffers: The components of the buffers used are as follows: PBSSC (137 mM NaCl, 2.7 mM KCl, 1.5 mM KH_2PO_4, 8 mM Na_2HPO_4 (pH 7.2)); Hypotonic buffer (5 mM Tris and 2 mM EDTA (pH 7.5)); TME (20 mM Tris-HCl (pH 7.4), 5 mM $MgCl_2$, 1 mM EDTA); Binding buffer (TME with 5 mg/mL BSA); Wash buffer (TME with 1 mg/mL BSA); Purification Buffer (50 mM Tris, 200 mM NaCl, 5 mM $MgCl_2$, 20 % glycerol (pH 7.5)); FSEC buffer 1 (Purification buffer with 0.06% CHAPS, 0.01% DM, and 0.01% CHS); FSEC buffer 2 (Purification buffer with 0.15% CHAPS, 0.3% DM, 0.03% CHS); Sol Buffer (Purification buffer with 0.6% CHAPS, 0.1% DM, 0.1% CHS); and Elution Buffer (Sol buffer with 200 μM nonapeptide corresponding to the rho1D4 antibody epitope); Lysis Buffer (50 mM Tris, 50 mM NaCl, 5 mM $MgCl_2$, 50 uM GDP, 0.1 mM PMSF, 5 mM β-ME, pH 8); Buffer A (20 mM Tris, 50 mM NaCl, pH 8); bg-buffer (10 mM Tris, 0.5 mM $MgCl_2$, 0.1 mM PMSF, 4 ug/mL Leupeptin, 1 X Protease Inhibitor Cocktail (PIC – Roche), 1mM DTT)

2.3.2 Construction of shCB1 mutants. Site-directed mutants, truncations and fusion constructs were made using overlap extension PCR to generate EcoRI & NotI fragments, EcoRI & XhoI fragments, XhoI & NotI, XhoI & NheI fragments and NheI & XhoI fragments in the pMT4 plasmid. The sequence of the primers are as follows: Primer A, GTGGCTCCTGCACTCGAGCTGGTGCCGCG; Primer B, ATAGTTTAG CGGCCGCTCAGTGATGGTGGTG; Primer C, TTTCTCTCCACAGGTGTCC ACTCC; Primer E , GGAATTCCACCATGGACATCGAGTGCTTC; Primer F, CATCGCCTCGAGGCCCTCGCACGAGGG; Primer G, GGAATTCCACCATGGACA TCGAGGCCTTC; Primer H, CATCGCCTCGAGGCCCTCGGCCGAGGG ; Primer I, CCGCTCGAGACAGAGACGTCCCAAGTG; Primer J, GCCGATTCATTAATGC AGAATTAATTC ; Primer K, GCCCTGAGCTGTCCCCCCCCCCC; Primer N, CGCTACATCAGCTGGCACAGGCCTCTG; Primer O,CAGAGGCCTGTGCC AGCTGATGTAG CG; Primer P,GAATTCCACCATGTCCTTCAAGGAGAACGAG.

The shCB1-GFP fusion construct was created by using primers A and B with pCGFP-EU as a template (Kawate). This created a PCR product that was digested to create a XhoI & NotI fragment of GFP. Using primers C and D with shCB1(synthetic human CB_1) as a template (described previously [199]) created a PCR product that was digested to yield an EcoRI & XhoI fragment containing shCB1. In a three part ligation, enzyme cut overlap extension products were ligated with EcoR1 & Not1 cut pMT4 plasmid to yield CB1-I.

The N-terminally truncated construct, Δ103-I, was created by using primers E and D to create an overlap extension product that was digested with EcoR1 & Xho1 and subsequently ligated with EcoR1 & Xho1 cut pMT4 plasmid. This created a truncated

shCB1 gene with a Kozak consensus sequence upstream of the initiator methionine (M103).

The C-terminally truncated product was created using primers C and F to create an overlap extension PCR product that was digested with EcoRI & XhoI and ligated with EcoRI & XhoI cut pMT4 plasmid. The resulting gene, termed Δ417-I would encode for a C-terminally truncated protein lacking CB_1 residues downstream of amino acid residue 417. The N and C-terminally truncated gene, termed Δ103/Δ417-I, was created by using primers E and F to create a PCR product that was digested with EcoR1 & Xho1 and ligated with EcoR1 & Xho1 cut pMT4 plasmid. The resulting gene encodes both N-terminally truncated (at amino acid 103) and C-terminally truncated protein (lacking CB_1 residues downstream of amino acid residue 417).

Previously, we have shown that 4 cysteine residues confer sulfhydryl modifying reagent insensitivity when assessed via ligand binding [199]. This construct, termed shCB1-C4-386A, contains only four cysteine residues (C257,C264, C355, and C382). We suspected that this reduced cysteine mutant might help minimize inappropriate disulfide formation. Thus, we used shCB1-C4-386A as a template along with primers G and H, to produce an N and C-terminally truncated construct termed C4-Δ417-I. Alternatively, primers E and H were used to create Δ103-C4-Δ417-I. To enhance purification, GFP was replaced with the last 9 amino acids of rhodopsin (1D4 epitope), thus enabling antibody purification. To make this construct, primers I and J where used on a shCB1 vector to create a PCR product containing the 1D4 epitope, termed Δ417-III. This product digested with Xho1 & Nhe1 was then ligated with Xho1 & Nhe1 fragments containing the respective shCB1 gene to create a N and C-terminally truncated CB_1

receptor that contained only four cysteine residues and the 1D4 epitope. Finally, Δ88/Δ417-II and Δ88/Δ417-III were created using primer P and K and Δ417-II as a template (or Δ417-III). All mutations were verified using restriction enzyme analysis and the dideoxynucleotide sequencing method.

2.3.3 Transfection. Wt and mutant shCB1 genes were expressed in transiently transfected monkey kidney cells (COS-1) using polyethylenimine (PEI). Briefly, 30 μg of DNA was added to 100 μg PEI (polysciences) in 5 mL of Opti-mem (invitrogen) and allowed to incubate for 20 min before adding to COS-1 monolayer supplemented with 15 mL of Fresh DMEM/High glucose (Hyclone), containing 10% Fetal Bovine Serum (Hyclone), 1% Penicillin (100 units/ml, Gibco), 1% Streptomycin (100μg/ml, Gibco) and 1 % glutamine dipeptide (2 mM, Hyclone). Samples were incubated for 65 hours at 5% CO_2, 75% relative humidity, and 37^{o}C. The cells were then harvested in PBSSC, the pellets were snap frozen in liquid nitrogen and stored at -80^{o}C.

2.3.4 Membrane preparations. Membranes were prepared for further studies as previously described with some modifications [199]. Briefly, cell pellets were homogenized via 30 strokes in a glass mortar and pestle in a final volume of 1 mL/plate of hypotonic buffer. The homogenized cells were then centrifuged at 40,000 x g for 45 min. For membrane binding assays, the pellets were resuspended in TME with Protease Inhibitor Cocktail (PIC, Roche), and protein concentration was determined using the modified DC protein assay kit (Bio-Rad). For solubilization studies, the samples were subjected to a salt wash, via resuspension in Pur Buffer (or hypotonic buffer with 100 mM KCl) and then homogenized via 30 strokes. Samples where then centrifuged again at 40,000 x g and re-homogenized in purification buffer (~0.5 mL/plate). Membrane

preparations were snap frozen in liquid nitrogen as aliquots and stored at -80^{o}C.

2.3.5 SDS PAGE and Immunoblot Analysis of Cannabinoid Receptor Mutants. SDS-PAGE and immunoblot analysis were performed according to previously published procedures [199]. Protein staining was carried out using Imperial Protein Stain (Thermo Scientific) as described in the manufactures protocol.

2.3.6 Fluorescence Size-exclusion Chromatography (FSEC). For non-purified proteins, membrane preparations were brought to 2 mg/mL in Sol Buffer with PIC, supplemented with 5 μg/ml leupeptin, 10 mM benzamadine, 0.5 mM PMSF, and 1 mM EDTA. Samples were allowed to nutate for one hour and then centrifuged at 100,000 x g for 1 hour. The amount of GFP tagged protein in the resulting supernatant was quantified by comparing its fluorescence intensity against purified enhanced-GFP standards to determine the percent of the sample that was retained in the supernatant. A fraction of the resulting supernatant (~100 μL of 20-100 nM via [GFP]) was loaded onto a 60 mL (34 cm x 1.5 cm diameter) Superdex 200 (prep grade) column equilibrated in FSEC buffer 1 and run at a flow rate of 0.5 mL/min. The elutions were monitored via a RF-551 fluorescence HPLC monitor (Shimadzu) with excitation wavelength set at 470 nm and emission wavelength set at 507 nm for GFP. Purified (10-20 nM) GFP-tagged protein was monitored as described above using FSEC buffer 2.

2.3.7 Purification of cannabinoid receptor mutants. Membranes containing mutant CB_1 receptor were suspended in Solubilization buffer and gently nutated for 2-3 hours at 4^{o}C. Samples were then centrifuged for 1 hour at 100,000 x g. The supernatant was added to an appropriate volume of 1D4 antibody-Sepharose beads (binding capacity ~1μg of rhodopsin/ug resin) in Solubilization buffer supplemented with PIC, 5 μg/ml leupeptin,

10 mM benzamadine, 0.5 mM PMSF, and 100 nM SR141716A and allowed to bind via gentle agitation at 4^{o}C for ~5 hours. Next, beads were washed with ~5 mLs protease inhibitor supplemented Solubilization buffer, and twice with 1 mL washes of solubilization buffer. Overnight or three hours after incubation of 1D4 antibody-Sepharaose beads with elution buffer (containing 200 μM nonapeptide), beads were gently centrifuged at 1,000 x g in a tabletop centrifuge for 5 min and the eluted protein was collected.

2.3.8 Soluble Radioligand Binding. The competitive inhibition binding of [^{3}H]SR141716A to solublized receptors was analyzed as follows: 10 nM of soluble receptors were incubated with ~20 nM [^{3}H]Ligand, in the presence of increasing amounts of agonist for 1 hour at 30^{o}C in a total volume of 100 μl of FSEC buffer supplemented with 0.1% BSA (w/v). Separation of bound ligand from free was achieved by gel filtration on Bio-Spin 30 Tris Columns (Bio Rad). Columns were packed with 1.5 ml of 1:1 slurry of Bio-Gel P-30 (Bio Rad), equilibrated overnight at 4^{o}C in BCD-PBSSC and washed with 0.5 ml of 5 mM BCD-PBSSC and 0.1% DM prior to use. The columns were precooled to 4^{o}C and prespun for 2 min at 1,000 x g before 75 μL of the assay mix was loaded on to the columns. Proteins were collected in the void volume at 1,000 x g (4^{o}C) for 4 min and bound ligand was then analyzed by liquid scintillation counting. One-site competition equation was used to fit the data using the pharmacology features in Sigma Plot, where the K_d and B_{max} values were estimated using previously described methods [202].

2.3.9 Radioligand Binding to Membrane. The ligand binding properties of the CB_1 receptor mutants were measured using a previously described competitive inhibition

binding assay [199]. Briefly, 50 μg of membranes (total membrane protein) were incubated at 30^{o}C for an hour in 500 μL of bind buffer with ~1 nM tritated ligands and increasing amounts of agonist or antagonist. Binding reactions were filtered over 0.2% (w/v) polyethyleneimine treated Whatman GF/B filters using a Brandel 24 or 48 well filtration apparatus, with three 5 mL washes with wash buffer. Radioactivity was detected and quantified by liquid scintillation. A similar model was used to fit the data, as described above.

2.3.10 CMC determination of CHAPS/DM/CHS detergent cocktail. The critical micelle concentration (CMC) of the detergent cocktail employed in our buffering system was determined fluorometrically as previously described [203]. Briefly, this approach utilizes the solvent sensitive properties of diphenylhexatriene (DPH), a fluorescent hydrocarbon that is essentially non-fluorescent in aqueous environment. However, DPH exhibits robust fluorescence when it is intercalated into hydrophobic environments (such as the interior of a micelle). Thus, the point of micelle formation can be determined as the onset of fluorescence as a function of detergent concentration. Steady-state fluorescence measurements were performed using a PTI fluorescence spectrometer at room temperature. The excitation wavelength was 358 nm (1 nm slit settings) and the emission was collected at 430 nm (with 3 nm slit settings). Fluorescence was detected in a time based manner and the first 3 seconds were averaged for each sample reading. In brief: 2.5 μM of DPH (final concentration) was dissolved in tetrahydrofuran (THF) and added to a serial dilution of detergent dissolved in purification buffer. Tubes were vortexed and then incubated in the dark for 30 minutes at room temperature. Duplicate sets of samples

were prepared. Any photoisomerization of DPH was allowed reverse by incubating the sample in the fluorometer for 30 seconds prior to shutter opening and data acquisition.

2.3.11 Preparation of the $G\alpha_i\beta\gamma$ heterotrimer. Purification of rat $G\alpha_i$ was performed essentially as previously described [204]. In brief, N-terminally-(6)HIS tagged rat $G\alpha_i$ in pT7-5 expression vector (a gift from H. Hamm's laboratory) was expressed in BL2 *E. coli* cells. One liter in 2xYT media supplemented with 100 μg/ml of ampicillin was grown at room temperature and induced with 30 μM IPTG. After ~20 hours, 5 g of wet cell pellet were lysed in lysis buffer by French press, and clarified by centrifugation. Subsequently, the cell lysate was supplemented with A buffer containing 20 mM imidizole. This mixture was then loaded onto a 1 mL HiTrap Chelating HP column and eluted in a gradient with 200 mM imidizole. Imidozole was removed by overnight dialysis in buffer A, and then loaded onto a 1 mL HiTrap Q column and eluted in a gradient with 1 M NaCl. The elution was dialyzed in buffer A and concentrated, using Aquacade II (Calbiochem). The transducin βγ subunit was purified from ROS essentially as described [205]. In brief, ROS membranes were prepared as previously described [206], and soluble proteins were extracted by exposure of ROS membranes to light and re-suspension in bg buffer. Next, membranes were collected by centrifugation at 100,000 x g for 45 min. This extraction was repeated three times and the pooled supernatants loaded onto to a HiTrap Blue proceeding in line with a HiTrap Q. The beta gamma subunits collected on the HiTrap Q were eluted using NaCl gradient, the elution was dialyzed in bg-buffer (w/o EDTA) and concentrated. The heterotrimer was generated by overnight incubation at 4°C on ice; $G\alpha_i$ and βγ combined at a 1:1 molar ratio (~2 μM of

each) with 1.5 mM DTT and 75 μM GDP. $G\alpha_i\beta\gamma$ heterotrimers were then aliquoted, snap frozen in liquid nitrogen, and stored at -80°C.

2.3.12 Cannabinoid function assessed by $G\alpha_i\beta\gamma$ heterotrimer. $G\alpha_i$ assays were done in a similar manner to rhodopsin transducin assays [207]. The final reaction mixture contained 20 mM Tris, 100 mM NaCl, 0.1% BSA, 0.06% CHAPS, 0.01% DM, 0.01% CHS and 0.016% Asolectin, 50 μM GDP, 1-2 μM G protein heterotrimer, 50-300 nM Cannabinoid Receptor, and 4.5 μM GTPγS. The samples were assayed using [^{35}S]GTPγS that was added to the receptor:G protein mixture and immediately transferred into tubes containing 5 μM final volume of either agonist (CP 55940) or antagonist (SR141716A), 10 μL aliquots were removed at different time points, spotted onto pre-wetted Millipore MF 0.45 μm HA membrane filters using a modified Brandell M-24 cell harvester. Spotted filters were washed three times with 4 mLs of TME w/ 100 mM NaCl, removed and radioactivity on each filter was measured by liquid scintillation spectroscopy.

2.4: RESULTS

2.4.1 Screening for optimal CB_1 mutants and detergent conditions.

Our first goal was to choose the best detergent, and after screening several, we settled on more rigorously testing two different types. The first, n-Dodecyl β-D-maltoside (DM) was chosen because it has long been used as the detergent of choice for solubilizing rhodopsin, as well as many other membrane proteins. The second choice was a mixture of 0.6% CHAPS, 0.1% DM and 0.1% CHS (CCD), as this "cocktail" has previously been shown to functionally solubilize CB_2 as well as other GPCRs [194, 195, 208]. We thus set out to test both detergent types on CB_1. Our preliminary screen

showed that the CCD cocktail was superior to DM, as assessed by comparing radioactive binding of crude membranes before and after solubilizing (Figure 2.S1). Additionally, we were able to measure agonist stimulated GTPγS binding in soluble cell extracts for the CCD mixture (Figure 2.S1).

Encouraged by these results, we focused on using the CCD cocktail and set out to identify an optimal CB_1 gene constructs for purification. Here, we employed GFP tagged CB_1 receptors to enable rapid screening for mutations that improved solubility (Figure 2.1 and 2.2). Initial screens showed that the solubility of full length 'Wt' CB_1-GFP in the CCD cocktail was fairly low, at ~15% (Figure 2.3A). Thus, we next tested if deleting parts of CB_1 would increase its solubility. We made a construct in which the first 102, residues were deleted, because the full-length N-terminus of CB_1 has been shown to inhibit efficient transport of the receptor to the cell surface and also enhance proteolytic processing [34]. We also made a construct that deleted the C-terminus from residue 417 onward, as evidence exist that GPCR interacting proteins (GIPs) may bind to the C-terminus of CB_1 [96, 97], and the ΔC-terminus truncation was previously found to retain G protein-coupling by Michel and colleagues [197]. Interestingly, the initial solubility screen data indicates the extreme N-terminal deletion, Δ103-I, showed increased expression (Figure 2.3A).

We then analyzed these samples using a flourescence detected size-exclusion chromatography (FSEC) approach, to assess how well-behaved the solublized receptor were in detergent (i.e., whether they were monodisperse or aggregated) [201]. These analyses show that deletion of the CB_1 C-terminus decreases the high molecular weight aggregation species which elutes at the void volume (~950 seconds, Figure 2.3B).

Interestingly, a N-terminal and C-terminal double truncation mutant, Δ103/Δ417-I, seemed to exhibit the best properties of both single deletions. This construct showed enhanced solubility and an elution profile similar to the C-terminal mutant, and additionally, its expression seemed to be moderately enhanced over the full length or the C-terminal deletion mutant (Figure 2.3B).

2.4.2 Optimization of solubilization conditions and determination of CMC values.

Using this information, we next focused on further optimizing receptor solubility by focusing on the ΔC-terminal mutant, as this deletion mutant seemed to produce the most promising FSEC profile and contained the full N-terminus. To alleviate any potential for aggregation caused by inappropriate disulfide formation, we also mutated 9 of the 13 cysteine residues in CB_1 to alanine. We have previously established that the resulting construct, termed previously shCB1-C4-386A (for the 4 remaining cysteines, C257, C265, C355, and C382) retains ligand binding and G protein binding properties [199].

However, before proceeding with further purification attempts, we next determined the critical micelle concentration (CMC) for the CCD detergent mixture. To do this, we used a previously established fluorescence technique that measures the increase in diphenylhexatriene (DPH) fluorescence as a function of detergent concentration [203, 209]. This assay is based on the increase in fluorescence for DPH that occurs when it enters a micelle, and thus monitoring DPH fluorescence as a function of detergent concentration can be used to identify when a micelle has formed.

We first "calibrated" our use of this methodology by determining the CMC values for DM and CHAPS. Our assay found these to be 0.01% and 0. 4% in water, respectively

(Figure 2.4A and 2.4B), values in close agreement with previously published values [203, 209, 210], thus verifying that this methodology worked in our hands

Interestingly, we find that for the CCD cocktail, the enhancement of DPH fluorescence as a function of increasing detergent concentration displays a shallow phase before the more typical sharp rise (Figure 2.4D). We found that the 'intermediate phase' (the shallow slope) was due to the presence of CHS, as CHAPS and DM alone (at a 6:1 ratio) was biphasic (with a CMC of 0.3% with respect to CHAPS, in water – Figure 2.4C). The CMC for the CCD cocktail at the end of this 'intermediate phase' was 0.05/0.08/0.08% CHAPS/DM/CHS (Figure 2.4D) in 20% glycerol and 200 mM NaCl. Thus, to be safely above the CMC for the initial solubilization trials, we used CCD detergent cocktail concentrations that were 10 fold above this value.

Now that we had established a 'safe' region for our CCD cocktail concentration we next determined the optimal amount of detergent to receptor ratio, using GFP quantitation in addition to FSEC analysis. These analyses showed that at a ratio at or above 100,000:1 for CCD to GFP (with respect to CHAPS) resulted in maximum solubility of receptor from crude membrane (Figure 2.5A), as well as a diminished presence of receptor aggregation (seen in the void of the FSEC, Figure 2.5B). Interestingly, the peak maximum for the non-aggregate seems to shift to a smaller weight as the detergent:receptor ratio is increased, perhaps suggesting a shift in receptor multimers to monomer.

2.4.3 Selection of an optimal CB_1 receptor mutant candidate for purification.

In addition to focusing on the Δ417 C-terminal truncation mutant (Δ417-II), we also combined this truncation with a less severe N-terminal truncation mutant, termed

Δ88/Δ417-II. This N-terminal deletion retained more of the highly conserved part of the CB_1 N-terminus (see Chapter 4), and we suspected it may contain an unidentified, functional role. The site of Δ88 deletion was ultimately chosen based on sequence conservation between CB_1 with CB_1 isoforms (CB_1a & CB_1b see Figure 1.2). We found this Δ88 N-terminal deletion combined with the C-terminal deletion (Δ417) exhibited superior expression and was also more soluble compared to the full N-terminal construct (Figure 2.6A). Both of the above constructs also had the last nine amino acids of rhodopsin attached C-terminally to GFP, in order to introduce the so-called "1D4" antibody epitope, for western blotting and immunoaffinity purification.

Immunoaffinity purification of these samples was carried out as follows. The samples were solubilized and then bound to 1D4 antibody-sepharose beads. Impurities and unbound receptor were washed off, and then the receptor was eluted off the beads using a peptide corresponding to the 1D4 epitope. The immunopurified samples were then subjected to SDS-PAGE analysis (Figures 2.6B), which showed that the wild-type N-term (Δ417-II) construct displayed significant proteolytic N-terminal degradation. In contrast, the Δ88/Δ417-II construct was less sensitive to aggregation and degradation (Figure 2.6B and 2.6C). Thus, our subsequent purification attempts focused on the Δ88/Δ417-II construct in order to obtain homogenous purified protein.

We further characterized the purified Δ88/Δ417-II using FSEC and pharmacological methods. Shown in Figure 2.6C, this purified construct shows a clear, monodisperse homogenous symmetrical FSEC peak that centers on a molecular weight of about 165 kDa. These results agree with the expected molecular weight for a truncated CB_1 receptor GFP chimera (~60 kDa) in a ~100 kDa detergent micelle.

We next developed a method to measure the pharmacological ligand binding properties of these detergent solubilized receptors, using mini size-exclusion columns to separate bound from free ligand in order to measure binding. It was critical to develop such an assay, so that we could establish if our samples were capable of binding ligands. These assays were carried out using a CCD concentration of 0.06/0.01/0.01% CHAPS/DM/CHS, which is above the empirically determined CMC (Figure 2.4D). Importantly, these detergent concentrations have previously been shown amenable for ligand binding and G protein activation in the neurotensin receptor NTS1 [208]. The fractional amount of ligand binding for the purified receptors was determined by comparing the B_{max} values obtained from radioligand binding to the total GFP present (calculated from GFP absorbance). From these data, we estimate that Δ88/Δ417-II possessed about 85% retention of ligand binding per total GFP tagged protein (Figure 2.6D).

We then set out to test if the purified optimal CB_1 construct was able to functionally couple with G protein. To minimize potential interference with G protein binding and activation, for these assays we used a construct with the C-terminal GFP tag removed and the 9 amino acid 1D4 epitope was fused directly to the C-terminus for purification (after Δ417, see Figure 2.7A). This construct is referred to as Δ88/Δ417-III.

We first expressed and purified the Δ88/Δ417-III construct (Figure 2.7A) and confirmed that it was also capable of binding antagonist (Figure 2.7B). Next, we tested its ability to activate G protein. To do this we, reconstituted G protein (consisting of *E. coli* expressed rat $G\alpha_i$ and $\beta\gamma$ from bovine transducin) and measured the time course of $S^{35}GTP\gamma S$ binding performed in the presence of agonist or antagonist and purified

Δ88/Δ417-III (Figure 2.7C). The results indicate that purified CB_1 showed a G protein activation rate of about 43 ± 14 fmoles/min/pmole of CB_1. Interestingly, this rate is about 20 fold lower than that of ROS for $G\alpha_i\beta\gamma_T$ heterotrimers (data not shown).

2.5: DISCUSSION

Here, we describe our efforts to develop a general platform for purifying functional CB_1 receptor. We began by developing an assay that enabled measuring cannabinoid ligand binding in solution, and then used this assay to screen detergents to identify those that enabled the receptor to retain ligand binding. These studies showed that the CCD detergent mixture was optimal. We then employed GFP tagged receptors, combined with size-exclusion chromatography and fluorescence detection, to rapidly quantify levels of receptor expression and solubility and began iterations to further optimize both of these parameters. We focused our optimization approaches primarily on truncation mutants, removal of non-required cysteines, and employing appropriate detergent to receptor ratios.

The use of GFP-tagged receptor in the early stages of our experiments was essential to the success, for a number of reasons: 1) it enabled rapid screening of solubility and expression; 2) unpurified solubilized lysate could be analyzed by FSEC to evaluate the mono/poly dispersity of the sample; 3) optimization and quantification of yields was facilitated by the rapid identification throughout the purification process (via GFP fluorescence); and 4) tracking the receptor was useful in developing size-exclusion ligand binding methods. For example, coupling ligand binding with GFP quantification made it possible to more accurately determine of the functional fraction (with respect to

ligand binding). Additionally, this also allows for assessment of GFP-tagged receptors that may stick to the separation media.

The use of FSEC with GFP receptors proved especially advantageous. The FSEC required as little as ~15 ng of CB_1-GFP tagged and also helped to identify optimal conditions. Monodispersed, properly folded protein will typically appear as a Gaussian peak in FSEC profiles, whereas aggregated protein will appear in the void fraction, and polydisperse, unstable, or unfolded proteins will exist as multiple asymmetric peaks [201]. Indeed, for our purified Δ88/Δ417-II construct, we observe a symmetrical peak and little to no peak in the void volume (shown in Figure 2.6C), thus indicating the CB_1 was in a stable monodisperse state, a key requirement for future crystallization studies.

Importantly, we also empirically determined the CMC of the detergent system used in our experiments using a fluorescence based approach [203]. Determining this value is critical. Different buffering conditions (such as salt and glycerol often required for maintaining receptor stability) can alter the CMC of the detergent or detergent cocktail employed [209], and it is usually important to be at or above the CMC to retain the receptor in a detergent soluble form. Conversely, for functional assays, it is best to not be too high above the CMC, as values far above the CMC (at least for DM) have been shown to impair G protein activity [211]. Moreover, in the case of hydrophobic cannabinoid ligands, excess detergent increases the difficulty of separating bound versus free ligand by size-exclusion chromatography.

Interestingly, we observe a shallow slope for the CCD detergent mixture. While, Chattopadhyay et al. caution that values within 5-10% of the CMC should be ignored, as fluorescence intensity within this region can exhibit a curved dependence upon detergent

concentration [203]. However, this “extra slope” in the CCD mixture is striking and due to the presence of CHS (Figure 2.4). A possibility for this phenomenon is that cholesterol gradually alters the mixed micelle morphology within this shallow slope region.

The immunoaffinity purification step, which employed a 9-residue tag from the C-terminus of rhodopsin and an anti-rhodopsin 1D4 immunoaffinity column, enabled efficient extraction of highly purified receptor. It is noteworthy that the 1D4 epitope attached C-terminally to GFP also functions in immunopurification (Figure 2.6). Thus, one can imagine a GFP-1D4 tag could be a “module” that acts as a useful "detection/purification tag," and be broadly applicable to use on the initial characterization of difficult to purify membrane proteins.

Assessment of ligand binding by size-exclusion chromatography yielded high retention of ligand binding capability for our optimal CB_1 construct (~85%). Additionally, the functionality of the purified receptor was further demonstrated using reconstituted G protein, however, this rate is about twenty fold lower than that of rhodopsin for $G\alpha_i\beta\gamma_T$. A similar, lower rate of activation is observed in the visual GPCR parapinopsin [126]. Site directed fluorescence labeling data suggest that this may be due to a decreased magnitude of movement in the G protein-coupling domain of parapinopsin [126]. While a possibility, our lower rates could also be due to suboptimal conditions, differential selectivity to the $\beta\gamma$ subunits, or lack of post translational modifications.

Finally, it is important to note that measurement of agonist induced G protein activation can serve not only as a test for functional purified receptor, but can also be

used early on in the screening process (using a GPCR-Gα fusion protein), if radioligands are unavailable or the putative orthosteric ligand is of low affinity.

2.5.1 Conclusion: The approach we outlined here to identify optimal conditions to solubilize and purify CB_1 was successful. The method relied on using GFP fusion tagged proteins, to rapidly quantify and optimize a number of parameters important for purification and subsequent analysis, and employed the rhodopsin affinity 9-residue motif tag to enable a straightforward single-step immunoaffinity purification, resulting in highly pure receptor. The general strategy described here, combined with automation and high-throughput screening methodologies, could be generally applied for structural determination and biophysical characterization for a large number of membrane proteins that have proven difficult to purify. This approach is used for purifying CB_1 receptor mutants described in subsequent chapters of this dissertation.

Notes on the Δ88/Δ417-III construct

The final cysteine construct ultimately employed here (containing C257, C264, C355 and C382) was used as an initial antigen to challenge mice with (further discussed in Chapter 5). However, it was unsuitable for subsequent site directed labeling (SDL) studies, due to high background labeling with fluorescent probe. In the next chapter this construct was further optimized for SDL studies (by removing C355 and C382).

Table 2.1: Cannabinoid receptor purification publications

Expression System/ construct	Yield	Purification/%Purity	Detergent	Functionality (Before purification)	Functionality (After purification)	Ref
E. coli. MBP fusion	None	None	None	No membrane binding observed	ND	(1)
E. coli. Nt-10 or 6 HIS muCB1	300-350 mg/L	IMAC & SEC/~50%	DM/Cymal-6 (refolded from SDS/BCD)	Refolded	~5pmoles/mg SR/CP ~30% functional	(2)
E. coli. CB1-GFP-His Coexpression w/ FtsH	?/~250 ± 100 CPMs ~80% Non-specific binding	IMAC/~60-70%	Cymal-7 (screened other detergents)	Only membrane binding	ND	(3)
Pichia pastoris *α-factor-flag-CB1-myc-his*	3.6 pmoles/mg TMP (starting amount)	Anti-Flag/>90% Some degradation	FC12	Only membrane binding	ND	(4)
Sf21 C-term His Tag	45% (from 7.4 pmoles/mg TMP)	IMAC/~20%	DM	Only membrane binding	ND	(5)
Sf9 FHTCB1STII (C-term truc @417)	52 pmoles/mg TMP (starting amount)	Co-IP/ND	DM/CHS	Only Membrane binding	ND	(6)
COS cells	~10-20 µg/plate	Anti-Rho/~95%	DM/CHAPS/ CHS	~10 pmoles/mg TMP	~50-80% functional	Present work

ND = Not Determined, TMP = total membrane protein, IMAC = ion metal affinity chromatography, SEC = size exclusion chromatography

Purity was either from published value or if possible determined by quantification of the published band using pixel integration software ImageJ.

1. Calandra, B., Tucker, J., Shire, D., and Grisshammer, R. (1997) *Biotechnology Letters* **19**, 425-428
2. Michalke, K., Huyghe, C., Lichiere, J., Graviere, M. E., Siponen, M., Sciara, G., Lepaul, I., Wagner, R., Magg, C., Rudolph, R., Cambillau, C., and Desmyter, A. (2010) *Anal Biochem* **401**, 74-80
3. Link, A. J., Skretas, G., Strauch, E. M., Chari, N. S., and Georgiou, G. (2008) *Protein Sci* **17**, 1857-1863
4. Kim, T. K., Zhang, R., Feng, W., Cai, J., Pierce, W., and Song, Z. H. (2005) *Protein Expr Purif* **40**, 60-70
5. Xu, W., Filppula, S. A., Mercier, R., Yaddanapudi, S., Pavlopoulos, S., Cai, J., Pierce, W. M., and Makriyannis, A. (2005) *J Pept Res* **66**, 138-150
6. Chillakuri, C. R., Reinhart, C., and Michel, H. (2007) *FEBS J* **274**, 6106-6115

Figure 2.1

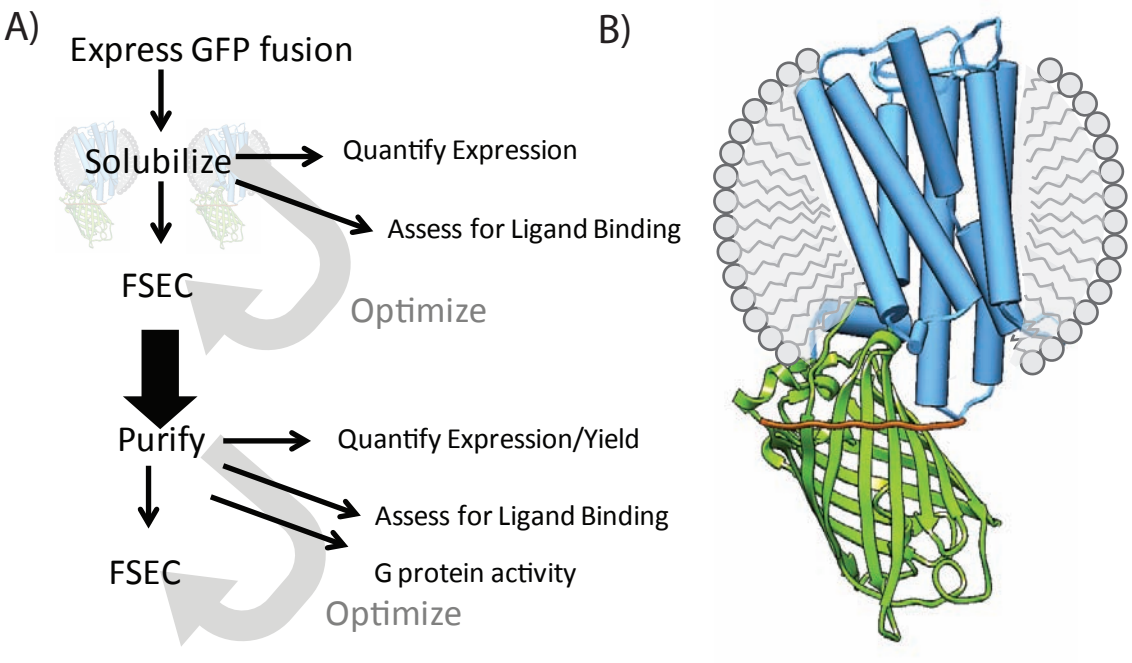
A)
Express GFP fusion
Solubilize
Quantify Expression
Assess for Ligand Binding
FSEC
Optimize
Purify
Quantify Expression/Yield
Assess for Ligand Binding
G protein activity
FSEC
Optimize
B)

Figure 2.1. General scheme for identifying and optimizing conditions for purifying CB_1 receptor. (A) Flow chart of the experimental approach. Retention of ligand binding in various detergents is a crucial first step. Coupling this with a FSEC-based screening approach allows for identification and characterization of optimal mutant CB_1-GFP constructs, without the need for purification. This approach can be used to rapidly identify and optimize receptor gene constructs, optimize for expression level, monodispersity, molecular volume, and stability. Next, a second round of screening/optimization (using the previously determined conditions as a start point) was performed on the purified CB_1 mutants. The immunopurified CB_1 mutants were subjected to similar FSEC analysis in addition to traditional pharmacological test for receptor function. **(B)** A model of CB_1 (blue) showing a C-terminal GFP fusion protein (green) and immunoaffinity tag (orange) in a hypothetical detergent micelle.

Figure 2.2

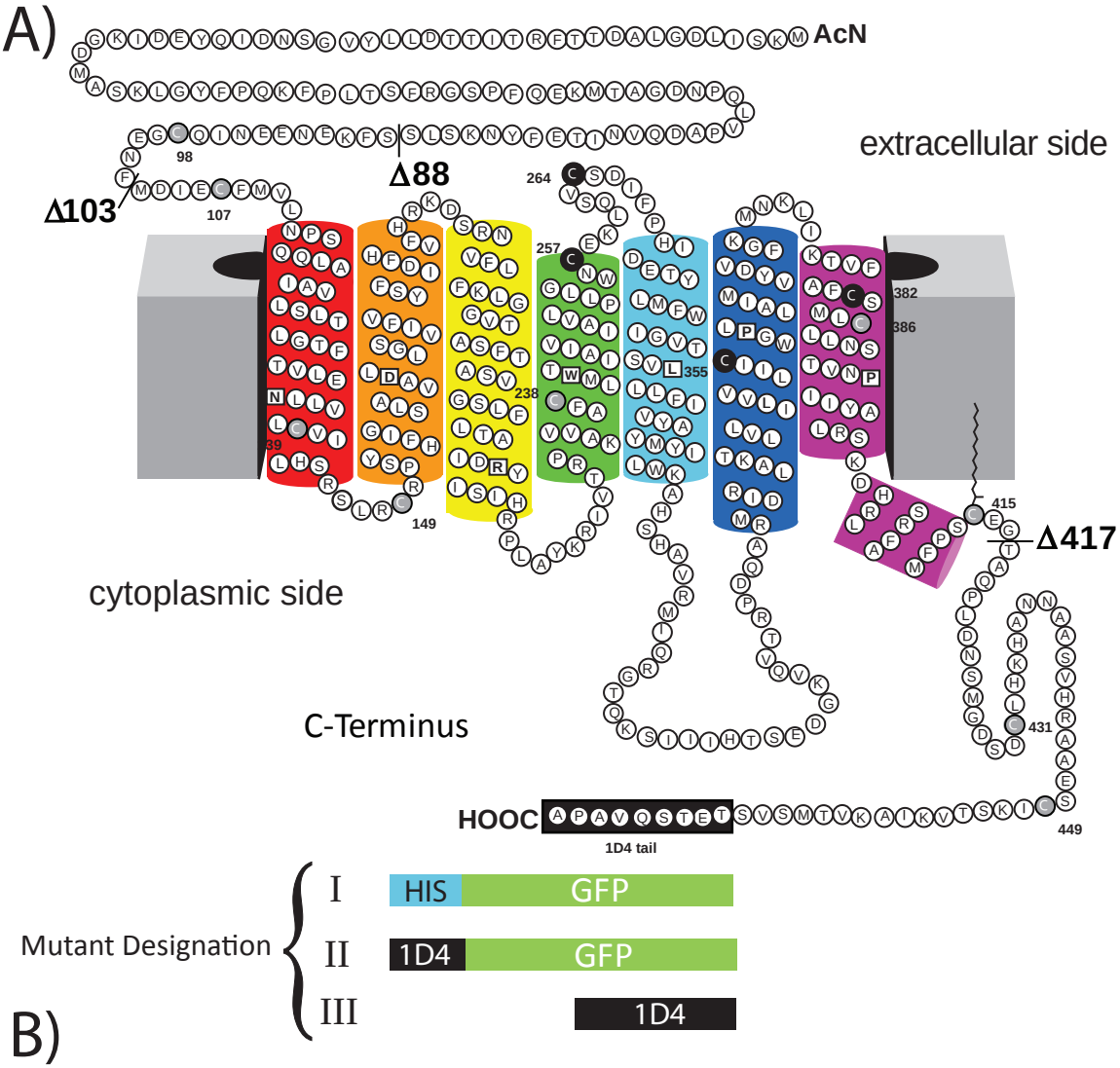

Table of different mutants used in this chapter.

	Name	N-term	C-term	Type of C-terminal Tag	Cys	GFP	HIS	1D4
Figure 3	CB1-I	+	+	I[a]	13	+	+	-
	Δ103-I	Δ103	+		12	+	+	-
	Δ417-I	+	Δ417		11	+	+	-
	Δ103/Δ417- I	Δ103	Δ417		10	+	+	-
Figure 5	Δ417-II	+	Δ417	II[b]	4	+	-	+
Figure 6	Δ417-II	+	Δ417		4	+	-	+
	Δ88/Δ417-II	Δ88	Δ417		4	+	-	+
Figure 7	Δ88/Δ417-III	Δ88	Δ417	III[c]	4	-	-	+

[a] I denotes a C-terminal GFP_{HIS}
[b] II denotes a CB1 construct C4 (containing cysteines C257, C264, C355, and C386) tagged with GFP_{1D4}
[c] III denotes CB1 construct C4 without GFP and in its place the 9-residue tag from the C-terminus of rhodopsin (1D4)

Figure 2.2. Diagram of CB_1-GFP chimeras and truncation mutants used in screening for optimal purification candidates. (A) 2D snake plot of CB_1 illustrating truncation sites and fusions used. Amino acid residues are indicated as their letter abbreviations. Cysteine residues are labeled by residue number, and shown as white letters on either grey or black background (for C4's cysteine residues). The Δ103, Δ88 and Δ417 indicate the location of N and C terminal truncations, respectively. Residues highly conserved in GPCRs are depicted with boxes and bold letters. Modifications to the C-terminus are further designated as either: I) the GFP fusion construct, II) the GFP fusion construct containing the 1D4 epitope or III) only the 1D4 epitope. See Experimental Procedures for more details. **(B)** Table and nomenclature for the different CB_1 constructs used in the present work. The variable number of CB_1 cysteines present in the chimeras shaded in blue is due to their presence in the deleted portion of the respective truncation mutant.

Figure 2.3

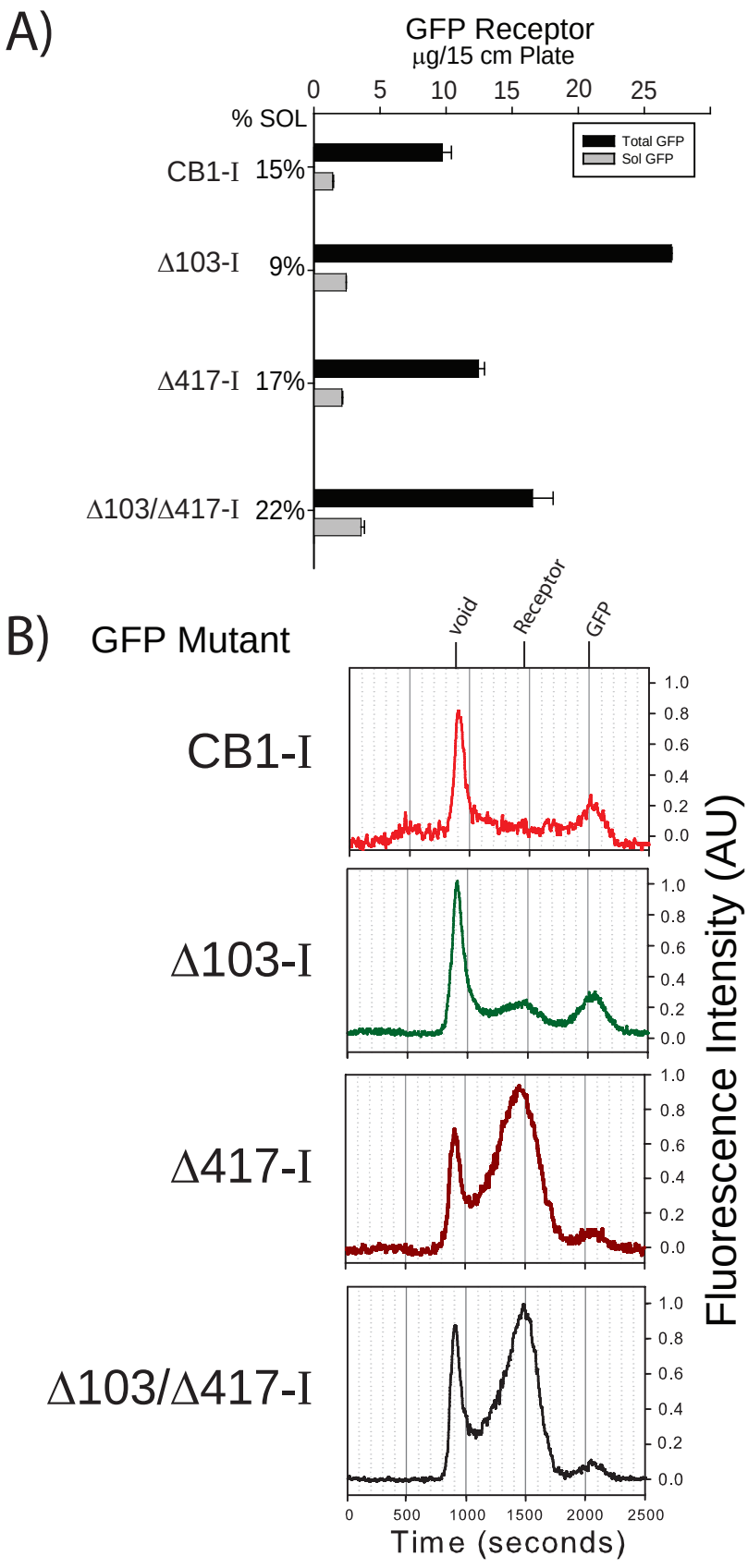
A)
GFP Receptor
µg/15 cm Plate
0
5
10
15
20
25
% SOL
Total GFP
Sol GFP
CB1-I 15%
Δ103-I 9%
Δ417-I 17%
Δ103/Δ417-I 22%
B)
GFP Mutant
void
Receptor
GFP
CB1-I
Δ103-I
Δ417-I
Δ103/Δ417-I
1.0
0.8
0.6
0.4
0.2
0.0
Fluorescence Intensity (AU)
0
500
1000
1500
2000
2500
Time (seconds)

Figure 2.3. Deletion of the CB_1 N-terminus improves receptor expression, while deletion of the C-terminus improves solubility and FSEC behavior. (A) Solubility screen of full length, CB1-I, extreme N-terminal truncation mutant Δ103-I, C-terminal truncation mutant (Δ417-I) and the double truncated Δ103/Δ417- I mutant. The total GFP fluorescence is normalized to μg/plate as determined from purified GFP standards. This is shown as black bars, and the same sample after solubilization and centrifugation (at 100,000 x g) is indicated in gray bars. Below the mutant name is the percent soluble. Data is the mean ± range between two sets. **(B)** Fluorescence-detected size-exclusion chromatography (FSEC) traces of the solubilized CB_1 truncation mutants compared to CB1-I. The top panel shows the FSEC profiles of 2 nM C-terminally GFP tagged shCB1 (Wt), all other constructs were at 5 nM.

Figure 2.4

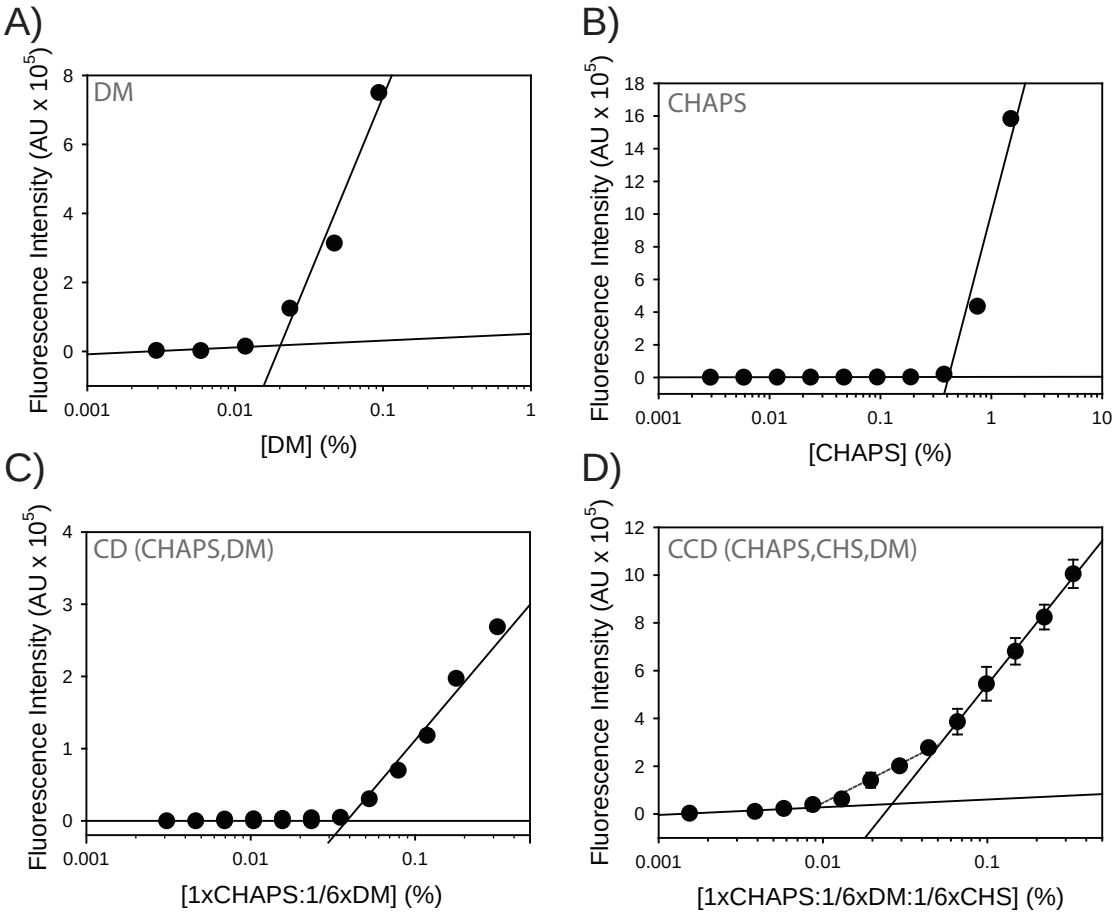
A)
DM
Fluorescence Intensity (AU x 10^5)
[DM] (%)
B)
CHAPS
Fluorescence Intensity (AU x 10^5)
[CHAPS] (%)
C)
CD (CHAPS,DM)
Fluorescence Intensity (AU x 10^5)
[1xCHAPS:1/6xDM] (%)
D)
CCD (CHAPS,CHS,DM)
Fluorescence Intensity (AU x 10^5)
[1xCHAPS:1/6xDM:1/6xCHS] (%)

Figure 2.4. Characterizing the CMC for different detergents and detergent mixtures. Assay is based on increase in fluorescence of the hydrophobic fluorophore DPH as it enters a detergent micelle. Dependence of DPH fluorescence on the detergent concentration of: **(A)** DM, **(B)** CHAPS, **(C)** a mixture of CHAPS:DM (at a 6:1 ratio) and **(D)** for a mixture of CHAPS:CHS:DM (at a 6:1:1 ratio). Both (A), (B) and (C) were tested in H_2O and (D) was tested in our buffering system (20% glycerol, 200 mM NaCl). Note the shallow initial slope observed when cholesteryl hemisuccinate (CHS) is added to the CHAPS:DM mixture. Data were collected using 2.5 μM DPH in indicated detergent concentrations. CMC value for the detergents was found to be 0.01% for DM, 0.04% for CHAPS, 0.03%/0.005% (CHAPs/DM), and 0.05%/.008%/.008% (CHAPS/DM/CHS). See Experimental Procedures for more details.

Figure 2.5

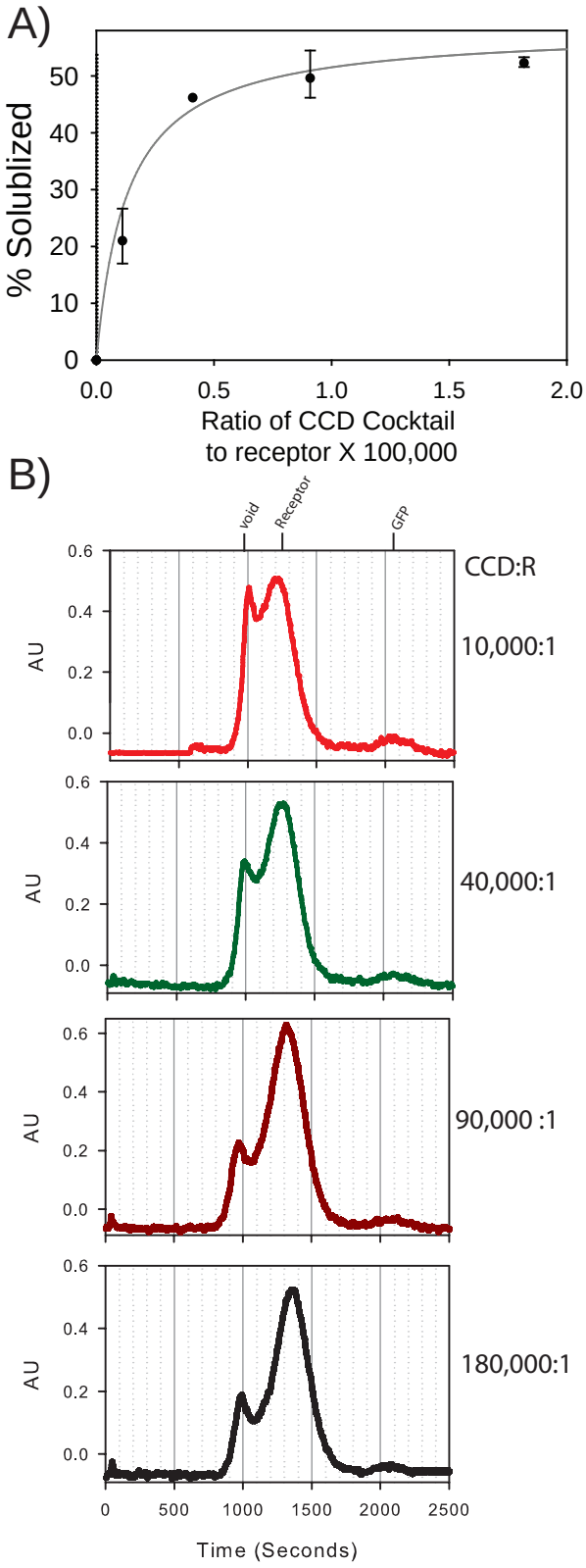
A)
% Solublized
0
10
20
30
40
50
0.0
0.5
1.0
1.5
2.0
Ratio of CCD Cocktail
to receptor X 100,000
B)
Void
Receptor
GFP
CCD:R
10,000:1
40,000:1
90,000 :1
180,000:1
AU
0.0
0.2
0.4
0.6
0
500
1000
1500
2000
2500
Time (Seconds)

Figure 2.5. Optimization of detergent solubility for Δ417-II. (A) Solubility screen of Δ417-II. Data are based on GFP quantification of pre and post solubilization, compared to the molar ratio of CHAPS in the CHAPS/CHS/DM 1:0.17:0.17 detergent cocktail to GFP tagged protein. **(B)** FSEC traces of this mutant at different protein to detergent ratios (~15 nM GFP sample loaded per run). Note the reduction in aggregate species (~ 950 seconds), and the shift in the peak max for the second peak (from 1209, 1248, 1316, and 1358) seconds with increasing detergent cocktail-to-protein ratios.

Figure 2.6

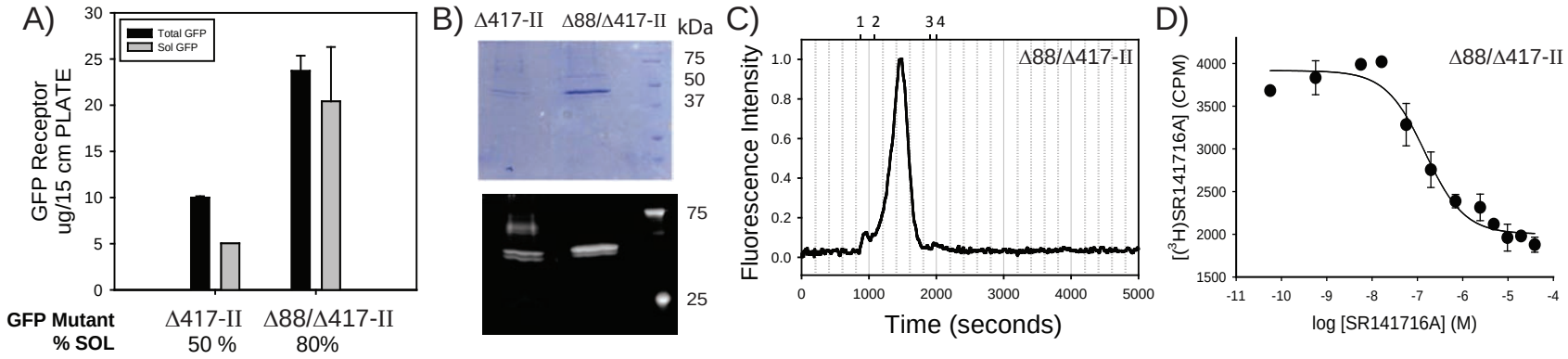
A)
Total GFP
Sol GFP
GFP Receptor
ug/15 cm PLATE
30
25
20
15
10
5
0
GFP Mutant
% SOL
Δ417-II
50 %
Δ88/Δ417-II
80%
B)
Δ417-II
Δ88/Δ417-II
kDa
75
50
37
75
25
C)
1 2
3 4
Δ88/Δ417-II
Fluorescence Intensity
1.0
0.8
0.6
0.4
0.2
0.0
0
1000
2000
3000
4000
5000
Time (seconds)
D)
Δ88/Δ417-II
[3H)SR141716A] (CPM)
4000
3500
3000
2500
2000
1500
-11
-10
-9
-8
-7
-6
-5
-4
log [SR141716A] (M)

Figure 2.6. Selection of Δ88/Δ417-II as an optimal CB_1 receptor. A) Comparison of solubility screen of C4 constructs, Δ417-II and Δ88/Δ417-II, under the higher detergent to protein ratios determined from Figure 5. Data is the mean ± range between at least two independent experiments. **B)** SDS-PAGE analysis of immuno-purified Δ417-II and Δ88/Δ417-II. Coomassie stain is depicted top, and in gel GFP fluorescence (prior to staining) is shown on the bottom. **C)** FSEC traces of the solubilized truncation mutant. 1, 2, 3, & 4 represent molecular weight standards (void volume, 669 kDa, 43 kDa, and 27 kDa, respectively). The peak height for the purified Δ88/Δ417-II construct is centered on a time corresponding to ~165 kDa. **D)** Competitive inhibition binding profile of antagonist binding, SR141716A on the purified Δ88/Δ417-II construct shows receptor is able to bind antagonist. The ratio from the B_{max} value and total GFP tagged protein is about 0.85, thus indicating a relatively high level of functional receptor. The radioactive binding represents the mean ± S.E.M from three independent experiments. Further details are provided in the Experimental Procedures.

Figure 2.7

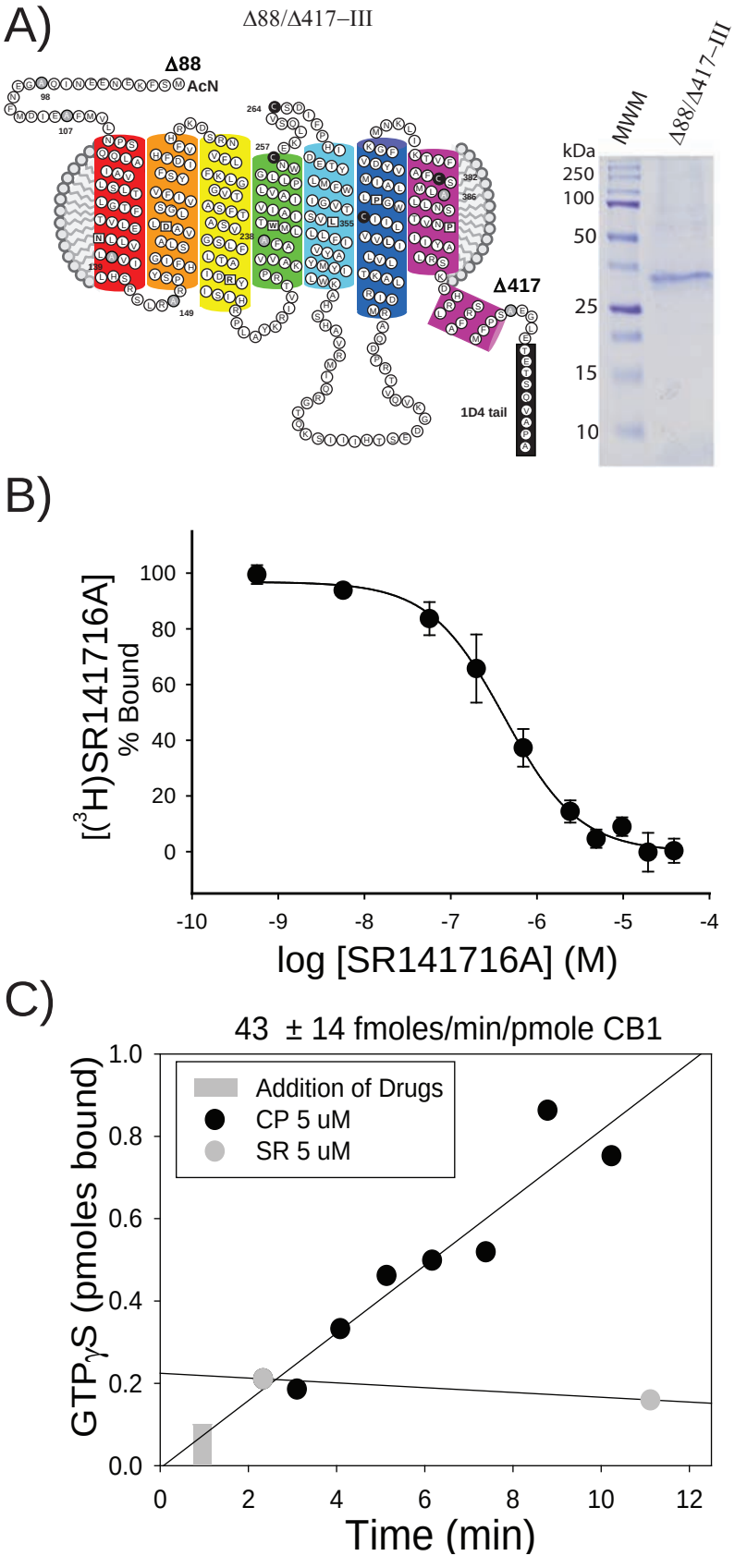
A)
Δ88/Δ417–III
Δ88
AcN
Δ417
1D4 tail
MWM
Δ88/Δ417–III
kDa
250
100
50
25
15
10
B)
[(3H)SR141716A]
% Bound
100
80
60
40
20
0
-10
-9
-8
-7
-6
-5
-4
log [SR141716A] (M)
C)
43 ± 14 fmoles/min/pmole CB1
Addition of Drugs
CP 5 uM
SR 5 uM
GTPγS (pmoles bound)
1.0
0.8
0.6
0.4
0.2
0.0
0
2
4
6
8
10
12
Time (min)

Figure 2.7. A CB_1 construct (Δ88/Δ417-III) devoid of GFP can be purified by immunoaffinity and retain its ability to bind ligand and activate G protein. A) SDS-PAGE analysis of immunoaffinity purified CB_1. **B)** Solution based binding, on the Δ88/Δ417-III construct shows receptor binds antagonist with a K_d = 423 ± 118 nM, and a B_{max} = 14 ± 3 nM. Protein concentration was set to be roughly 10 nM and was estimated from absorbance of the protein (extinction coefficient calculated to be 42,525 $M^{-1}cm^{-1}$). **C)** The detergent solublized, purified CB_1 mutant can activate G protein as indicated by the representative plot of agonist bound CB_1 stimulated [^{35}S]GTPγS incorporation as a function of time. The initial rate for this process is 43 ± 13 fmoles/min/pmole of CB_1. All radioactive binding values are the mean ± S.E.M for at least 3 independent experiments. Further details are provided in the Experimental Procedures.

Supplemental Figure

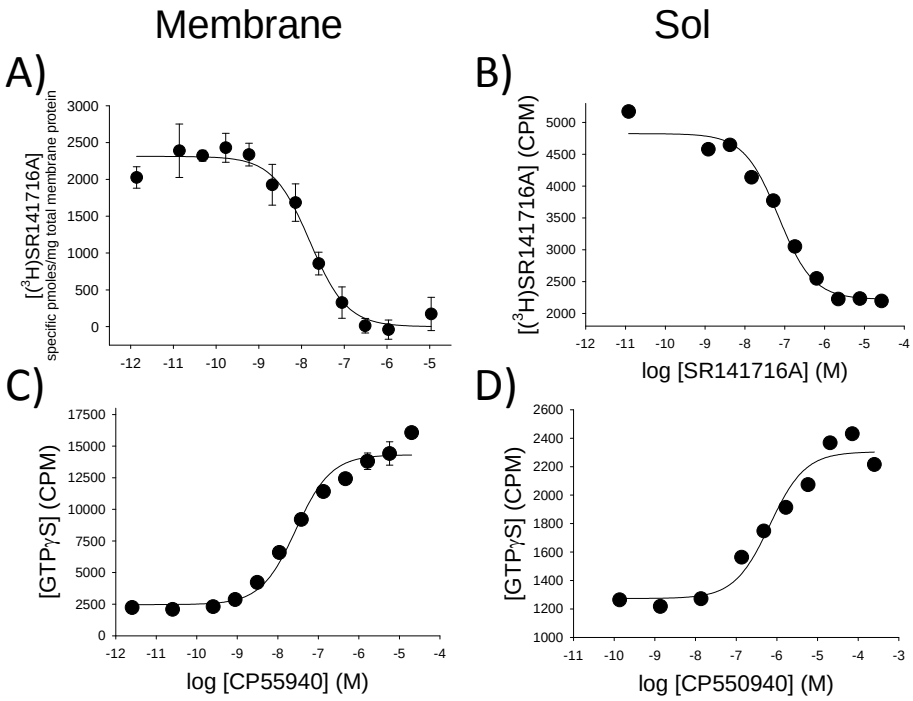

Figure 2.S1. Antagonist binding and G protein activation of membrane and solubilized CB_1-$G\alpha_i$ fusion construct. Homologous displacement binding study of the antagonist SR141716A for **(A)** crude membrane preparations and **(B)** crude solubilized membranes containing CB_1-$G\alpha_i$. Agonist (CP55940) stimulation of GTPγS binding by CB_1-$G\alpha_i$ for **(C)** crude membranes or **(D)** crude solubilized membranes. Data represent the mean of one binding experiments performed in duplicate ± the range for crude membrane and done once in singlicate for radioactive solution based pharmacological assays. All membrane radioactive pharmacological assays were performed using filter binding experiments as previously described [199] and solution assays were performed using mini size-exclusion columns. See Experimental Procedures for more details.

Chapter 3

A key agonist-induced conformational change in the cannabinoid receptor CB_1 is blocked by the allosteric ligand Org 27569

Jonathan F. Fay[1] & David L. Farrens[1]

[1] *Department of Biochemistry and Molecular Biology, Oregon Health and Science University, Portland, Oregon 97239*

Running Title: Structural changes in CB_1 are blocked by a novel allosteric ligand

3.1: SUMMARY

Allosteric ligands that modulate how G protein-coupled receptors respond to traditional orthosteric drugs are an exciting and rapidly expanding field of pharmacology. An allosteric ligand for the cannabinoid receptor CB_1, Org 27569, exhibits an intriguing effect – it increases agonist binding, yet blocks agonist-induced CB_1 signaling. Here we explored the mechanism behind this puzzling behavior, using a site-directed fluorescence labeling approach (SDFL). Our results show that Org 27569 blocks conformational changes in CB_1 that accompany G protein binding and/or activation, and thus inhibit formation of a fully active CB_1 structure. The underlying mechanism behind this behavior is intriguing—it shows simultaneous binding of Org 27569 produces a unique agonist-bound conformation, one that may resemble an intermediate structure formed on the pathway to full receptor activation.

All of the experiments and data analysis reported in this chapter were performed by the author of this dissertation. The data presented in this chapter were presented as an invited talk at the 2011 Molecular Pharmacology Gordon-Merck Research Seminar, Ventura, CA, and as a poster (2624-Pos Board B394) at the 56th Annual Biophysical Society Meeting, San Diego, CA, 2012.

The data presented in this chapter has been accepted for publication in The *Journal of Biological Chemistry*.

3.2: INTRODUCTION

G protein-coupled receptors (GPCRs) comprise ~3% of the protein-coding human genome [77]. Due to their involvement in a vast number of signaling systems, these membrane receptors are targeted by numerous therapeutic agents. An exciting field of GPCR research has emerged with the discovery that allosteric ligands can bind to some GPCRs and modulate their activity [212]. Allosteric ligands bind to a different site than traditional competitive agonists and antagonists, thus they may affect receptor signaling (efficacy) through new mechanisms. Knowing how allosteric GPCR ligands induce their effect is of great therapeutic interest, as they can complement endogenous ligands, have less potential for overdose, and specifically target receptor subtypes due to greater evolutionary divergence for allosteric binding sites [160]. Clearly, these novel ligands enrich the pharmacological dimensions of GPCR signaling, and provide additional ways to further "dial in" GPCR responses.

One of the highest expressed GPCRs in the central nervous system (CNS) is the human neuronal cannabinoid receptor, CB_1 [33]. Although initial interest in CB_1 was linked to its role as the target for psychotropic agents in marijuana [12], CB_1 has subsequently been implicated in a wide array of clinically relevant conditions, including Parkinson's disease, Alzheimer's disease, depression, inflammation, neuropathic pain and obesity. However, despite its ubiquitous presence in the CNS and its therapeutically exploitable nature, structural and biophysical information about CB_1 is limited. The lipophilic nature of cannabinoid ligands have made ligand binding assays technically challenging. Moreover, the CB_1 receptor has proven refractory to purification of significant quantities in a functional form [193, 196, 197, 213-215].

In this manuscript, we show it is possible to purify significant amounts of CB_1 in a functional form, and investigate how an allosteric ligand interacts with the purified CB_1. This ligand, Org 27569, exhibits an interesting behavior – it increases agonist binding to CB_1, yet in contrast, inhibits CB_1 signaling (i.e., it is a positive allosteric modulator of agonist affinity yet a negative allosteric modulator of agonist signaling efficacy) [163].

One possibility is that Org 27569 places the receptor in a distinct, agonist bound, non-signaling conformational state or (since the previous studies of Org 27569 were all carried out using unpurified cell membranes) acts indirectly through unidentified component(s) of the CB_1 signaling pathway.

We set out to experimentally test both possibilities, by determining if Org 27569 acts directly on CB_1, and testing if it evokes these opposing effects by inducing a distinct structural state in the CB_1 receptor. To do this, we first established conditions under which we could obtain a functional, purified CB_1 receptor. We then studied this purified CB_1 using a site-directed fluorescent labeling (SDFL) approach, in which we placed a fluorescent label on the cytoplasmic end of transmembrane helix six (TM6), a helix shown to move during activation in other GPCRs by SDFL [126, 134, 139, 206, 216, 217]. We then monitored this probe to determine if Org 27569 altered conformational changes in or around TM6 when agonists bound to the receptor.

Our results clearly show that agonist binding induces some kind of movement in the cytoplasmic end of TM6 of CB_1, whereas antagonist binding does not. We also confirm that Org 27569 stimulates agonist binding, both in membranes and for purified CB_1 in detergent. Our SDFL studies of agonist-bound CB_1 show that Org 27569 blocks

the agonist-induced conformational change at TM6 described above. Together, these results explain how Org 27569 can elicit differential effects on CB_1 agonist affinity and efficacy: Org 27569 traps the receptor in a distinct agonist bound, but non-signaling conformational state.

3.3: EXPERIMENTAL PROCEDURES

3.3.1 Buffers: The buffers used are defined as: PBSSC (137 mM NaCL, 2.7 mM KCL, 1.5 mM KH_2PO_4, 8 mM Na_2HPO_4 (pH 7.2)); Hypotonic buffer (5 mM Tris and 2 mM EDTA (pH 7.5)); TME (20 mM Tris-HCl (pH 7.4), 5 mM $MgCl_2$, 1 mM EDTA); Binding buffer (TME with 5 mg/mL BSA); Wash buffer (TME with 1 mg/mL BSA); Purification Buffer (50 mM Tris (pH 7.5, 200 mM NaCl, 5 mM $MgCl_2$, 20 % glycerol, 0.12% CHAPS, 0.02% CHS, 0.02% DM); Detergent Buffer ; (50 mM Tris (pH 7.5, 200 mM NaCl, 5 mM $MgCl_2$, 20 % glycerol, 0.6% CHAPS, 0.1% CHS, 0.1% DM)

3.3.2 *Construction of shCB1 mutants.* The site-directed mutants and truncation constructs were made using overlap extension PCR to generate the mutants in the shCB1(synthetic human CB_1) gene [198]. The non-reactive mutant, θ, contains only two of the original 13 cysteines (C257 & C264), which appear to be required for a functional receptor [199]. We previously established that θ is insensitive to sulfhydryl modifying reagents when assessed by ligand binding [199]. To facilitate purification we further modified θ, by deleting the N and C termini and then introducing the last 9 amino acids of rhodopsin (1D4 epitope: TETSQVAPA) to the C-terminus to enable immunoaffinity purification.

For the site-specific fluorescence labeling studies, we then introduced a unique

reactive cys on TM6 at residue A342C (6.34) into the θ background using a two-step PCR procedure. All mutations were verified using restriction enzyme analysis and the dideoxynucleotide sequencing method.

3.3.3 *Transfection.* The mutant shCB1 genes were expressed in transiently transfected monkey kidney cells (COS-1) in 15 cm plates. Samples were incubated for ~65 hours at 5% CO_2, 75% relative humidity, and 37^{o}C. The cells were then harvested in PBSSC, the pellets were snap frozen in liquid nitrogen and stored at -80^{o}C.

3.3.4 *SDS PAGE and Immunoblot Analysis of Cannabinoid Receptor Mutants.* SDS-PAGE and immunoblot analysis were performed according to previously published procedures [199]. PDT-bimane labeling of the samples was visualized by measuring the in-gel fluorescence using an Alpha Innotech gel doc system. Subsequently, Coomassie protein staining was carried out using Imperial Protein Stain (Thermo Scientific) as described in the manufacturer's protocol.

3.3.5 *Purification of cannabinoid receptor mutants.* COS1 cell membranes containing mutant CB_1 receptor protein were suspended in Detergent buffer supplemented with protease inhibitor tablet (Roche), as well as 5 μg/ml leupeptin, 10 mM benzamadine, 0.5 mM PMSF and 1 μM SR141716A and gently nutated for 2-3 hours at 4^{o}C. Samples were then centrifuged for 1 hour at 100,000 x g in Beckman optima LE-80K ultracentrifuge with a TI60 rotor. The supernatant was removed, and then added to an appropriate volume of 1D4 antibody-Sepharose beads (binding capacity ~1ug of rhodopsin/μg resin) and allowed to bind via gentle agitation at 4^{o}C for 4-5 hours. Next, the receptor-bound beads were washed, first with ~5 mLs buffer containing protease inhibitor and antagonist SR141716A, and then two times with 1 mL washes of buffer. Alternatively, for

fluorescence labeling of mutant of CB_1 receptors, the CB_1 bound to 1D4 beads was incubated with 50 μM PDT-bimane overnight, followed by extensive washes to remove non-reactive free bimane label. The samples were then eluted from the 1D4 antibody-Sepharaose beads with Purification buffer containing 200 μM nonapeptide.

3.3.6 *Solution Radioligand Binding Measurements.* The ability of the detergent solublized receptors to bind [^{3}H]CP 55940 or [^{3}H]SR141716A was measured using mini size-exclusion chromatography columns, as follows: 50-150 nM of soluble receptors were incubated with ~25-75 nM [^{3}H]Ligand, in the presence of increasing amounts of agonist or antagonist for 1 hour at 30^{o}C in a total volume of 100 μl of buffer. Separation of bound from free ligand was achieved by gel filtration, and then analyzed by liquid scintillation counting to determine the amount of bound ligand. The one-site competition binding model in Sigma Plot was fit to our data. The K_d and B_{max} values were estimated using previously described methods [202]. Data was globally fit and error estimates for the parameters were derived from least square fits.

Additionally, an allosteric ternary complex model, described previously [162], was used to fit our data:

$$Y = \frac{[A]}{[A] + \frac{K_A\left(1 + \frac{[B]}{K_B}\right)}{\left(1 + \frac{\alpha[B]}{K_B}\right)}} \qquad (\mathbf{3.1})$$

where Y denotes the specific bound orthosteric ligand divided by the total concentration of orthosteric ligand [A]. [B] denotes the total concentration of allosteric ligand. K_A and K_B are the dissociation constants for the orthosteric and allosteric ligand respectively and α is the binding cooperativity factor between the orthosteric and allosteric ligands. The

[A] value was the average radioactive orthoesteric ligand concentration employed in the binding assays, and K_A was estimated from the fraction bound and [A]. Values of α and K_B were determined from least-squares fitting of equation (3.1).

3.3.7 *Binding Measurements in COS1 Membranes.* The ligand binding properties of the unpurifed CB_1 receptor mutants in cell membranes were measured using a previously described competitive inhibition binding assay [199]. Briefly, this involved incubating 50 μg of membranes (total membrane protein) at 30°C for an hour in 500 μL of binding buffer with ~1 nM tritated ligands and increasing amounts of agonist or antagonist. The binding reactions were then filtered over 0.2% (w/v) polyethyleneimine treated Whatman GF/B filters using a Brandel 24 or 48 well filtration apparatus, then washed three times with 5 mL washes of wash buffer. Radioactivity was detected and quantified by liquid scintillation. Data was fit as described above.

3.3.8 Preparation of the $G\alpha_i\beta\gamma$ heterotrimer. Purification of rat $G\alpha_i$ was performed essentially as previously described [204]. The transducin βγ subunit was purified from rod outer segments (ROS) essentially as described [218]. In brief, after transducin extraction subunits were collected contemporaneously on a HiTrap Blue (for the Gα) and a HiTrap Q (for the βγ) columns. The beta gamma subunits collected on the HiTrap Q were eluted using NaCl gradient. The elution was then subjected to dialysis and further concentrated. The $G\alpha_i\beta\gamma$ heterotrimer was generated by overnight incubation at 4°C on ice; $G\alpha_i$ and βγ combined at a 1:1 molar ratio (~2 μM of each) with 1.5 mM Dithiothreitol and 75 μM GDP. $G\alpha_i\beta\gamma$ heterotrimers were then aliquoted, snap frozen in liquid nitrogen and stored at -80°C.

3.3.9 Cannabinoid functional efficacy assessed by reconstitution with $G\alpha_i\beta\gamma$ heterotrimer. $G\alpha_i$ assays were done in a similar manner to rhodopsin transducin assays [207]. The final reaction mixture contained 200 to 300 nM purified, labeled CB_1 in detergent and appropriate buffer, 1 μM G protein heterotrimer and 2 μM GTPγS. The samples were assayed using [^{35}S]GTPγS that was added to the receptor: G protein mixture and immediately transferred into tubes containing various ligands to be tested. 10 μL aliquots were removed after 30 min and spotted onto pre-wetted Millipore MF 0.45 μm HA membrane filters using a modified Brandell M-24 cell harvester. Spotted filters were washed three times with 4 mLs of wash buffer [10 mM Tris, 100 mM NaCl, 5 mM $MgCl_2$ and 0.1 mM EDTA pH 7.5] removed and radioactivity on each filter was measured by liquid scintillation spectroscopy.

3.3.10 *Fluorescence Assays.* Steady-state fluorescence measurements were performed using a PTI fluorescence spectrometer at room temperature. The excitation wavelength was 380 nm (2 nm slit settings) and the emission was collected from 400-650 nm (with 12 nm slit settings). Prior to measurements, the CB_1 receptor concentration was diluted to a final concentration of 200 nM in Purification buffer. The CB_1 receptor concentrations were estimated from absorbance value at 280nm (corrected for the contribution of bimane at this wavelength), using an extinction coefficient of 42,525 L mol^{-1} cm^{-1} estimated from the protein sequence (ExPASy ProtPram tool). All ligands were diluted, such that the final solvent concentration was less than 1%. The fluorescence spectra were buffer subtracted and corrected for dilution.

The variable slope sigmoidal dose-response function was fit globally to our bimane response (change in bimane fluorescence) with respect to Org 27569

concentration. The error estimates for the parameters were derived from least square fits.

An operational model of allosterism, as previously described by Price et al. [163], that assumes the allosteric modulator does not process any intrinsic efficacy was also fit to our data, equation (**3.2**):

$$E = \frac{E_{max}\tau^n[A]^n\left(1+\frac{\alpha\beta[B]}{K_B}\right)^n}{\left[[A]\left(1+\frac{\alpha[B]}{K_B}\right)+K_A\left(1+\frac{[B]}{K_B}\right)\right]^n+\tau^n[A]^n\left(1+\frac{\alpha\beta[B]}{K_B}\right)^n} \qquad (\mathbf{3.2})$$

[A], K_A, and are as defined above in equation (3.1). E represents the bimane effect, *n* is a logistic slope factor, τ is a measure of orthosteric ligand efficacy, and β is the empirical proportionality constant describing the modulation of an allosteric ligand on agonist mediated efficacy. When β is less than 1 there is an inhibition of signaling efficacy imparted on the receptor by the allosteric modulator. The fitting used 10 μM for [A]; values obtained from equation (3.1) from our solution binding assay for K_A, K_B, and α; and set E_{max} to the mean of our empirically derived value from our data sets, and restricted β to be greater than 0.

3.3.11 *TCA Precipitation Method to Determine the Extent of Free Label Contamination.* To assess if free (unattached, non-reacted) bimane label was present in the samples, we used a slightly modified version of our previous procedure [139, 219]. Briefly, this involves determining if any bimane fluorescence is present in a sample after TCA precipitation of the protein. To do this, the total bimane fluorescence of a sample containing PDT-bimane labeled CB_1 was measured immediately after adding 10% TCA. The protein was then precipitated by placing the sample on ice for 20 min, and then subjected to centrifugation at 14k RPM at 4^{o}C for 20 min using a bench-top eppendorf centrifuge. The supernatant was then collected and fluorescence emission was measured.

This approach exploits the fact that the 10% TCA precipitates essentially all protein, whereas free bimane is not precipitated. Thus, any fluorescence remaining in the supernatant must be due to (free) bimane that is not attached to the protein. Comparison of these two emission max values gave a relative amount of free label in the sample. In all cases the measured free label concentration was essentially negligible (< 1% see Figure 3.S1).

3.3.12 *Fluorescence Quenching Experiments.* Measurements of the accessibility of the bimane probe were carried out by Stern-Volmer quenching studies to determine the bimolecular quenching coefficient (Figure 3.2). Briefly, the bimane labeled CB_1 samples were incubated in 20 μM CP 55940 or SR141716A for 30 min prior to measurements. For the KI quenching assays, the added total salt concentration was kept at ~40 mM by the addition of a corresponding amount of KCl, and 0.1 nM Na_2SO_4 was present to inhibit formation of I_3 [126, 139]. Fluorescence lifetime measurements were carried out using a Pico Quant Fluo Time 200 equipped with a Hamamatsu R3809U-5X series microchannel-plate photomultiplier. The excitation was from a 405 nm diode-laser, and emission was monitored at 490 nm with 2 nm slits. The average fluorescent lifetime $<\tau>$ and slopes from the KI quenching assay (Ksv) were used to calculate kq ($kq = Ksv / <\tau>$) [220]. The bimolecular quenching coefficient (kq) is a direct measure of the efficiency of quenching ($M^{-1}s^{-1}$).

3.4: RESULTS

3.4.1 *Expression, purification & site-specific labeling of CB_1.*

Before introducing unique cysteines into CB_1 for labeling with a fluorophore, we

first had to establish a mutant that showed no background cysteine labeling. To do this, we used our gene construct, called θ, which contains only two cysteines, C257 and C264 [199]. These two cysteines are required to produce a functional receptor [199, 221], and we have previously shown that all other cysteines can be mutated to alanine while still retaining a functional CB_1 receptor. Together, these results strongly suggest (but do not definitively prove) C257 and C264 form a disulfide bond [199, 221].

In order to obtain a unique site for attaching the fluorescent label, we then introduced a cysteine at the cytoplasmic end of TM6, in the θ construct, at residue 342 (or 6.34 via the Weinstein and Ballestros nomenclature). We hereafter refer to this cysteine mutant as A342C/θ.

The θ and A342C/θ gene constructs were expressed in COS cells. Subsequently, the membranes containing mutant CB_1 receptors were solubilized in detergent, the samples were clarified by centrifugation, and the supernatant then applied to a 1D4 immuno-affinity antibody column (IAC). The bound CB_1 receptors were then incubated with an ~20 fold excess of PDT-bimane for ~16 hours, and the excess fluorescent label was then washed from the receptor bound IAC. The purified receptors were then eluted from the IAC using an excess of nonapeptide corresponding to the 1D4 binding epitope. The yield from this process is ~ 15 μg purified, bimane-labeled receptor per 15 cm plate of transfected COS1 cells.

3.4.2 *The purified CB_1 is specifically labeled at TM6.*

SDS-PAGE analysis shows that the eluted proteins are pure (Figure 3.1C and D). Moreover, the lack of fluorescence in θ when this gel was irradiated with UV light (prior

to Coomassie staining) indicates that the 'background' receptor is not reactive to the bimane label (Figure 3.1C and D). Notably, treating θ with a reducing agent, prior to labeling, resulted in label incorporation (Figure 3.1C), providing further direct evidence that cysteines C257/C264 form a disulfide bond in CB_1.

In contrast to θ, mutant A342C/θ showed robust labeling with the PDT-bimane (Figure 3.1D). This result indicates the fluorophore is specifically attached to the cysteine at site 342. The labeling efficiency was ~60-80% based on comparison of the ratio of $280nm_{(protein)}/390nm_{(bimane)}$ absorbance. The samples were free of non-reacted label, as determined by TCA precipitation analysis (see Figure 3.S1).

3.4.3 The purified, bimane-labeled CB_1 retains its functional affinity & efficacy for cannabinoid ligands.

Figure 3.1D and 3.1E show that the purified, bimane-labeled A342C/θ mutant is functional in respect to its pharmacological properties. It can bind both agonist and antagonist in a solution binding assay, exhibiting K_d values of 187 ± 27 nM and 47 ± 23 nM for agonist and antagonist, respectively or 398 ± 58 nM and 52 ± 37 respectively, when fit using Swillens approximation to account for possible ligand depletion [222] . These values are ~ 50-100 fold higher than what we (and others) typically observe in membranes [198, 199]. This shift may be partially due to the absence of G proteins in our purified samples, as well as non-specific effects of the detergent on the receptor. To test if our bimane labeled, purified receptor retains functional efficacy, we measured its ability to stimulate $GTP\gamma S^{35}$ binding when reconstituted with G protein ($G\alpha_i$) and agonist. The results confirm an agonist-induced stimulation of G protein activation and $GTP\gamma S^{35}$ binding compared to the basal or antagonist bound states (Figure 3.3B). It is

unclear why SR141716A did not affect basal G protein activity. Possibly the intrinsic activity of our G protein preparation could mask this effect and/or our purified samples lack endocannabinoids that may be present in previous *in vivo* assays that demonstrate basal activity.

3.4.4 Binding of agonist to CB_1 induces a conformational change in the cytoplasmic end of TM6, as detected by changes in the fluorescence of the bimane probe.

The addition of agonist, CP 55940, causes an ~35% increase in the fluorescence intensity of the attached bimane label (Figure 3.2A). This fluorescence increase is clearly due to agonist-induced structural changes in CB_1 altering the environment around the probe. CP 55940 itself is non fluorescent at the excitation and emission wavelengths used (Figure 3.S2). The agonist-induced fluorescence increase is dose dependent, exhibiting an EC_{50} of 430 ± 86 nM (Figure 3.2Bi). No further increase is seen at ligand concentrations greater than ~10 μM. A fluorescence increase occurs upon addition of the endocannabinoid analogue meAEA or the CB_1 agonist WIN55212-2. Interestingly, the three cannabinoids we tested have the same rank order of potency (CP>WIN>AEA) for their ability to induce the bimane fluorescence response in CB_1 as they are observed in more traditional pharmacological assays (see Figure 3.2Bi). We also found that the partial agonist AEA appears to cause less of a fluorescent change, which can be overcome by the addition of more CP 55940 (Figure 3.2Bii). However, we found meAEA and WIN55212-2 more difficult to work with than CP 55940, due to solubility issues and their lower affinities resulting in substantially noisier data. Thus, we did not further explore their behavior in more detail and focused instead on CP 55940.

In contrast to agonists, adding antagonist (SR141716A) caused no significant

fluorescence change in the sample (Figure 3.2C). The antagonist could also reverse the agonist induced fluorescence increase (Figure 3.2D), and it did so much more rapidly ($t_{1/2}$ ~1.5 min) than the slow rate of agonist induced fluorescence increase ($t_{1/2}$ ~ 4.7 min).

3.4.5 The bimane label on TM6 moves to a more polar environment upon addition of the agonist, CP 55940.

Along with the fluorescence increase, addition of agonist also induced an ~ 6 nm red-shift in the bimane fluorescence compared to the SR141716A form (Figure 3.2E,i). We have previously shown that for a soluble protein, the bimane fluorescence emission λ max reflects the solvent accessibility at the site of attachment [219, 223].

However, CB_1 is a membrane protein, thus the λ max shifts could also be affected by interaction of bimane with detergent. Thus, to assess the exposure of the probe to solvent, we carried out fluorescence quenching studies using the aqueous quenching agent, KI. The results show the probe collides more frequently with I^- (i.e., it has a larger bimolecular quenching constant) in the agonist bound form (Figure 3.2E,ii). Together, these data confirm that agonist binding causes the probe to relocate to a more solvent exposed environment, as is expected if CB_1 activation involves a conformational change in TM6 (modeled in Figure 3.2F), as is observed in other GPCRs (rhodopsin, B2AR, and A2AR).

3.4.6 The allosteric ligand Org 27569 promotes agonist binding to CB_1, yet blocks the agonist induced conformational changes in TM6.

Previous reports have shown Org 27569 (Figure 3.3A) inhibits the ability of CB_1 to elicit agonist-induced downstream signaling [163]. To test if this effect occurred at the level of the G protein interaction with the receptor, we measured agonist stimulated

guanine nucleotide exchange for the labeled, purified receptor reconstituted with $G\alpha_i$. The results show that agonist stimulated GTPγS binding is completely inhibited in the presence of Org 27569 (Fig 3B).

We next confirmed previous reports [163] that the allosteric ligand Org 27569 enhances CP 55940 binding for CB_1 in membranes (Figure 3.3C). We then confirmed that Org 27569 also enhances agonist binding to the detergent solubilized, purified, bimane-labeled CB_1 (Figure 3.3D). Importantly, this data clearly establishes that Org 27569 can enhance specific CP 55940 binding <u>independent</u> of the G protein coupling state of the receptor, as our purified, detergent solubilized CB_1 samples are devoid of G protein (see Figure 3.3D).

Additionally, when an allosteric ternary complex (Equation 3.1) is fit to our data the allosteric cooperativity factor is 2.74 ± 0.41 and 2.75 ± 0.23 for membrane and solution binding respectively (Table 3.1). Both of these values are nearly the same and are greater than one, indicating positive cooperativity.

Interestingly, the affinity of the orthosteric ligands are significantly lower in our detergent purified samples than in membranes, yet the Org 27569 enhancement of agonist binding is essentially unchanged (Figure 3.3C, 3.3D, Table 3.1). We are not sure why this is, it is possible that the allosteric site is insensitive to the G protein-coupling state of the receptor (in contrast to the orthosteric ligands) and/or there is a differential “detergent effect” on the samples.

After establishing that Org 27569 does not block but rather increases agonist binding, we next tested the effect of Org 27569 on the agonist-induced conformational changes in TM6 detected by the fluorescence from the bimane probe. Interestingly, the

data show that Org 27569 blocks the agonist-induced fluorescence increase of the bimane probe on TM6 (Figure 3.4A). Org 27569 can also rapidly reverse the fluorescence increase induced by agonist binding (Figure 3.4B and 3.4C). Org 27569 also reversed the fluorescence increase that occurs upon addition of the endocannabinoid analogue meAEA or the CB_1 agonist WIN55212-2, although again, the use of these compounds resulted in substantially noisier data (Figure 3.4D and 3.4E).

Importantly, the inhibition of agonist-induced fluorescence occurs in a dose-dependent manner that closely parallels radioligand CP 55940 binding enhancement (compare Figures 3.3D and 3.4F). When fit to an operational model of allostery (Equation 3.2), we find the β value (magnitude of the allosteric modulation of agonist efficacy) to be less than one and in fact approaches zero (Table 3.1). This indicates an insurmountable allosteric antagonism of the observable, the bimane response, which we interpret to be transition of the receptor into the active state. The implications of these results are discussed below.

3.5: DISCUSSION

In this paper we set out to determine how the allosteric CB_1 ligand Org 27569 can enhance agonist binding, yet at the same time inhibit receptor function, a phenomenon first reported by Price and co-workers [163]. GPCRs are inherently under allosteric regulation by G proteins – a bound G protein induces a high-affinity agonist binding site in the receptor that is lost when the G protein is activated and released [150]. Recently, the cause of this effect has been localized to specifically involve binding of the G protein C-terminus to a site exposed by TM6 movement in the receptor [109, 152]. Thus, we hypothesized that Org 27569 binding might affect key conformational changes in the

cytoplasmic face of the receptor that typically accompany agonist binding and receptor activation/G protein-coupling.

To test this hypothesis, we employed an SDFL approach. We introduced a unique and reactive cysteine residue into CB_1, and then labeled it with an environmentally sensitive fluorophore, PDT-bimane. We put this probe on the cytoplasmic end of TM6, since this helix has been shown to move during activation in a number of GPCRs [117, 121, 126, 139, 141, 142, 144, 145, 152, 224-226]. Thus, we anticipated activation would cause a change in the fluorescence of the bimane probe.

Our results clearly show activation-induced changes in fluorescence caused by increased solvent exposure for the bimane probe on TM6 upon agonist binding (Figure 3.2). Although these results do not delineate precisely how TM6 moves (or the extent) in CB_1, they are consistent with an outward TM6 movement observed in other GPCRs (Figure 3.2F) [109, 117, 121, 126, 139, 141, 142, 144, 145, 152, 225, 227].

Significantly, the agonist concentration that yields half-maximal bimane fluorescence response (EC_{50}) essentially matches the agonist affinity determined from radioligand binding (compare Figure 3.2B with Figure 3.1D). The fact that antagonist binding causes no dramatic fluorescence change (Figure 3.2C), and can even rapidly reverse the slower agonist induced changes (Figure 3.2D) indicates that the fluorescence increase is specifically linked to agonist-activation.

It is unclear as to why the agonist-induced fluorescence change is so slow. The Kobilka lab observes a similar slow change in their SDFL studies of the B2AR [124], which they determined is due to a multi-step binding phenomenon of the ligand to the receptor [128]. Thus, the slow change we see for CB_1 may represent an analogous multi-

step binding phenomenon.

Alternatively, the slow fluorescence change we see in CB_1 may be caused by interactions of the hydrophobic cannabinoid ligands with the detergent micelles used in our experiments. Interaction of the ligand with empty micelles could slow the amount of agonist cannabinoid ligand available to a receptor/micelle complex. Thus, the more hydrophobic CP 55940 would have a slower apparent rate of repartitioning from an empty micelle to a micelle containing a receptor, and this could thus contribute to the slower observed fluorescence change/conformational change in the labeled CB_1. Similarly, the faster rate of change observed for the antagonist SR141716A might be partially due to its greater aqueous solubility (lower octanol/water partition coefficient compared to agonist -1×10^5 *v.* 1.6×10^6, respectively) [59, 228]. Notably, multi-step binding models have previously been proposed for cannabinoid ligands to take into account their interaction with membranes [229, 230].

How can we reconcile our Org 27569 data with an activation model of CB_1? We propose that the binding of the allosteric modulator Org 27569 induces or stabilizes a new ligand-specific conformation, a state that has an agonist bound, but lacks conformational changes in TM6. These results are in agreement with predictions of the allosteric two-state model where the allosteric ligand has positive cooperativity with agonist binding but negative cooperativity with receptor activation [231].

Figure 3.5 demonstrates how a multi-state model can explain our data. The model shows agonist binding accompanies a movement of TM6 (right), whereas the antagonist-bound state does not (left). Org 27569 binds with the agonist to CB_1, but at least partially inhibits and/or reverses the agonist-induced TM6 movements (middle). Previous

experimental studies as well as models have also suggested multiple GPCR conformations are possible [127, 155, 232]. The model in Figure 3.5 is consistent with our data, which show that Org 27569 puts the CB_1 receptor in a distinct conformational state, one in which the binding pocket is occupied by an agonist (Figure 3.3B and 3.3C), yet lacks conformational change(s) in TM6 (Figure 3.4).

Lack of full TM6 movement explains the observed negative allosteric effect Org 27569 has on CB_1 signaling efficacy [163]. Inhibiting structural changes in the cytoplasmic face of CB_1 should impact receptor signaling, since movement in this region is associated with a GPCR's ability to bind and activate its cognate G protein [117, 121, 126, 139, 152, 225].

It is tempting to speculate that the CB_1-agonist-Org 27569 complex represents not a new conformational state, but rather, the stabilization of an already existing intermediate structure, one that is on the pathway that flows from agonist binding to full receptor activation.

There is ample precedence for this possibility. Rhodopsin, the GPCR involved in vision, clearly undergoes several spectrally distinct conformational changes during the conversion of the inactive state to fully activated receptor [130, 131]. Structures for many of these inactive intermediates have been solved, and they show that although the agonist (*all-trans*-retinal) is in the binding pocket of the receptor, only limited changes have propagated throughout the protein to the cytoplasmic face, especially regarding TM6 movements [227, 233-235]. Similarly, a structure of a 'low-affinity' B2AR containing an irreversibly bound agonist shows diminished TM6 movement [236]. These examples demonstrate the difficulty of trapping a fully active GPCR conformation, even

one which contains a covalently attached agonists.

One way that Org 27569 could trap such an early activation intermediate would be by exploiting or lowering the energy of an early agonist-bound intermediate state, and/or increasing the energy barrier required for the receptor to take on the active conformation. Interestingly, a similar concept was recently used to determine the structure of an energetic intermediate of the A2A adenosine and B1A receptors, by extensive mutagenesis designed to produce a more thermally stable receptor. The resulting structures show an intermediate conformation between the inactive and active state, with TM6 partially occluded [148, 237, 238]. Interestingly, one would expect the inhibition of full TM6 movement by Org 27569 and the trapping of CB_1 in an intermediate state on the pathway to full activation would also increase the dwell time of agonist in the binding pocket. This should enhance the apparent amount of agonist bound to CB_1 in the presence of Org 27569, exactly as we observed in our data (Figure 3.3).

Understanding how allosteric ligands exert their effects is an exciting and crucial new field of GPCR study [239]. Our results here provides insight into one way an allosteric ligand can alter the signaling of its cognate GPCR – by either inducing (or capturing) a previously unidentified and unique receptor conformation, or trapping an existing intermediate state formed on the way to receptor activation. These findings also suggest that GPCR intermediate structures may prove to be better templates for designing and screening new allosteric GPCR drugs than either the fully active or the fully inactive state structures.

ATCM	**Membrane Binding**	**Solution Binding**
Parameters	Figure 3.3C	Figure 3.3D
K_B	6.8 ± 4.2 μM	2.28 ± 0.82 μM
α	2.74 ± 0.41	2.75 ± 0.23
Operational Model	**Bimane Response**	
Parameters	Figure 3.4F	
β	0.00 ± 0.24	

TABLE 3.1. Allosteric ternary complex model (ATCM) and allosteric operational model parameter values for Org 27569. ATCM best fit parameter values for crude membranes expressing A342C/θ, as well as for purified bimane labeled A342C/θ. K_B is the equilibrium dissociation constant for Org 27569, and α is the allosteric cooperativity factor. A value of $\alpha > 1$ indicates positive cooperativity and governs the magnitude that the allosteric modulator enhances agonist binding. The reported parameter values represent the mean ± S.E.M. determined from least-squares fitting of equation (3.1) from two experiments performed in duplicate.

An operational model of allostery was used to fit the data in Figure 3.4F. A value of $\beta < 1$ indicates attenuation of the orthosteric induced observable, and it governs the magnitude of this event (in this case the bimane response). Values not shown in the Table are the calculated intrinsic efficacy of the orthosteric ligand ($\tau = 2.21 \pm 0.95$) and the calculated 'fitting' factor ($n = 2.03 \pm 1.30$). The reported parameter values represent the mean ± S.E.M. determined from least-squares fitting of equation (3.2) from two independent experiments.

Figure 3.1

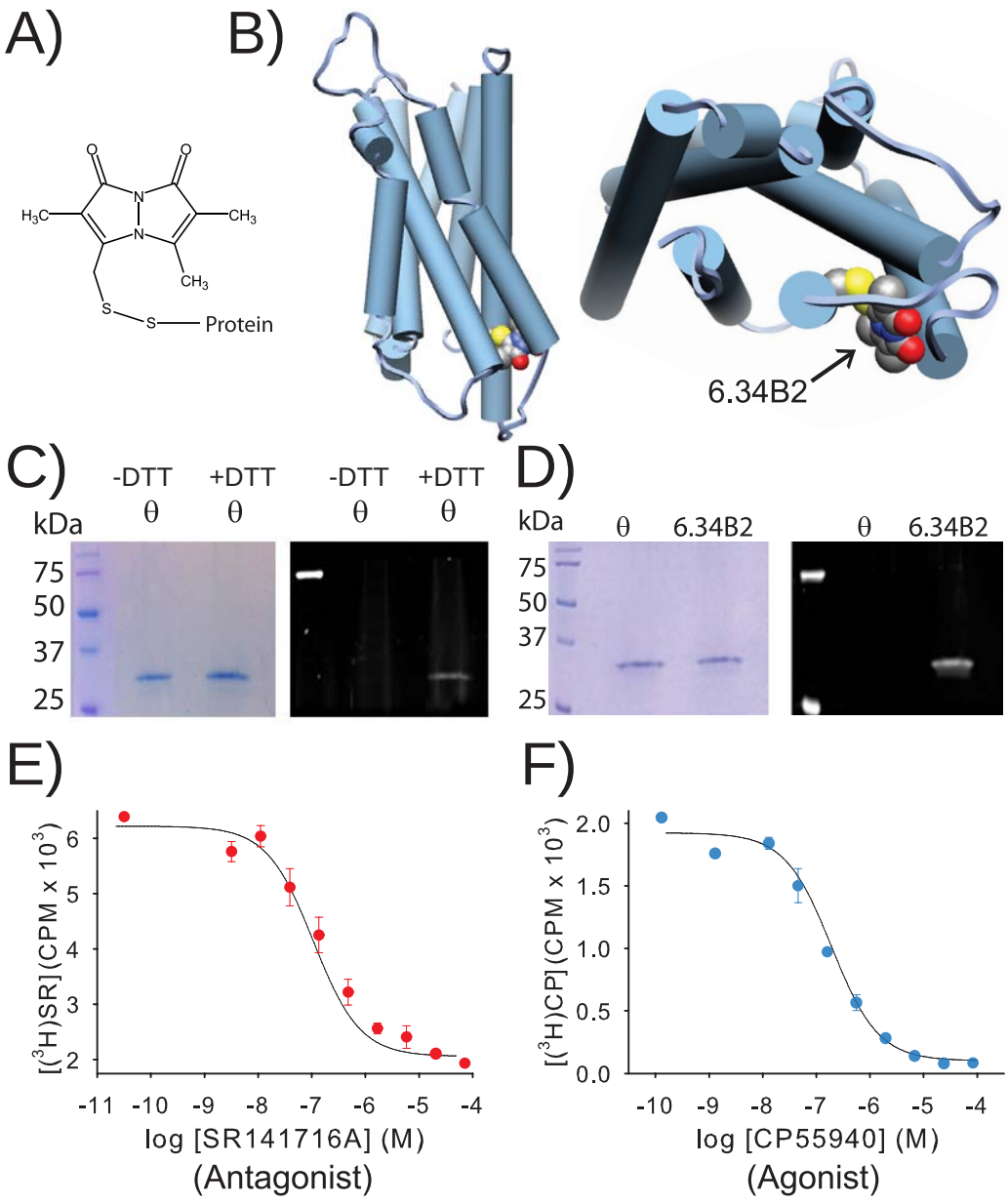
A)
B)
H3C
CH3
CH3
S
S
Protein
6.34B2
C)
-DTT
+DTT
-DTT
+DTT
kDa
θ
θ
θ
θ
75
50
37
25
D)
kDa
θ
6.34B2
θ
6.34B2
75
50
37
25
E)
[3H]SR](CPM x 10^3)
6
5
4
3
2
-11
-10
-9
-8
-7
-6
-5
-4
log [SR141716A] (M)
(Antagonist)
F)
[3H]CP](CPM x 10^3)
2.0
1.5
1.0
0.5
0.0
-10
-9
-8
-7
-6
-5
-4
log [CP55940] (M)
(Agonist)

FIGURE 3.1. A purified CB_1 receptor, specifically labeled with a bimane fluorophore at site 6.34 on TM6, can still bind agonist and antagonist. **(A)** The structure of PDT-bimane. **(B)** A model of CB_1 showing the probe covalently attached at A342C (C6.34) on the cytoplasmic face of TM6. **(C)** Coomassie stained SDS-PAGE gel (left) of purified minimal-cysteine construct mutant θ (which contains only C257 and C264). Ultraviolet irradiation of the same gel (right), before staining, shows that θ does not react with PDT-bimane unless it is first reduced with DTT, prior to labeling (note the bimane fluorescence in the DTT treated sample). This result provides direct chemical evidence that C257 and C264 are in a disulfide bond in CB_1. **(D)** (left) A Coomassie-stained SDS-PAGE gel showing that the immuno-purified CB_1 mutants θ and A342C/θ can be purified to homogeneity. (right) In-gel fluorescence of the same gel before Coomassie staining shows only the A342C/θ mutant exhibits fluorescence, indicating the bimane is uniquely and specifically covalently attached at A342C in TM6. The same purified, detergent solubilized, bimane-labeled A342C/θ from (D) is functional, as indicated by its ability to bind antagonist, SR141716A **(E)** and agonist, CP 55940 **(F)** in solution. Further details are provided in the Experimental Procedures.

Figure 3.2

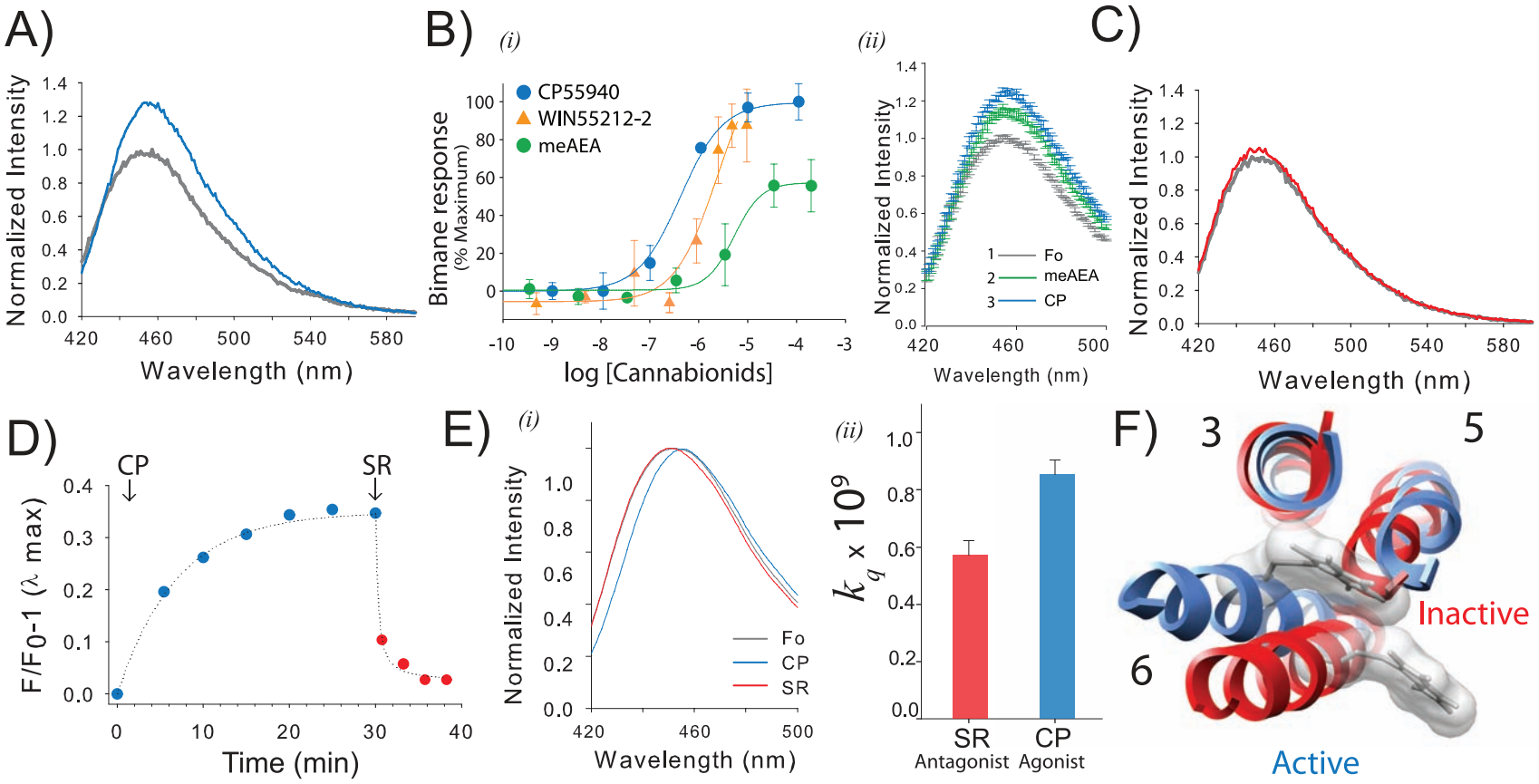
A)
Normalized Intensity
Wavelength (nm)
B)
(i)
CP55940
WIN55212-2
meAEA
Bimane response
(% Maximum)
log [Cannabionids]
(ii)
Normalized Intensity
1 Fo
2 meAEA
3 CP
Wavelength (nm)
C)
Normalized Intensity
Wavelength (nm)
D)
CP
SR
F/F0-1 (λ max)
Time (min)
E)
(i)
Normalized Intensity
Fo
CP
SR
Wavelength (nm)
(ii)
kq x 10^9
SR
Antagonist
CP
Agonist
F)
3
5
Inactive
6
Active

FIGURE 3.2. Agonist binding to CB_1 induces a conformational change that is detected by a probe at site 6.34 (or 342) on TM6. **(A)** The addition of agonist CP 55940 (CP) causes an ~35% increase in fluorescence intensity for PDT-bimane labeled mutant sample A342C/θ. The spectra, normalized to the apo state (Fo, gray), show before and after a 30 minute incubation with 10 μM CP 55940 (blue). **(B)** (*i*) The dose-response plot of the agonists (CP 55940, WIN55212-2 and meAEA) report the stimulated increase in fluorescence (data normalized to the maximum increase in fluorescence for CP 55940). The apparent EC_{50} are 430 ± 86 nM for CP, 3 ± 0.4 μM for WIN and 6.6 ± 4.0 μM for mAEA. The bimane dose response plots are the means of at least three independent experiments fit with a sigmoidal dose response function. (*ii*) The partial increase in fluorescence induced by meAEA addition (50 μM, green) is further increased by subsequent addition of CP 55940 (35 μM, blue). Each data point in the spectra show the range of the S.E.M. from three independent experiments. **(C)** In contrast to agonists, adding antagonist (5 μM SR141716A, red) has essentially no effect on the fluorescence compared to the ligand-free receptor (Fo, gray). **(D)** The agonist-induced increase in fluorescence (10 μM CP 55940, blue) occurs slowly, whereas subsequent addition of antagonist (5 μM SR141716A, red) causes a rapid reversal. **(E)** Agonist binding induces the probe to move into a more polar, solvent accessible environment, as indicated by: (*i*) the shift in the λmax of the normalized emission spectra (blue, 10 μM CP 55940; red, 5 μM SR141716A; gray, absence of ligands), and (*ii*) a comparison of the bimolecular quenching constants (*kq*) determined from the Stern-Volmer quenching experiments. Error estimates come from the least-squares fitting. **(F)** A movement of the probe on A342C into a more polar environment is consistent with the presumed location of the probe in CB_1 models based on rhodopsin in the inactive state (red, PDB: 1GZM) and active state (blue, PDB: 3DQB). For clarity, the figure only shows the probe and TM3, TM5 and TM6. See Experimental Procedures for more details.

Figure 3.3

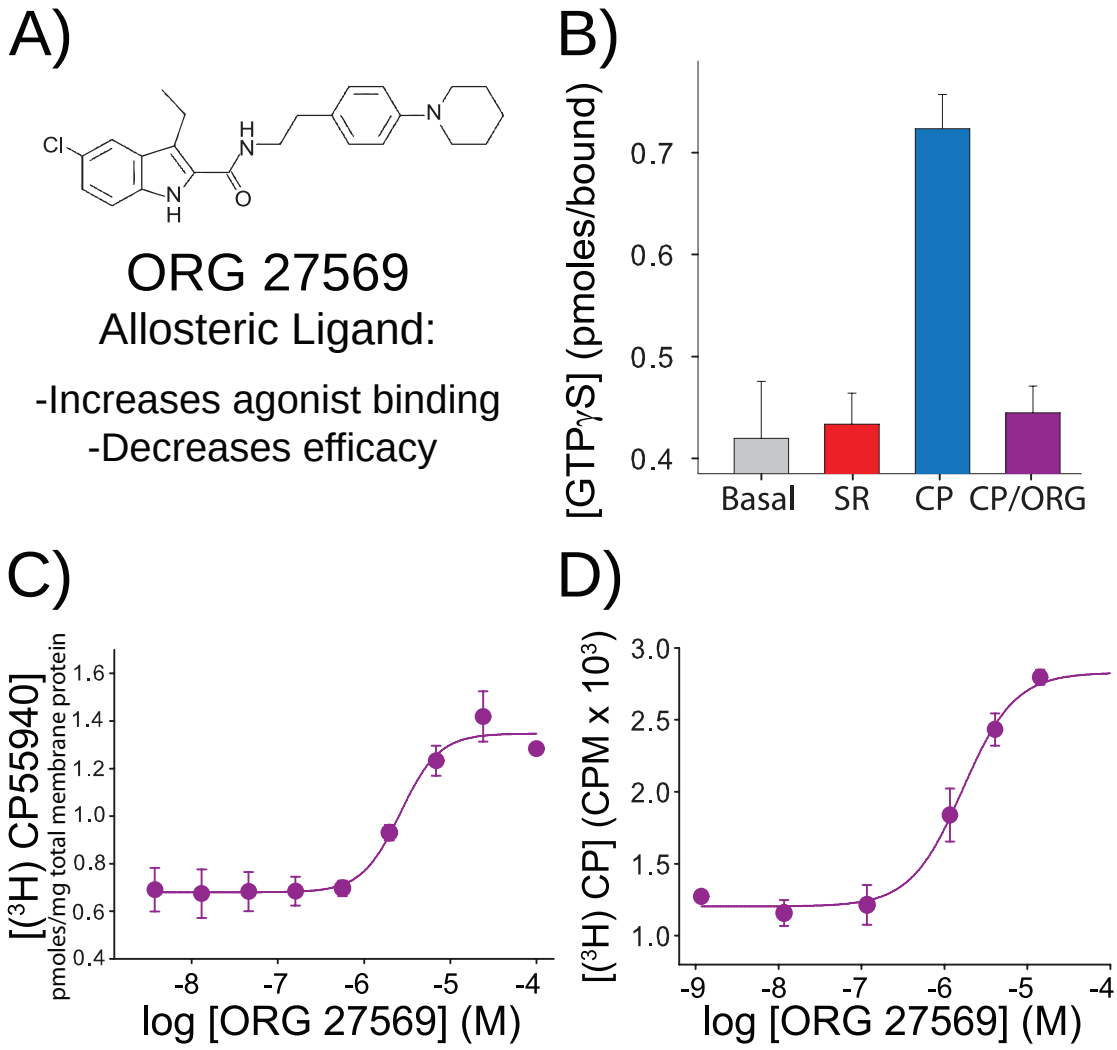
A)
Cl
H
N
N
H
O
N
ORG 27569
Allosteric Ligand:
-Increases agonist binding
-Decreases efficacy
B)
[GTPγS] (pmoles/bound)
0.7
0.6
0.5
0.4
Basal
SR
CP
CP/ORG
C)
[(3H) CP55940]
pmoles/mg total membrane protein
1.6
1.4
1.2
1.0
0.8
0.6
0.4
-8
-7
-6
-5
-4
log [ORG 27569] (M)
D)
[(3H) CP] (CPM x 10³)
3.0
2.5
2.0
1.5
1.0
-9
-8
-7
-6
-5
-4
log [ORG 27569] (M)

FIGURE 3.3. The allosteric CB_1 modulator Org 27569 enhances agonist (CP 55940) binding yet inhibits agonist-induced G protein activation. **(A)** Molecular structure of the allosteric ligand Org 27569. **(B)** The purified, detergent-solubilized bimane labeled CB_1 mutant A342C/θ is functionally active – it stimulates G protein activation upon addition of agonist (10 μM CP 55940, blue) as measured by GTPγS^{35} binding to purified $G\alpha_i\beta\gamma$. In contrast, no agonist ligand (gray bar) or antagonist (10 μM SR141716A, red bar) show less GTPγS binding. Allosteric ligand Org 27569 block G protein activation when added along with agonist (10 μM Org 27569 + 10 μM CP 55940, purple). Note that Org 27569 does not act as a traditional competitive antagonist, in fact it actually increases agonist binding ([^{3}H] CP 55940) to CB_1. We observed this phenomenon for CB_1 mutant A342C/θ **(C)** in membranes (EC_{50} for CP 55940 binding enhancement = 2.7 ± 0.7 μM), and **(D)** in a bimane-labeled, detergent solubilized, purified form (EC_{50} for CP 55940 binding enhancement = 1.9 ± 0.6 μM). Together, these results confirm that Org 27569 is not a competitive inhibitor for the orthosteric binding site. Moreover, panel (D) proves that Org 27569: i) binds to the purified bimane labeled CB_1 receptor, and ii) acts directly on the CB_1 receptor. All radioactive binding studies are representative of two independent experiments performed in duplicate, shown as mean ± S.E.M. The specific equilibrium binding of [^{3}H] CP 55940 in (C) and (D) were determined in the presence of various concentrations of Org 27569 compared to saturating amounts of cold CP 55940. The EC_{50} values were determined by fitting a variable slope sigmoidal dose-response function to the combined respective data sets, and errors were determined from least squares fitting. See Experimental Procedures for more details.

Figure 3.4

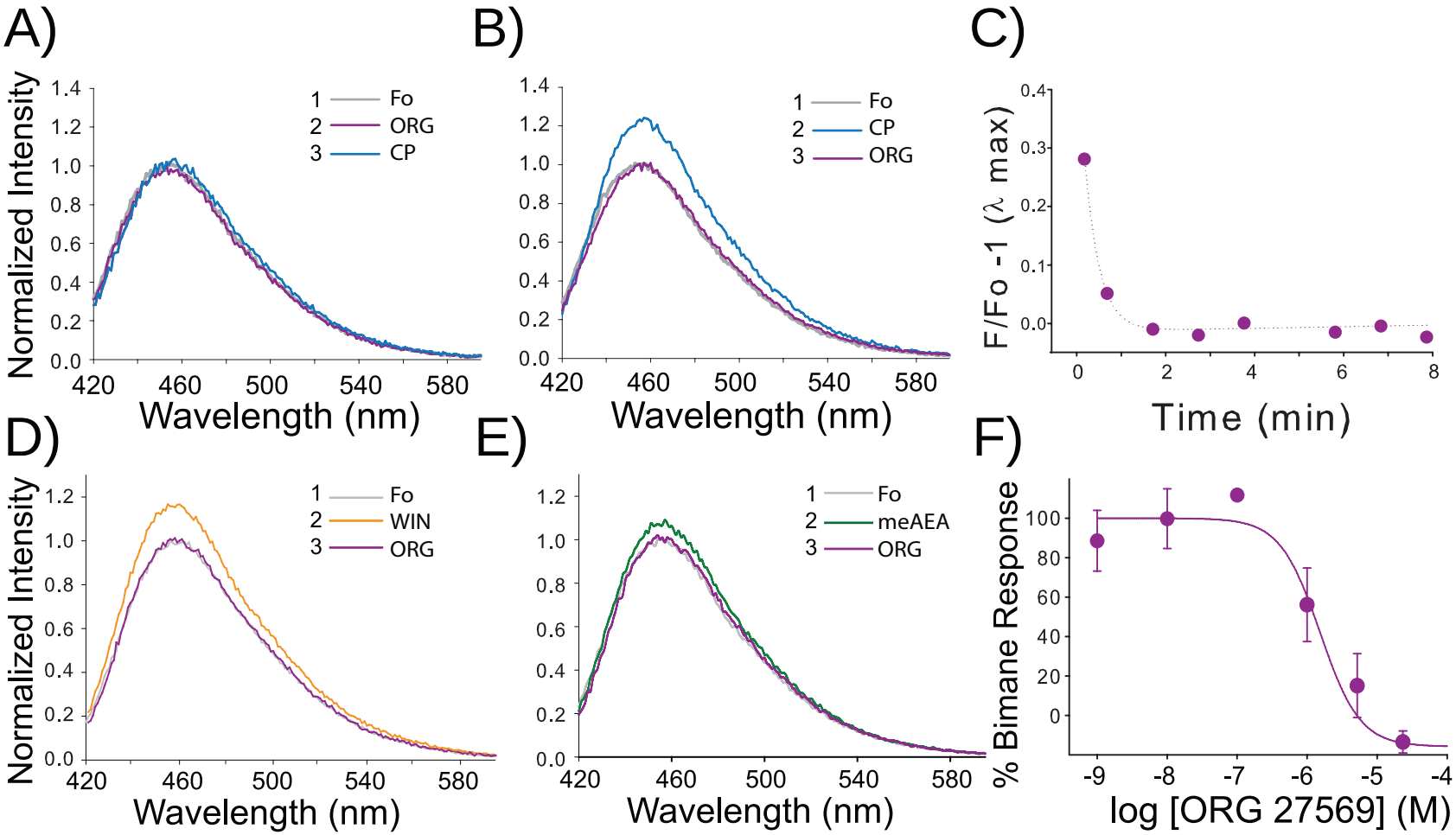
A)
B)
C)
D)
E)
F)
Normalized Intensity
Wavelength (nm)
1 Fo
2 ORG
3 CP
1 Fo
2 CP
3 ORG
F/Fo -1 (λ max)
Time (min)
1 Fo
2 WIN
3 ORG
1 Fo
2 meAEA
3 ORG
% Bimane Response
log [ORG 27569] (M)

FIGURE 3.4. The allosteric modulator Org 27569 inhibits agonist-induced TM6 movement in CB_1 detected by a fluorescent probe on site 342. The order in which indicated drugs were added is denoted by the number and compound (inset). Fo represents the ligand-free or apo state (gray). **(A)** Org 27569 impairs TM6 movements in CB_1. When Org 27569 is pre-incubated with the bimane-labeled CB_1 mutant A342C/θ (purple) for 30 min before adding agonist (10 μM CP 55940, blue), the agonist-induced fluorescence change for the bimane probe on TM6 (blue) is no longer observed. **(B)** Org 27569 can also reverse agonist induced TM6 movements. Adding Org 27569 (10 μM, purple) reverses the agonist (10 μM CP 55940) induced fluorescence increase in the bimane-labeled CB_1 A342C/θ mutant (blue). **(C)** The Org 27569 (5 μM) induced reversal seen in (B) is rapid; with a $t_{1/2} < 1$ min. Data is representative of one experiment performed more than 3 times. Org 267569 also reverses the fluorescence increase caused by CB_1 agonists **(D)** WIN55212-2 (10 μM, 30 min) and **(E)** meAEA (38 μM, 30 min). **(F)** Importantly, the dose-response plot for Org 27569 inhibition of agonist (CP 55940) induced TM6 movement (stimulated increase in fluorescence, $EC_{50} = 2.2 \pm 1.2$ μM) matches the dose response for Org 27569 enhancement of agonist CP 55940 binding (shown in Figure 3.3D). The bimane dose response plot represents the mean of two independent experiments. All spectra are background subtracted from buffer and ligands, and are normalized to the background-subtracted emission for the bimane-labled mutant CB_1 in the apo form (Fo, gray). For comparison, the data for the Org 27569 enhancement of fluorescence was normalized to the maximum increase in fluorescence. Further details are provided in the Experimental Procedures.

Figure 3.5

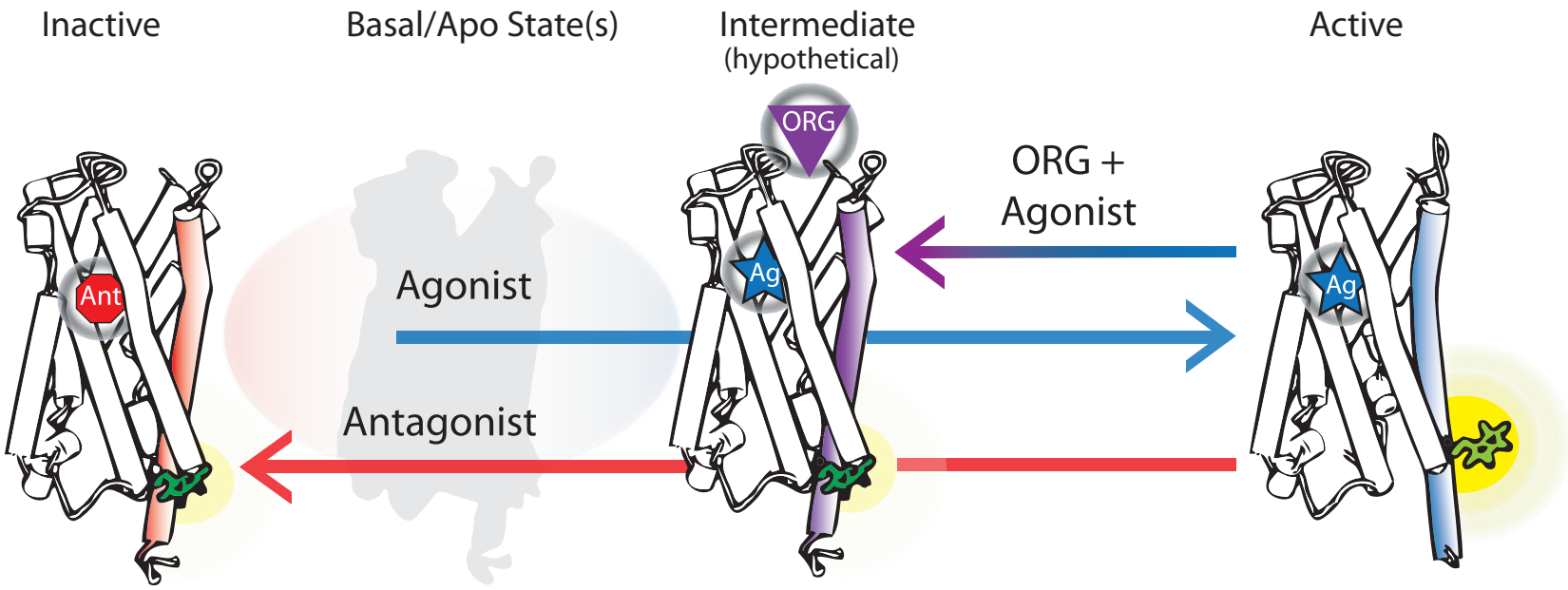
Inactive
Basal/Apo State(s)
Intermediate
(hypothetical)
Active
ORG
ORG +
Agonist
Ant
Ag
Ag
Agonist
Antagonist

FIGURE 3.5. Cartoon model proposing that discrete CB_1 receptor structures are induced by a bound agonist, antagonist or agonist plus allosteric ligand. The model suggests that occupation of the traditional (orthosteric) binding site by an agonist alone (Ag, right) accompanies a conformational change in TM6 (blue), detected as an increase in fluorescence from an attached bimane probe (green). In contrast, antagonist alone binding (Ant, left) causes no change in TM6 (red). When the allosteric ligand Org 27569 (ORG) binds to its (currently unknown) site on an agonist-bound CB_1, the conformational change in TM6 (purple haze) is either blocked or reversed. This model proposes that ORG binding traps a distinct and different agonist-bound CB_1 structure, which may be a structural intermediate on the pathway to full receptor activation. The basal (ligand free) CB_1 state is depicted in light gray.

Supplemental Figures

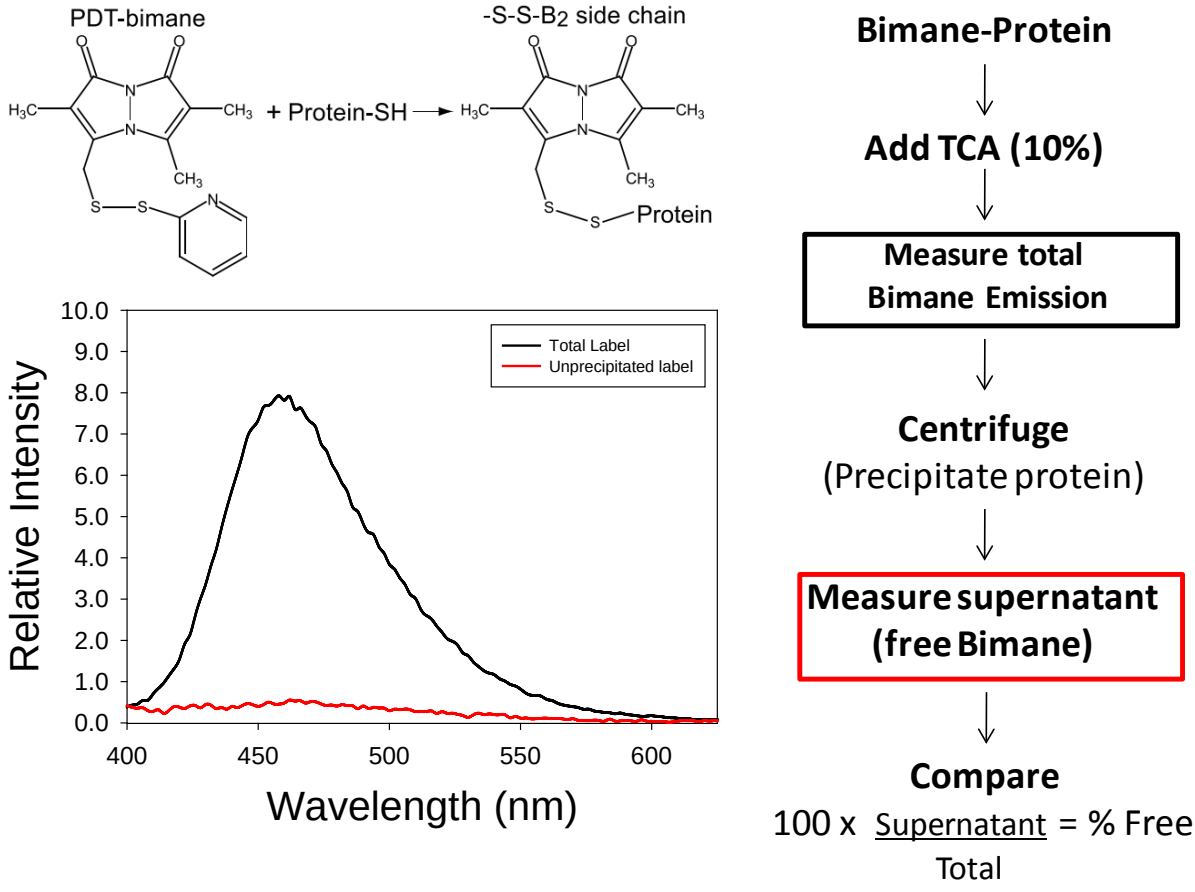

Figure 3.S1. Essentially no-free label is present in our bimane labeled CB_1 samples. Above, PDT-bimane reaction scheme. Right, a flow chart depicting the TCA precipitation method for testing the presence of free label. Bottom left, bimane emission spectra of the sample before (black) and after TCA precipitation (red). Note that nearly all of the bimane fluorescence is lost in the supernatant after protein precipitation and removal of the sample by centrifugation, indicating that most of the bimane is indeed attached to protein and thus precipitates. For more details see Experimental Procedures.

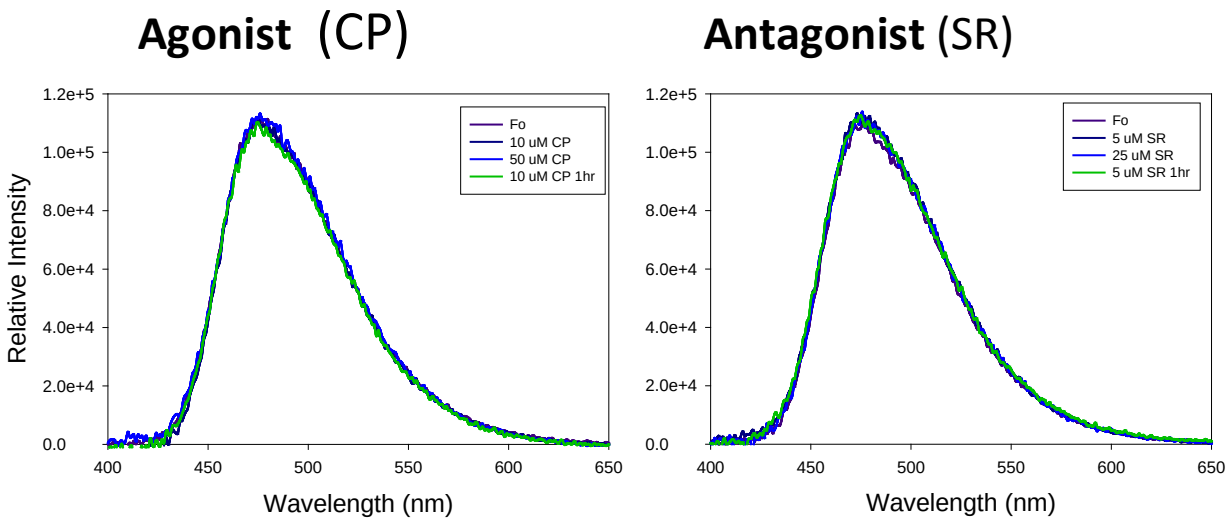

Figure 3.S2. **The CB_1 ligands CP 55940 and SR141716A do not alter (quench or enhance) bimane fluorescence**. This control experiment tested the effect of various concentrations of agonist (CP 55940) and antagonist (SR141716A) on bimane fluorescence emission. Bimane emission spectra were collected on a sample of 200 nM PDT-bimane labeled L-cysteine in buffer in the presence of various ligand concentrations (as indicated in the figure, inset). All spectra were background subtracted from buffer and ligands. The data above clearly show that the ligands alone do not affect or alter bimane fluorescence, thus the fluorescence changes observed for bimane-labeled CB_1 are due to conformational changes in the receptor induced by the ligands.

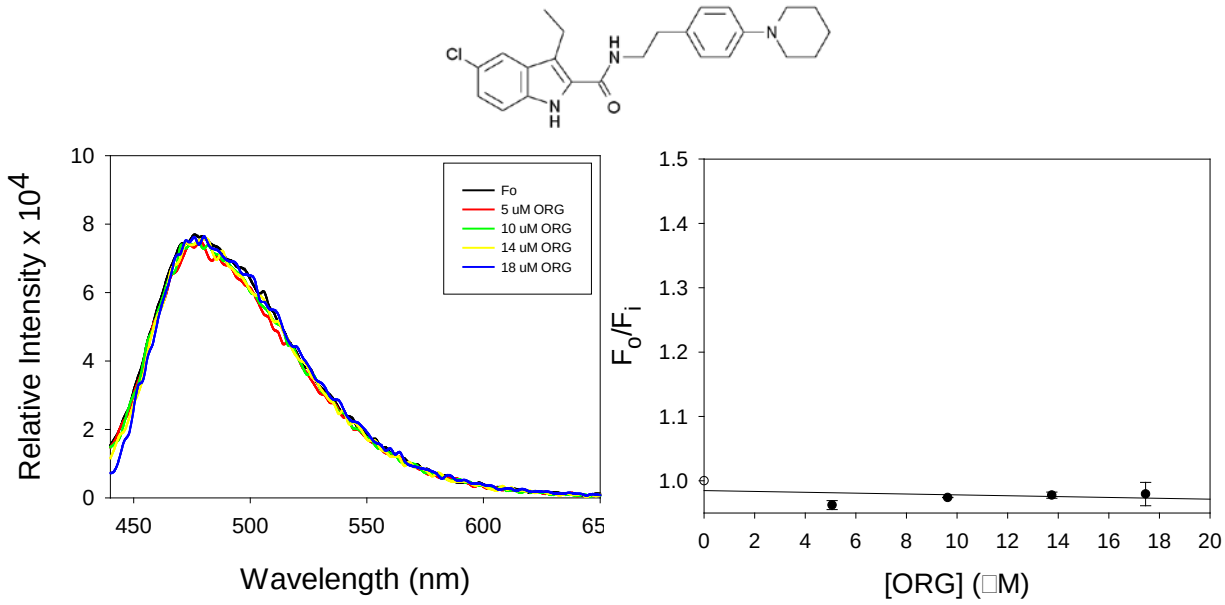

Figure 3.S3. Org 27569 does not quench or enhance free bimane fluorescence. This control experiment demonstrates that Org 27569 (structure above) does not affect the fluorescence of free bimane. The data show no effect of increasing concentrations of Org 27569 on free bimane fluorescence (200 nM PDT-bimane reacted with L-cysteine in buffer), indicating that Org 27569 does not directly interact with bimane to change its fluorescence, at least under the concentration range used in our experiments. All spectra were background subtracted from buffer and ligands.

Chapter 4

Extracellular cysteine residues in the N-terminus of human neuronal cannabinoid receptor allosterically regulate ligand affinity

Jonathan F. Fay[1] & David L. Farrens[1]

[1]*Department of Biochemistry and Molecular Biology, Oregon Health and Science University, Portland, Oregon 97239*

4.1: SUMMARY

The human cannabinoid receptor, CB_1, like all G protein-coupled receptors (GPCRs), is an intrinsically dynamic membrane protein that transduces signals across the cell membrane. Here we explore a potential role for the CB_1 N-terminus. Specifically, we investigated if there is an extracellular disulfide bond in the N-terminus, and if so, what role it might play in ligand binding. Our results provide evidence that the conserved cysteine residues C98 and C107 do form a disulfide in the N-terminus, and regulate ligand binding in a way that can be quantitatively analyzed by an allosteric model. These results provide insight into how the CB_1 N-terminus and extracellular loop two act together to form a high-affinity orthosteric ligand binding site.

All of the experiments and data analysis reported in this chapter were performed by the author of this dissertation.

4.2: INTRODUCTION

The cannabinoid receptor, CB_1, is a G protein-coupled receptor (GPCR) found in high concentrations in the central nervous system [185]. CB_1 has been shown to mediate neurotransmitter release in pre-synaptic terminals [92, 240, 241], by coupling with G_i or G_o proteins, which then inhibit adenylate cyclase [17, 177], N- and P/Q-type calcium channels [93], and activate A-type inwardly rectifying potassium channels [94]. These modulations have been shown to modulate the amplitude or frequency of neurotransmission and thus presumably the psychotropic affects known to accompany cannabis use.

Here we focused on the CB_1 N-terminus (Figure 4.1). The role of this relatively long (~110 amino acids) extracellularly located N-terminus has been puzzling, because endogenous and synthetic CB_1 ligands are lipophilic, and are thus likely partitioned into the membrane. As summarized below, to date the role of this region and its contribution to ligand binding and/or receptor stability is still unclear.

Sequence analysis indicates the CB_1 N-terminus contains two putative N-linked glycosylation sites (N77 and N83), but these residues are apparently <u>not</u> required for efficient translocation to the plasma membrane, and their absence does not alter agonist (CP 55940) binding [34]. Truncation of the first 63 residues in CB_1 has been reported to have no dramatic effect on binding the agonist CP 55940 [34], and we also find truncation of the N-terminus even up to residue 103 has no apparent effect on agonist, antagonist or G protein activation (see Results). It should be noted that the CB_1 membrane proximal region (at residue 113) of the amino terminus does appear to be critical for binding of agonist (CP 55940) but not antagonist (SR141716A), based on the

negative effect observed in dipeptide insertions studies [242]. Furthermore, truncation of the N-terminus, or addition of a signal sequence has been shown to increase cell surface expression of CB_1 [34].

One aspect of the CB_1 N-terminus that has been intriguing is the presence of two cysteines, at residue number 98 and 107, that are highly conserved across N-termini of CB_1 from mammals, birds, fish, and amphibians (Figure 4.1A). Previous studies (including our own) have found no obvious consequence of mutating these residues (to alanine or serine) on agonist and antagonist binding, or G protein activation [199, 221]. Thus, it has been surmised that no crucial disulfide bridge exists between these two cysteines, and their role has remained a mystery. Because of the above anomalies, and some accidental discoveries on our part (*vide infra*), in the present work we carried out structure/function studies of the CB_1 N-terminus, focusing on assessing if two conserved cysteine residues found in the N-terminus of CB_1 might play a heretofore unappreciated role. Specifically, we investigate if these two residues can form a disulfide, and if so, what functional role it may play in forming and stabilizing the orthosteric ligand binding pocket of CB_1.

4.3: EXPERIMENTAL PROCEDURES

4.3.1 Buffers. The definitions for buffers are: PBSSC [0.137 M NaCL, 2.7 mM KCl, 1.5 mM KH_2PO_4, 8 mM Na_2HPO_4]; Hypotonic Bufffer [5 mM Tris·HCL, 2 mM EDTA, PIC, pH 7.5]; TME [20 mM Tris·HCl, 1 mM EDTA, 5 mM $MgCl_2$, pH 7.4]; Rat A [320 mM sucrose, 2 mM Tris·EDTA, & 5 mM of $MgCl_2$]; and Rat B: [50 mM Tris·HCl, pH 7, 2 mM 2 mM Tris·EDTA & 5 mM $MgCl_2$].

4.3.2 Expression and membrane preparations of shCB_1 *genes in COS-1 cells.* Expression and membrane preparations of shCB_1 genes occurred in COS-1 cells utilizing transient transfection methods as previously described previously [199] .

4.3.3 Purification of C2 and C2/Nt2 – labeling and SDS-PAGE gel shift. Purification, labeling, and SDS-PAGE analysis was performed as described previously in Chapter 3. In brief, CB_1 constructs were purified using a one-step immunoaffinity approach. While bound to the column samples were either subjected to a 20 fold molar excess of PDT-bimane (or not) prior to elution and SDS PAGE analysis in the absence or presence of reducing agent DTT. At least two separate gels were loaded to confirm the curious gel-shift initially observed.

4.3.4 Membrane preparations of Rat cannabinoid receptors. Rat cortices were purchased from Pel Freeze Biologicals (Rogers, AR) and membrane preparations were performed as previously described [12]. Briefly: 6 g of cortices were homogenized in 45 ml of Rat A and centrifuged (1600 x g for 10 min), washed twice as above, and combined supernatant fractions were centrifuged at 39,000 x g for 15 min. The resuspended pellet (RAT B, 90 mls) was incubated at 37°C for 10 min, and subsequently centrifuged at 11,000 x g for 15 min whereupon the pellet was again resuspended in Rat B, and incubated at 30°C for 40 min. Final centrifugation occurred at 11,000 x g for 15 min and pellets were homogenized to suspension in TME aliquoted, snap frozen and stored at -80°C until use. Protein concentration was determined using the modified DC protein assay kit (Bio-Rad).

4.3.5 DTT treatment. Membrane preparations containing receptor protein were diluted to 4.4 mg/ml of total protein. Importantly, samples were passed through a 24 gauge

needle 5 times and allowed to sit on ice for 1 hour prior to treatments. Treatments consisted of diluting membrane preparations to 2.2 mg/ml in various concentrations of DTT (0-300 mM) and allowing the treated samples to nutate at room temperature for 20 min. Pretreated membranes were then immediately used for equilibrium binding studies.

4.3.6 Ligand binding studies. The ligand binding experiments were carried out as previously described [199]. Data was globally fit and error estimates for the parameters were derived from least square fits. All radioactive binding experiments were performed at least twice in duplicate, unless otherwise indicated. Additionally, an allosteric two-site model (equation **4.1**), described previously [155], was used to fit our data:

$$Fraction\ Bound = \frac{[A]\left(1+\frac{\alpha[B]}{K_{B2}}\right)}{[A]\left(1+\frac{\alpha[B]}{K_{B2}}\right)+K_A\left(1+\frac{[B]}{K_{B1}}+\frac{[B]}{K_{B2}}\left(1+\frac{\beta[B]}{K_{B1}}\right)\right)} \qquad (\mathbf{4.1})$$

where R denotes the receptor; A denotes the orthosteric ligand and B denotes the allosteric ligand. The K_A, K_{B1} and K_{B2} are the dissociation constants where the subscript B1 and B2 represent the two sites that the allosteric ligand can interact with, orthosteric site and allosteric site, respectively. The cooperativity factors, α and β, denote the allosteric interaction between A and B or between the two molecules of B.

4.4: RESULTS

Below we describe relatively simple observations that led us to re-examine the possible existence of, and role for, a disulfide between C98 and C107 in the CB_1 N-terminus (see Figure 4.1B). As mentioned in the Introduction, we were able to confirm previous reports that deletion of the N-terminus has no dramatic, obvious role on ligand binding to CB_1. As shown in Figure 4.2, we find that a mutant in which the first 102

residues are truncated (Δ103) still exhibits wild-type like binding to agonist (CP 55940) and antagonist (SR141716A). In addition, the Δ103 deletion mutants can still elicit G protein activation (Figure 4.S1). These results clearly demonstrate, the N-terminal region of the receptor is not required and does not have an obvious role in the binding of synthetic high-affinity ligands.

During our previous work developing optimal conditions for preparing a stable, pure CB_1 (Chapter 2 and 3), we made an interesting observation. As anticipated, a purified CB_1 construct, which contains only 2 cysteine residues 257 and 264 (termed C2, or θ in Chapter 3) was not reactive to thiol reactive fluorophores (Figure 4.3A). This was expected, because these two cysteines in extracellular loop two (EL2) are thought to be in a disulfide bond. One intriguing aspect of CB_1 is that it has this disulfide bond, instead of the canonical disulfide bridge connecting EL2 to transmembrane helix 3 present in most Class A GPCRs.

We found that a second construct, which also contained N-terminal cysteines 98 and 107, in addition to C257 and C264 (called Nt2/C2), also showed no bimane labeling (Figure 4.3B). Of course, the lack of labeling of the two N-terminal cysteines in Nt2/C2 does not prove or disprove they are in a disulfide, as they may simply be structurally inaccessible to the label. These results were intriguing enough, however, for us to look further into the possibility that C98 and C107 form a disulfide in the N-terminus.

We hypothesized we might detect evidence for a disulfide between the Nt2 cysteine residues as a gel shift under non-reducing SDS-PAGE conditions. Thus, we compared the mobility of C2 versus Nt2/C2, by running the samples both with and without reducing agent. The results show dithiothreitol (DTT) caused the purified

Nt2/C2 receptor to run more slowly, similarly to its C2 counterpart (Figure 4.3C), supporting the possibility of an N-terminal disulfide which potentially imparts structure and/or stability to the CB_1 receptor.

Encouraged by these results, we turned to assessing what functional effect cleaving this putative disulfide might have on ligand binding. To do this, we used a traditional membrane binding approach, and monitored the effects of DTT on ligand binding to 'Wt' CB_1 (shCB1-C13) receptors expressed in COS-1 cells (Table 4.1). In our COS-1 expression system, the changes appeared to reflect K_d changes and B_{max} changes. However, in rat membranes there was an increase in B_{max} and not K_d (Table 4.2). We were unsure how to interpret these findings, and instead decided to explore this phenomenon using a different approach.

We reasoned that the changes imparted by reducing the putative N-terminal disulfide bond might only subtly modulate ligand binding, since clearly the whole N-terminus has no extreme effect. Therefore, we next systematically monitored binding of both agonist and antagonist as a function of DTT, using transiently expressed shCB1-C13 receptors in COSH-1 cells (Figure 4.4A). These results show that DTT causes a decrease in agonist binding, while surprisingly, causing a concomitant increase in antagonist binding (Figure 4.4A). To test if this reduction-dependent effect involved the two cysteines residues in the N-terminus, we mutated them to alanine (C98A and C107A) in a shCB1-C13 background (termed C11). As seen in Figure 4.4B, the C11 mutant does not show the DTT dependent increase and decrease in antagonist and agonist binding, only the decrease in both at very high DTT concentrations. We also confirmed that these results were not simply an artifact of our transient expression system, by testing if this

effect occurs in native cannabinoid receptors in rat cerebral cortex, and found a similar behavior (Figure 4.4C).

In all cases, higher DTT concentrations abolish binding of both ligands. The likely cause for the loss in binding at the higher DTT concentrations is the reduction of the disulfide bond between 257 and 264, in EL2, as this disulfide is required for function CB_1 ligand binding [199, 221]. To confirm this, we tested the effect of DTT on our previously characterized shCB1-C2 mutant [199] and found it behaves in a manner similar to shCB1-C11 (Figure 4.S2). These results are consistent with the interpretation that the C257/264 disulfide bond in EL2 confers stability to the CB_1 receptor orthosteric site. Importantly, the C257/264 disulfide requires a high concentration of DTT before ligand binding is effected, indicating that it likely exists in a more inaccessible region and/or is more readily reversible. Interestingly, TCEP treatment did not appear to effect antagonist binding, perhaps due to its larger size and/or higher solubility (Figure 4.S3), again supporting the presumably inaccessible location of the C257/C264 disulfide.

The behavior seen in Figure 4.4 is highly indicative of an allosteric effect, in which reducing the allosteric N-terminal disulfide imparts either positive or negative cooperativity to the orthosteric (antagonist or agonist) ligand binding site. Thus, we tested if an allosteric two-site model could be used to quantify and interpret these results [155]. This model is represented in a structural cartoon from in Figure 4.5A and schematically in Figure 4.5B. The model presumes that the DTT dependent enhancement/decrease of binding at the N-terminal disulfide is the “other site” (i.e., allosteric), whereas the disulfide in EL2 makes up part of the orthosteric site, as it is known that the EL2 disulfide is required for orthosteric ligand binding [199, 221]. It is

important to note that in this two-site model, DTT is not binding to these sites in a traditional sense, but rather, acting by modifying/interacting with these two sites in a manner that can be interpreted (for the case of this model) as 'binding.'

We began the modeling by using the C11 data to first isolate and evaluate the properties of the C257/264 disulfide, since the suspected 'allosteric effect' disulfide in the N-terminus (between C98 and C107) is absent in the C11 construct. We began by fitting the C11 data with the following equation (**4.1**), derived from the scheme shown in Figure 4.5:

$$Fraction\ Bound = \frac{[A]\left(1+\frac{\alpha[B]}{K_{B2}}\right)}{[A]\left(1+\frac{\alpha[B]}{K_{B2}}\right)+K_A\left(1+\frac{[B]}{K_{B1}}+\frac{[B]}{K_{B2}}\left(1+\frac{\beta[B]}{K_{B1}}\right)\right)} \qquad (\mathbf{4.1})$$

where A is the orthosteric ligand (agonist CP 55940 or antagonist SR141716A) and B is the allosteric ligand (in this case DTT). The K_A, K_{B1} and K_{B2} are their respective dissociation constants. The subscript B1 and B2 represent the two sites that can interact with the allosteric ligand. To reiterate, for the purposes of our model, B1 is defined as the 'orthosteric effect' (C257/264 disulfide) and B2 the 'allosteric effect' (C98/107 disulfide). The cooperativity factor, α, denotes the allosteric interaction between A and B. The cooperativity factor, β, denotes allosteric interaction between the two different orthosteric and allosteric effect disulfides. Note that cooperativity values greater than 1 denote positive cooperativity (increased affinity), values less than one denote negative cooperativity (decreased affinity), and values equal to one are neutral.

We first fit out C11 data by restricting K_{B2} to a very low dissociation value (to reflect its absence – and 'permanently reduced state'). This enabled us to determine the

K_{B1} from our fits. We then used this K_{B1} value (57 mM) to enable determination of the K_{B2} value for the C13 construct data. The fits of C13 indicated a dissociation constant for the allosteric site (K_{B2}) of 2.5 mM.

The cooperatively factor, α, provides DTT dependent positive and negative cooperativity values of 1.85 for antagonist and 0.77 and agonist binding, respectively. In comparison, the cooperativity factor, β (the interaction between the two sites), was found to be neutral. This model appears to fit our finding with coefficient of determination values greater than 0.85 (Figure 4.5 and Table 4.3).

Although not perfect, this two-state model provides a unique way to conceptualize and quantify our novel data. The fits indicate that there is either positive or negative cooperativity (α) imparted on the orthosteric ligand by modulation of the 'allosteric effect' disulfide in the N-terminus. One important caveat of our data is that dissociation values derived from our fits are most likely dependent on the experimental conditions (time, temperature, concentration, etc.). Formally, these data could also be fit with a dimer/oligomer model, but we have not yet done so. The implications of this model are discussed in greater detail below.

4.5: DISCUSSION

Our data suggest that the N-terminus of CB_1 can affect the ligand binding properties of the receptor, although in a subtle and previously unappreciated way. Specifically, our data indicate that an intramolecular disulfide can occur in the N-terminus, and this disulfide can stabilize a more compact structure and/or confer denaturation resistance to CB_1 (as shown in Figure 4.2). The N-terminal disulfide

appears susceptible to DTT. Most interestingly, binding data showing the mediating effects of DTT can be fit to a two-site allosteric model (Figure 4.5), where breaking of the C257/264 disulfide in EL2 at high DTT concentrations obliterates the orthosteric binding site. The effect of breaking the C257/C264 disulfide in EL2 is consistent with previous studies that find mutation of one or both of these cysteine residues to a sereine or alanine is detrimental to the stability of the orthosteric ligand binding site [199, 221]. At lower DTT concentrations, it appears that cleaving the N-terminal disulfide (the 'allosteric effect' disulfide) with DTT imparts either positive or negative cooperativity (α) on the orthosteric ligand binding site – with respect to antagonist or agonist respectively. Importantly, these values can be quantified by using the allosteric two-site model, thus providing affinities and cooperativity factors (Table 4.3 and Figure 4.5).

In our model (Figure 4.5A and B) the cooperativity factor, α, defines how the K_{B2} site affects the orthosteric site. For instance, an α of 1.85 would give a 1.85 fold enhancement in affinity. This was as expected when antagonist binding studies were conducted in the presence or absence of a fixed concentration of DTT (Table 4.1). For agonist binding we would expect the determined cooperativity factor ($\alpha = 0.77$) to impart a higher K_d , however, we observed the opposite (Table 4.1). This observation may be further complicated by the presence of the G protein. At the present moment, we do not have a good explanation for this discrepancy.

Interestingly, the higher fractional occupancy observed for our C11 constructs is in agreement with the lower K_d values observed in the presence of 10 mM DTT (Figure 4.5 and Table 4.1). Based on the K_{B1} and K_{B2} values determined from the model (Table 4.3), we find the EL2 disulfide (K_{B1}) has an approximately 20-fold higher dissociation

constant than the N-terminal disulfide (K_{B2}). This would suggest that loop E2 is less accessible to reducing agents than the N-terminal disulfide.

What insights do these data and analysis provide about the role of the CB_1 N-terminus? One can use these data to speculate that the N-terminus couples to the orthosteric site, perhaps because (as depicted in our model in Figure 4.6) part of the N-terminus forms a 'lid' over the orthosteric binding site.

Note that the two disulfides in CB_1 (Nt and EL2) do not appear to be coupled, as the cooperatively factor that governs their interaction is neutral (i.e., β does not significantly deviate from 1). In other words, the reduction of one disulfide does not seem to enhance or diminish the reactivity of the other. The near neutral cooperativity factor suggests that breaking of the N-terminal disulfide produces only subtle structural changes. This could mean that either these changes confer equal protection to the EL2 disulfide, or EL2 is so buried that it is inaccessible to DTT whether or not the N-terminal disulfide is reduced.

Precedence for an inaccessible disulfide in EL2 of a GPCR has been observed in rhodopsin; the highly conserved disulfide between EL2 and TM3 is completely buried and inaccessible to reducing agents (in the absence of denaturants) [243]. Furthermore, this interpretation is not necessarily at odds with our gel-shift data, as denaturing conditions may enhance the observed difference and the EL2 disulfide seems to be only accessible to high concentration of DTT. Indeed, FSEC analysis suggest that samples with and without N-terminal disulfides under non-reducing conditions provide nearly identical elution profiles, however, the sensitivity of our setup may not be able to distinguish between these subtle differences, especially in mild

detergents (see Chapter 2).

Our findings clearly suggest that addition of the reducing agent, DTT, can act on N-terminal cysteines in CB_1. In doing so, DTT appears to allosterically regulate the binding characteristic for the orthosteric site on CB_1 for agonist and antagonists in a reciprocal manner. Intriguingly, this reciprocity is illustrated by the cooperativity factors – for instance, the inverse of the positive cooperatively value for antagonist binding ($\alpha_{SR}^{-1} = 0.54 \pm 0.35$) is close to the negative cooperative for agonist binding ($\alpha_{CP} = 0.77 \pm 0.12$). It is also reasonable to assume the converse effects may exist, where agonist binding is enhanced by the presence of an N-terminal disulfide, and antagonist specific binding is reduced by the presence of an N-terminal disulfide.

The disulfide in the CB_1 N-terminus, suggested by our data may play several roles. It may serve as a switch linking between distant cysteines, into constrained positions, leading to a subtle conformational and functional states in the receptor. These results also indicate that the N-terminus of CB_1 can allosterically regulate the orthosteric binding site of CB_1 in a subtle way, which may help explain its highly conserved nature, yet still unclear role.

The N-terminal disulfide in CB_1 could also act to help stabilize CB_1's N-terminus, which in turn could act as a domain over loop E2 in CB_1. A similar role for the N-terminus has been proposed for rhodopsin, where disulfide bonds engineered to constrain the N-terminus yield a receptor with enhanced thermostability [106]. Similarly, destabilizing mutations in loop E2 lead to reduced rhodopsin thermostability [105]. Such effects have also been observed for other GPCRs. Altering the position/flexibility of loop E2 by disulfide engineering impairs orthosteric ligand binding in the M2 receptor [107],

and ligand specific loop E2 conformations have also been observed in the B2AR [99]. Moreover, reactivity studies on the angiotensin II receptor support ligand specific domain coupling between the N-terminus and EL2 [100]. One can envisage a similar domain coupling between the N-terminus and EL2 of CB_1, where reduction of the exposed N-terminal disulfides can perturb the N-terminal domain structure and thus the entire conformational landscape of the extracellular domain. Moreover, similar enhancements of ligand binding by DTT have been previously observed for the angiotensin II GPCR [244]. In contrast, some chemokine receptors also contain an extra cellular disulfide, though in this case, mutations of these cysteines appears to inhibit chemokine binding [245] suggesting they play an important structural role in maintaining ligand binding site [246]. Interestingly, the matabatropic glutamate and calcium sensing receptors have been reported to have intermolecular disulfides between receptors [247, 248], but we so far have no evidence for this in CB_1.

Finally, it is tempting to speculate that the N-terminal disulfide in CB_1 could act as a redox sensor. Redox-dependent structural switches have been observed in other proteins, for example OxyR, INAD, and angiotensinogen [249]. For the case of CB_1 such a switch could be subtle and result in a minor allosteric modulation of the receptor ligand affinity, thereby altering receptor ligand occupancy and changing the ‘set point’ at which it can respond to endogenous signals.

One can envisage such a redox sensor playing a neuroprotective role for CB_1. Traumatic brain injury has been shown to release endocannabinoids in addition to reactive oxygen intermediates [187, 250]. Taken together, such a redox-switch could potentially enhance CB_1 receptor ligand occupancy and in part modulate the

neuroprotective role of CB_1 activation.

The antioxidant tripeptide glutathione (GSH) can be released from neurons in a depolarization-dependent fashion [251] and has been shown to play a role in modulation of excitatory neurotransmission [252] similar to endocannabinoids [253]. Thus, GSH release may be a way to locally regulate presynaptic CB_1 receptor 'set points.' Moreover, impaired GSH homeostasis or increase in reactive oxygen species is associated with diseases [254] that coincide with CB_1 receptor associated disease states, including Parkinson's and Alzheimer's [185] . The importance of the disulfide bond-mediated redox sensitivity in normal and diseased states has implications in the development of antioxidant-based therapeutic approaches and warrants further exploration.

Whatever their ultimate role, our data suggest the extracellular cysteine residues in the N-terminus of CB_1 may be more important than previously thought, and may confer a physiological role in the receptor response to environmental stress. This possibility should spark further investigation.

Table 4.1: K_d and B_{max} values of [^{3}H]CP 55940 and [^{3}H]SR141716A binding and B_{max} values from shCB1-C13 receptor transiently expressed in COS-1 cells[a].

[DTT]	CP 55940 K_d (nM)	CP 55940 B_{max} (pmoles/mg total protein)	SR141716A K_d (nM)	SR141716A B_{max} (pmoles/mg total protein)
10 mM	4.4 ± 1.2	3.3 ± 0.3	7.2 ± 0.7	18.9 ± 1.9
0 mM	9.8 ± 2.5	10.6 ± 1.3	14.1 ± 1.0	24.3 ± 1.7

[a] Competitive Displacement binding assays were performed, and K_d and B_{max} values were calculated as described in Experimental Procedures. Data represents the mean ± the S.E.M. of at least two independent experiments each performed in duplicate.

Table 4.2: K_d and B_{max} values of [^{3}H]CP 55940 and [^{3}H]SR141716A binding and B_{max} values from cannabinoid receptors found in Rat Cerebral Cortex[a].

[DTT]	CP 55940 K_d (nM)	CP 55940 B_{max} (pmoles/mg total protein)	SR141716A K_d (nM)	SR141716A B_{max} (pmoles/mg total protein)
10 mM	2.6 ± 0.3	2.9 ± 0.0	4.9 ± 0.6	7.0 ± 0.8
0 mM	2.6 ± 0.1	3.7 ± 0.2	5.5 ± 0.2	4.5 ± 0.0

[a] Competitive Displacement binding assays were performed, and K_d and B_{max} values were calculated as described in Experimental Procedures. Data represents the mean ± the S.E.M. of at least two independent experiments each performed in duplicate.

Table 4.3: Allosteric two-site model parameters for DTT effect on shCB1-C13 and shCB1-C11 for agonist and antagonist binding. [A] is the concentration of the orthosteric ligand, K_A is the dissociation constant for the orthosteric ligand, K_{B1} and K_{B2} are the dissociation constants for the orthosteric and allosteric effector disulfide respectively. The α value is the cooperativity factor between A and B and, and β is the allosteric interaction between B.

	shCB1-C13 SR141716A	shCB1-C11 SR141716A	shCB1-C13 CP 55940	shCB1-C11 CP 55940
[A]	9.4 pM	8.7 pM	7.0 pM	8.6 pM
K_A	6.4 nM	3.3 nM	8.5 nM	6.9 nM
K_{B1}	57 mM	57 mM	57 mM	20 mM
K_{B2}	2.5 ± 2.0 mM	0 ± 25 nM	2.5 ± 5.5 mM	0 ± 27 μM
α	1.85 ± 0.35	1.91 ± 0.10	0.77 ± 0.12	1.25± 0.10
β	1.00 ± 0.34	0.98 ± 0.22	1.00 ± 0.41	1.00 ± 0.47

Figure 4.1

A)

```
                    *       20      *       40      *       60      *       80      *      100      *
Human       : MKSILDGLADTTFRTITTDLLYVGSNDIQYEDIKGDMASKLGYFPQKPLTSFRGSPFQEKMTAGDNPQLVPADQVNITEFYNKSLSSFKENEENIQCGENFMDIECFMVLNPSQQ
Chimp       : MKSILDGLADTTFRTITTDLLYVGSNDIQYEDIKGDMASKLGYFPQKPLTSFRGSPFQEKMTAGDNPQLVPADQVNITEFYNKSLSSFKENEENIQCGENFMDIECFMVLNPSQQ
Macaque     : MKSILDGLADTTFRTITTDLLYVGSNDIQYEDIKGDMASKLGYFPQKPLTSFRGSPFQEKMTAGDNPQLVPADQVNITEFYNKSLSSFKENEENIQCGENFMDIECFMVLNPSQQ
Marmoset    : MKSILDGLADTTFRTITTDLLYVGSNDIQYEDTKGDMASKLGYFPQKPLTSFRGSPFQEKMTAGDNPQLVPADQVNITEFYNKSLSSFKENEENIQCGENFMDIECFMVLNPSQQ
Elephant    : MKSILDGLADTTFRTITTDLLYVGSNDIQYEDIKGDMASKLGYFPQKPLTSFRGSPFQEKMTAGDNPQLVPADQVNITEFYNKSLSSYKENEENIQCGENFMDMECFMILNPSQQ
Panda       : MKSILDGLADTTFRTITTDLLYVGSNDIQYEDIKGDMASKLGYFPQKPLTSFRGSPFQEKMTAGDNGQLVPADQVNITEFYNKSLSSYKENEENIQCGENFMDMECFMILNPSQQ
Dog         : MKSILDGLADTTFRTITTDLLYVGSNDIQYEDIKGDMASKLGYFPQKPLTSFRGSPFQEKMTAGDNAQLVPADQVNITEFYNKSLSSYKENEENIQCGENFMDMECFMILNPSQQ
Cat         : MKSILDGLADTTFRTITTDLLYVGSNDIQYEDIKGDMASKLGYFPQKPLTSFRGSPFQEKMTAGDNSQLVPADQVNITEFYNKSLSSYKENEENIQCGENFMDMECFMILNPSQQ
Armadillo   : MKSILDGLADTTFRTITTDLLYVGSNDIQYEDIKGDMASKLGYFPQKPLTSFRGSPFQEKMTAGDSPQLVPADQVNITEFYNKSLSSYKENEENIQCGENFMDMECFMILNPSQQ
Platypus    : MKSILDGLADTTFRTITTDLLYVGTNDIQYEDLKGDMASKLGYFPQKPLTSSRGNPFQEKMTAGNDLLVAPLDPINITEFYNKSLSSYKGNEENIQCGENFMDMECFMILNPSQQ
Rabbit      : MKSILDGLADTTFRTITTDLLYVGSNDIQYEDIKGDMASKLGYFPQKPLTSFRGSPFQEKMTAGDNAQLVPGDPLNMTEFYNKSLSSYKENEENIQCGENFMDMECFMILNPSQQ
Hedgehog    : MKSVLDGLADTTFRTITTDLLYVGSNDIQYEDIKGDMASKLGYFPQKPLTSFRGSPFQEKMTAGDNPQLVPADQVNITEFYNKSLSSYKENEENIQCGENFMDMECFMILNPSQQ
GuineaPig   : MKSMLDGLADTTFRTITTDLLYVGSNDIQYEDIKGDMASKLGYFPQKPLTSYRGSPFQEKMTAGDSAQLVPADPGNLTEFYNKSLSSYKENDENIQCGENFMDMECFMILNPSQQ
Rat         : MKSILDGLADTTFRTITTDLLYVGSNDIQYEDIKGDMASKLGYFPQKPLTSFRGSPFQEKMTAGDNSPLVPADTTNITEFYNKSLSSFKENEENIQCGENFMDMECFMILNPSQQ
Mouse       : MKSILDGLADTTFRTITTDLLYVGSNDIQYEDIKGDMASKLGYFPQKPLTSFRGSPFQEKMTAGDNSPLVPADTTNITEFYNKSLSSFKENEDNIQCGENFMDMECFMILNPSQQ
Newt        : MKSILDGLADTTFRTITTDLLYMGSNDVQYEDTKGEMASKLGYFPQKPLSSFRRDHSPDKMTIGDDNLLSPLDQFNVTEFFNRSVSTFKENDDNLKCGENFMDMECFMILTASQQ
Opossum     : MKSNLDGLADTTFRTITTDLLYAGSNDIQYEDIKGNMASKLGYFPQKPLTSFRGSPFQEKMTAGDNPQLIPSDQINITEFYNKSLSSYKDNDENIQCGENFMDMECFMILNPSQQ
Shrew       : MKSILDGLADTTFRTITTDLLYVGSNDIQYEDIKGDMASKLGYFPQKPLTSFRGSPFQEKMTAGDSPQLVPADQVNITEFYNKSLSSYKENEENIQCGENFMDMECFMILNPSQQ
Bat         : MKSILDGLADTTFRTITTDLLYVGSNDIQYEDIKGDMASKLGYFPQKPLTSFRGSPFQEKMTAGDSPQLVPADQVNITEFYNKSLSSYKENE-NIQCGENFMDMECFMILNPSQQ
Chicken     : MKSILDGLADTTFRTITTDLLYVGSNDIQYEDMKGDMASKLGYYPQKPLSSFRGDPFQEKMTAGDDPLLSPSDQINITEFYNKSLSTFKENEENIQCGENFMDMECFMILNPSQQ
ZebraFinch  : MKSILDGLADTTFRTITTDLLYVGSNDIQYEDMKGDMASKLGYYPQKPLSSFRGDPFQEKMTGGDDSLLSIIPQVNITEFYNKSLSTFKDNEENIQCGENFMDMECFMILNPSQQ
Pufferfish  : MKLALHRIAGATMAALTTEVQYLGSNDASYEDPQADAALMKSRFNFEKPYSASSSLHRL---IPGNKELIYGGLSTILPTNASDFPLSNGSGEATQCGEDIVDMECFMILTPAQQ
Sticklebac  : IKMALHRIAGTAMSSLTTGVQYLGSNDASYDDASVDSTLIKNRFHFEKPNSASISNSFPGLVP-VNKEVIYSGLAPIFPTNVSDFLLGNGTSVESQCGEDFVDMECFMILTPSQQ
Ricefish    : VKVAVPRVTQATMSTLATGVRYLGSNDASYDDPSADSGLVKNGLRFGKHPS-LSSSFPEIFPESKEVFYAAVSPIFPMNVSDVGNVTSVEIGGAHQCSENFADNECFMILTPGQQ
Zebrafish   : VKSVLDGVAETTFRTITSGLQYIGSNDIGYDDHIIDGDSKSGYPLPKPFAAYRRSSFADKVAPDEELIVKGLPFYPTNSSDVFGNWSHAED-GSLQCGENFMDMECFMILTPSQQ
Frog        : MKSILDGLADTTFRTITTDLLYLGPNEVQYDDSKGDISSKLVYFPQKPLSSLRGDPLHEKMTIIDDPLLSIPLDQINATDFYNKSIIFKDTDDNVQCGKNFMDMECFMILTPSQQ
```

B)

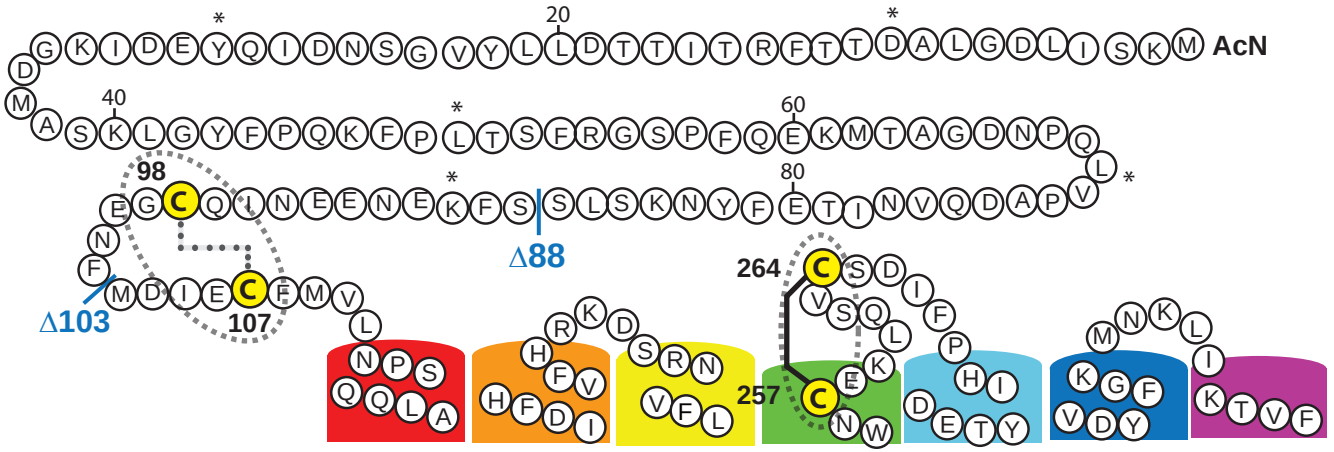

Figure 4.1. Two cysteines in the N-terminus of CB_1 are highly conserved across species. (A) Sequence alignment of CB_1 protein sequence from a select group of mammals, birds, fish, and amphibian (sequences were extracted from GPCR.org). Shading is based on the following sequence identity parameters: 100% (blue), >80% (lighter blue), and <80% is not shaded. The conserved N-terminal cysteines (human C98 and C107) are colored in yellow. **(B)** Two-dimensional model of human cannabinoid (CB_1) receptor showing the extracellular region and sites of cysteines and deletions studied in the present work. Cysteines C98, C107, C257 and C264 are depicted as filled yellow circles. The amino acid position of truncation mutants Δ88 and Δ103 are respectively labeled in blue.

Figure 4.2

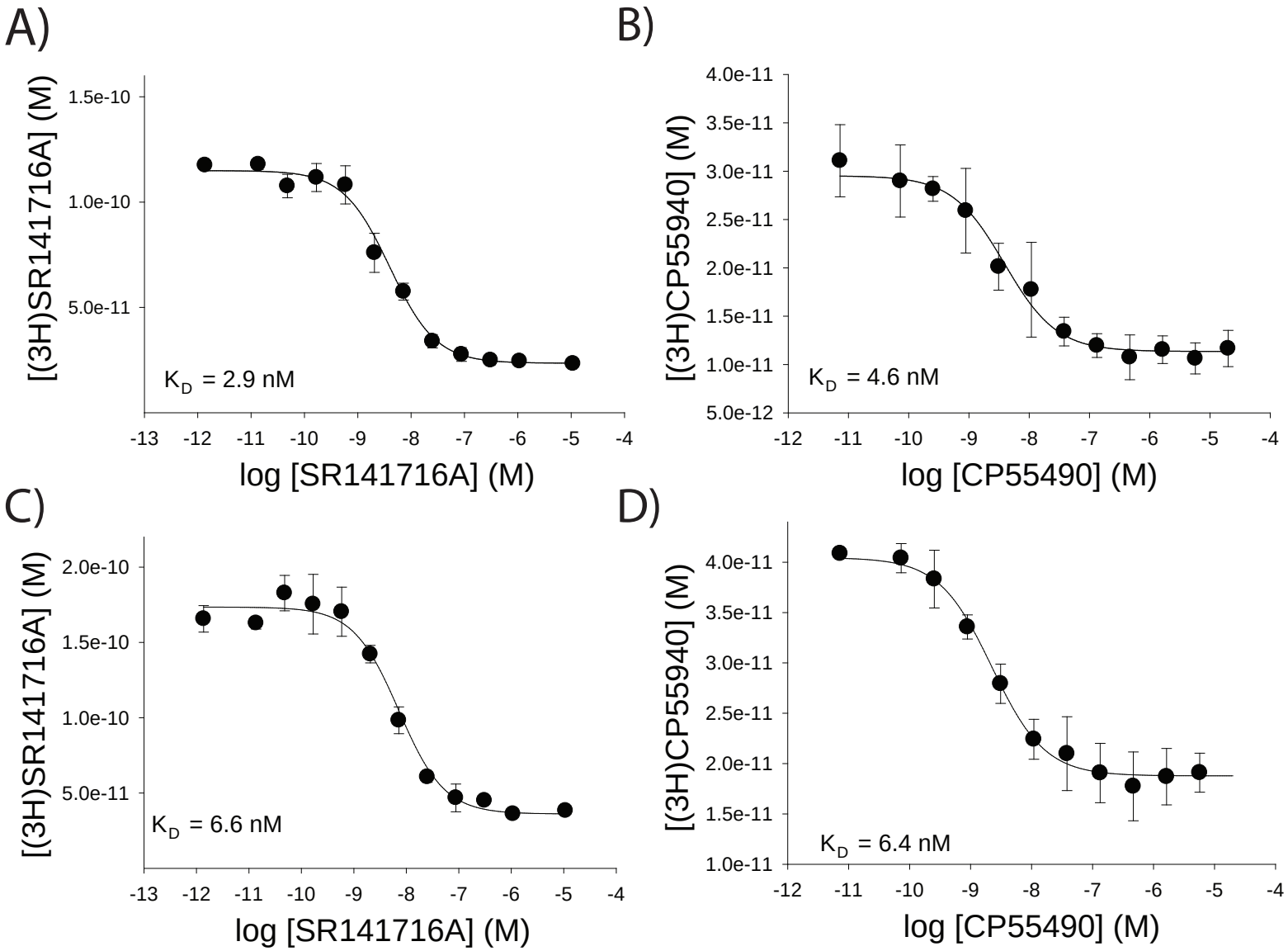
A)
[(3H)SR141716A] (M)
1.5e-10
1.0e-10
5.0e-11
K_D = 2.9 nM
-13 -12 -11 -10 -9 -8 -7 -6 -5 -4
log [SR141716A] (M)
B)
[(3H)CP55940] (M)
4.0e-11
3.5e-11
3.0e-11
2.5e-11
2.0e-11
1.5e-11
1.0e-11
5.0e-12
K_D = 4.6 nM
-12 -11 -10 -9 -8 -7 -6 -5 -4
log [CP55490] (M)
C)
[(3H)SR141716A] (M)
2.0e-10
1.5e-10
1.0e-10
5.0e-11
K_D = 6.6 nM
-13 -12 -11 -10 -9 -8 -7 -6 -5 -4
log [SR141716A] (M)
D)
[(3H)CP55940] (M)
4.0e-11
3.5e-11
3.0e-11
2.5e-11
2.0e-11
1.5e-11
1.0e-11
K_D = 6.4 nM
-12 -11 -10 -9 -8 -7 -6 -5 -4
log [CP55490] (M)

Figure 4.2. An extreme deletion of the CB_1 N-terminus (Δ103) does not abolish ligand binding. Competitive inhibition binding studies comparing 'Wt' shCB1 (A & B) with Δ103 (C & D). (A & C) antagonist SR141716A binding. (B & D) Agonist CP 55940 binding. Binding was carried out using a Brandel 24-well filtration apparatus, and the data fit with a one-site binding model. Data represent one binding experiment performed in duplicate. See Experimental Procedures for more details.

Figure 4.3

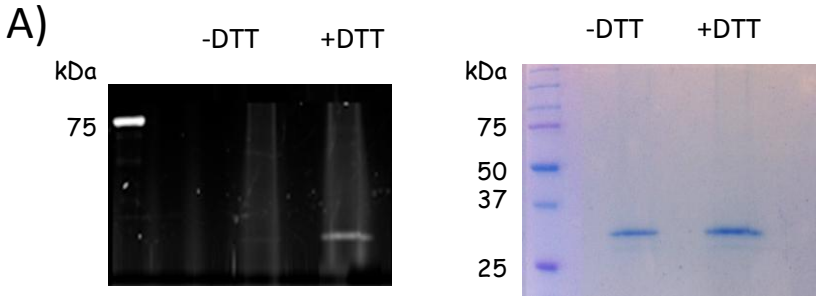
A)
-DTT
+DTT
kDa
75
-DTT
+DTT
kDa
75
50
37
25

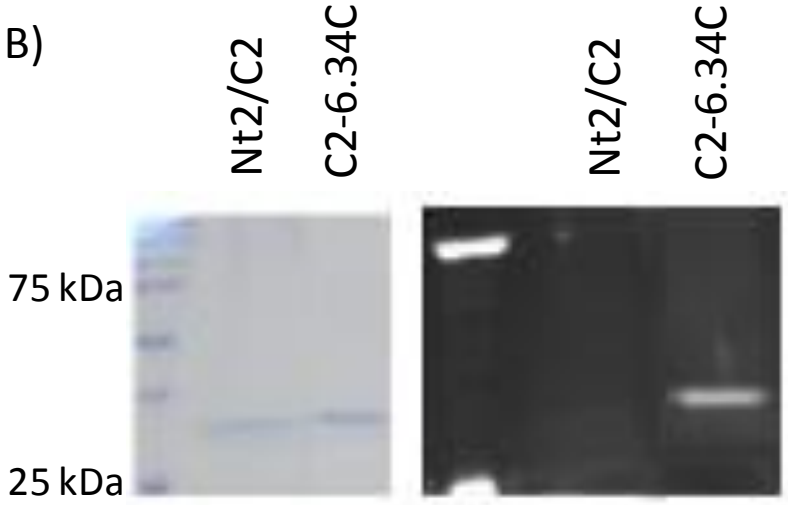
B)
Nt2/C2
C2-6.34C
Nt2/C2
C2-6.34C
75 kDa
25 kDa

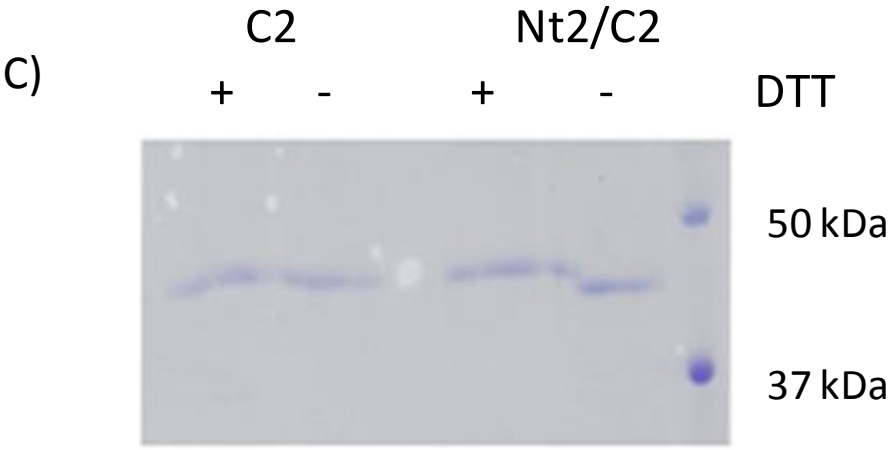
C)
C2
Nt2/C2
+
-
+
-
DTT
50 kDa
37 kDa

Figure 4.3. Evidence for a disulfide between C98/C107 in the CB_1 N-terminus: both cysteines are unreactive to thiol specific probes and their presence in a non-reduced sample causes a faster running species on SDS-PAGE. (A) The purified, minimal-cysteine construct mutant C2 (or θ see Chapter 3 – which contains only C257 and C264) does not react to thiol reactive fluorophore PDT-bimane. However, reducing the sample with DTT, prior to bimane labeling, results in label incorporation (+DTT). This is observed as a lack of detectable fluorescence in the in-gel bimane fluorescence (left), even though equivalent amounts of protein are present (right, coomassie staining of the same gel). **(B)** Similarly, the purified construct with also contains two cysteines in the N-terminus (C98,C107, C257, and C264 – termed Nt/C2) is insensitive to bimane labeling. Coomassie stained SDS-PAGE gel (left) of Nt2/C2 and positive control C2-6.34C (which contains only C257, C264, and a reactive cysteine introduced at 342 - 6.34 in Ballesteros-Weinstein numbering). Ultraviolet irradiation of the same gel (right), before staining, shows that Nt2/C2 does not react with PDT-bimane. In contrast, the positive control which contains a 3rd reactive cysteine residue inTM6 (see Chapter 3), called C2-6.34C, does show incorporation of bimane label. **(C)** Comparison of mobility for the purified CB_1 receptor C2 or Nt2/C2 in the presence or absence of DTT. Notice that in non-reducing conditions, Nt2/C2 runs faster than C2, but when treated with DTT it collapses back to the C2 like molecular weight.

Figure 4.4

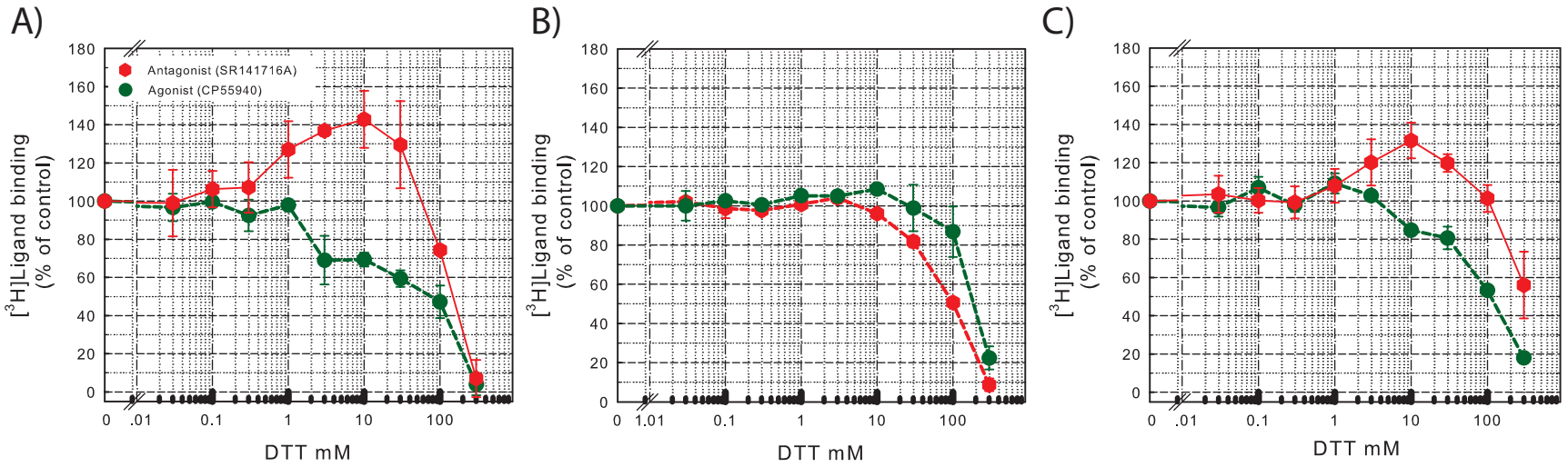
A)
B)
C)
Antagonist (SR141716A)
Agonist (CP55940)
[3H]Ligand binding
(% of control)
DTT mM
0
20
40
60
80
100
120
140
160
180
.01
0.1
1
10
100
1.01

Figure 4.4. **The reducing agent DTT causes allosteric modulation of ligand binding to CB_1.** The data show the effect of increasing concentrations of DTT on binding of tritated agonist (CP 55940 – green circles) or antagonist (SR141716A – red hexagons). **(A)** Effect of DTT on ligand binding to "wild-type" (shCB1-C13) receptors expressed in COS-1 cells. **(B)** Effect of DTT on ligand binding to shCB1-C11 receptors lacking N-terminal cysteines (containing C98A and C103A) expressed is COSH-1 cells. **C)** Binding to wild-type cannabinoid receptors present in membranes prepared from rat cortices. All experiments were performed at least twice in duplicate and are presented as the mean ± S.E.M. Data is normalized to specific fraction bound for respective radioligands determined in the absence or presence of saturating concentration of respective cold. For more details see Experimental Procedures.

Figure 4.5

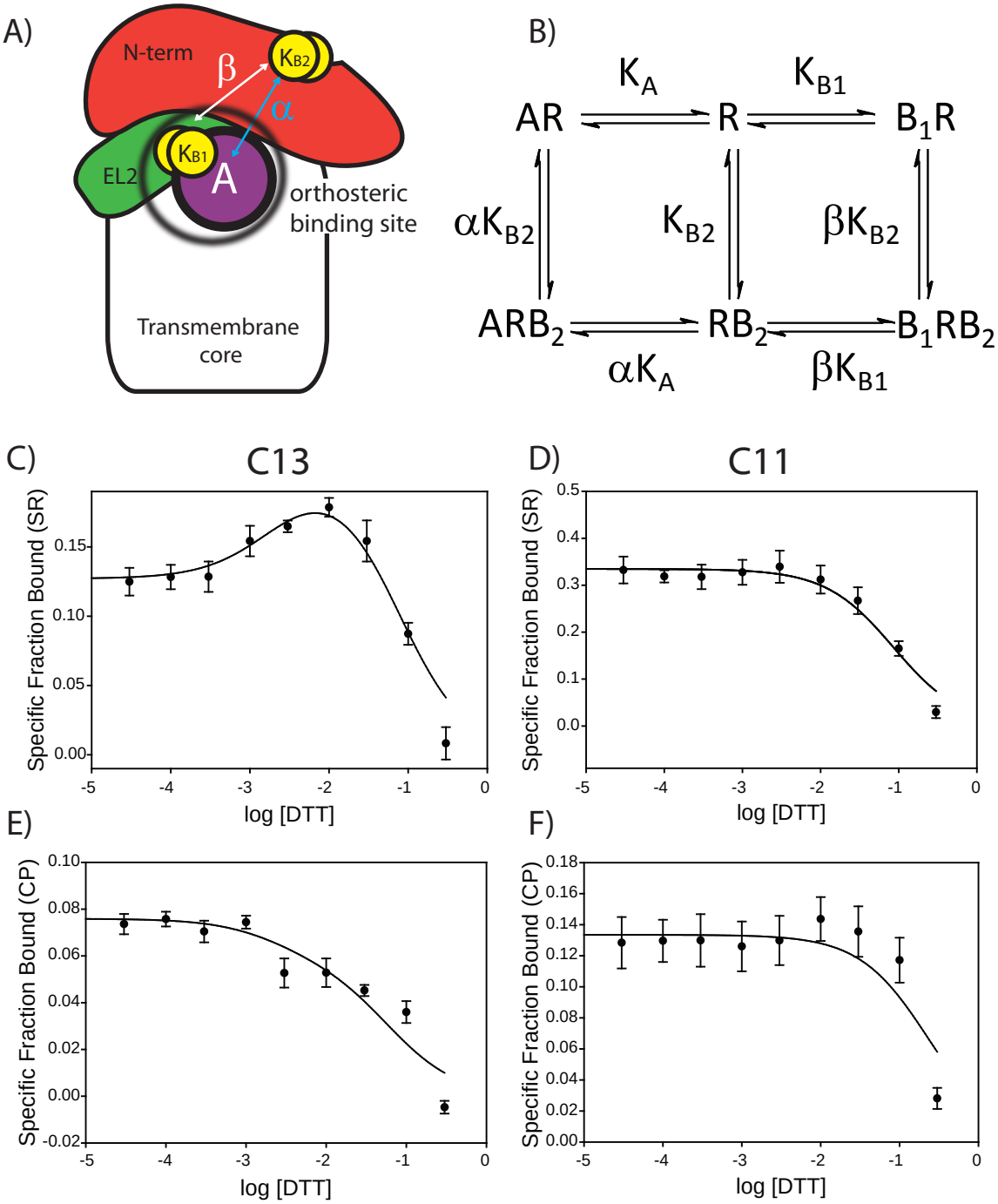
A)
N-term
β
K_{B2}
α
K_{B1}
A
EL2
orthosteric
binding site
Transmembrane
core
B)
K_A
K_{B1}
AR
R
B_1R
αK_{B2}
K_{B2}
βK_{B2}
ARB_2
RB_2
B_1RB_2
αK_A
βK_{B1}
C)
C13
Specific Fraction Bound (SR)
log [DTT]
D)
C11
Specific Fraction Bound (SR)
log [DTT]
E)
Specific Fraction Bound (CP)
log [DTT]
F)
Specific Fraction Bound (CP)
log [DTT]

Figure 4.5. An allosteric two-site model can be used to fit the effect of DTT on CB_1 ligand binding. **(A)** Cartoon describing the allosteric two-site model as related to our system. The orthosteric ligand, A (purple circle), is bound in the orthosteric binding pocket (black circle) also comprised of C257/264 EL2 (green) disulfide (K_{B1} – yellow circles). The allosteric N-terminal (red) disulfide (K_{B2} – yellow circles). The cooperativity factors that govern the interaction between K_{B2} and the orthosteric site (α) or between the two disulfides (β) are represented by blue and white arrows, respectively, showing the linkage between the sites. **(B)** A schematic representation of the allosteric two-site model where R denotes the receptor; A denotes the orthosteric ligand (CP 55940 or SR141716A) and B denotes the allosteric ligand (in this case DTT). The K_A, K_{B1} and K_{B2} are their respective dissociation constants. The subscript B1 and B2 represent the two sites that the allosteric ligand can interact with, B1 is the orthosteric site (C257/264 disulfide) and B2 is the allosteric site (C98/107 disulfide). The cooperativity factor, α, denotes the allosteric interaction between A and B. The cooperativity factor, β, denotes allosteric interaction between the two molecules of B. Cooperativity values greater than 1 denote the magnitude of positive cooperativity (increased affinity), values less than one denote the magnitude of negative cooperativity (decreased affinity) and values equal to one are neutral. **(C-F)** Effect of varying concentrations of DTT on tritiated antagonist (C and D) or agonist (E and F), for C13 (C and E) and C11 (D and F). Equation (4.1) was used to fit the data. K_{B1}, was determined from fits of the C11 data, and used as a fixed parameter in determination of values for subsequent fitting of the C13 data. The coefficient of determination was calculated to be 0.9162, 0.8944, 0.9122, 0.9844 and 0.8729 for C13SR, C11SR, C13CP and C11CP respectively. Calculated parameter values from the fits are shown in Table 4.3. See Experimental Procedures for more details.

Figure 4.6

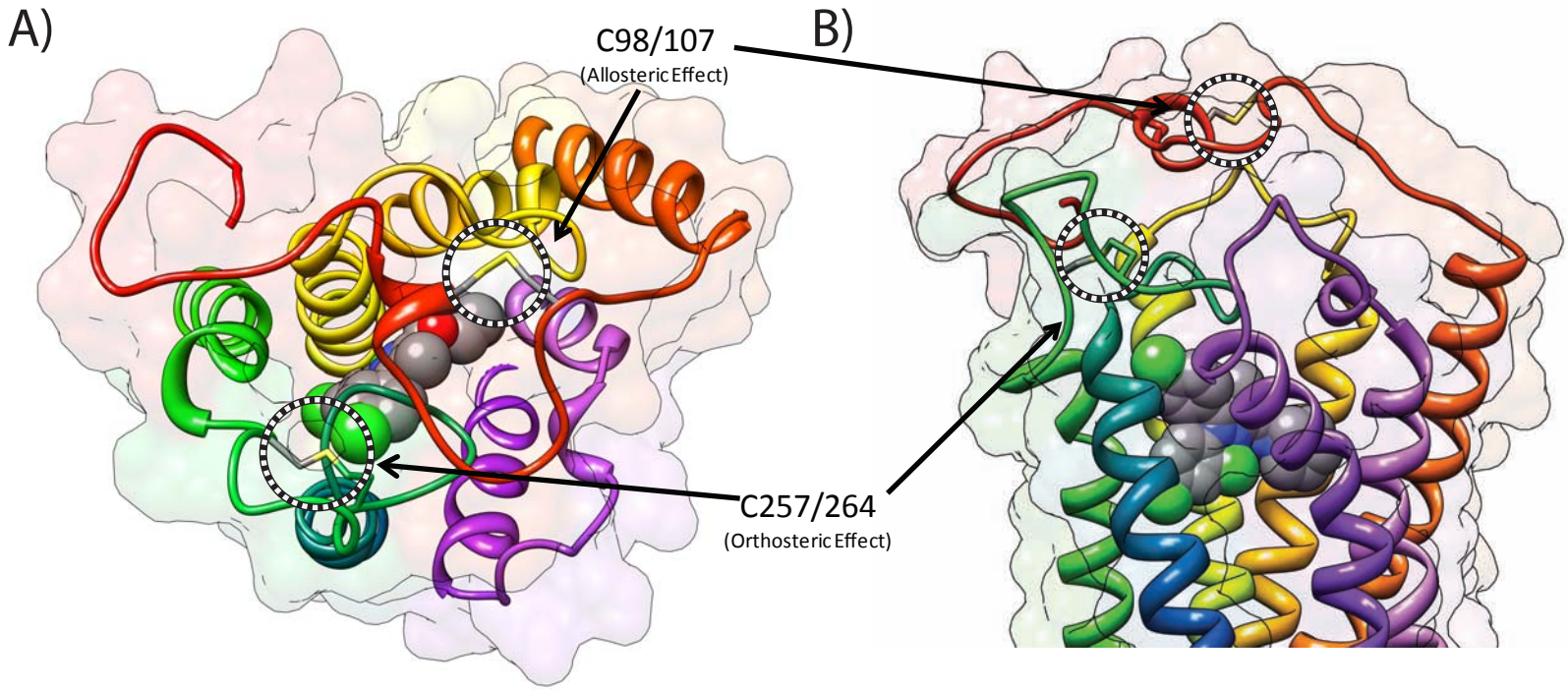

Figure 4.6. **Structural model illustrating how CB_1 disulfides can play a role in hypothesized domain coupling between the N-terminus and loop E2 in CB_1.** Model of CB_1 extracellular face (left) and side view (right). Depicted are N-terminal 'allosteric effect' disulfide (red, C98/107) and the EL2 'orthosteric effect' disulfide (green, C257/264). The antagonist SR141716A is shown bound in the binding pocket. Ribbons are colored in rainbow (from red to violet – N to C terminus) to help orientate the helices. Our model suggests that perturbations of N-terminal disulfides may disrupt ability of the N-terminal domain to couple with the orthosteric site. Possibly by interaction with EL2 and thus subtly alter ligand binding. Note that N-terminal residues from 1-87 were omitted from the model.

Supplemental Figures

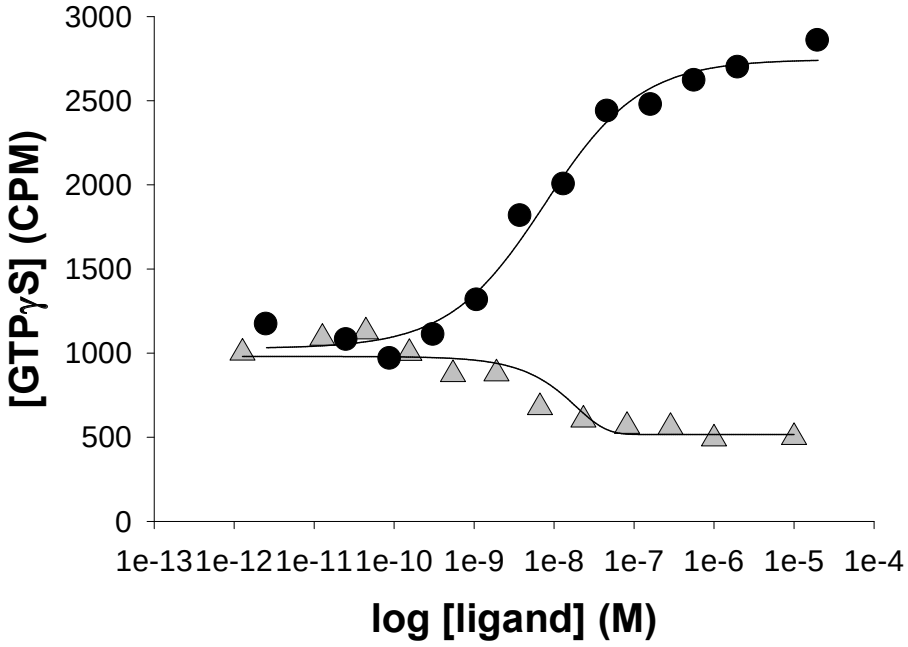

Figure 4.S1. Ligand binding and stimulation of GTPγS binding by Δ103 CB_1/Gαi fusion protein. Ability of increasing concentrations of agonist or antagonist to affect GTPγS binding to Δ103-CB_1/$G\alpha_i$. Assays used 50 μg membranes containing Δ103-CB_1/Gαi fusion. Notice the GTPγS binding decreases for the antagonist. Data represent one binding experiment performed in singlicate. For details see Experimental Procedures.

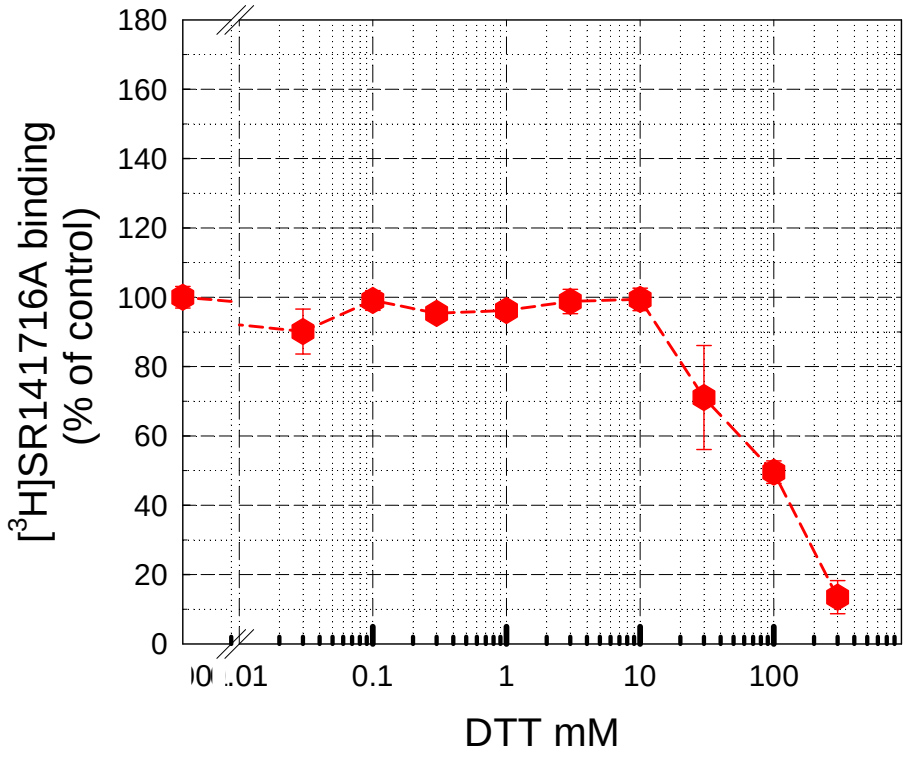

Figure 4.S2. **Reducing agent, DTT, reduces a disulfide bond between 257 and 264, in EL2 of CB_1.** Effect of varying concentrations of DTT on tritiated antagonist (SR141716A) on a mutant containing only two cysteines residues, C257 and C264 (shCB1-C2). Representative experiments were performed at least twice in duplicate and are presented as the means ± range. Data is normalized to specific fraction bound for [^{3}H]SR141716A determined in the absence or presence of saturating concentration of respective cold. For more details see Experimental Procedures.

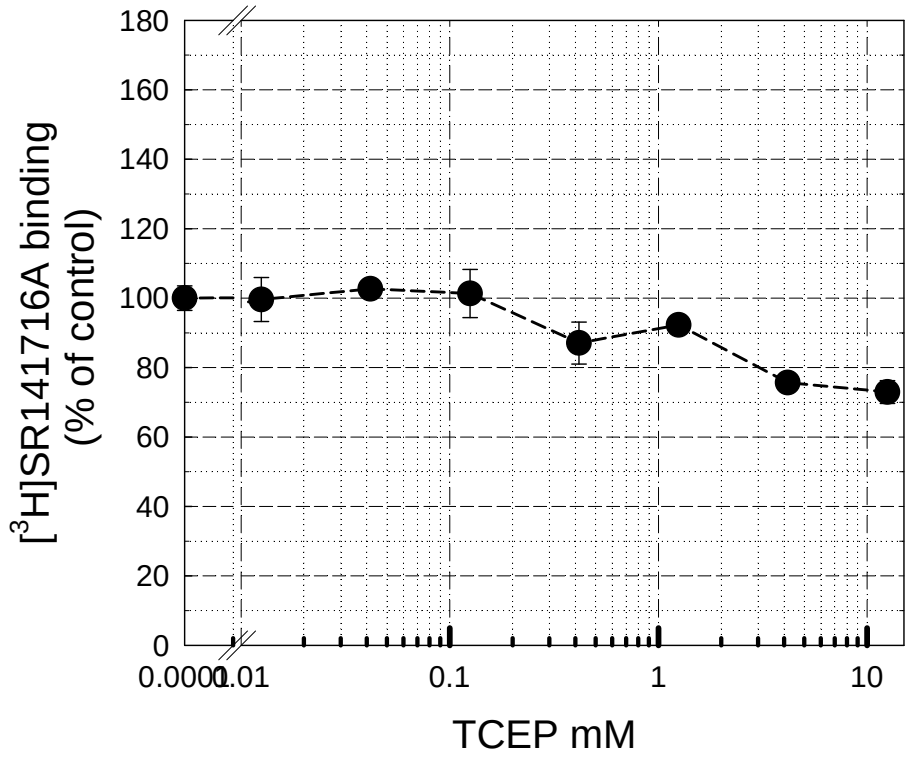

Figure 4.S3. **The reducing agent, TCEP, does not appear to exhibit an allosteric effect in rat cortices.** Effect of varying concentrations of TCEP on tritiated antagonist (SR141716A) binding to endogenous rat cannabinoid receptors. Experiment was performed once in duplicate and is presented as the means ± range. Data is normalized to specific fraction bound for [^{3}H]SR141716A determined in the absence or presence of saturating concentration of respective cold. For more details see Experimental Procedures.

Chapter 5

Generation and initial characterization of novel CB_1 receptor monoclonal antibodies

Jonathan F. Fay[1] & David L. Farrens[1]

[1] *Department of Biochemistry and Molecular Biology, Oregon Health and Science University, Portland, Oregon 97239*

Acknowledgements: I would like to thank D. Cawley for monoclonal antibody production and ELISA screening.

5.1: SUMMARY

We have used purified, functional CB_1 receptor to generate several new and unique mouse monoclonal antibodies that should prove useful for future structure function studies. The antibodies can be separated into three general categories, based on the regions they recognize: (1) N-terminal, between residues 88-103; (2) intracellular loop 3 (IL3); and (3) an extracellular region group. Here, we describe a characterization of these antibodies, some of their novel properties (for example, one of the IL3 antibodies binds preferentially to activated receptor), how they were generated, and examples of their use for structure/function studies of CB_1.

All of the experiments and data analysis reported in this chapter were performed by the author of this dissertation. D. Cawley was instrumental in the generation of monoclonal antibody production and ELISA screening. Parts of the data presented here have previously been presented in a poster (2624-Pos Board B394) at the 56th Annual Biophysical Society Meeting, San Diego, CA, 2012.

5.2: INTRODUCTION

In this chapter, I describe the production and characterization of novel antibodies directed against the neuronal cannabinoid G protein-coupled receptor, CB_1. Previously, in order to generate CB_1 antibodies, short peptide sequences corresponding to N-terminal, C-terminal, or 3rd intracellular loop regions were used as antigens, as purified functional CB_1 was not available [255]. An early and now widely used anti-CB_1 antibody is a rabbit polyclonal antibody directed against the first 77 residues of the N-terminus. More recently, peptides corresponding to residues 27-41 of the N-terminus have been used to generate a different class of rat antibodies [256]. However, to date I am unaware of any monoclonal antibodies that have been generated against functional CB_1 receptor.

In addition to serving as chaperones for crystallization [257, 258] and their role in autoimmune disease [259, 260], antibodies represent powerful research tools. They can even act as drugs themselves, regulating receptors by blocking constitutive activity or inducing activation. Alternatively, they can be utilized to target drug delivery payloads. Creating additional antibodies against GPCRs may also unlock other hidden allosteric domains, perhaps unmasking key regions that can be allosterically modulated, thus paving the way for alternative pharmaceutical targets. Some antibodies can probe the receptor activation state [261, 262] and it is possible these types of antibodies can be used for applications in high-throughput screening for drug discovery programs.

Due to our currently unique ability to purify functional CB_1 (see Chapter 2 and 3) we decided to develop our own unique antibodies against CB_1. Because our CB_1 purification construct is devoid of the majority of N-terminus – where most previous CB_1 antibodies have been targeted (see above) – by default any new CB_1 specific antibodies

we generated would be by definition “new.” In this manuscript I present initial characterization of some of these unique primary clones and then focus on the behavior of an interesting allosterically activating antibody.

5.3: Experimental Procedures

5.3.1 Buffers. The definitions of the buffers that were are: PBSSC [0.137 M NaCl, 2.7 mM KCl, 1.5 mM, KH2PO4, and 8 mM Na2HPO4], hypotonic buffer [5 mM Tris-HCl, 2 mM EDTA, and PIC (pH 7.5)], TME [20 mM Tris-HCl (pH 7.4), 5 mM $MgCl_2$, and 1 mM EDTA], MAB buffer [5 mM TRIS (pH 7.5) at 23^{o}C, 200 mM NaCl,5 mM $MgCl_2$,2% Glycerol,0.06%/0.01/0.01 CHAPS/DM/CHS], Purification Buffer [50 mM Tris (pH 7.5), 200 mM NaCl, 5 mM $MgCl_2$, 20 % glycerol], FSEC buffer [20 mM TRIS (pH 7.5), 150 mM NaCL, 1 mM EDTA, 0.05% DM], 2xFSEC buffer [Purification buffer with 0.12% CHAPS, 0.02% DM, 0.02% CHS]; Solubilization Buffer [Purification buffer with 0.6% CHAPS, 0.1% DM, 0.1% CHS]; Elution Buffer [2XFSEC buffer with 200 μM nonapeptide corresponding to the rho1D4 antibody epitope], Digestion Buffer [PBSSC + 20 mM cysteine-HCL, 10 mM EDTA, pH 6.4], and ELISA buffer [20 mM Tris:150 mM NaCl, 5mM MgCl2, 1 mM DM , 5% glycerol and 2 mg/mL BSA].

5.3.2 Nomenclature of shCB1 Mutants used in this chapter. Our ‘wild-type’ CB_1 gene, called shCB1-C13 (or C13 for short), has been described previously [198, 199]. Notably, this construct has the last 8 residues replaced with the last 9 of rhodopsin to enable immunodetection. CB_1a is a CB_1 human splice variant that contains a modified amino terminus. The CB_1a N-terminus [19] was cloned into our shCB1-C13 gene. The initial antigen used to challenge mice was Δ88/Δ417-III (see Chapter 2) and is termed in this

chapter as Δ88. This construct contains only four of the thirteen cysteines residues in CB_1 (C257,C264, C355, and C382) [199], in addition to an N-terminal truncation at residue number 88 (Δ88) and a C-terminal truncation at residue number 417 (Δ417). Additionally, this mutant contains the last 9 amino acids of rhodopsin (1D4 epitope) facilitating immuno-affinity purification. Δ103/Δ417-II is a similar mutant, but has an extreme N-terminal purification deletion mutant described in Chapter 2; here this mutant is termed Δ103. The construct termed θ is a minimal cysteine construct of the Δ88/Δ417-III mutant CB_1 containing only C257 and C264 as discussed in Chapter 3. Notably, this mutant is a minimal cysteine construct that contains no reactive cysteine residues. C407 was introduced into θ to create θ/407C. The construct termed ΔIL3 is a θ mutant where residues 307-326 corresponding to part of intracellular loop 3 (IL3) have been removed. The GFP tagged CB_1 receptor variant of Δ88/Δ417-III , is called Δ88/Δ417-II (described previously in Chapter 2).

5.3.3 Construction of mutants. The Sequence of the primers is as follows: **Rho1:** TTT CTC TCC ACA GGT GTC CAC TCC, **Rho2:** GCC CTG AGC TGT CCC CCC CCC CCC, **RevNhe:** CTC GCC AAA AAA GCT AGC GCA GCA GC. **407C**: GAT CTG CGG CAC TGC TTC CGC AGC, **ΔIL3**: GCC GTG CGG CAA GTG ACC CGC. The 407C mutant was constructed using θ as a template in a two part overlap extension using primers Rho1, Rho2, 407C and its complement. The IL3 deletion mutant was created in a similar fashion using θ as a template and primers Rho1, Rho2, ΔIL3 and its complement. The Δ103, Δ88/Δ417-II, and Δ88/Δ417-III were made previously as discussed in Chapter 2. CB_1a gene was created by ordering the following gene from Genscript in a Puc57 vector and sub cloning into shCB1-C13 using restriction enzymes EcoR1 and Ava1:

aagaattccaccATGGCCCTGCAGATCCCCCCCAGCGCCCCCAGCCCCCTGACCAGC
TGCACCTGGGCCCAGATGACCTTCAGCACCAAGACCAGCAAGGAGAACGAG
GAGAACATCCAGTGCGGCGAGAACTTCATGGATATCGAGTGCTTCATGGTGCT
GAACCCCAGTCAGCAATTGGCCATCGCCGTGCTGTCCCTGACCCTAGGCACCT
TCACCGTGCTGGAAAATCTGCTAGTACTGTGCGTGATCCTGCACAGCCGAAGC
TTGCGGTGCCGCCCCAGCTACCACTTCATCGGATCCCTGGCCGTGGCAGATCT
TCTGGGCAGCGTGATCTTCGTGTACAGCTTCATCGACTTCCACGTGTTCCACCG
CAAGGACTCCCGCAACGTGTTCCTGTTCAAGCTCGGG

5.3.4 Transfection. Wild-type and mutant shCB1 genes were expressed in transiently transfected COSH-1 using polyethylenimine (PEI) as previously described in Chapter 2 & 3. Briefly, 30-50 μg of DNA was incubated with 100 μg PEI (Polysciences) in 5 mL of Opti-mem (Invitrogen), which was then added to COSH-1 monolayer supplemented with 15 mL of DMEM/High glucose (Hyclone), containing 10% Fetal Bovine Serum (Hyclone), 1% Penicillin (100 units/ml, Gibco), 1% Streptomycin (100μg/ml, Gibco) and 1 % glutamine dipeptide (2 mM, Hyclone). Cells were allowed to grow for 55-65 hours at 5% CO_2, 75% relative humidity, and 37^{o}C. The cells were then harvested in PBSSC, and the pellets were snap frozen in liquid nitrogen and stored at -80^{o}C.

5.3.5 Membrane preps. Membranes were prepared as previously described [199]. Briefly, wet cell pellets were homogenized in a volume of 1 mL/plate of hypotonic buffer. The homogenized cells were then subjected to 40,000 g centrifugation for 45 min. The pellets were re-suspended in TME with Protease Inhibitor Cocktail (PIC, Roche) at 0.5 mL/ 15 cm plate. Membrane preparations were snap frozen in liquid nitrogen as aliquots and stored at -80^{o}C.

5.3.6 Purification of cannabinoid receptor mutants. COS cells expressing CB_1 receptor protein were suspended in Solubilization buffer at a ratio of 0.1g of wet cell pellet:mL and gently nutated for 3 hours at 4^{o}C. The supernatant from clarified solubilized lysate (centrifuged for 1 hour at 100,000 x g) was added to an appropriate volume of 1D4 antibody-Sepharose beads (binding capacity ~1μg of rhodopsin/μg resin) in Solubilization buffer supplemented with PIC, 5 μg/ml leupeptin, 10 mM benzamadine, 0.5 mM PMSF, and 100 nM SR141716A and allowed to bind via gentle agitation at 4^{o}C for ~5 hours. Next, beads were washed with ~5 mLs protease inhibitor supplemented Solubilization buffer, and 2 times with 1 mL washes of solubilization buffer. Three hours after incubation of 1D4 antibody-Sepharaose beads with elution buffer (containing 200 μM nonapeptide), beads were gently centrifuged, 1,000 x g in table top centrifuge for 5 min and eluted protein was collected. Alternatively, antigen preparation samples were washed with 2xFSEC buffer and then with MAB buffer 3 times prior to elution in MAB buffer supplemented with nonapeptide. All labeling was performed as previously described in Chapter 3.

5.3.7 Monoclonal antibody generation and Fab purification. Monoclonal antibodies and Fab fragments. Mouse monoclonal antibodies (IgG2a/b, kappa) against Δ88/Δ417-III (Chapter 1) and Nt2/C2 (Chapter 4) were generated by standard methods using respective purified protein in detergent as antigen [263]. In brief, 4 Balb/c mice are injected each with 10-25 μg of purified CB_1 four times (on day 0, 21 ,51, and 55). Spleen cells were fused with P3X mouse myeloma cells, and hybridoma supernatants were assayed on day 66-67 via ELISA. Screening was performed using Streptavidin-CB_1 biotin capture ELISA based assays using ELISA buffer. Biotin labeled θ/407C was purified and labeled

with Malemide-PEG11-Biotin (Thermo Scientific Prod #21911). Alternatively, Biotin labeled Nt2/C2-407C was also used, however, no obvious differences were observed. From these screens, we isolated a number of hybridoma supernatants that were further characterized.

Antibody clones 3A3, 5G3, 2C12 and 1E10 were purified from hybridoma supernatants using a mercaptoethylpyridine/protein A chromatography. Fab fragments were generated by papain digestion at 23-25^{o}C without agitation for 3 hours. Papain was diluted in digestion buffer and added to a 1:20 dilution with antibody in PBSSC such that the final EDTA concentration was 1 mM and the 3A3 monoclonal antibody to papain molar ratio was 1:100. Digestion of 3A3 was quenched with 6 mM freshly prepared iodoacetamide for 30 minutes. Fab fragments were purified on a Protein A column, followed by 7kDa size-exclusion chromatography step to remove Fc molecules and undigested material. This was then concentration in a 3 kDa molecular weight cut off Amicon concentrator to the desired concentration. Fab concentration was estimated from absorbance at 280 nm with an extinction coefficient (1 mg/mL) of 1.35.

5.3.8 Immunoblot Analysis. A known concentration of IgG standard monoclonal to green fluorescent protein at 22 μg/mL in the hybridoma medium were run on SDS-PAGE gel along with unknown concentration of IgG in hybridoma supernatants, and then the gel was transferred to Immobilon-P membrane and immunoblotted with 1:5000 dilution of peroxidase-conjugated goat anti-mouse IgG (H+L) (Pierce), and visualized using enhanced chemiluminescence. The relative intensities of the standards and unknowns were determined via pixel density.

Hoefer Slot Blot Manifold was used to transfer the indicated concentrations of

purified CB_1 constructs, Δ88, ΔIL3, and Δ103 to Immobilon-P membranes (Millipore) and immunoblotted with hybridoma supernatant diluted to a final titer of 10 ng/mL. Immunoblots were visualized with Blue Lite Autorad Film (GeneMate Cat.No F-90248X10), photos were captured using an iPhone with the film on a Vernier White light transilluminator. The relative intensities of the standards and unknowns were determined via pixel density using a ImageJ image processing program (National Institutes of Health, Washington, DC).

5.3.9 Peptide inhibition assays to map epitopes. Peptides, ^{88}SKFENEENIQ^{97} (pH 10) , ^{307}MIQRGTQK^{314}, ^{315}SIIIHTSED^{323} (pH 10) and ^{323}DGKVQVTRP^{331} were supplied by GenScript at >95% purity. Dissolved in 0.2 μ filtered $DDIH_2O$ or 10 mM CAPS buffer pH 10 (where indicated).

Crude membrane preparations of COSH-1 expressing indicated CB_1 constructs were subjected to SDS-PAGE and immunoblotting. CB_1 concentration was estimated to be about ~100 ng. This is roughly about a 1/6th dilution of crude membranes at 0.5 mL TME +PIC/15 cm plate. After addition of primary antibody (at a titer of 10 ng/mL), the blots were washed in PBSSC +0.1% Tween-20, then a final wash was performed that contained 100 μM indicated peptides for 1 hour prior to exposure to peroxidase-conjugated goat anti-mouse IgG (H+L) and subsequent work up.

5.3.10 Cell imaging Microscopy. HEK293FT cells were transfected with CB_1 receptors using lipofectamine 2000 after seeded onto 12-mm glass-bottomed slides (BD Biocoat^{TM}) precoated with poly-D-lysine. Cells were treated with different ligands for various lengths of time as indicated in the figures and then washed three times with PBS, followed by fixation with 4% paraformaldehyde for 15 min at room temperature. For

intracellular antibodies, cells were permeabilized with 0.2% Triton X-100 in PBSSC containing 5% BSA, pH 7.6. After incubating with blocking solution (5% BSA) for 30 min at room temperature, the cells were incubated with the diluted antibody at 1:1000 for 30 min at room temperature, followed by 1:2000 dilution of goat anti-mouse Alexa 594 (Invitrogen). Cells were mounted in Vectashield mounting medium (Vector Laboratories, CA) and visualized using Zeiss Axiovert 200M deconvolution microscope. Images were collected from at least 2 independently transfected cell dishes and processed for presentation in figures using Adobe Photoshop 6.0 (Adobe Systems, San Jose, CA).

5.3.11 Fluorescence Size-exclusion Chromatography (FSEC). Was performed essentially as described in Chapter 2. In brief, indicated concentrations of a CB_1-GFP chimera (Δ88/Δ417-II) were applied to a 60 mL Superdex 200 column equilibrated in FSEC buffer and run at a flow rate of 0.5 mL/min. GFP fluorescence was monitored using a RF-551 fluorescence HPLC monitor (Shimadzu) with excitation wavelength set at 470 nm and emission wavelength set at 507 nm.

5.3.12 Fluorescence Assay. Steady-state fluorescence measurements were performed essentially as previously described (Chapter 3) using a PTI fluorescence spectrometer with temperature controlled at ~23^{o}C. The excitation wavelength was set at 380 nm and the emission was collected from 400-650 nm. The bimane labeled θ/342C receptor concentration was 200 nM. All ligands were diluted, such that the final solvent concentration was less than 1%. The purified 3A3 Fab was supplemented with detergents such that the final detergent concentration remained constant. All fluorescence spectra were buffer subtracted and corrected for dilution.

5.4: RESULTS

5.4.1 Initial generation of antibodies

In order to generate unique CB_1 monoclonal antibodies, we expressed and purified CB_1 (Δ88/Δ417-III, see Chapter 3 – termed Δ88 in this chapter) which lacks the majority of the N and C terminus (truncated at 88 and 417 for N and C termini respectively) and used it as an initial antigen. Monoclonal antibodies were generated by Dr. Dan Cowley at VGTI Monoclonal Antibody Core using a conventional fusion protocol [263]. Isolated spleen cells from 4 mice were fused to myeloma cells, yielding 13 high-affinity hybridoma clones that produced antibody to CB_1, as determined by an initial CB_1 biotin capture ELISA.

5.4.2 Initial slot-blot screen to identify antibody epitopes on non-denatured CB_1

We suspected the most likely accessible and antigenic regions were the remaining N-terminus (88-110) and intracellular loop 3 (IL3). Thus, to help identify if the new antibodies bound in either of these regions, we created two CB_1 variants that we could use as targets for screening the antibodies. One mutant had an additional 15 resides in the N-terminus (Δ103) deleted, and one mutant lacked IL3 (residues 307-326, termed ΔIL3) (Figure 5.1B). These mutant CB_1 receptor construct were purified, and then probed with each of the hybridoma supernatants using a slot blot approach, along with initial antigen as a control (Figure 5.1C).

As seen in Figure 5.1, the initial characterization could be used to separate the clones into three classes of antibodies: 1) a group that is sensitive to the extreme Δ103 N-terminal deletion, 2) a group that is sensitive to the IL3 deletion and 3) a group that is insensitive to both deletions. Moreover, all the different hybridoma supernatants could

bind to the initial antigen (Δ88). These classes of CB_1 specific antibodies are graphically illustrated by the cartoon in Figure 5.1A.

5.4.3 Screen of antibodies by traditional SDS-PAGE and Western blot

Next, I set out to examine if any of the antibodies were conformationally sensitive by probing their ability to detect the different CB_1 constructs after denaturation by SDS-PAGE and subsequent immunoblot analysis. Again, all of the clones selected from each of these groups could detect the original Δ88 antigen (Figure 5.2).

Surprisingly, only the antibodies sensitive to the IL3 deletion could recognize the full length 'wild-type' shCB1-C13 (or C13 for short). The clones from the N-terminal deletion sensitive group, and a clone that was insensitive to both Δ103 and ΔIL3 deletions mutants could not recognize C13. Two of the N-terminus group clones (1E10 and 3D5) also were unable to detect our full length N-terminal purified CB_1 receptor (despite significant amino terminal proteolysis) using slot blot analysis. However hybridoma clone 8E3, a member of the IL3 and N-term deletion insensitive group, was capable of detecting the presence of this construct (Figure 5.S1). This observation, coupled with the SDS-PAGE analysis in Figure 5.2A, suggests that 8E3 may bind to an extracellular region (that is not the N-terminus) of CB_1 and this epitope can be masked by the full N-terminus.

5.4.4 Characterization of antibodies that bind an N-terminal epitope

Data in Fig 5.1C suggest that hybridoma clones 1E10 and 3D5 appear to bind to an epitope contained within residues 88 and 103. We further characterized this N-terminal epitope by measuring the ability of a peptide corresponding to part of this region in CB_1 (^{88}SKFENEENIQ^{97}) to block binding of this antibody. As can be seen in Figure

5.2B, the peptide significantly reduces the binding of antibody 1E10 to the Δ88 CB_1 antigen, suggesting the epitope for 1E10 and 3D5 most likely includes this region of the CB_1 N-terminus. Additionally, CB_1a, an amino-terminal splice variant of CB_1 [19], can also mask detection of the 1E10 epitope.

5.4.5 Characterization of antibodies that bind the IL3 epitope

Antibodies fragments that bind at (or around) IL3 have proven successful chaperones in crystallization of GPCRs, but one necessary criterion is that they can recognize the receptor in detergent, under non-denaturing conditions. Thus, we decided to further characterize how well the antibodies 3A3 and 5G3 interact with purified receptor in solution [98, 264]. This was accomplished by using fluorescence size-exclusion chromatography (FSEC) to measure their ability to bind purified green fluorescent protein (GFP) tagged Δ88 (Δ88/Δ417-II, described in Chapter 2). The mobility shift observed in the presence of 3A3 and 5G3 indicates both antibodies are capable of recognizing a native, detergent solubilized CB_1 receptor (Figure 5.3).

We also assessed how low in concentration we could still detect binding for these two antibodies by testing complete FSEC mobility shifts under different receptor-antibody concentrations (at a1:1 ratio). Both 5G3 and 3A3 could detect the GFP tagged Δ88 mutant in the nano molar concentration range. Interestingly, the 3A3 required a higher receptor: antibody concentration in order to induce a full mobility shift on the FSEC (Figure 5.3A), indicating that 5G3 is of higher affinity (10s vs 100s of nM).

We also assessed the ability of IL3 antibody 3A3 to visualize CB_1 expressed in cells in imaging studies, and found 3A3 was able to detect CB_1 receptors transiently expressed in HEK293 cells (Figure 5.3D-E).

5.4.6 IL3 antibody 3A3 preferentially binds active CB_1

During the initial screening of constructs, we observed that the antibody 3A3 binding to CB_1 was enhanced in the presence of agonist CP 55940 in a slot blot assay. Moreover, pre-incubation of the receptor in SDS reduces 3A3's affinity to CB_1 (Figure 5.4A). These results indicate that the epitope recognized by 3A3 is denaturation sensitive (i.e., not merely a linear epitope), and is also conformationally sensitive — i.e., it preferentially binds the activated form of the receptor.

Due to the promising nature of this clone, we next generated and purified Fab produced from 3A3. We tested the effect of these 3A3 Fabs on the conformation of CB_1, using the fluorescence assay we previously used to monitor agonist-induced conformational changes in TM6 of CB_1 (see Chapter 3 for more details). These experiments showed a startling result — the 3A3 Fabs can themselves cause an increase in fluorescence of the bimane labeled CB_1— presumably by an allosteric interaction with an epitope in IL3 (Figure 5.4C). The change is similar to agonist CP 55940, which also causes an increase bimane labeled CB_1's fluorescence. Importantly, the increase is blocked by preincubation with an antagonist (Figure 5.4D). Interestingly, the allosteric ligand Org 27569 alone does not appear to block the 3A3-induced fluorescent change, but in the presence of Org 27569 and agonist, the 3A3 Fab does not induce a fluorescence change (Figure 5.S2). This intriguing finding will be discussed below.

5.5: DISCUSSION

To our knowledge, our new antibodies represent the first mouse monoclonal antibodies directed at several currently untargeted epitope domains in the CB_1 receptor.

The antibodies can be grouped into three different categories, based on the epitope regions they recognize: (1) N-terminal residues 88-103, (2) intracellular loop three (IL3), and (3) a yet unidentified region that we suspect is in the extracellular region of the receptor. The characteristics and implication of these different antibodies are discussed below.

5.5.1 Antibodies that bind an N-terminal epitope on CB_1

Several antibodies (1E10, 3D5, 2C12, 3D12, 10F4, 1B1 and 6E7) were generated that localize to the N-terminus. Interestingly, a subsequent sequence-based analysis of the N-terminus of CB_1 predicts residues 83-95 to be especially antigenic (Figure 5.S3). This region overlaps with our 88-103 region of the N-terminal antibody group.

Curiously, this epitope of CB_1 is inaccessible for the full length N-terminus, and the shorter CB_1a isoform, even under denaturing SDS-PAGE conditions. Thus, it is tempting to speculate that perhaps the N-terminus of CB_1 serves an immuno-protective role for this region, "shielding" it from the immune system. One antibody, 1E10, clearly locates to this region, based on peptide competition assays (Figure 5.2B). Thus, this peptide and antibody may serve as a useful combination for immunoaffinity purification and be commercially exploited as a system to purify other proteins, as has been the case for FLAG and 1D4 antibodies [265, 266].

5.5.2 Antibodies that do not bind either N-terminal or IL3 epitopes

Perhaps the most uncharacterized class of antibodies I identified is the "extracellular region" antibodies (or EC region). We propose these antibodies bind in the

EC region because they are able to bind purified CB_1 constructs even with an extreme N-terminal deletion (Δ103) or IL3 deleted, indicating that they do not need residue 1-102, 307-326, or 417-472 to bind CB_1. However, they cannot bind to the receptor when the full CB_1 N-terminus is present (even under denaturation conditions).

How can we explain this conundrum? One possibility is that the CB_1 N-terminus forms a structure that sits over and shields this antigenic region recognized by these antibodies, as we think occurs for the N-terminal antibodies discussed in previous section. These interpretations would again support the notion that the CB_1 N-terminus likely forms a lid over the receptor that occludes the EC region similar to that as seen in crystallographic models of lipid-type ligand GPCRs, rhodopsin and S1P1 [120, 173]. Formally, it is possible these antibodies might instead bind to transmembrane helices (TM) in CB_1, although this is highly unlikely, due to the lack of exposure and antigenicity of TMs. It will be interesting in future studies to examine if this class of antibodies affects receptor ligand binding or activation for our extreme N-terminal deletion construct.

5.5.3 Antibodies that bind to an IL3 epitope on CB_1

The IL3 of GPCRs is well known to play a role in G protein-coupling. Moreover, IL3 exhibits a high degree of sequence divergence (and length) between GPCRs, and this fact suggests it plays a key role in receptor bias to different G proteins. Additionally, IL3 is highly mobile in electron paramagnetic resonance and deuterium exchange mass spectrometry studies [119, 267]. Furthermore, the B-factors observed in crystallographic models of IL3 are often high, indicating each model represents an ensemble of conformations; also IL3 can exist in different poses in various atomic resolution

structural models [116, 120]. Given the flexibility of this region and its involvement in the G protein interaction (which is well known to allosterically modulate receptor transitions), it is not surprising that proteins that bind to and restrict the conformational landscape of IL3 can also modulate GPCRs.

Indeed, recent advancements in GPCR crystallography often replace this region of the receptor with a crystallization chaperone (such as T4 Lysozyme) and/or employ antibody fragments directed at this region of the receptor. Recently, some of these antibody fragments have been shown to stabilize/induce conformations in the receptor that (allosterically) modulate receptor transitions [98, 109, 264, 268].

We find a similar effect with our antibody 3A3 and Fab fragments, which we find to have a higher affinity for the agonist bound receptor. Furthermore, Fabs from antibody 3A3 induce a fluorescent change in CB_1 that appears identical to that produced by agonist binding, and this change is inhibited by first pre-incubating the receptor with antagonist (Figure 5.4). This finding suggests that 3A3 stabilizes or induces an active-like state in the receptor (Figure 5.4E). Thus, 3A3 may serve as a promising candidate for further structure/function studies that probe allosteric modulation of receptor transitions.

Importantly, it may also be possible to exploit the ability of 3A3 to preferentially bind to an agonist-bound CB_1 receptor in some kind of diagnostic probe for drug discovery programs. Whole-cell imaging using 3A3 antibodies appears possible (Figure 5.3B), suggesting promise for this antibody in biological screening of CB_1 and its isoforms. Finally, we note that two IL3 antibodies appear to bind to the soluble form of the receptor, as indicated by the shifts in the CB_1-GFP FSEC mobility, and thus they represent promising crystallization chaperone candidates (Figure 5.3A and 5.3B).

Figure 5.1

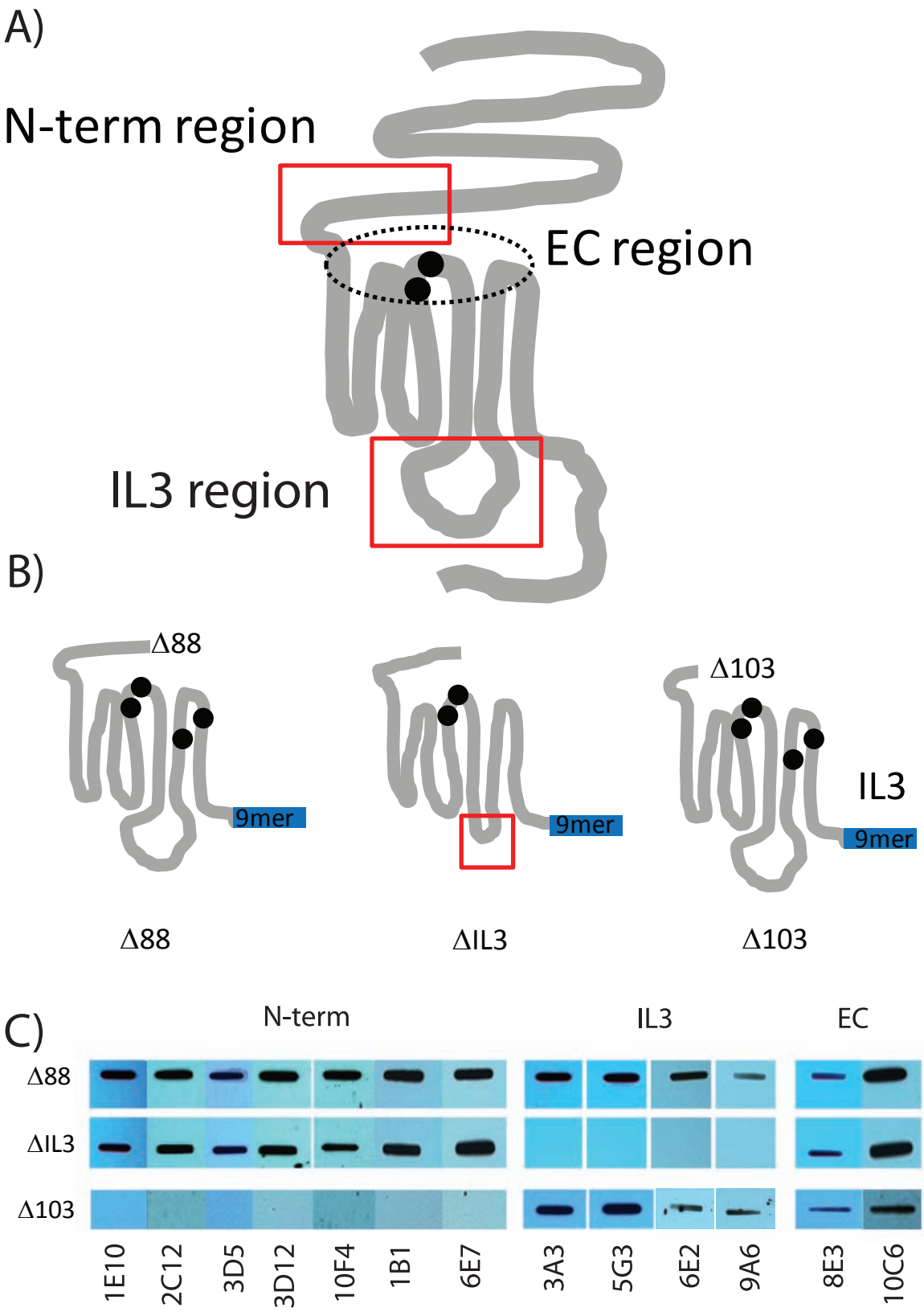
A)
N-term region
EC region
IL3 region
B)
Δ88
9mer
9mer
Δ103
IL3
9mer
Δ88
ΔIL3
Δ103
C)
N-term
IL3
EC
Δ88
ΔIL3
Δ103
1E10
2C12
3D5
3D12
10F4
1B1
6E7
3A3
5G3
6E2
9A6
8E3
10C6

Figure 5.1. Characterization of CB_1 mouse monoclonal antibodies (MAB)

(A) Cartoon illustration depicting proposed sites of antibody binding to the CB_1 receptor. Red boxes indicate that deletion mutation in these regions inhibits antibody binding. The dashed ellipse indicates a proposed binding region. The three classes of antibodies are (1): 'N-term' - a group that binds to residues 88-103 in the N-terminus, (2): 'IL3' - a group sensitive to the IL3 deletion and (3): 'EC region' – a group that does not bind the N-terminus or IL3. **B**) Illustration depicting the CB_1 mutants used in panel C. Our initial antigen Δ88 (right) containing four cystiene residues CB_1 (C257,C264, C355, and C382), in addition to a C-terminal truncation (Δ417) followed by the rhodopsin C-terminal nine amino acid affinity motif that is detected by an anti-rhodopsin antibody, 1D4 (9mer, blue). (Middle) The construct termed ΔIL3 is a θ mutant (containing only cysteines residues C257 and C264), where residues 307-326 corresponding to part of intracellular loop 3 (IL3) have been removed. (Right) The construct termed Δ103, similar to Δ88, however, is N-terminally truncated at residue 103. **C)** Slot blot analysis showing three different classes of CB_1 antibodies. Top row is 250 ng of purified antigen Δ88, middle row (ΔIL3) IL3 deletion mutant (deletion of residues 308-327) and the last row is 250 ng of purified extreme N-terminal, Δ103 deletion mutant lacking residues 1-102. This slot blot was performed with an overnight exposure to primary at 1:1000 dilution corrected for antibody concentration (determined by MAB immunotblot to a known standard) in supernatant such that the concentration was approximately 10 μg/mL before dilution. Secondary was at 1:5000 for 2 hours. Blots are representative of at least two independent experiments. See Experimental Procedures for more details

Figure 5.2

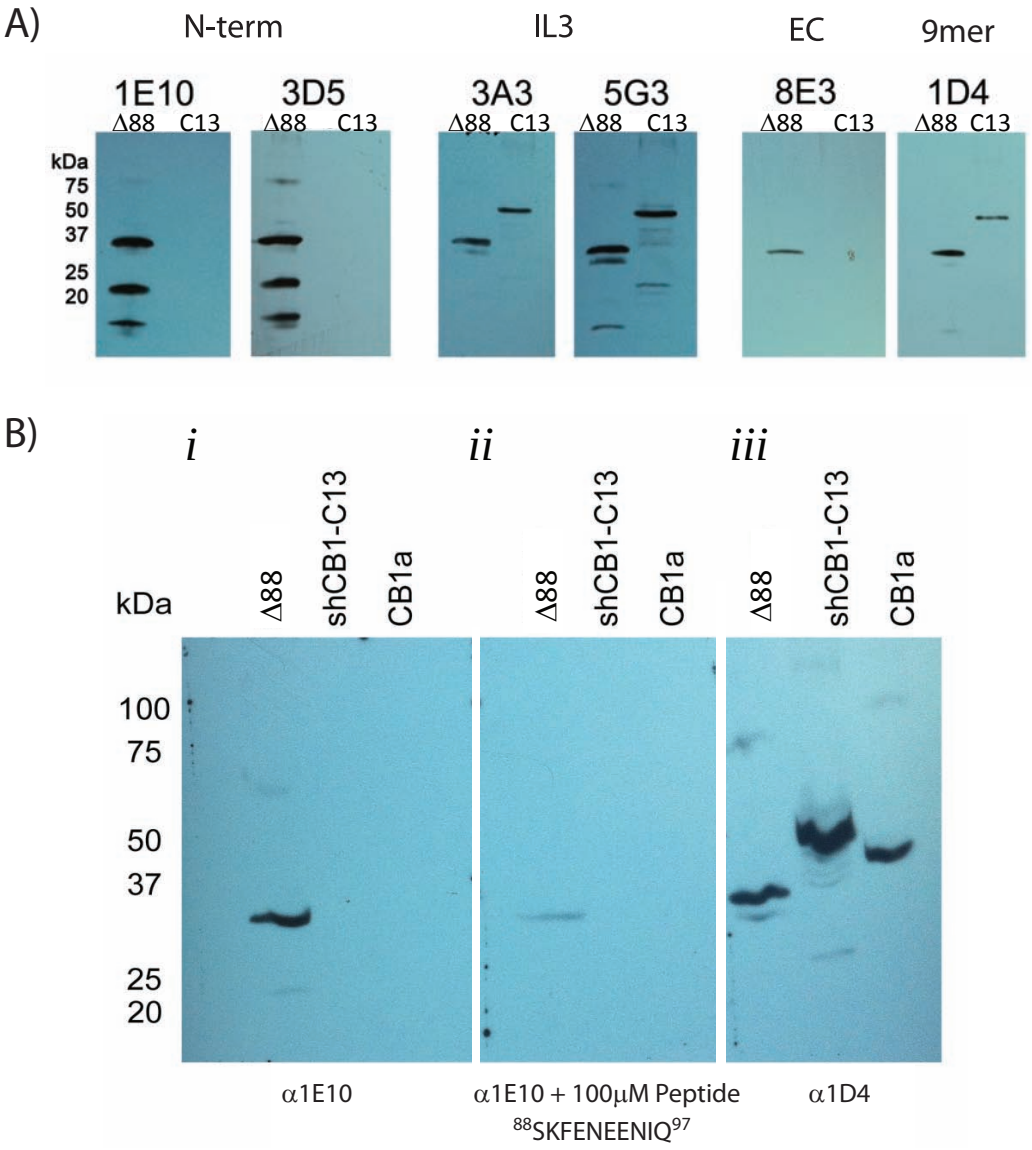
A)
N-term
IL3
EC
9mer
1E10
3D5
3A3
5G3
8E3
1D4
Δ88 C13
kDa
75
50
37
25
20
B)
i
ii
iii
kDa
Δ88
shCB1-C13
CB1a
100
75
50
37
25
20
α1E10
α1E10 + 100μM Peptide
88SKFENEENIQ97
α1D4

Figure 5.2. Analysis of select clones by SDS-PAGE and Western blotting. (A) The full CB_1 N-terminus apparently blocks the binding epitope for both the EC region and N-term antibodies, even under denaturing conditions (SDS-PAGE). SDS-PAGE and Western blot of crude membranes expressing Δ88 or 'wild-type' (C13) CB_1 constructs. The amounts of CB_1 protein on the gel is in 50-100 ng range, assuming a receptor expression level of ~20 μg/plate. The Western blot used an overnight exposure to primary antibodies 1:1000 dilution (corrected for antibody concentration in supernatant such that the concentration was approximately 10 μg/mL before dilution). The secondary antibody was at 1:5000 dilution for 1 hour. As a positive control, 1D4, an antibody against the last 9 amino acids of rhodopsin (a tag present on both constructs) was also used to probe at a 1:5000 dilution (CB_1 protein for this antibody was in tens of ng range). **(B)** A peptide corresponding to the sequence in the N-terminal epitope appears to compete with binding of antibody 1E10. No binding is seen for CB_1a (a CB_1 isoform with a shorter N-terminus). SDS-PAGE and Western blot of crude membranes expressing Δ88 , 'wild-type' (C13) CB_1 constructs, or CB_1a. *i*) using 1E10 to probe *ii*) using 1E10 probe in the presence of a peptide ^{88}SKFENEENIQ^{97}and *iii*) a 1D4 control lane showing the presence of all three CB_1 receptor constructs

Figure 5.3

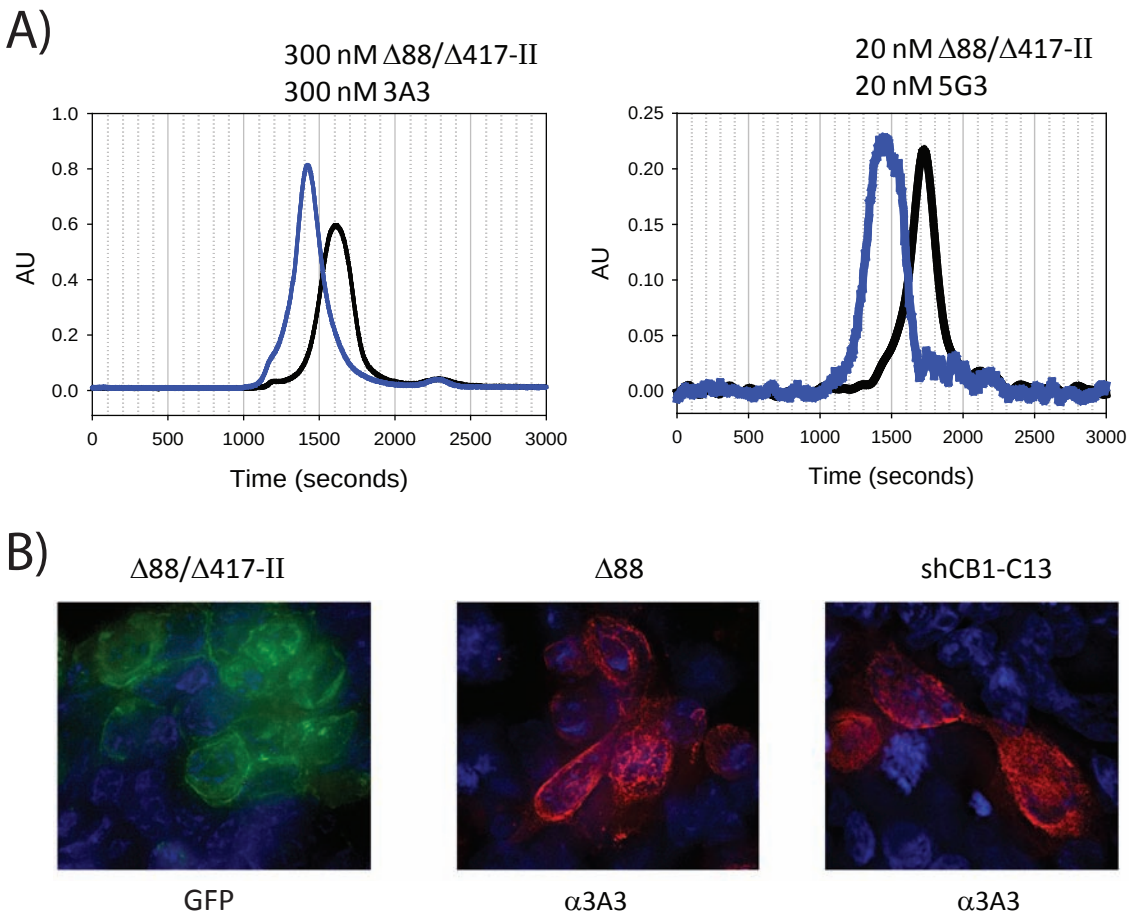
A)
300 nM Δ88/Δ417-II
300 nM 3A3
AU
1.0
0.8
0.6
0.4
0.2
0.0
0
500
1000
1500
2000
2500
3000
Time (seconds)
20 nM Δ88/Δ417-II
20 nM 5G3
AU
0.25
0.20
0.15
0.10
0.05
0.00
0
500
1000
1500
2000
2500
3000
Time (seconds)
B)
Δ88/Δ417-II
Δ88
shCB1-C13
GFP
α3A3
α3A3

Figure 5.3. Further characterization of monoclonal antibodies that bind to IL3 (3A3 and 5G3). (A) Antibody 3A3 (left) and 5G3 (right) can bind solubilized, purified CB_1-GFP chimera (Δ88/Δ417-II), as assessed by an FSEC mobility shift assay. Compare receptor alone (in black trace) and receptor antibody at indicated concentration (in blue trace). The 5G3 antibody appears to have higher affinity, as it can cause a complete shift at lower concentrations. Purified antibody was added to receptor at indicated concentrations. Samples were incubated in 2XFSEC at indicated concentrations and nutated for 1 hour, then injected onto a 60 mL (34 cm x 1.5 cm diameter) Superdex 200 (prep grade) using 20 mM TRIS pH 7.5, 150 mM NaCl, 1mM EDTA and 0.05% DM at a flow rate of 0.5 mL/min. The elutions were monitored via a RF-551 fluorescence HPLC monitor (Shimadzu) with the excitation wavelength set at 470 nm and the emission wavelength set at 507 nm for GFP **(B)** The 3A3 antibody can be used in immunoflourescence imaging studies of cells. Flourescence from a GFP fusion construct (Δ88/Δ417-II, far left) compared to immunofluorescence visualization of CB_1 with 3A3 antibody for the antigen Δ88 (middle) and our 'wild-type' receptor shCB1-C13 (right).

Figure 5.4

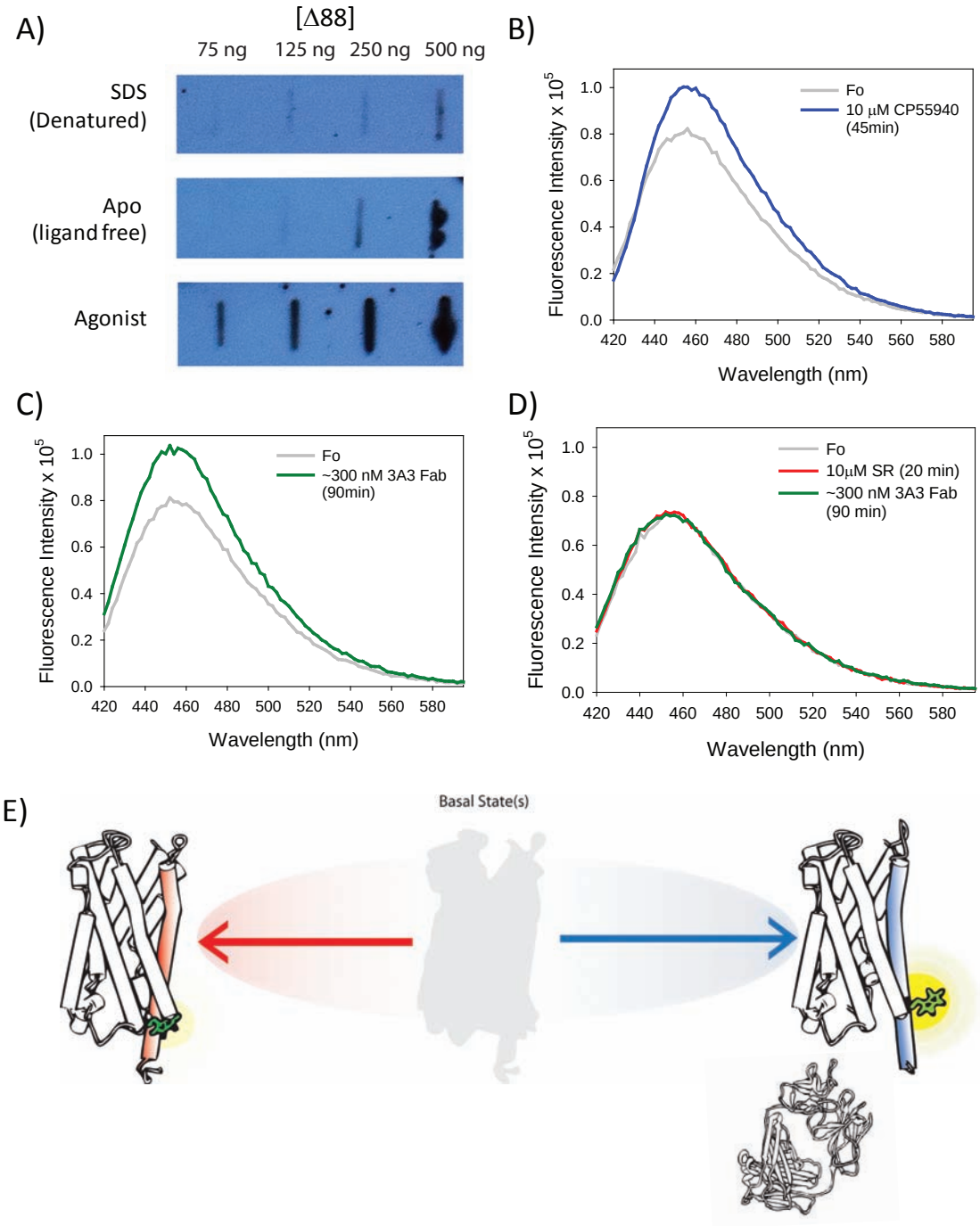
A)
[Δ88]
75 ng
125 ng
250 ng
500 ng
SDS
(Denatured)
Apo
(ligand free)
Agonist
B)
Fluorescence Intensity x 10^5
Fo
10 μM CP55940
(45min)
Wavelength (nm)
C)
Fluorescence Intensity x 10^5
Fo
~300 nM 3A3 Fab
(90min)
Wavelength (nm)
D)
Fluorescence Intensity x 10^5
Fo
10μM SR (20 min)
~300 nM 3A3 Fab
(90 min)
Wavelength (nm)
E)
Basal State(s)

Figure 5.4. Fab fragments of IL3 binding antibody 3A3 induce or stabilize an active like state. A) An immunotblot slot blot assay shows the conformational sensitivity of CB_1 to 3A3. The initial antigen (Δ88) was diluted such that the final protein concentration per well was 75, 125, 250, and 500 ng. (Top) Denatured samples were prepared by incubation of receptor in dye free SDS-PAGE loading buffer prior to blot. (Bottom) To test sensitivity to agonist, the CB_1 samples were diluted into 2XFSEC buffer containing 1 μM agonist, CP 55940 (Middle - the apo sample, contains no ligands). All samples were incubated in their respective buffers for 20 min at room temperature prior to performing the slot blot. The primary antibody 3A3 was blotted at 1:1000 and secondary was at 1:5000. Blocking, primary and secondary were all done for one hour. **B)** The addition of agonist (10 μM, CP 55940) causes an ~35% increase in fluorescence intensity for PDT-bimane labeled mutant sample A342C/θ, which we interpret to indicate a conformational change in TM6 (See Chapter 3). **C)** Addition of 3A3 Fab alone (in the absence of agonist) induces a slow change in fluorescence that mimics agonist binding. **D)** Pre-incubation with the antagonist (10 μM, SR141716A) inhibits the 3A3 Fab induced change in bimane's fluorescence. All spectra are background subtracted from buffer and ligands. **E)** Cartoon model showing that occupation of the traditional binding site by an agonist accompanies a conformation change in TM6 (blue), detected as an increase in fluorescence from an attached bimane probe (green). This model proposes that our Fab binding traps a distinct and different CB_1 structure — i.e., a ligand free receptor state with, 3A3 Fab bound (to IL3) which appears to be in an active like state. The basal (ligand free) CB_1 state is depicted in light gray.

Supplemental Figures

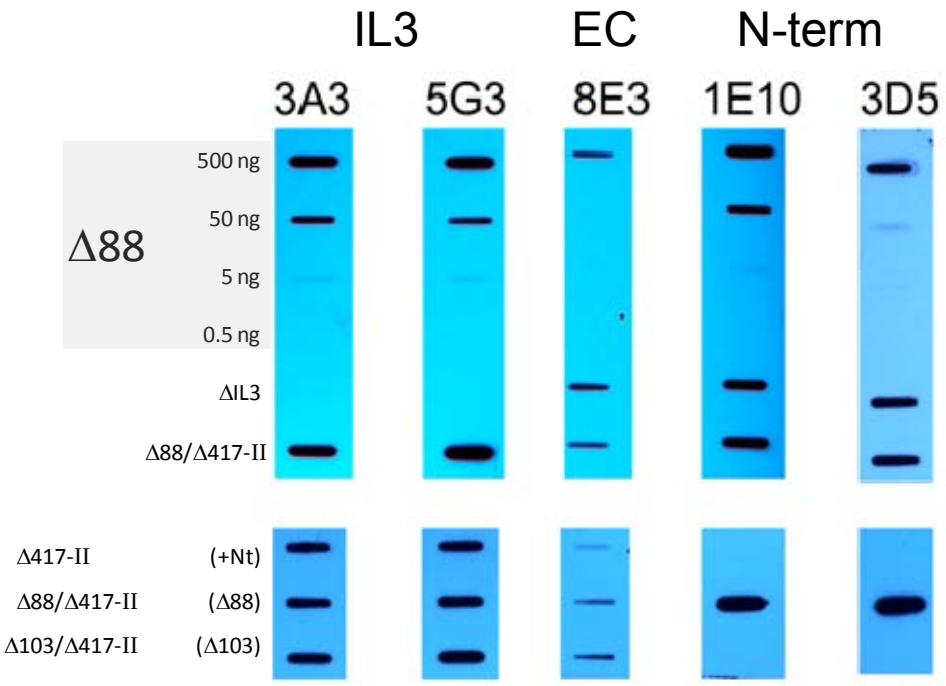

Figure 5.S1. Slot blot analysis showing three different classes of CB_1 antibodies. This slot blot was performed with an overnight exposure to indicated primary at 1:1000 dilution corrected for antibody concentration in supernatant such that the concentration was approximately 10μg/mL before dilution. Secondary was at 1:5000 for 2 hours and the rest is as previously described. Purified CB_1 mutants were transferred to PVDF membranes at indicated concentrations. Mutants, Δ88 (Δ88/Δ417-III), ΔIL3, and CB_1-GFP chimera (Δ88/Δ417-II) used 500 ng of protein (top). All N-terminal mutants used 250 ng of protein (bottom).

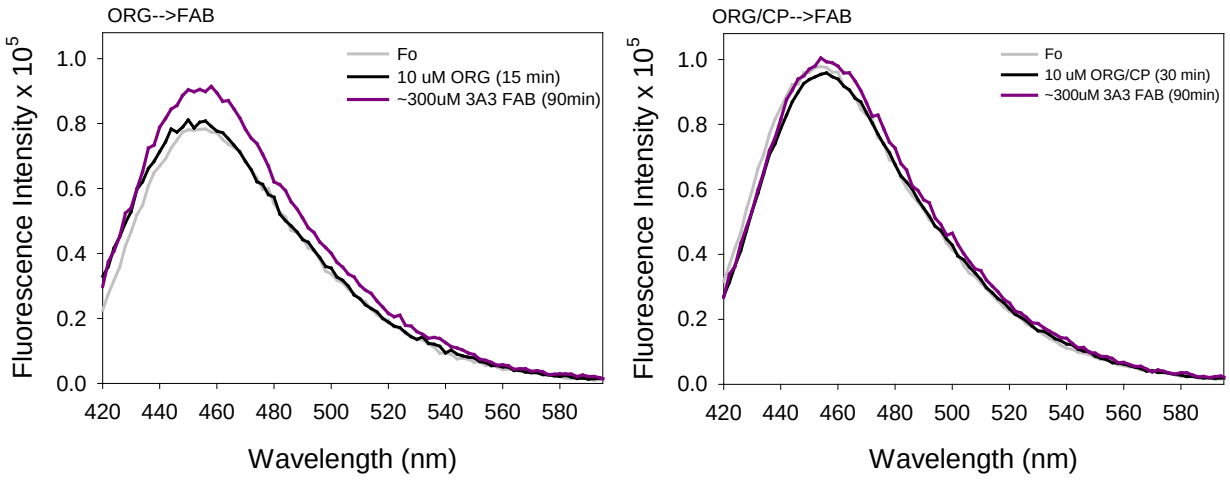

Figure 5.S2. Allosteric CB_1 ligand Org 27569 alone does not appear to block the effects of 3A3, however Org 27569 and agonist renders the receptor insensitive to Fab 3A3's effects. (Left) The fluorescence intensity for 200 nM PDT-bimane labeled mutant sample A342C/θ (Fo, initial spectra gray) pretreated with 10 μM Org 27569 for 15 min (black) and then after a 90 minute incubation with 300 μM 3A3 Fab (purple). (Right) Fluorescence intensity for 200 nM PDT-bimane labeled mutant sample A342C/θ (Fo, initial spectra gray) pretreated with 10 μM Org 27569 and 10 μM CP 55940 for 30 min (black) and then after a 90 minute incubation with 300 μM 3A3 Fab (purple). All spectra are background subtracted from buffer and ligands. Further details are provided in the Experimental Procedures

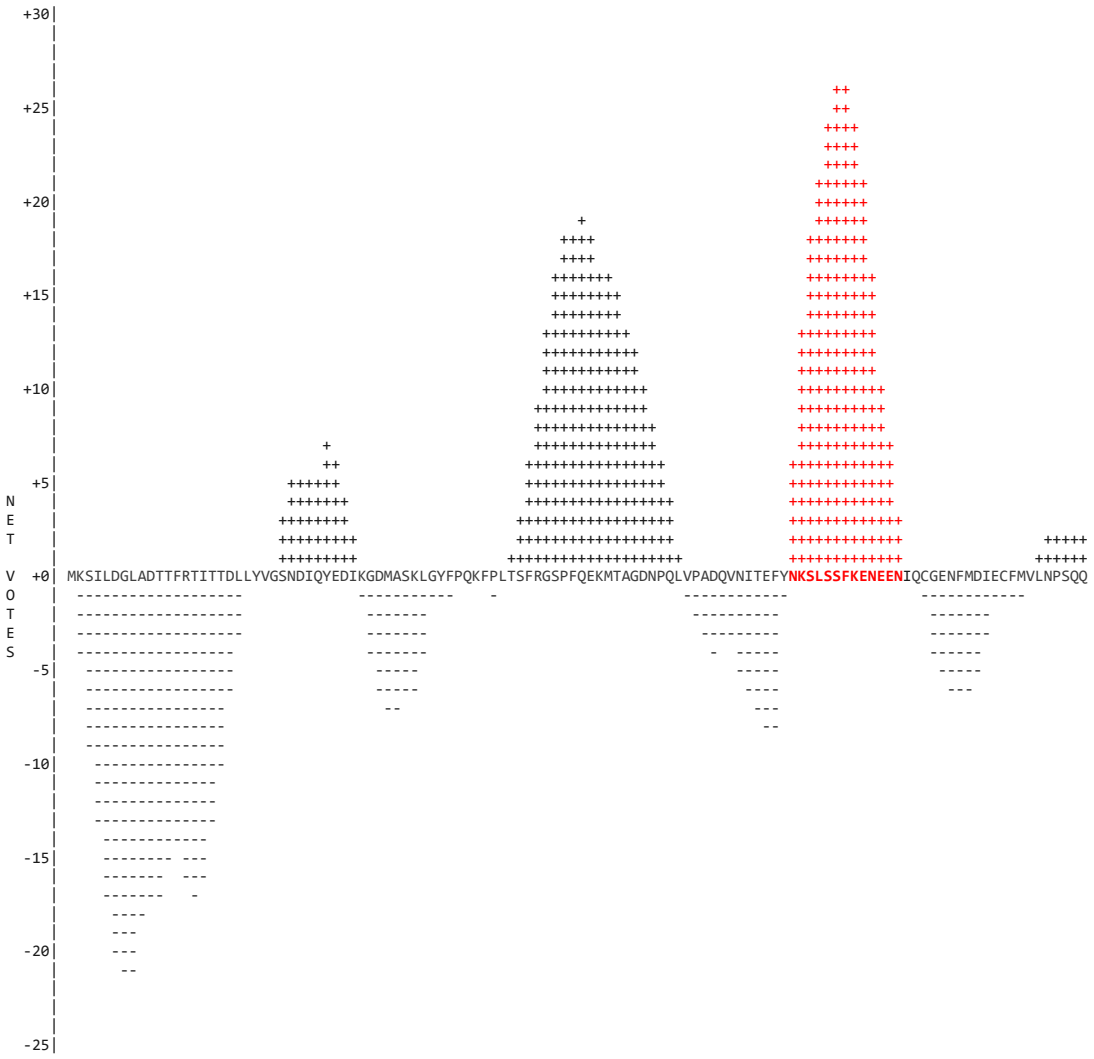

Figure 5.S3. Predicted antigenic propensity score for CB_1 N-terminus. Shown in red are residues 83-95. Predictions were performed using COBEpro [269]. N-terminal group antibodies recognize a region that overlaps with this predicted highly antigenic region and is consistent with assignment of that antibody epitope from both deletion mutants and peptide competition studies. Interestingly, the full Wt CB_1 N-term appears to shield this region from detection, despite its predicted highly antigenicity.

Chapter 6

Summary and Conclusions

6.1: Overview

In this dissertation, I have described the purification, biochemical and biophysical characterization of the CB_1 receptor. In Chapter 2, I describe a systematic approach I developed to purify CB_1 and demonstrated high retention of ligand binding and functionality. Then, in Chapter 3, I studied the dynamic structural changes in CB_1 using site directed fluorescent labeling (SDFL) and addressed how a novel allosteric CB_1 ligand exerts its effects. In Chapter 4, I expanded on observations made during purification of CB_1 and discovered a subtle allosteric role for cysteine residues in the CB_1 N-terminus. Finally, in Chapter 5, I detail the creation and characterization of several novel CB_1 specific monoclonal antibodies, using the purified CB_1 receptor as an antigen.

Below, I will discuss the most germane findings and conclusions for each chapter, and then discuss unresolved issues and aspects that warrant further exploration and future experimentation.

6.2: **Summary of Chapter 2:** *Purification of functional human cannabinoid receptor CB_1 from a mammalian cell expression system*

My studies indicate that CB_1 can be successfully purified from a mammalian expression system. The yield from this process is ~15-20 μg of purified receptor per 15 cm plate of transfected COS1 cells. Moreover, the purification construct I identified (through systematic trial and error) is functional: it retains high percentage of ligand binding (85%) and is able to elicit agonist stimulated guanine nucleotide exchange when reconstituted with G protein.

Notably, the rate of G protein activation for this purified CB_1 mutant is about 20 fold lower than that of rhodopsin for $G\alpha_i$. One reason could be that our purification construct lacks cysteine number 415, at the end of juxtamembrane helix 8, a cysteine that is generally conserved in most rhodopsin like GPCRs. Cysteines residues around this region are palmitoylated in rhodopsin and B2AR [270, 271] and their mutation to an alanine in CB_1 inhibits G protein activation [272]. However, in previous studies I found mutation of this cysteine in a CB_1-G protein fusion construct had no deleterious effects, although the chimera construct, may mask any change in signaling due to mutation of the palmitoylation site [199].

Future directions for analysis of purified CB_1

The ability to produce purified, functional CB_1 now makes it possible to study cannabinoid receptors using reductionist approaches and some future possible experiments are briefly discussed below. For example, it could prove informative to explore the palmitoylation status of the above mentioned cysteine in an *in vitro*

reconstitution assay, in order to determine what effects palmitoylation of this residue has on G protein-coupling and activation. It would also be important to explore the effects of lipids on G protein activation by CB_1, as others have found the presence of lipids enhanced receptor stimulated G protein activity and even arrestin binding. [195, 273, 274].

One way to do this would be to incorporate purified CB_1 into 'nanodiscs' (soluble discoidal lipid bilayers). Nanodiscs are comprised of a small portion of membrane that has been solubilized by the addition of two molecules of an amphipathic protein, the so-called membrane scaffold protein (MSP), which are derivatives of apolipoprotein A-1 (apo A-1) [275]. The MSP wraps around the hydrophobic core of the lipids, creating a soluble, caged membrane that allows for study of the receptor in a native membrane environment. In our laboratory, we have employed this system for studies of rhodopsin [131, 276]. I have also been able to prepare CB_1 receptors in these discoidal membranes, using bimane labeled θ/342C (described in Chapter 3), and I observed an agonist dependent change in fluorescence in this system. However, I was not able to accurately assess the radioligand binding properties in these preliminary studies, due to high non-specific ligand binding and low yields of receptor/nanodiscs.

Solution based radioligand binding studies

One caveat regarding the data presented in Chapter 2 is the methodology I used in thoes first studies measuring solution based radioligand binding assay was unfortunately less effective for agonist CP 55940 binding and homologous CP 55940 binding assays suffered from low signal-to-noise. I was later able to improve and optimize this assay, as shown in Chapter 3.

The use of Δ88/Δ417-III construct

The final cysteine construct ultimately employed in Chapter 2 (containing C257, C264, C355 and C382) had high background labeling of fluorophores and thus was unsuitable for subsequent SDFL studies. As C257 and C264 are in a disulfide bond ([199, 221] and Chapters 3) this labeling could be due to the remaining cysteines (C355 and 382). However, I suspect C382 is more likely the reactive cysteine, as the CB_1 -T4L fusion construct (detailed in Appendix 2) is not susceptible to labeling, yet contains C355.

6.3: Summary of Chapter 3: *A key agonist-induced conformational change in the cannabinoid receptor CB_1 is blocked by the allosteric ligand Org 27569*

In Chapter 3 of this dissertation, I performed an SDFL study on CB_1. Here I first created and validated a minimal cysteine construct that could be specifically labeled with a thiol reactive fluorophore. In this case, the fluorophore bimane was attached at the cytoplasmic end of TM6, as this region of CB_1 is thought to move upon ligand binding. The bimane labeled sample appeared to bind agonist (CP 55940) and antagonist (SR141716A), using an improved radioligand solution binding assay.

Addition of the agonist, CP 55940, to this labeld-CB_1 resulted in an increase in fluorescence that could be reversed by the antagonist, SR141716A. Moreover, the agonist bound receptor showed increased collisions with an aqueous quencher, when compared to antagonist bound receptor. These results suggest that a label on TM6 moves into an environment that is more exposed upon activation, which is consistent with other models of GPCR activation. Importantly, other cannabinoid agonists were also able to

produce a similar increase in fluorescence. For example, the non-classical agonist WIN55212-2 and the partial agonist, endocannabinoid analogue of anadamide (meAEA) were both capable of eliciting an increase in fluorescence. Notably, the meAEA increase was less dramatic in intensity than WIN55212-2 or CP 55940 and could be overcome by the additional addition of saturating amounts of CP 55940. These later results suggest that the magnitude of TM6 change may be less for partial agonists (or the partial agonist receptor complex spends less time in the fully active state). When the change in bimane fluorescence was measured as a function of drug concentration, we found a similar rank order of potency as is observed for CB_1 G protein activity assays (i.e., CP>WIN>AEA).

I then explored the behavior of the curious allosteric CB_1 ligand, Org 27569 [163] in the *in vitro* purified CB_1 system. I observed that Org 27569 does not act as traditional orthosteric ligand. In fact, Org 27569 enhances agonist binding, yet inhibits G protein activation in the presence of agonist. My studies on Org 27569 using our purified biochemical assays prove that Org 27569 binds to the purified bimane labeled CB_1 receptor, and acts directly on the CB_1 receptor. When used in our fluorescence based assay, Org 27569 pre-incubation blocks the agonist induced fluorescence change yet reverses the fluorescence change when added after agonist. Org 27569 was also able to reverse the agonist induced fluorescence change due to WIN55212-2 and meAEA.

When the change in agonist induced bimane fluorescence was measured as a function of allosteric Org 27569 ligand concentration, I observed a dose dependent decrease in fluorescence (Figure 3.4F). Moreover, when we fit an operational model of allostery (Equation 3.2) to our data we find the magnitude of the allosteric modulation of agonist efficacy (defined as the β value) to be less than one and, in fact, approaches zero

(Table 3.1). This indicates "insurmountable allosteric antagonism" of the observable, the bimane response, which we interpret to be transition of the receptor into the active state. Furthermore our findings are in agreement with predictions of the allosteric two-state model, where the allosteric ligand has positive cooperativity with agonist binding (enhances agonist binding) but negative cooperativity with receptor activation (a β value less than one) [231] (this is discussed in further detail in the Allosteric Appendix).

Based on our SDFL fluorescence assay, we conclude that Org 27569 places the receptor in a unique conformation – i.e., an agonist bound state that lacks TM6 movement. We speculate that Org 27569 traps the CB_1 receptor in an intermediate conformation on the pathway to an activated receptor. Recently, studies from Dr. Kendall's laboratory (published online after submission of our manuscript) suggests that a constitutively active CB_1 mutant was not altered by Org 27569 [181]. Their observation is not inconsistent with our hypothesis. Constitutively active receptors possibly reduce the energy barrier towards an activated receptor species and thus could attenuate the actions of Org 27569 in trapping a now energetically less-favorable species.

Furthermore, Org 27569 may act as a functionally selective ligand. Evidence suggest that on its own, Org 27569 can enhance G protein *independent* pathways [181]. Recent structural and dynamic evidence suggest that GPCR mediated, non-G protein signaling pathways involve structural changes at or around TM7 of the receptor [136-138]. Indeed, I have carried out preliminary experiments that seem to suggest Org 27569 enhances spectroscopic changes at or around the TM7/H8 interface. Future experiments aimed at further exploring the conformational transitions of the CB_1 receptor's cytoplasmic surface may help further illuminate mechanisms of CB_1 receptor function.

6.4: **Summary of Chapter 4:** *Extracellular cysteine residues in the N-terminus of human neuronal cannabinoid receptor allosterically regulate ligand affinity*

I explored the puzzling nature of the relatively long CB_1 receptor N-terminus in Chapter 4. While monitoring reactivity of purified CB_1 mutants to bimane, I stumbled upon an interesting observation. The Nt2/C2 purified mutant, which contains two cysteines in the N-terminus (C98 and C107) and two cysteines in a known disulfide (C257 and C264) runs faster than C2 on a Coomassie stained SDS-PAGE gel (Figure 4.3). I only fortuitously noticed this because the PDT-bimane fluorophore attaches to free thiols via a disulfide bond thus I ran my gels in the absence of reducing agent. Upon further investigation of this shift, I found that the presence of DTT in the loading buffer causes this purified receptor to run more slowly, like its C2 counterpart (Figure 4.3). This initial finding indicates that perhaps an N-terminal disulfide potentially exists.

To address the possible role of an N-terminal disulfide, I conducted radioligand binding studies as a function of DTT, and found an unanticipated and surprising result. The reducing agent DTT appeared to *inhibit* agonist (CP 55940) binding, and in contrast, *enhanced* antagonist (SR141716A) binding.

From my research into allosteric models (Chapter 3 and the Allosteric Appendix) I realized these finding were consistent with an allosteric effect. Thus, I employed a two-site allosteric model to try and fit my observations. The model fits the data with reasonable coefficients of determination, and reasonably describes and quantifies my observations. Thus, these results suggest a role for the N-terminus, one that involves conformational coupling between the extracellular surface of CB_1 and its orthosteric ligand binding site. Specifically, an N-terminal disulfide can serve to allosterically

enhance antagonist binding or inhibit agonist binding. We further speculate that the N-terminal disulfide serves as a redox sensor that may alter the receptor's response to stress, although we do not yet have experimental data to support this speculation.

Future Directions

Ultimately, I would like to see if the DTT phenomena I observed for non-purified CB_1 in membranes can be recapitulated using purified CB_1. This would rule out other unidentified components as potential reasons for the reduction dependent allosteric modulation of CB_1. Furthermore, it would provide a set of controls that would allow for us to investigate if the N-terminal disulfide affects conformational dynamics in CB_1 (using SDFL approaches). Future experiments should also explore if endocannabinoid binding is also allosterically regulated by N-terminal disulfides, and what effect these N-terminal disulfides have on their efficacy.

6.5 Summary of Chapter 5: *Generation and initial characterization of novel* CB_1 *receptor monoclonal antibodies*

In Chapter 5 I used our functional purified CB_1 to have monoclonal antibodies generated by the Vaccine & Gene Therapy Institute. I was able to initially approximate where these antibodies bound on CB_1 using deletion mutants, and found they could be grouped into 3 categories, based on the regions in which they presumably recognize on the receptor: (1) an N-terminal group, (2) an extracellular region group, and (3) an intracellular loop 3 (IL3) group. These early characterizations set the stage for future experiments and possible commercially exploitable biological products.

For example, the binding of one of the N-terminal group antibodies, 1E10, can be inhibited by peptides corresponding to the binding epitope and thus this antibody/epitope combination might be usefully applied on other proteins, like the rhodopsin 1D4 tag. Moreover, the IL3 antibodies (3A3 and 5G3) are of high affinity, and can recognize wild-type CB_1 receptors. Current CB_1 antibodies are of low affinity, and this class of antibodies represents a major improvement in immunodetection of CB_1.

Interestingly, we find the antibody 3A3 appears to be conformationally sensitive, given its higher affinity for an agonist bound state. This property also has potential to be exploited, for example as a way to probe the active states of the receptor or in the testing of cannabimimetic analytes. I also have promising (preliminary) results that suggest that purified CB_1 bound to 3A3 antibody beads can be selectively eluted off using elution buffers containing antagonist. This might be useful for the selection of more biologically active CB_1 receptor species. These findings, however, have not been included in this thesis, as they require replication and optimization.

Future Directions

Many additional questions remain to be addressed regarding our novel anti-CB_1 antibodies. For instance, do IL3 antibodies disrupt G protein-coupling, and allosterically modulate ligand binding? What receptor conformation(s) do they recognize (or induce)? NMR or crystallography with IL3 peptides, as well as 3A3 and 5G3 Fabs could prove informative for understanding IL3 conformations. Additional biophysical characterization of antibody induced conformations could be explored using SDFL and even crystallographic approaches. Together, these investigations could provide further insight into the conformational landscape of CB_1.

It would also be interesting to see if the extracellular region antibodies (EC) may function as surrogate N-termini (for mutant receptors lacking the N-terminus). Due to the precedence of allosteric modulation of orthosteric ligand binding by the N-terminal disulfides presented in Chapter 4, a similar role of EC antibody binding may be possible (i.e., binding of these EC antibodies may allosterically alter the receptors ligand binding or functional properties). Moreover, the regions that the EC antibodies bind to could potentially be targeted, and thus represent an as of yet unidentified 'druggable' region – potentially facilitating the creation of pharmacological probes that can uniquely manipulate the receptor.

6.6: Concluding Statements

The methodologies I have set forth here allow for purification of CB_1 and the assesment of radioligand binding, thus providing the framework for a myriad of future experiments. The creation of a minimal cysteine CB_1 construct allows for many future SDL studies (both fluorescence and electron paramagnetic resonance). I used our unique capabilites in this way to explore the role of allostery in CB_1, and my data suggest that the allosteric ligand Org 27569 bound with agonist together inhbit transition of the receptor into the active state. Moreover, I have disovered what (we interpret to be) conformational coupling between the N-termininus and the orthosteric site in CB_1, hinting at a role for this mysterious extracellular region. Finally, my generation and characterization of CB_1 antibodies provides new reagents that may be used to elucidate structural mechanism of receptor activation. Together, I anticipate the methodologies, discoveries, and tools described herein will prove useful in the design of new pharmaceutical therapeutics.

References

1. Starks, M., *Marijuana Chemistry: Genetics, Processing & Potency.* 1990, Berkeley, Ca: Ronin Publishing, Inc.
2. Elsohly, M.A. and D. Slade, *Chemical constituents of marijuana: the complex mixture of natural cannabinoids.* Life Sci, 2005. **78**(5): p. 539-48.
3. Fellermeier, M., et al., *Biosynthesis of cannabinoids. Incorporation experiments with (13)C-labeled glucoses.* Eur J Biochem, 2001. **268**(6): p. 1596-604.
4. Fellermeier, M. and M.H. Zenk, *Prenylation of olivetolate by a hemp transferase yields cannabigerolic acid, the precursor of tetrahydrocannabinol.* FEBS Lett, 1998. **427**(2): p. 283-5.
5. de Meijer, E.P., et al., *The inheritance of chemical phenotype in Cannabis sativa L.* Genetics, 2003. **163**(1): p. 335-46.
6. McGilveray, I.J., *Pharmacokinetics of cannabinoids.* Pain Res Manag, 2005. **10**(A): p. 15A-22A.
7. Mechoulam, R. and Y. Gaoni, *A Total Synthesis of Dl-Delta-1-Tetrahydrocannabinol, the Active Constituent of Hashish.* J Am Chem Soc, 1965. **87**: p. 3273-5.
8. Watson, S.J., J.A. Benson, Jr., and J.E. Joy, *Marijuana and medicine: assessing the science base: a summary of the 1999 Institute of Medicine report.* Arch Gen Psychiatry, 2000. **57**(6): p. 547-52.
9. Yamamoto, I., et al., *Recent advances in the metabolism of cannabinoids.* Int J Biochem Cell Biol, 1995. **27**(8): p. 741-6.
10. Gertsch, J., R.G. Pertwee, and V. Di Marzo, *Phytocannabinoids beyond the Cannabis plant - do they exist?* Br J Pharmacol, 2010. **160**(3): p. 523-9.
11. Devane, W.A., et al., *A novel probe for the cannabinoid receptor.* J Med Chem, 1992. **35**(11): p. 2065-9.
12. Devane, W.A., et al., *Determination and characterization of a cannabinoid receptor in rat brain.* Mol Pharmacol, 1988. **34**(5): p. 605-13.
13. Howlett, A.C., et al., *International Union of Pharmacology. XXVII. Classification of cannabinoid receptors.* Pharmacol Rev, 2002. **54**(2): p. 161-202.
14. Howlett, A.C., *Inhibition of neuroblastoma adenylate cyclase by cannabinoid and nantradol compounds.* Life Sci, 1984. **35**(17): p. 1803-10.
15. Howlett, A.C. and R.M. Fleming, *Cannabinoid inhibition of adenylate cyclase. Pharmacology of the response in neuroblastoma cell membranes.* Mol Pharmacol, 1984. **26**(3): p. 532-8.
16. Matsuda, L.A., et al., *Structure of a cannabinoid receptor and functional expression of the cloned cDNA.* Nature, 1990. **346**(6284): p. 561-4.
17. Gerard, C.M., et al., *Molecular cloning of a human cannabinoid receptor which is also expressed in testis.* Biochem J, 1991. **279 (Pt 1)**: p. 129-34.
18. Munro, S., K.L. Thomas, and M. Abu-Shaar, *Molecular characterization of a peripheral receptor for cannabinoids.* Nature, 1993. **365**(6441): p. 61-5.
19. Shire, D., et al., *An amino-terminal variant of the central cannabinoid receptor resulting from alternative splicing.* J Biol Chem, 1995. **270**(8): p. 3726-31.
20. Ryberg, E., et al., *Identification and characterisation of a novel splice variant of the human CB1 receptor.* FEBS Lett, 2005. **579**(1): p. 259-64.

21. Sawzdargo, M., et al., *Identification and cloning of three novel human G protein-coupled receptor genes GPR52, PsiGPR53 and GPR55: GPR55 is extensively expressed in human brain.* Brain Res Mol Brain Res, 1999. **64**(2): p. 193-8.
22. Brown AJ, W.A., *Identification of modulators of GPR55 activity*. 2001. .
23. Drmota T, G.P., Groblewski T, *Screening assays for cannabinoid-ligand type modulators of GPR55*. 2004.
24. McHugh, D., et al., *Delta(9) -Tetrahydrocannabinol and N-arachidonyl glycine are full agonists at GPR18 receptors and induce migration in human endometrial HEC-1B cells.* Br J Pharmacol, 2012. **165**(8): p. 2414-24.
25. Zygmunt, P.M., et al., *Vanilloid receptors on sensory nerves mediate the vasodilator action of anandamide.* Nature, 1999. **400**(6743): p. 452-7.
26. Jordt, S.E., et al., *Mustard oils and cannabinoids excite sensory nerve fibres through the TRP channel ANKTM1.* Nature, 2004. **427**(6971): p. 260-5.
27. Pertwee, R.G., *Receptors and channels targeted by synthetic cannabinoid receptor agonists and antagonists.* Curr Med Chem, 2010. **17**(14): p. 1360-81.
28. Sun, Y. and A. Bennett, *Cannabinoids: a new group of agonists of PPARs.* PPAR Res, 2007. **2007**: p. 23513.
29. Tsou, K., et al., *Immunohistochemical distribution of cannabinoid CB1 receptors in the rat central nervous system.* Neuroscience, 1998. **83**(2): p. 393-411.
30. Matsuda, L.A., T.I. Bonner, and S.J. Lolait, *Localization of cannabinoid receptor mRNA in rat brain.* J Comp Neurol, 1993. **327**(4): p. 535-50.
31. Herkenham, M., et al., *Characterization and localization of cannabinoid receptors in rat brain: a quantitative in vitro autoradiographic study.* J Neurosci, 1991. **11**(2): p. 563-83.
32. Sim, L.J., et al., *Differences in G-protein activation by mu- and delta-opioid, and cannabinoid, receptors in rat striatum.* Eur J Pharmacol, 1996. **307**(1): p. 97-105.
33. Piomelli, D., *The molecular logic of endocannabinoid signalling.* Nat Rev Neurosci, 2003. **4**(11): p. 873-84.
34. Andersson, H., et al., *Membrane assembly of the cannabinoid receptor 1: impact of a long N-terminal tail.* Mol Pharmacol, 2003. **64**(3): p. 570-7.
35. Baczynsky, W.O. and A.M. Zimmerman, *Effects of delta 9-tetrahydrocannabinol, cannabinol and cannabidiol on the immune system in mice. I. In vivo investigation of the primary and secondary immune response.* Pharmacology, 1983. **26**(1): p. 1-11.
36. Klein, T.W., C. Newton, and H. Friedman, *Inhibition of natural killer cell function by marijuana components.* J Toxicol Environ Health, 1987. **20**(4): p. 321-32.
37. Klein, T.W., C. Newton, and H. Friedman, *Cannabinoid receptors and immunity.* Immunol Today, 1998. **19**(8): p. 373-81.
38. Klein, T.W., et al., *Delta 9-tetrahydrocannabinol injection induces cytokine-mediated mortality of mice infected with Legionella pneumophila.* J Pharmacol Exp Ther, 1993. **267**(2): p. 635-40.
39. Klein, T.W., et al., *The effect of delta-9-tetrahydrocannabinol and 11-hydroxy-delta-9-tetrahydrocannabinol on T-lymphocyte and B-lymphocyte mitogen responses.* J Immunopharmacol, 1985. **7**(4): p. 451-66.
40. Newton, C.A., T.W. Klein, and H. Friedman, *Secondary immunity to Legionella pneumophila and Th1 activity are suppressed by delta-9-tetrahydrocannabinol*

injection. Infect Immun, 1994. **62**(9): p. 4015-20.
41. Pertwee, R.G., *Pharmacology of cannabinoid CB1 and CB2 receptors.* Pharmacol Ther, 1997. **74**(2): p. 129-80.
42. Ryberg, E., et al., *The orphan receptor GPR55 is a novel cannabinoid receptor.* Br J Pharmacol, 2007. **152**(7): p. 1092-101.
43. Balenga, N.A., et al., *GPR55 regulates cannabinoid 2 receptor-mediated responses in human neutrophils.* Cell Res, 2011. **21**(10): p. 1452-69.
44. Chin, C.N., et al., *Ligand binding and modulation of cyclic AMP levels depend on the chemical nature of residue 192 of the human cannabinoid receptor 1.* J Neurochem, 1998. **70**(1): p. 366-73.
45. Pertwee, R.G., et al., *O-1057, a potent water-soluble cannabinoid receptor agonist with antinociceptive properties.* Br J Pharmacol, 2000. **129**(8): p. 1577-84.
46. Martin, B.R., et al., *Pharmacological evaluation of dimethylheptyl analogs of delta 9-THC: reassessment of the putative three-point cannabinoid-receptor interaction.* Drug Alcohol Depend, 1995. **37**(3): p. 231-40.
47. Reggio, P.H., et al., *Investigation of the role of the phenolic hydroxyl in cannabinoid activity.* Mol Pharmacol, 1990. **38**(6): p. 854-62.
48. Ryan, W., et al., *A novel class of potent tetrahydrocannabinols (THCS): 2'-yne-delta 8- and delta 9-THCS.* Life Sci, 1995. **56**(23-24): p. 2013-20.
49. Melvin, L.S., et al., *Structure-activity relationships defining the ACD-tricyclic cannabinoids: cannabinoid receptor binding and analgesic activity.* Drug Des Discov, 1995. **13**(2): p. 155-66.
50. D'Ambra, T.E., et al., *Conformationally restrained analogues of pravadoline: nanomolar potent, enantioselective, (aminoalkyl)indole agonists of the cannabinoid receptor.* J Med Chem, 1992. **35**(1): p. 124-35.
51. Reggio, P.H., et al., *The bioactive conformation of aminoalkylindoles at the cannabinoid CB1 and CB2 receptors: insights gained from (E)- and (Z)-naphthylidene indenes.* J Med Chem, 1998. **41**(26): p. 5177-87.
52. Huffman, J.W., et al., *3-Indolyl-1-naphthylmethanes: new cannabimimetic indoles provide evidence for aromatic stacking interactions with the CB(1) cannabinoid receptor.* Bioorg Med Chem, 2003. **11**(4): p. 539-49.
53. Estep, K.G., et al., *Conformationally restrained aminoalkylindoles: potent, stereoselective ligands at the cannabinoid binding site.* NIDA Res Monogr, 1990. **105**: p. 300-1.
54. Huffman, J.W., et al., *Design, Synthesis and Pharmacology of Cannabimimetic Indoles.* Bioorganic & Medicinal Chemistry Letters, 1994. **4**(4): p. 563-566.
55. Eissenstat, M.A., et al., *Aminoalkylindoles: structure-activity relationships of novel cannabinoid mimetics.* J Med Chem, 1995. **38**(16): p. 3094-105.
56. Hosohata, Y., et al., *AM630 antagonism of cannabinoid-stimulated [35S]GTP gamma S binding in the mouse brain.* Eur J Pharmacol, 1997. **321**(1): p. R1-3.
57. Rinaldi-Carmona, M., et al., *SR141716A, a potent and selective antagonist of the brain cannabinoid receptor.* FEBS Lett, 1994. **350**(2-3): p. 240-4.
58. Bays, H.E., *Current and investigational antiobesity agents and obesity therapeutic treatment targets.* Obes Res, 2004. **12**(8): p. 1197-211.
59. Katoch-Rouse, R., et al., *Synthesis, structure-activity relationship, and evaluation*

of SR141716 analogues: development of central cannabinoid receptor ligands with lower lipophilicity. J Med Chem, 2003. **46**(4): p. 642-5.
60. Wiley, J.L., et al., *Novel pyrazole cannabinoids: insights into CB(1) receptor recognition and activation.* J Pharmacol Exp Ther, 2001. **296**(3): p. 1013-22.
61. Lange, J.H. and C.G. Kruse, *Keynote review: Medicinal chemistry strategies to CB1 cannabinoid receptor antagonists.* Drug Discov Today, 2005. **10**(10): p. 693-702.
62. Lan, R., et al., *Structure-activity relationships of pyrazole derivatives as cannabinoid receptor antagonists.* J Med Chem, 1999. **42**(4): p. 769-76.
63. Hurst, D.P., et al., *N-(piperidin-1-yl)-5-(4-chlorophenyl)-1-(2,4-dichlorophenyl)-4-methyl-1H-pyrazole -3-carboxamide (SR141716A) interaction with LYS 3.28(192) is crucial for its inverse agonism at the cannabinoid CB1 receptor.* Mol Pharmacol, 2002. **62**(6): p. 1274-87.
64. Ruiu, S., et al., *Synthesis and characterization of NESS 0327: a novel putative antagonist of the CB1 cannabinoid receptor.* J Pharmacol Exp Ther, 2003. **306**(1): p. 363-70.
65. Francisco, M.E.Y., et al., *Structure elucidation of a novel ring-constrained biaryl pyrazole CB1 cannabinoid receptor antagonist.* Magnetic Resonance in Chemistry, 2003. **41**(4): p. 265-268.
66. Devane, W.A., et al., *Isolation and structure of a brain constituent that binds to the cannabinoid receptor.* Science, 1992. **258**(5090): p. 1946-9.
67. Stella, N., P. Schweitzer, and D. Piomelli, *A second endogenous cannabinoid that modulates long-term potentiation.* Nature, 1997. **388**(6644): p. 773-8.
68. Savinainen, J.R., et al., *Despite substantial degradation, 2-arachidonoylglycerol is a potent full efficacy agonist mediating CB(1) receptor-dependent G-protein activation in rat cerebellar membranes.* Br J Pharmacol, 2001. **134**(3): p. 664-72.
69. Sugiura, T., et al., *Evidence that the cannabinoid CB1 receptor is a 2-arachidonoylglycerol receptor. Structure-activity relationship of 2-arachidonoylglycerol, ether-linked analogues, and related compounds.* J Biol Chem, 1999. **274**(5): p. 2794-801.
70. Di Marzo, V., et al., *Formation and inactivation of endogenous cannabinoid anandamide in central neurons.* Nature, 1994. **372**(6507): p. 686-91.
71. Cravatt, B.F., et al., *Molecular characterization of an enzyme that degrades neuromodulatory fatty-acid amides.* Nature, 1996. **384**(6604): p. 83-7.
72. Di Marzo, V., *Endocannabinoids: synthesis and degradation.* Rev Physiol Biochem Pharmacol, 2008. **160**: p. 1-24.
73. Mechoulam, R., E. Fride, and V. Di Marzo, *Endocannabinoids.* Eur J Pharmacol, 1998. **359**(1): p. 1-18.
74. Abadji, V., et al., *(R)-methanandamide: a chiral novel anandamide possessing higher potency and metabolic stability.* J Med Chem, 1994. **37**(12): p. 1889-93.
75. Rouzer, C.A., K. Ghebreselasie, and L.J. Marnett, *Chemical stability of 2-arachidonylglycerol under biological conditions.* Chem Phys Lipids, 2002. **119**(1-2): p. 69-82.
76. Howlett, A.C., et al., *Endocannabinoid tone versus constitutive activity of cannabinoid receptors.* Br J Pharmacol, 2011. **163**(7): p. 1329-43.
77. Lagerstrom, M.C. and H.B. Schioth, *Structural diversity of G protein-coupled*

receptors and significance for drug discovery. Nat Rev Drug Discov, 2008. **7**(4): p. 339-57.
78. Fredriksson, R., et al., *The G-protein-coupled receptors in the human genome form five main families. Phylogenetic analysis, paralogon groups, and fingerprints.* Mol Pharmacol, 2003. **63**(6): p. 1256-72.
79. Downes, G.B. and N. Gautam, *The G protein subunit gene families.* Genomics, 1999. **62**(3): p. 544-52.
80. Clapham, D.E. and E.J. Neer, *G protein beta gamma subunits.* Annu Rev Pharmacol Toxicol, 1997. **37**: p. 167-203.
81. Schmidt, C.J., et al., *Specificity of G protein beta and gamma subunit interactions.* J Biol Chem, 1992. **267**(20): p. 13807-10.
82. Oldham, W.M. and H.E. Hamm, *Heterotrimeric G protein activation by G-protein-coupled receptors.* Nat Rev Mol Cell Biol, 2008. **9**(1): p. 60-71.
83. Milligan, G., *A day in the life of a G protein-coupled receptor: the contribution to function of G protein-coupled receptor dimerization.* Br J Pharmacol, 2008. **153 Suppl 1**: p. S216-29.
84. Terrillon, S. and M. Bouvier, *Roles of G-protein-coupled receptor dimerization.* EMBO Rep, 2004. **5**(1): p. 30-4.
85. Howlett, A.C., L.C. Blume, and G.D. Dalton, *CB(1) cannabinoid receptors and their associated proteins.* Curr Med Chem, 2010. **17**(14): p. 1382-93.
86. Oddi, S., et al., *Functional characterization of putative cholesterol binding sequence (CRAC) in human type-1 cannabinoid receptor.* J Neurochem, 2011. **116**(5): p. 858-65.
87. Parnas, H. and I. Parnas, *The chemical synapse goes electric: Ca2+- and voltage-sensitive GPCRs control neurotransmitter release.* Trends Neurosci, 2007. **30**(2): p. 54-61.
88. Stanfield, P., *Voltage sparks a GPCR.* Nat Cell Biol, 2006. **8**(12): p. 1323-5.
89. Changeux, J.P. and S. Edelstein, *Conformational selection or induced fit? 50 years of debate resolved.* F1000 Biol Rep, 2011. **3**: p. 19.
90. Kreitzer, A.C. and W.G. Regehr, *Cerebellar depolarization-induced suppression of inhibition is mediated by endogenous cannabinoids.* J Neurosci, 2001. **21**(20): p. RC174.
91. Wilson, G. and A. Karlin, *Acetylcholine receptor channel structure in the resting, open, and desensitized states probed with the substituted-cysteine-accessibility method.* Proc Natl Acad Sci U S A, 2001. **98**(3): p. 1241-8.
92. Ohno-Shosaku, T., T. Maejima, and M. Kano, *Endogenous cannabinoids mediate retrograde signals from depolarized postsynaptic neurons to presynaptic terminals.* Neuron, 2001. **29**(3): p. 729-38.
93. Twitchell, W., S. Brown, and K. Mackie, *Cannabinoids inhibit N- and P/Q-type calcium channels in cultured rat hippocampal neurons.* J Neurophysiol, 1997. **78**(1): p. 43-50.
94. Deadwyler, S.A., et al., *Cannabinoids modulate voltage sensitive potassium A-current in hippocampal neurons via a cAMP-dependent process.* J Pharmacol Exp Ther, 1995. **273**(2): p. 734-43.
95. Howlett, A.C., *Cannabinoid receptor signaling.* Handb Exp Pharmacol, 2005(168): p. 53-79.

96. Stadel, R., K.H. Ahn, and D.A. Kendall, *The cannabinoid type-1 receptor carboxyl-terminus, more than just a tail.* J Neurochem, 2011. **117**(1): p. 1-18.
97. Martini, L., et al., *Ligand-induced down-regulation of the cannabinoid 1 receptor is mediated by the G-protein-coupled receptor-associated sorting protein GASP1.* FASEB J, 2007. **21**(3): p. 802-11.
98. Rasmussen, S.G., et al., *Crystal structure of the human beta2 adrenergic G-protein-coupled receptor.* Nature, 2007. **450**(7168): p. 383-7.
99. Bokoch, M.P., et al., *Ligand-specific regulation of the extracellular surface of a G-protein-coupled receptor.* Nature, 2010. **463**(7277): p. 108-12.
100. Unal, H., et al., *Ligand-specific conformation of extracellular loop-2 in the angiotensin II type 1 receptor.* J Biol Chem, 2010. **285**(21): p. 16341-50.
101. Bourne, H.R. and E.C. Meng, *Structure. Rhodopsin sees the light.* Science, 2000. **289**(5480): p. 733-4.
102. Lin, S., U. Gether, and B.K. Kobilka, *Ligand stabilization of the beta 2 adrenergic receptor: effect of DTT on receptor conformation monitored by circular dichroism and fluorescence spectroscopy.* Biochemistry, 1996. **35**(46): p. 14445-51.
103. Klco, J.M., et al., *Essential role for the second extracellular loop in C5a receptor activation.* Nat Struct Mol Biol, 2005. **12**(4): p. 320-6.
104. Shi, L. and J.A. Javitch, *The second extracellular loop of the dopamine D2 receptor lines the binding-site crevice.* Proc Natl Acad Sci U S A, 2004. **101**(2): p. 440-5.
105. Janz, J.M., J.F. Fay, and D.L. Farrens, *Stability of dark state rhodopsin is mediated by a conserved ion pair in intradiscal loop E-2.* J Biol Chem, 2003. **278**(19): p. 16982-91.
106. Standfuss, J., et al., *Crystal structure of a thermally stable rhodopsin mutant.* J Mol Biol, 2007. **372**(5): p. 1179-88.
107. Avlani, V.A., et al., *Critical role for the second extracellular loop in the binding of both orthosteric and allosteric G protein-coupled receptor ligands.* J Biol Chem, 2007. **282**(35): p. 25677-86.
108. Ahn, K.H., et al., *Dual role of the second extracellular loop of the cannabinoid receptor 1: ligand binding and receptor localization.* Mol Pharmacol, 2009. **76**(4): p. 833-42.
109. Rasmussen, S.G., et al., *Structure of a nanobody-stabilized active state of the beta(2) adrenoceptor.* Nature, 2011. **469**(7329): p. 175-80.
110. Deupi, X., J. Standfuss, and G. Schertler, *Conserved activation pathways in G-protein-coupled receptors.* Biochem Soc Trans, 2012. **40**(2): p. 383-8.
111. Angel, T.E., M.R. Chance, and K. Palczewski, *Conserved waters mediate structural and functional activation of family A (rhodopsin-like) G protein-coupled receptors.* Proc Natl Acad Sci U S A, 2009. **106**(21): p. 8555-60.
112. Katritch, V., V. Cherezov, and R.C. Stevens, *Diversity and modularity of G protein-coupled receptor structures.* Trends Pharmacol Sci, 2012. **33**(1): p. 17-27.
113. Kruse, A.C., et al., *Structure and dynamics of the M3 muscarinic acetylcholine receptor.* Nature, 2012. **482**(7386): p. 552-6.
114. Wess, J., *Molecular basis of receptor/G-protein-coupling selectivity.* Pharmacol Ther, 1998. **80**(3): p. 231-64.
115. Ulfers, A.L., et al., *Structure of the third intracellular loop of the human*

cannabinoid 1 receptor. Biochemistry, 2002. **41**(38): p. 11344-50.
116. Moukhametzianov, R., et al., *Two distinct conformations of helix 6 observed in antagonist-bound structures of a beta1-adrenergic receptor.* Proc Natl Acad Sci U S A, 2011. **108**(20): p. 8228-32.
117. Park, J.H., et al., *Crystal structure of the ligand-free G-protein-coupled receptor opsin.* Nature, 2008. **454**(7201): p. 183-7.
118. Shimamura, T., et al., *Crystal structure of squid rhodopsin with intracellularly extended cytoplasmic region.* J Biol Chem, 2008. **283**(26): p. 17753-6.
119. Zhang, X., et al., *Dynamics of the beta2-adrenergic G-protein coupled receptor revealed by hydrogen-deuterium exchange.* Anal Chem, 2010. **82**(3): p. 1100-8.
120. Palczewski, K., *G protein-coupled receptor rhodopsin.* Annu Rev Biochem, 2006. **75**: p. 743-67.
121. Farrens, D.L., et al., *Requirement of rigid-body motion of transmembrane helices for light activation of rhodopsin.* Science, 1996. **274**(5288): p. 768-70.
122. Altenbach, C., et al., *Structural features and light-dependent changes in the cytoplasmic interhelical E-F loop region of rhodopsin: a site-directed spin-labeling study.* Biochemistry, 1996. **35**(38): p. 12470-8.
123. Altenbach, C., et al., *High-resolution distance mapping in rhodopsin reveals the pattern of helix movement due to activation.* Proc Natl Acad Sci U S A, 2008. **105**(21): p. 7439-44.
124. Gether, U., S. Lin, and B.K. Kobilka, *Fluorescent labeling of purified beta 2 adrenergic receptor. Evidence for ligand-specific conformational changes.* J Biol Chem, 1995. **270**(47): p. 28268-75.
125. Gether, U., et al., *Agonists induce conformational changes in transmembrane domains III and VI of the beta2 adrenoceptor.* EMBO J, 1997. **16**(22): p. 6737-47.
126. Tsukamoto, H., et al., *The magnitude of the light-induced conformational change in different rhodopsins correlates with their ability to activate G proteins.* J Biol Chem, 2009. **284**(31): p. 20676-83.
127. Ghanouni, P., et al., *Functionally different agonists induce distinct conformations in the G protein coupling domain of the beta 2 adrenergic receptor.* J Biol Chem, 2001. **276**(27): p. 24433-6.
128. Swaminath, G., et al., *Probing the beta2 adrenoceptor binding site with catechol reveals differences in binding and activation by agonists and partial agonists.* J Biol Chem, 2005. **280**(23): p. 22165-71.
129. Swaminath, G., et al., *Sequential binding of agonists to the beta2 adrenoceptor. Kinetic evidence for intermediate conformational states.* J Biol Chem, 2004. **279**(1): p. 686-91.
130. Okada, T., et al., *Activation of rhodopsin: new insights from structural and biochemical studies.* Trends Biochem Sci, 2001. **26**(5): p. 318-24.
131. Tsukamoto, H., et al., *Rhodopsin in Nanodiscs Has Native Membrane-like Photointermediates.* Biochemistry, 2011. **50**(22): p. 5086-91.
132. Mansoor, S.E., H.S. McHaourab, and D.L. Farrens, *Mapping proximity within proteins using fluorescence spectroscopy. A study of T4 lysozyme showing that tryptophan residues quench bimane fluorescence.* Biochemistry, 2002. **41**(8): p. 2475-84.
133. Mansoor, S.E., M.A. Dewitt, and D.L. Farrens, *Distance mapping in proteins*

using fluorescence spectroscopy: the tryptophan-induced quenching (TrIQ) method. Biochemistry, 2010. **49**(45): p. 9722-31.
134. Yao, X., et al., *Coupling ligand structure to specific conformational switches in the beta2-adrenoceptor.* Nat Chem Biol, 2006. **2**(8): p. 417-22.
135. Kenakin, T., *Ligand-selective receptor conformations revisited: the promise and the problem.* Trends Pharmacol Sci, 2003. **24**(7): p. 346-54.
136. Liu, J.J., et al., *Biased signaling pathways in beta2-adrenergic receptor characterized by 19F-NMR.* Science, 2012. **335**(6072): p. 1106-10.
137. Rahmeh, R., et al., *Structural insights into biased G protein-coupled receptor signaling revealed by fluorescence spectroscopy.* Proc Natl Acad Sci U S A, 2012. **109**(17): p. 6733-8.
138. Kirchberg, K., et al., *Conformational dynamics of helix 8 in the GPCR rhodopsin controls arrestin activation in the desensitization process.* Proc Natl Acad Sci U S A, 2011. **108**(46): p. 18690-5.
139. Janz, J.M. and D.L. Farrens, *Rhodopsin activation exposes a key hydrophobic binding site for the transducin alpha-subunit C terminus.* J Biol Chem, 2004. **279**(28): p. 29767-73.
140. Scheerer, P., et al., *Structural and kinetic modeling of an activating helix switch in the rhodopsin-transducin interface.* Proc Natl Acad Sci U S A, 2009. **106**(26): p. 10660-5.
141. Scheerer, P., et al., *Crystal structure of opsin in its G-protein-interacting conformation.* Nature, 2008. **455**(7212): p. 497-502.
142. Choe, H.W., et al., *Crystal structure of metarhodopsin II.* Nature, 2011. **471**(7340): p. 651-5.
143. Deupi, X., et al., *Stabilized G protein binding site in the structure of constitutively active metarhodopsin-II.* Proc Natl Acad Sci U S A, 2012. **109**(1): p. 119-24.
144. Standfuss, J., et al., *The structural basis of agonist-induced activation in constitutively active rhodopsin.* Nature, 2011. **471**(7340): p. 656-60.
145. Xu, F., et al., *Structure of an agonist-bound human A2A adenosine receptor.* Science, 2011. **332**(6027): p. 322-7.
146. Chung, K.Y., et al., *Conformational changes in the G protein Gs induced by the beta2 adrenergic receptor.* Nature, 2011. **477**(7366): p. 611-5.
147. Van Eps, N., et al., *Interaction of a G protein with an activated receptor opens the interdomain interface in the alpha subunit.* Proc Natl Acad Sci U S A, 2011. **108**(23): p. 9420-4.
148. Lebon, G., et al., *Agonist-bound adenosine A2A receptor structures reveal common features of GPCR activation.* Nature, 2011. **474**(7352): p. 521-5.
149. Changeux, J.P., *50th anniversary of the word "allosteric".* Protein Sci, 2011. **20**(7): p. 1119-24.
150. De Lean, A., J.M. Stadel, and R.J. Lefkowitz, *A ternary complex model explains the agonist-specific binding properties of the adenylate cyclase-coupled beta-adrenergic receptor.* J Biol Chem, 1980. **255**(15): p. 7108-17.
151. Lefkowitz, R. *bioseminar*. 2010; Available from: http://www.youtube.com/user/ibioseminars?feature=watch.
152. Rasmussen, S.G., et al., *Crystal structure of the beta2 adrenergic receptor-Gs protein complex.* Nature, 2011. **477**(7366): p. 549-55.

153. Samama, P., et al., *A mutation-induced activated state of the beta 2-adrenergic receptor. Extending the ternary complex model.* J Biol Chem, 1993. **268**(7): p. 4625-36.
154. Weiss, J.M., et al., *The cubic ternary complex receptor-occupancy model. III. resurrecting efficacy.* J Theor Biol, 1996. **181**(4): p. 381-97.
155. Christopoulos, A. and T. Kenakin, *G protein-coupled receptor allosterism and complexing.* Pharmacol Rev, 2002. **54**(2): p. 323-74.
156. Kenakin, T., *New concepts in drug discovery: collateral efficacy and permissive antagonism.* Nat Rev Drug Discov, 2005. **4**(11): p. 919-27.
157. Christopoulos, A., *Allosteric binding sites on cell-surface receptors: novel targets for drug discovery.* Nat Rev Drug Discov, 2002. **1**(3): p. 198-210.
158. Lazareno, S., et al., *Thiochrome enhances acetylcholine affinity at muscarinic M4 receptors: receptor subtype selectivity via cooperativity rather than affinity.* Mol Pharmacol, 2004. **65**(1): p. 257-66.
159. Gao, Z.G., et al., *Allosteric modulation of A(3) adenosine receptors by a series of 3-(2-pyridinyl)isoquinoline derivatives.* Mol Pharmacol, 2001. **60**(5): p. 1057-63.
160. May, L.T., et al., *Allosteric modulation of G protein-coupled receptors.* Annu Rev Pharmacol Toxicol, 2007. **47**: p. 1-51.
161. Valant, C., et al., *The best of both worlds? Bitopic orthosteric/allosteric ligands of g protein-coupled receptors.* Annu Rev Pharmacol Toxicol, 2012. **52**: p. 153-78.
162. Ehlert, F.J., *Estimation of the affinities of allosteric ligands using radioligand binding and pharmacological null methods.* Mol Pharmacol, 1988. **33**(2): p. 187-94.
163. Price, M.R., et al., *Allosteric modulation of the cannabinoid CB1 receptor.* Mol Pharmacol, 2005. **68**(5): p. 1484-95.
164. Piscitelli, F., et al., *Indole-2-carboxamides as Allosteric Modulators of the Cannabinoid CB(1) Receptor.* J Med Chem, 2012.
165. Horswill, J.G., et al., *PSNCBAM-1, a novel allosteric antagonist at cannabinoid CB1 receptors with hypophagic effects in rats.* Br J Pharmacol, 2007. **152**(5): p. 805-14.
166. Wang, X., et al., *Effects of the allosteric antagonist 1-(4-chlorophenyl)-3-[3-(6-pyrrolidin-1-ylpyridin-2-yl)phenyl]urea (PSNCBAM-1) on CB1 receptor modulation in the cerebellum.* Mol Pharmacol, 2011. **79**(4): p. 758-67.
167. Navarro, H.A., et al., *Positive allosteric modulation of the human cannabinoid (CB) receptor by RTI-371, a selective inhibitor of the dopamine transporter.* Br J Pharmacol, 2009. **156**(7): p. 1178-84.
168. Gemma L. Baillie, G.F., Paul MacBeath, John Miskelly, Sonia Watson, Lesley A. Stevenson, Tesmol George, Anu Mahadevan, Raj K. Razdan, Roger G. Pertwee & Ruth A. Ross *ALLOSTERIC MODULATION OF THE CANNABINOID CB1 RECEPTOR: NOVEL ALLOSTERIC MODULATORS*, in *17th Annual Symposium on the Cannabinoids*. 2007: Saint-Sauveur, Québec Canada.
169. Lynda Adam, D.S., Lenka Rihakova, Stéphanie Lapointe, Stéphane StOnge, Jean Labrecque and Kemal Payza *POSITIVE ALLOSTERIC MODULATORS OF CB1 RECEPTORS* in *17th Annual Symposium on the Cannabinoids*. 2007: Saint-Sauveur, Québec Canada.
170. Reggio, P.H., *The cannabinoid receptors*. The receptors. 2009, New York:

Humana. xiv, 396 p., 6 p. of plates.
171. Grunbeck, A., et al., *Genetically Encoded Photo-cross-linkers Map the Binding Site of an Allosteric Drug on a G Protein-Coupled Receptor.* ACS Chem Biol, 2012.
172. Grunbeck, A., et al., *Mapping the ligand-binding site on a G protein-coupled receptor (GPCR) using genetically encoded photocrosslinkers.* Biochemistry, 2011. **50**(17): p. 3411-3.
173. Hanson, M.A., et al., *Crystal structure of a lipid G protein-coupled receptor.* Science, 2012. **335**(6070): p. 851-5.
174. Urban, J.D., et al., *Functional selectivity and classical concepts of quantitative pharmacology.* J Pharmacol Exp Ther, 2007. **320**(1): p. 1-13.
175. Bosier, B., et al., *Functionally selective cannabinoid receptor signalling: therapeutic implications and opportunities.* Biochem Pharmacol, 2010. **80**(1): p. 1-12.
176. Govaerts, S.J., E. Hermans, and D.M. Lambert, *Comparison of cannabinoid ligands affinities and efficacies in murine tissues and in transfected cells expressing human recombinant cannabinoid receptors.* Eur J Pharm Sci, 2004. **23**(3): p. 233-43.
177. Glass, M. and J.K. Northup, *Agonist selective regulation of G proteins by cannabinoid CB(1) and CB(2) receptors.* Mol Pharmacol, 1999. **56**(6): p. 1362-9.
178. Mukhopadhyay, S. and A.C. Howlett, *Chemically distinct ligands promote differential CB1 cannabinoid receptor-Gi protein interactions.* Mol Pharmacol, 2005. **67**(6): p. 2016-24.
179. Prather, P.L., et al., *Activation of cannabinoid receptors in rat brain by WIN 55212-2 produces coupling to multiple G protein alpha-subunits with different potencies.* Mol Pharmacol, 2000. **57**(5): p. 1000-10.
180. Mathiesen, J.M., et al., *Identification of indole derivatives exclusively interfering with a G protein-independent signaling pathway of the prostaglandin D2 receptor CRTH2.* Mol Pharmacol, 2005. **68**(2): p. 393-402.
181. Ahn, K.H., M.M. Mahmoud, and D.A. Kendall, *Allosteric modulator ORG27569 induces a CB1 Cannabinoid receptor high affinity agonist binding state, receptor internalization and Gi-independent ERK1/2 activation.* J Biol Chem, 2012.
182. Schwartz, T.W. and B. Holst, *Allosteric enhancers, allosteric agonists and ago-allosteric modulators: where do they bind and how do they act?* Trends Pharmacol Sci, 2007. **28**(8): p. 366-73.
183. Holst, B., et al., *Overlapping binding site for the endogenous agonist, small-molecule agonists, and ago-allosteric modulators on the ghrelin receptor.* Mol Pharmacol, 2009. **75**(1): p. 44-59.
184. Mannhold, R., et al., *Calculation of molecular lipophilicity: State-of-the-art and comparison of log P methods on more than 96,000 compounds.* J Pharm Sci, 2009. **98**(3): p. 861-93.
185. Reggio, P.H., *Pharmacophores for ligand recognition and activation/inactivation of the cannabinoid receptors.* Curr Pharm Des, 2003. **9**(20): p. 1607-33.
186. Bloom, A.S., et al., *9-nor-9beta-hydroxyhexahydrocannabinol, a cannabinoid with potent antinociceptive activity: comparisons with morphine.* J Pharmacol Exp Ther, 1977. **200**(2): p. 263-70.

187. Calignano, A., et al., *Control of pain initiation by endogenous cannabinoids.* Nature, 1998. **394**(6690): p. 277-81.
188. Cha, Y.M., et al., *Differential effects of delta9-THC on learning in adolescent and adult rats.* Pharmacol Biochem Behav, 2006. **83**(3): p. 448-55.
189. Hollister, L.E., *Health aspects of cannabis.* Pharmacol Rev, 1986. **38**(1): p. 1-20.
190. Miller, A.S. and J.M. Walker, *Electrophysiological effects of a cannabinoid on neural activity in the globus pallidus.* Eur J Pharmacol, 1996. **304**(1-3): p. 29-35.
191. Sulcova, E., R. Mechoulam, and E. Fride, *Biphasic effects of anandamide.* Pharmacol Biochem Behav, 1998. **59**(2): p. 347-52.
192. Calandra, B., et al., *Dual intracellular signaling pathways mediated by the human cannabinoid CB1 receptor.* Eur J Pharmacol, 1999. **374**(3): p. 445-55.
193. Michalke, K., et al., *Mammalian G protein-coupled receptor expression in Escherichia coli: II. Refolding and biophysical characterization of mouse cannabinoid receptor 1 and human parathyroid hormone receptor 1*. Anal Biochem, 2010. **401**(1): p. 74-80.
194. Yeliseev, A., L. Zoubak, and K. Gawrisch, *Use of dual affinity tags for expression and purification of functional peripheral cannabinoid receptor.* Protein Expr Purif, 2007. **53**(1): p. 153-63.
195. Kimura, T., et al., *Recombinant cannabinoid type 2 receptor in liposome model activates g protein in response to anionic lipid constituents.* J Biol Chem, 2012. **287**(6): p. 4076-87.
196. Kim, T.K., et al., *Expression and characterization of human CB1 cannabinoid receptor in methylotrophic yeast Pichia pastoris.* Protein Expr Purif, 2005. **40**(1): p. 60-70.
197. Chillakuri, C.R., C. Reinhart, and H. Michel, *C-terminal truncated cannabinoid receptor 1 coexpressed with G protein trimer in Sf9 cells exists in a precoupled state and shows constitutive activity.* FEBS J, 2007. **274**(23): p. 6106-15.
198. Farrens, D.L., et al., *Design, expression, and characterization of a synthetic human cannabinoid receptor and cannabinoid receptor/ G-protein fusion protein.* J Pept Res, 2002. **60**(6): p. 336-47.
199. Fay, J.F., T.D. Dunham, and D.L. Farrens, *Cysteine residues in the human cannabinoid receptor: only C257 and C264 are required for a functional receptor, and steric bulk at C386 impairs antagonist SR141716A binding.* Biochemistry, 2005. **44**(24): p. 8757-69.
200. Oprian, D.D., et al., *Expression of a synthetic bovine rhodopsin gene in monkey kidney cells.* Proc Natl Acad Sci U S A, 1987. **84**(24): p. 8874-8.
201. Kawate, T. and E. Gouaux, *Fluorescence-detection size-exclusion chromatography for precrystallization screening of integral membrane proteins.* Structure, 2006. **14**(4): p. 673-81.
202. DeBlasi, A., K. O'Reilly, and H.J. Motulsky, *Calculating receptor number from binding experiments using same compound as radioligand and competitor.* Trends Pharmacol Sci, 1989. **10**(6): p. 227-9.
203. Chattopadhyay, A. and E. London, *Fluorimetric determination of critical micelle concentration avoiding interference from detergent charge.* Anal Biochem, 1984. **139**(2): p. 408-12.
204. Skiba, N.P., H. Bae, and H.E. Hamm, *Mapping of effector binding sites of*

transducin alpha-subunit using G alpha t/G alpha i1 chimeras. J Biol Chem, 1996. **271**(1): p. 413-24.
205. Fukada, Y., *Prenylation and carboxylmethylation of G-protein gamma subunit.* Methods Enzymol, 1995. **250**: p. 91-105.
206. Dunham, T.D. and D.L. Farrens, *Conformational changes in rhodopsin. Movement of helix f detected by site-specific chemical labeling and fluorescence spectroscopy.* J Biol Chem, 1999. **274**(3): p. 1683-90.
207. Mansoor, S.E., K. Palczewski, and D.L. Farrens, *Rhodopsin self-associates in asolectin liposomes.* Proc Natl Acad Sci U S A, 2006. **103**(9): p. 3060-5.
208. White, J.F., et al., *Dimerization of the class A G protein-coupled neurotensin receptor NTS1 alters G protein interaction.* Proc Natl Acad Sci U S A, 2007. **104**(29): p. 12199-204.
209. Chattopadhyay, A. and K.G. Harikumar, *Dependence of critical micelle concentration of a zwitterionic detergent on ionic strength: implications in receptor solubilization.* FEBS Lett, 1996. **391**(1-2): p. 199-202.
210. Kaufmann, T.C., A. Engel, and H.W. Remigy, *A novel method for detergent concentration determination.* Biophys J, 2006. **90**(1): p. 310-7.
211. Ramon, E., et al., *Effect of dodecyl maltoside detergent on rhodopsin stability and function.* Vision Res, 2003. **43**(28): p. 3055-61.
212. Keov, P., P.M. Sexton, and A. Christopoulos, *Allosteric modulation of G protein-coupled receptors: a pharmacological perspective.* Neuropharmacology, 2011. **60**(1): p. 24-35.
213. Calandra, B., et al., *Expression in Escherichia coli and characterisation of the human central CB1 and peripheral CB2 cannabinoid receptors.* Biotechnology Letters, 1997. **19**(5): p. 425-428.
214. Link, A.J., et al., *Efficient production of membrane-integrated and detergent-soluble G protein-coupled receptors in Escherichia coli.* Protein Sci, 2008. **17**(10): p. 1857-63.
215. Xu, W., et al., *Purification and mass spectroscopic analysis of human CB1 cannabinoid receptor functionally expressed using the baculovirus system.* J Pept Res, 2005. **66**(3): p. 138-50.
216. Ghanouni, P., et al., *Agonist-induced conformational changes in the G-protein-coupling domain of the beta 2 adrenergic receptor.* Proc Natl Acad Sci U S A, 2001. **98**(11): p. 5997-6002.
217. Farrens, D.L., *What site-directed labeling studies tell us about the mechanism of rhodopsin activation and G-protein binding.* Photochem Photobiol Sci, 2010. **9**(11): p. 1466-74.
218. Matsuda, T. and Y. Fukada, *Functional analysis of farnesylation and methylation of transducin.* Methods Enzymol, 2000. **316**: p. 465-81.
219. Mansoor, S.E. and D.L. Farrens, *High-throughput protein structural analysis using site-directed fluorescence labeling and the bimane derivative (2-pyridyl)dithiobimane.* Biochemistry, 2004. **43**(29): p. 9426-38.
220. Lakowicz, J.R., *Principles of Fluorescence Spectroscopy*. 2006: Springer.
221. Shire, D., et al., *Structural features of the central cannabinoid CB1 receptor involved in the binding of the specific CB1 antagonist SR 141716A.* J Biol Chem, 1996. **271**(12): p. 6941-6.

222. Swillens, S., *Interpretation of binding curves obtained with high receptor concentrations: practical aid for computer analysis.* Mol Pharmacol, 1995. **47**(6): p. 1197-203.
223. Mansoor, S.E., H.S. McHaourab, and D.L. Farrens, *Determination of protein secondary structure and solvent accessibility using site-directed fluorescence labeling. Studies of T4 lysozyme using the fluorescent probe monobromobimane.* Biochemistry, 1999. **38**(49): p. 16383-93.
224. Sheikh, S.P., et al., *Rhodopsin activation blocked by metal-ion-binding sites linking transmembrane helices C and F.* Nature, 1996. **383**(6598): p. 347-50.
225. Yao, X.J., et al., *The effect of ligand efficacy on the formation and stability of a GPCR-G protein complex.* Proc Natl Acad Sci U S A, 2009. **106**(23): p. 9501-6.
226. Tsukamoto, H., A. Terakita, and Y. Shichida, *A pivot between helices V and VI near the retinal-binding site is necessary for activation in rhodopsins.* J Biol Chem, 2010. **285**(10): p. 7351-7.
227. Ye, S., et al., *Tracking G-protein-coupled receptor activation using genetically encoded infrared probes.* Nature, 2010. **464**(7293): p. 1386-9.
228. Kimura, T., et al., *Location, structure, and dynamics of the synthetic cannabinoid ligand CP-55,940 in lipid bilayers.* Biophys J, 2009. **96**(12): p. 4916-24.
229. Hurst, D.P., et al., *A lipid pathway for ligand binding is necessary for a cannabinoid G protein-coupled receptor.* J Biol Chem, 2010. **285**(23): p. 17954-64.
230. Makriyannis, A., *Cannabinoid Receptors*. Neuroscience Perspectives, ed. P. Jenner. 1995: Academic Press.
231. Hall, D.A., *Modeling the functional effects of allosteric modulators at pharmacological receptors: an extension of the two-state model of receptor activation.* Mol Pharmacol, 2000. **58**(6): p. 1412-23.
232. Kenakin, T., *Principles: receptor theory in pharmacology.* Trends Pharmacol Sci, 2004. **25**(4): p. 186-92.
233. Nakamichi, H. and T. Okada, *Local peptide movement in the photoreaction intermediate of rhodopsin.* Proc Natl Acad Sci U S A, 2006. **103**(34): p. 12729-34.
234. Ruprecht, J.J., et al., *Electron crystallography reveals the structure of metarhodopsin I.* EMBO J, 2004. **23**(18): p. 3609-20.
235. Salom, D., et al., *Crystal structure of a photoactivated deprotonated intermediate of rhodopsin.* Proc Natl Acad Sci U S A, 2006. **103**(44): p. 16123-8.
236. Rosenbaum, D.M., et al., *Structure and function of an irreversible agonist-beta(2) adrenoceptor complex.* Nature, 2011. **469**(7329): p. 236-40.
237. Lebon, G., et al., *Thermostabilisation of an agonist-bound conformation of the human adenosine A(2A) receptor.* J Mol Biol, 2011. **409**(3): p. 298-310.
238. Warne, T., et al., *The structural basis for agonist and partial agonist action on a beta(1)-adrenergic receptor.* Nature, 2011. **469**(7329): p. 241-4.
239. Unal, H. and S.S. Karnik, *Domain coupling in GPCRs: the engine for induced conformational changes.* Trends Pharmacol Sci, 2012. **33**(2): p. 79-88.
240. Kreitzer, A.C. and W.G. Regehr, *Retrograde inhibition of presynaptic calcium influx by endogenous cannabinoids at excitatory synapses onto Purkinje cells.* Neuron, 2001. **29**(3): p. 717-27.
241. Wilson, R.I. and R.A. Nicoll, *Endogenous cannabinoids mediate retrograde*

signalling at hippocampal synapses. Nature, 2001. **410**(6828): p. 588-92.
242. Murphy, J.W. and D.A. Kendall, *Integrity of extracellular loop 1 of the human cannabinoid receptor 1 is critical for high-affinity binding of the ligand CP 55,940 but not SR 141716A.* Biochem Pharmacol, 2003. **65**(10): p. 1623-31.
243. Karnik, S.S. and H.G. Khorana, *Assembly of functional rhodopsin requires a disulfide bond between cysteine residues 110 and 187.* J Biol Chem, 1990. **265**(29): p. 17520-4.
244. Feng, Y.H., Y. Saad, and S.S. Karnik, *Reversible inactivation of AT(2) angiotensin II receptor from cysteine-disulfide bond exchange.* FEBS Lett, 2000. **484**(2): p. 133-8.
245. Blanpain, C., et al., *Extracellular cysteines of CCR5 are required for chemokine binding, but dispensable for HIV-1 coreceptor activity.* J Biol Chem, 1999. **274**(27): p. 18902-8.
246. Wu, B., et al., *Structures of the CXCR4 chemokine GPCR with small-molecule and cyclic peptide antagonists.* Science, 2010. **330**(6007): p. 1066-71.
247. Romano, C., W.L. Yang, and K.L. O'Malley, *Metabotropic glutamate receptor 5 is a disulfide-linked dimer.* J Biol Chem, 1996. **271**(45): p. 28612-6.
248. Ward, D.T., E.M. Brown, and H.W. Harris, *Disulfide bonds in the extracellular calcium-polyvalent cation-sensing receptor correlate with dimer formation and its response to divalent cations in vitro.* J Biol Chem, 1998. **273**(23): p. 14476-83.
249. Ryu, S.E., *Structural mechanism of disulphide bond-mediated redox switches.* J Biochem, 2012. **151**(6): p. 579-88.
250. Mechoulam, R., *Discovery of endocannabinoids and some random thoughts on their possible roles in neuroprotection and aggression.* Prostaglandins Leukot Essent Fatty Acids, 2002. **66**(2-3): p. 93-9.
251. Zangerle, L., et al., *Screening of thiol compounds: depolarization-induced release of glutathione and cysteine from rat brain slices.* J Neurochem, 1992. **59**(1): p. 181-9.
252. Janaky, R., et al., *Glutathione and signal transduction in the mammalian CNS.* J Neurochem, 1999. **73**(3): p. 889-902.
253. Kano, M., et al., *Endocannabinoid-mediated control of synaptic transmission.* Physiol Rev, 2009. **89**(1): p. 309-80.
254. Moriarty-Craige, S.E. and D.P. Jones, *Extracellular thiols and thiol/disulfide redox in metabolism.* Annu Rev Nutr, 2004. **24**: p. 481-509.
255. Howlett, A.C., et al., *Characterization of CB1 cannabinoid receptors using receptor peptide fragments and site-directed antibodies.* Mol Pharmacol, 1998. **53**(3): p. 504-10.
256. Gupta, A., et al., *Conformation state-sensitive antibodies to G-protein-coupled receptors.* J Biol Chem, 2007. **282**(8): p. 5116-24.
257. Griffin, L. and A. Lawson, *Antibody fragments as tools in crystallography.* Clin Exp Immunol, 2011. **165**(3): p. 285-91.
258. Lieberman, R.L., et al., *Crystallization chaperone strategies for membrane proteins.* Methods, 2011. **55**(4): p. 293-302.
259. Unal, H., R. Jagannathan, and S.S. Karnik, *Mechanism of GPCR-Directed Autoantibodies in Diseases.* Adv Exp Med Biol, 2012. **749**: p. 187-99.
260. May, L.T., et al., *Allosteric modulation of G protein-coupled receptors.* Curr

Pharm Des, 2004. **10**(17): p. 2003-13.
261. Gupta, A., et al., *Antibodies against G-protein coupled receptors: novel uses in screening and drug development.* Comb Chem High Throughput Screen, 2008. **11**(6): p. 463-7.
262. Steyaert, J. and B.K. Kobilka, *Nanobody stabilization of G protein-coupled receptor conformational states.* Curr Opin Struct Biol, 2011. **21**(4): p. 567-72.
263. Harlow, E.L., D. , *Antibodies: A Laboratory Manual*, in *(Cold Spring Harbor Laboratory Press, 1988).*
264. Hino, T., et al., *G-protein-coupled receptor inactivation by an allosteric inverse-agonist antibody.* Nature, 2012. **482**(7384): p. 237-40.
265. Hopp, T.P., et al., *A Short Polypeptide Marker Sequence Useful for Recombinant Protein Identification and Purification.* Nat Biotech, 1988. **6**(10): p. 1204-1210.
266. Molday, R.S. and D. MacKenzie, *Monoclonal antibodies to rhodopsin: characterization, cross-reactivity, and application as structural probes.* Biochemistry, 1983. **22**(3): p. 653-60.
267. Hubbell, W.L., et al., *Rhodopsin structure, dynamics, and activation: a perspective from crystallography, site-directed spin labeling, sulfhydryl reactivity, and disulfide cross-linking.* Adv Protein Chem, 2003. **63**: p. 243-90.
268. Piscitelli, C.L., et al., *Equilibrium between metarhodopsin-I and metarhodopsin-II is dependent on the conformation of the third cytoplasmic loop.* J Biol Chem, 2006. **281**(10): p. 6813-25.
269. Sweredoski, M.J. and P. Baldi, *COBEpro: a novel system for predicting continuous B-cell epitopes.* Protein Eng Des Sel, 2009. **22**(3): p. 113-20.
270. Karnik, S.S., et al., *Palmitoylation of bovine opsin and its cysteine mutants in COS cells.* Proc Natl Acad Sci U S A, 1993. **90**(1): p. 40-4.
271. Cherezov, V., et al., *High-resolution crystal structure of an engineered human beta2-adrenergic G protein-coupled receptor.* Science, 2007. **318**(5854): p. 1258-65.
272. Oddi, S., et al., *Effects of palmitoylation of Cys(415) in helix 8 of the CB(1) cannabinoid receptor on membrane localization and signalling.* Br J Pharmacol, 2012. **165**(8): p. 2635-51.
273. Bubis, J., *Effect of detergents and lipids on transducin photoactivation by rhodopsin.* Biol Res, 1998. **31**(1): p. 59-71.
274. Sommer, M.E., W.C. Smith, and D.L. Farrens, *Dynamics of arrestin-rhodopsin interactions: acidic phospholipids enable binding of arrestin to purified rhodopsin in detergent.* J Biol Chem, 2006. **281**(14): p. 9407-17.
275. Bayburt, T.H. and S.G. Sligar, *Membrane protein assembly into Nanodiscs.* FEBS Lett, 2010. **584**(9): p. 1721-7.
276. Tsukamoto, H., et al., *Monomeric rhodopsin is the minimal functional unit required for arrestin binding.* J Mol Biol, 2010. **399**(3): p. 501-11.

Appendix 1

Allosteric Appendix

A1.1: Preamble

In this appendix I will give a more in-depth analysis to some of the models of allosterism that were touched upon in the introduction. For the following concepts I will be relying heavily of works written by Dr. Christopoulos and Dr. Kenakin, which expand or reiterate ideas put forth by drug-receptor forefathers including: Hill, Langmuir, Clark, Langley, Gaddum, Schild, Ariens, Stephenson, Black and Leff. For a less cursory review on the subject please see references at the end of this appendix.

A1.2: Competitive binding

Before we can discuss binding that is not competitive, we will first consider a case where binding is competitive. Namely, the case where radioligand A is displaced by nonradioactive ligand B. This is shown below schematically as:

$$BR \underset{}{\overset{K_B}{\rightleftharpoons}} R \overset{K_A}{\rightleftharpoons} AR$$

The binding affinities can expressed by the association constants K_a and K_b for both compounds:

$$K_a = \frac{[AR]}{[A][R]} \quad \text{and} \quad K_b = \frac{[BR]}{[B][R]}$$

The total amount of receptor is given as the sum of the species R_{total} = [R] + [AR] + [BR]. Solving for [BR] and [R] and replacing them in the R_{total} equation gives:

$$R_{total} = \frac{[AR]}{[A]K_a}(1 + K_b[B]) + [AR]$$

Dividing by [AR] generates:

$$\frac{R_{total}}{[AR]} = \frac{1}{[A]K_a}(1 + K_b[B]) + \frac{[A]K_a}{[A]K_a}$$

This can be simplified to:

$$\frac{R_{total}}{[AR]} = \frac{1 + K_b[B] + [A]K_a}{[A]K_a}$$

This can rearranged (to express as fractional occupancy) and association constants can be expressed as their dissociation constant (i.e. $1/K_A = K_a$):

$$\text{Fractional Occupancy} = \frac{[\text{RA}]}{\text{R}_{\text{total}}} = \frac{[A]/K_A}{1 + [B]/K_B + [A]/K_A}$$

This can be further simplified by multiplying both the numerator and denominator by K_A to yield equation **(A1.1):**

$$\text{Fractional Occupancy} = \frac{[A]}{[A] + K_A(1 + \frac{[B]}{K_B})} \qquad (\boldsymbol{A1.1})$$

Equation (A1.1) above will be used to simulate data where both ligands compete for the same binding domain on the receptor.

A1.3: Allosteric binding

The simplest model to describe an allosteric ligand binding to a receptor and modulating the affinity of an orthosteric ligands is the allosteric ternary complex model (ATCM) (1). This model is shown schematically below:

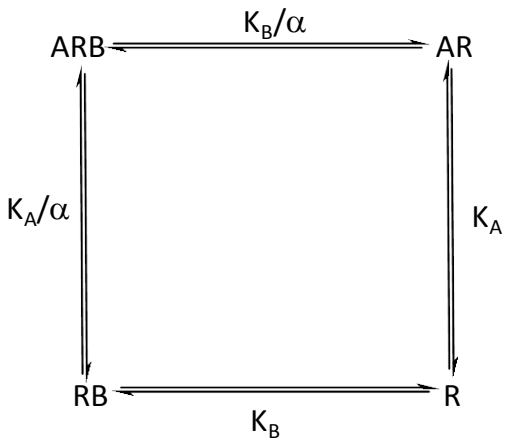

where K_A and K_B are the equilibrium dissociation constants for orthosteric ligand A and allosteric ligand B and α is the cooperativity factor for their interaction. This latter factor governs the magnitude by which one ligand can alter the affinity for the other when they form a ternary complex. Values of α greater than 1 denote positive cooperativity (increased affinity) and values less than one denote negative cooperativity (decreased affinity).

The binding affinities can expressed by the dissociation constants K_A and K_B for both compounds in the presence or absence of an allosteric modulator:

$$K_A = \frac{[A][R]}{[AR]} \qquad K_B = \frac{[B][R]}{[BR]} \qquad \alpha_d K_A = \frac{[BR][A]}{[ABR]} \qquad \alpha_d K_B = \frac{[AR][B]}{[ABR]}$$

The term α_d represents the inverse of the cooperativity factor α. The total amount of receptor is given as the sum of the species:

$$R_{total} = [R] + [AR] + [RB] + [ARB]$$

This can manipulated to express as fractional occupancy by multiplying both sides by (AR + ARB) to yield:

$$\text{Fractional Occupancy} = \frac{[AR] + [ARB]}{R_{total}} = \frac{[AR] + [ARB]}{[R] + [AR] + [RB] + [ARB]}$$

Multiplying the numerator and denominator by $([A][R])^{-1}$ gives:

$$\text{Fractional Occupancy} = \frac{\frac{[AR]}{[A][R]} + \frac{[ARB]}{[A][R]}}{\frac{[R]}{[A][R]} + \frac{[AR]}{[A][R]} + \frac{[RB]}{[A][R]} + \frac{[ARB]}{[A][R]}}$$

Then substituting the appropriate dissociation constants on the previous page provides:

$$\text{Fractional Occupancy} = \frac{\frac{1}{K_A} + \frac{[ARB]}{[X][R]}}{\frac{1}{[A]} + \frac{1}{K_A} + \frac{[RA]}{[A][R]} + \frac{[ARB]}{[A][R]}}$$

Using the following substitutions:

$$[\text{ARB}] = \frac{[AR][A]}{\alpha_d K_A} \quad ; \quad [R] = \frac{K_B[RB]}{[B]} \quad \& \quad \frac{[AR]}{[R][A]} = {K_A}^{-1}$$

Gives:

$$\text{Fractional Occupancy} = \frac{\frac{1}{K_A} + \frac{[B]}{\alpha_d K_A K_B}}{\frac{1}{A} + \frac{1}{K_A} + \frac{[B]}{\alpha_d K_B K_A} + \frac{[B]}{A * K_B}}$$

This can be simplified by multiplying the numerator and denominator by $K_A K_B[A]$:

$$\text{Fractional Occupancy} = \frac{[A]\left(K_B + \frac{[B]}{\alpha_d}\right)}{K_B[A] + K_A K_B + \frac{[A][B]}{\alpha_d} + K_A[B]}$$

Then combining terms:

$$\text{Fractional Occupancy} = \frac{[A]\left(K_B + \frac{[B]}{\alpha_d}\right)}{[A]\left(K_B + \frac{[B]}{\alpha_d}\right) + K_A(K_B + [B])}$$

This can be further simplified by dividing the numerator and denominator by

$(K_B + [B]/\alpha_d)$:

$$\text{Fractional Occupancy} = \frac{[A]}{[A] + \frac{K_A(K_B + [B])}{\left(K_B + \frac{[B]}{\alpha_d}\right)}} = \frac{[A]}{[A] + N}$$

Multiplying both the numerator and denominator of N by ($1/K_B$) and replacing α_d with α gives equation **(A1.2)**:

$$\text{Fractional Occupancy} = \frac{[A]}{[A] + \frac{K_A\left(1 + \frac{[B]}{K_B}\right)}{\left(1 + \frac{\alpha[B]}{K_B}\right)}} \qquad (\boldsymbol{A1.2})$$

When [B] is 0 there is no allosteric modulator the fractional occupancy is determined by the dissociation constant K_A. Notice that equation (A1.2) can essentially reduce to equation (A1.1) when $\alpha << 1$. This would define a case where the cooperativity is so negative that it essentially behaves like a competitive inhibitor. Also let us consider the other extreme case where the cooperativity factor is infinitely high ($\alpha >> 1$). This would lead to a condition where the fractional occupancy was 1 (i.e. fully bound – regardless of allosteric concentration – unless it was absent).

With these two equations in hand we can simulate data, to assess how the interplay between different factors affect the outcome. Shown in **Figure A1.1** is the effect of a competitive ligand (A) compared to a negative or positive allosteric modulator (Figure 1 B & C respectively). The dissociation constants for orthosteric ligand A and allosteric or competitive ligand was set to 10 nM. For B & C the cooperativty factor was set to .01 or 100 for negative and positive respectively. The data was simulated in the presence of 1 mM to 100 pM allosteric ligand each plotted on a log [A] scale. Competitive interactions (i.e. competing for the same site) led to a dextral shift in the orthosteric ligand binding. In contrast an allosteric ligand causes a shift whose limit is determined by the

cooperativity factor. In this case, there is a 100 fold shift in affinity (to 1 μM when α is 0.01 and 100 pM when α is 100). In other words, allosteric ligands saturate at a limit defined by αK_A. This phenomenon (the saturation effect) is expected as allosteric ligands do not bind to the orthosteric site, but instead to a limited allosteric site; thus the effect is limited when the allosteric site is fully bound.

Another way to measure allosteric modulation is to determine orthosteric ligand binding as a function of the allosteric ligand. This style of analysis is shown in **Figure A1.2 (A)** and can be especially useful when the cooperativity factor does not significantly deviate from one. There are, however, some drawbacks to this approach. Namely, at low orthosteric radioligand concentrations (where the fractional occupancy is low) negative allosteric modulation would be less pronounced (and the converse) (Figure A1.2 B & C).

A1.4: Binding and Receptor Function

The simplest model that accommodates affinity and efficacy (function) is the allosteric two-state model (ATSM) first described by Hall (2). The ATSM is shown schematically in **Figure A1.3** using the parameters he originally designated. For the sake of comparison I will discuss the ATSM as it is described schematically below:

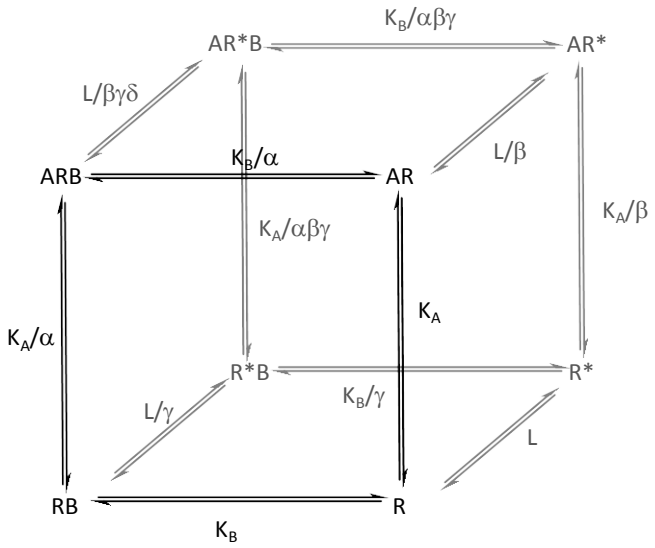

All this model does is expand the ATCM (in black above) by adding another state (hence the two-state) whereby the receptor can now exist in activated conformation (R*). The subsequent linkages are shown in gray. Now let's discuss some of these additional parameters. L is the isomerization constant. It is a ratio that expresses the receptors propensity to exist in the two populations R and R*. The parameter α (discussed above) governs the binding cooperativity factor for the inactive receptor state. The parameters γ and β defines the ability to modulate the transition to an active receptor state for the allosteric (B) and orthosteric (A) ligands, respectively (intrinsic efficacy). Finally, the parameter, δ, denotes the activation cooperativity factor for the ternary complex (ARB) that governs its ability to transition to the active state.

Using the equations that define binding and activity (shown in Figure A1.3 – Equations (A1.3) and (A1.4) respectively) we can now model conditions with various parameters. Let's consider a case akin to Org 27569. The molecule has positive cooperativity with respect to agonist binding and has negative cooperativity with respect to the transition to the active state. Modeling these conditions by adjusting the appropriate parameters

shown in **Figure A1.4** simulates a model that is consistent with our observations in Chapter 3. Namely, Org 27569 inhibits the receptor transition to an active state while increasing affinity for the orthosteric agonist.

Operational model

While the ATSM has utility in conceptualizing divergent allosteric modulator effects on ligand affinity versus efficacy (as illustrated in Figure A1.4), it is difficult to empirically determine many of the constants. With the current advances in single molecule fluorescence, however, one may be able to quantify such constants. An alternative methodology has been to combine an operational model of agonism (3) and the ATCM (4,5). This is shown below schematically:

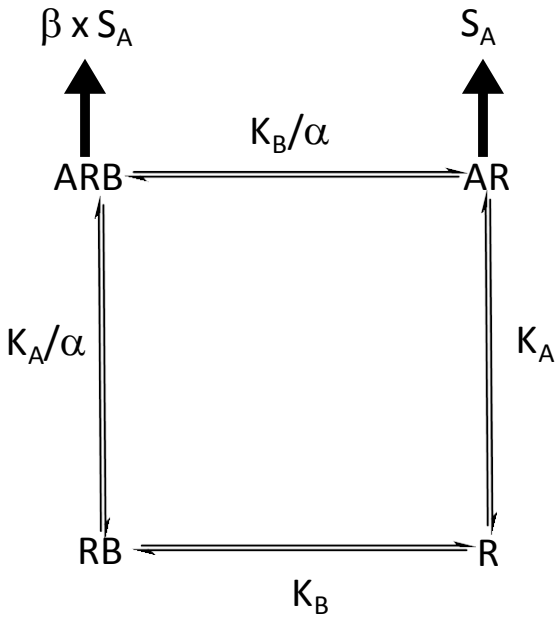

Considering for cases were modulators have no direct agonist effect yields the following equation **(A1.5)** for allosteric modulation of efficacy (E):

$$E = \frac{E_{max}\tau^n[A]^n\left(1+\frac{\alpha\beta[B]}{K_B}\right)^n}{\left[[A]\left(1+\frac{\alpha[B]}{K_B}\right)+K_A\left(1+\frac{[B]}{K_B}\right)\right]^n+\tau^n[A]^n\left(1+\frac{\alpha\beta[B]}{K_B}\right)^n} \quad (\boldsymbol{A1.5})$$

where E_{max} is the maximal response capability of the system, τ is the intrinsic efficacy of the orthosteric ligand, K_A and K_B are the equilibrium dissociation constants of the orthosteric and allosteric ligands and *n* is a 'fitting' factor. The parameter β denotes the effect the modulator has on efficacy defined as the signal imparted on the receptor system by orthosteric ligand A (S_A).

At first glance this equation may seem as equally ridiculous as the ATSM, however, this equation can actually be fitted to traditional pharmacological experimental data. The K_A, K_B, and α terms should remain constant between a given GPCR and its set of ligands[1]. The empirical parameter, β, governs the magnitude of an allosteric modulator's ability to modify efficacy of the ternary complex (ARB). Moreover, β may change depending on the signaling pathway that is being monitored (functional selectivity).

The α and β parameters are rheostats that govern orthosteric ligand occupancy and the agonist receptor generated signal. Using equation (A1.5) we can explore possible outcomes where α and β exhibit positive, negative, and neutral cooperativity on affinity and efficacy, respectively (for an agonist). First we will consider the case of *solely* manipulating α (**Figure A1.5 A & B**). Since, α is the cooperativiity factor for binding we see that only the potency is enhanced when $\alpha > 1$ (positive cooperativity) and decreased when $\alpha < 1$ (negative cooperativity). Similar to Figure A1.1 we observe the signal

[1] Of note, the operational binding cooperativity factor, α, is an amalgam of α, β, & γ discussed above for the ATSM.

imparted by the orthosteric ligand is only altered by the effect of the allosteric ligand's ability to modulate receptor occupancy.

Next, let's consider the case for *solely* manipulating β (**Figure A1.5 C & D**). The cooperativiity factor for efficacy, β enhances the potency and efficacy is when $\beta > 1$ (positive cooperativity) and decreases the potency and efficacy when $\beta < 1$ (negative cooperativity). Interestingly, if the intrinsic efficacy (τ) of the orthosteric ligand is very high then the allosteric modulation is initially observed as a reduction in only agonist potency.

Now, let's consider the log dose response profiles when an allosteric modulator can alter *both* affinity and efficacy (**Figure A1.6).** When both efficacy and affinity are positively modulated (Figure A1.6A) or both negatively modulated (Figure A1.6D) there are additive effects. The allosteric ligand increases (or decreases) agonist receptor occupancy and this combined with the increase (or decrease) in receptor generated signal, whose combined effects culminate in enhanced potency and efficacy (or the converse).

So what outcomes does the model provide when the rheostats (α and β) have opposite effects? Let's consider these divergent behaviors (illustrated in Figure A1.6B & C), where receptor occupancy is enhanced and the agonist receptor effect decreased (or the converse). When the orthosteric ligand occupancy is enhanced ($\alpha > 1$) combined with negative cooperativity with respect to efficacy ($\beta < 1$) we observe a small increase in potency combined with decreased total effect. When the opposite parameters are

employed ($\alpha < 1$; $\beta > 1$) we have a decrease in agonist receptor occupancy that is counterbalanced by the increase in signal generation, yielding small reduction in potency and a more noticeable enhancement of efficacy.

Ago-allosteric ligands

What if the modulator possesses intrinsic efficacy? The ability of an allosteric modulator to induce (or stabilize) a conformational state can also lead to intrinsic efficacy for the modulator is becoming more prevalent. To model this we just need to add a new term S_B, that is the signal imparted on the receptor by the allosteric ligand (in cyan):

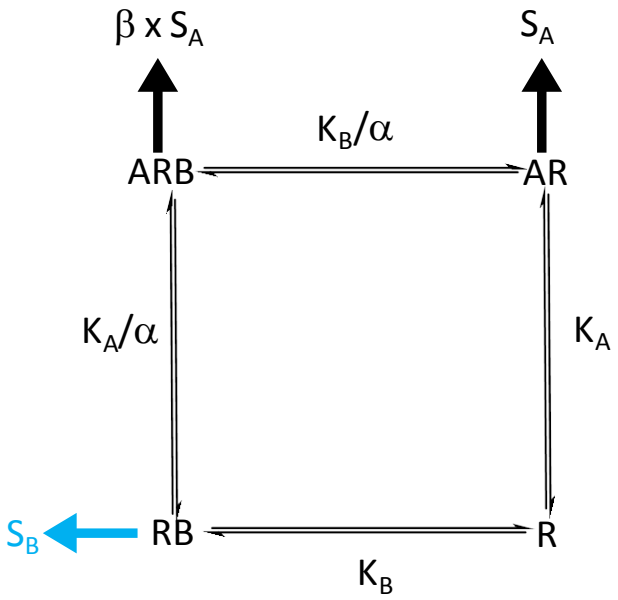

This provides the following equation (6) **(A1.6)**:

$$E = \frac{E_{max}(\tau_A[A](K_B + \alpha\beta[B]) + \tau_B[B]K_A)^n}{([A]K_B + K_AK_B + K_B[B] + \alpha[A][B])^n + (\tau_A[A](K_B + \alpha\beta[B]) + \tau_B[B]K_A)^n} \qquad (\boldsymbol{A1.6})$$

The terms are as described above for equation (A1.5). The intrinsic efficacy τ is now defined specifically for the allosteric ligand (τ_B) and the orthosteric ligand (τ_A). This provides us with yet another rheostat than enables modeling of conditions where the allosteric ligand has direct agonism. Moreover, this allows for modeling of up to nine

general types of possibilities for these complex behaviors. For the time being, let's just consider the simplest case where $\alpha=\beta=1$ and the allosteric ligand has direct agonism ($\tau_B = 0.25$). The modulator has no effect on the co-binding of agonist, however, it's direct agonism is additive to the system. This is illustrated in **Figure A1.7**.

A1.5: Conclusion

Allosteric GPCR ligands are becoming more commonplace, thus, pharmacological models need to adapt to account for these myriad of behaviors. Outlined above is a brief description of some select models relating to my thesis. The operational models have more recently emerged to help quantify allosteric GPCR ligands diverse phenomena. Furthermore, equation (A1.5) can even be used to model biased agonism. Thereby, thinking about GPCRs with respect to allostery can help generate models that define their known behaviors. For further reading please see the select references at the end of this appendix.

Figure A1.1

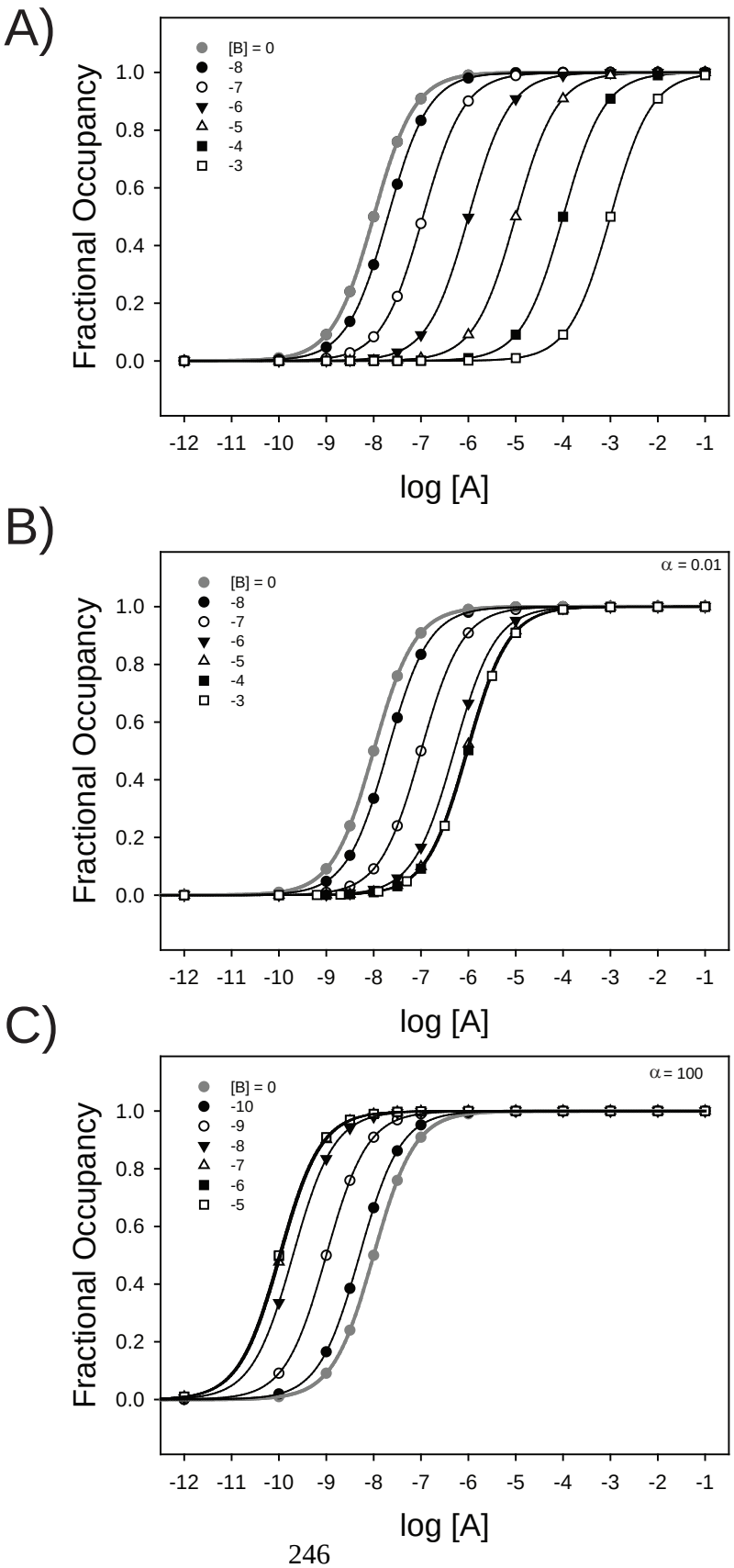
A)
[B] = 0
-8
-7
-6
-5
-4
-3
Fractional Occupancy
1.0
0.8
0.6
0.4
0.2
0.0
-12 -11 -10 -9 -8 -7 -6 -5 -4 -3 -2 -1
log [A]
B)
α = 0.01
[B] = 0
-8
-7
-6
-5
-4
-3
Fractional Occupancy
log [A]
C)
α = 100
[B] = 0
-10
-9
-8
-7
-6
-5
Fractional Occupancy
log [A]

Figure A1.1. Effect of: (A) a competitive ligand (B) a negative allosteric modulator (AM) or C) a positive AM on orthosteric binding. In gray in all panels is the effect of fractional occupancy in the absence the other ligand B. The fixed concentration of B present in each simulation is indicated (inset). Fractional occupancy is defined as $[AR]/[R_{total}]$ where A is the othosteric ligand and R is the receptor. [AR] is the orthosteric ligand, A bound receptor concentration and R_{total} is the total receptor concentration (formally for an allosteric ligand it should read $([AR]+[ARB])/[R_{total}]$). For all simulations the K_A and K_B the K_D of the orthosteric ligand A and other ligand B, respectively were set to 10 nM. Competitive simulation in A) was fit to equation (1) while allosteric behavior B) and C) was fit to the allosteric ternary complex model equation (2) with a cooperativity factor (a) set to a value less than one (0.01) or greater than 1 (100) for a negative and positive modulation of orthosteric binding by B an allosteric ligand (B and C, respectively – also inset). In these simulations competitive interactions (interaction for the same site) leads to a limitless shift in ligand A occupancy. In contrast, allosteric modulators modify orthosteric ligand A's binding to a limit by a factor of 100 (determined by the α factor).

Figure A1.2

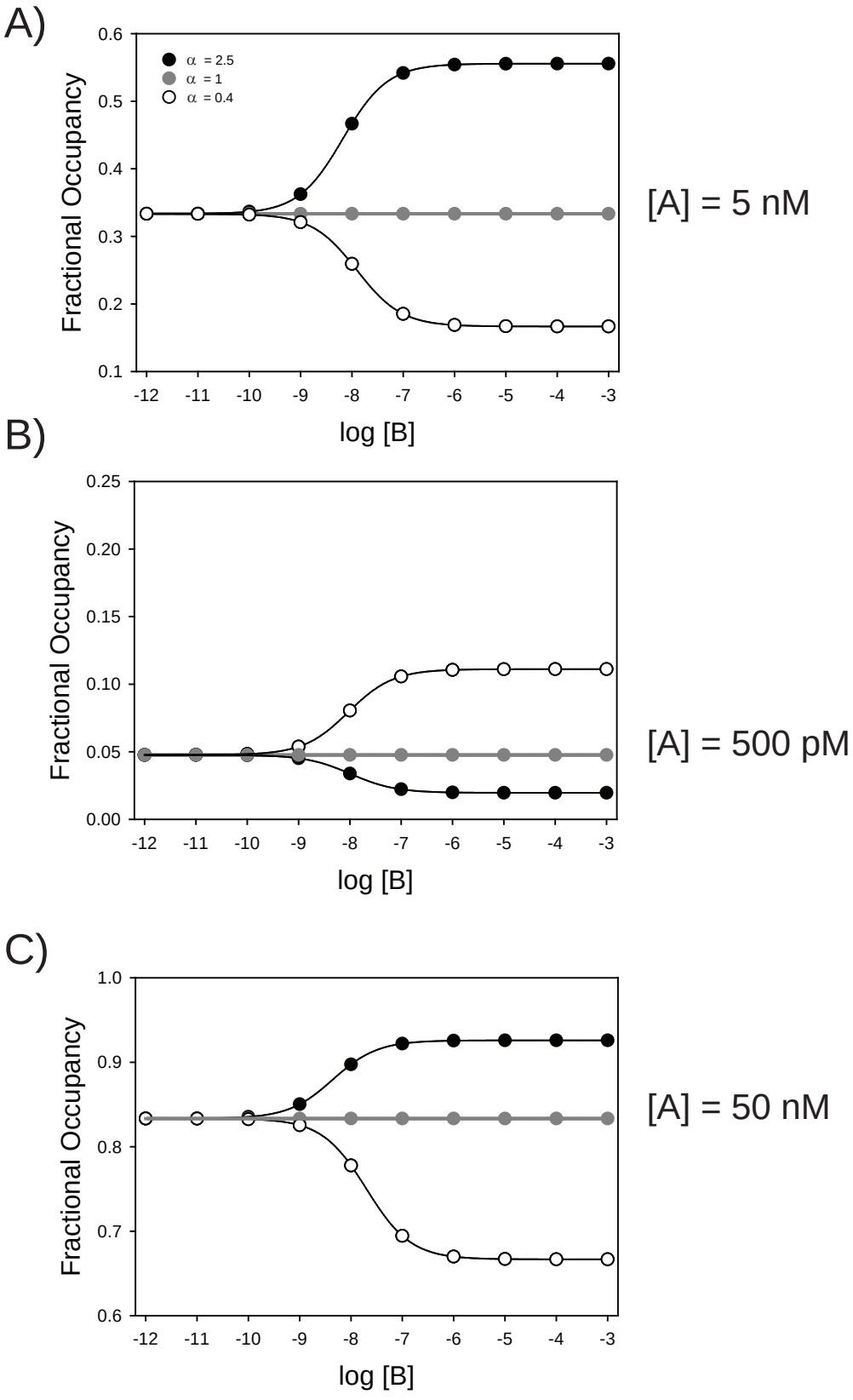
A)
α = 2.5
α = 1
α = 0.4
Fractional Occupancy
log [B]
[A] = 5 nM
B)
Fractional Occupancy
log [B]
[A] = 500 pM
C)
Fractional Occupancy
log [B]
[A] = 50 nM

Figure A1.2. Effect of a three set concentrations of radiolabeled orthosteric ligand ([A], 5 nM, 500 pM and 50 nM – for A, B, & C respectively) on increasing concentrations of an allosteric modulator ([B]). In gray in all panels is the effect of fractional occupancy when there is no cooperativity factor $\alpha = 1$ (this is in essence the fraction bound in the absence the allosteric ligand [B]). For all simulations the K_A and K_B the K_D of the orthosteric ligand A and other ligand B, respectively were set to 10 nM. The cooperativity factor was set to 2.5 (black circles – positive cooperativity) or 0.4 (white circles – negative cooperativity). This style of analysis is good for values that are close to 1. Also this predicts that positive cooperativity values are less pronounced when the factional occupancy is high (i.e. high a concentration of A) and negative cooperativity values are less observable when factional occupancy is low.

Figure A1.3

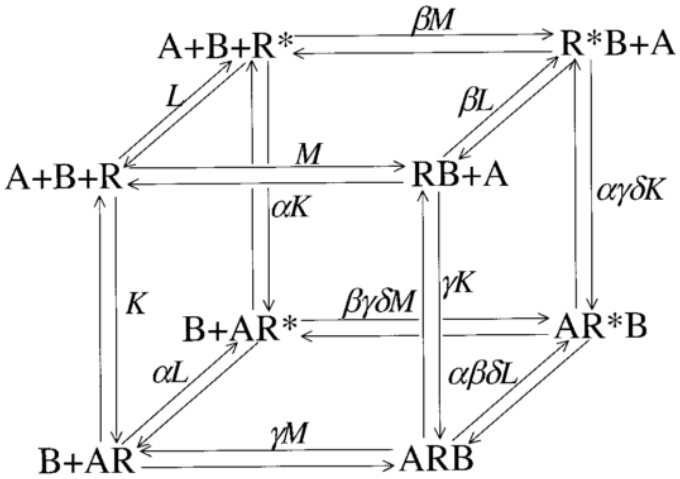

$$\frac{[A]_{Bound}}{[R]_{Total}} = \frac{K[A] + \gamma KM[A][B] + \alpha KL[A] + \alpha\beta\gamma\delta KLM[A][B]}{1 + L + M[B](1 + \beta L) + K[A]\big(1 + \alpha L + \gamma M[B](1 + \alpha\beta\delta L)\big)} \quad \textbf{(A1.3)}$$

$$\frac{[A]_{Active}}{[R]_{Total}} = \frac{L(1 + \alpha K[A] + \beta M[B](1 + \alpha\gamma d\delta[A]))}{1 + L + M[B](1 + \beta L) + K[A]\big(1 + \alpha L + \gamma M[B](1 + \alpha\beta\delta L)\big)} \quad \textbf{(A1.4)}$$

TABLE 1
Summary of the equilibrium constants of the allosteric two-state model

Parameter	Description	Definition
K	Association constant of A	$\frac{[AR]}{[A][R]}$
L	Receptor isomerization constant	$\frac{[R^*]}{[R]}$
M	Association constant of B	$\frac{[RB]}{[B][R]}$
α	Intrinsic efficacy of A: ratio of affinity (and therefore selectivity) of A for R* and R	$\frac{[R][AR^*]}{[R^*][AR]}$
β	Intrinsic efficacy of B: ratio of affinity of B for R* and R	$\frac{[R][R^*B]}{[R^*][RB]}$
γ	Binding cooperativity between A and B: ratio of affinity of A for BR and R or of B for AR and R	$\frac{[R][ARB]}{[AR][RB]}$
δ	Activation cooperativity between A and B: ratio of affinity of A for BR* and BR or of B for AR* and AR	$\frac{[R^*][AR][RB][AR^*B]}{[R][AR^*][R^*B][ARB]}$

Figure A1.3. The allosteric two-state model as described by Hall (2000). Equations (A1.3) and (A1.4) for binding and efficacy respectively. Derivations can be found in Hall (2000) (for equations 3 and 10). Table 1 taken directly from hall (2000) is a summary of equilibrium constants of the allosteric two-state model.

Figure A1.4

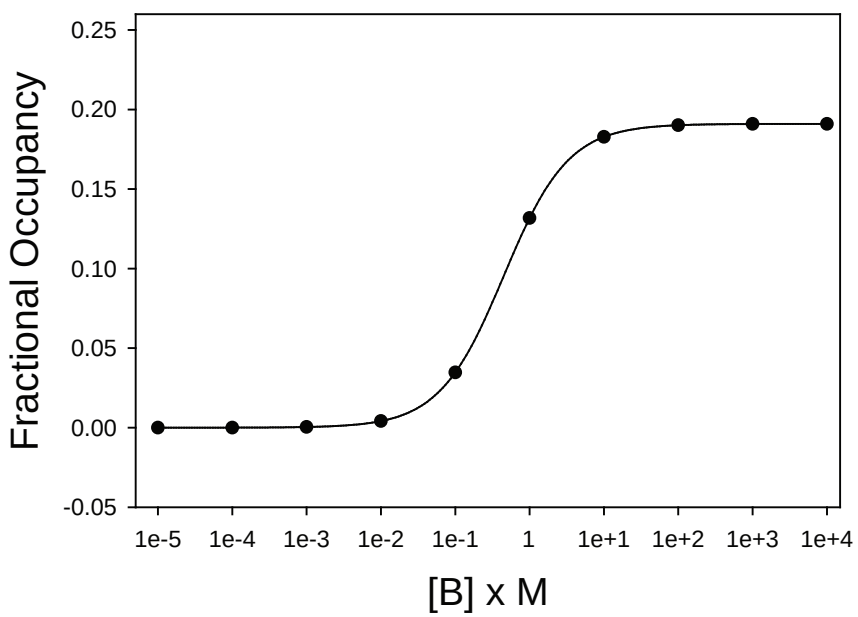
Fractional Occupancy
0.25
0.20
0.15
0.10
0.05
0.00
-0.05
1e-5
1e-4
1e-3
1e-2
1e-1
1
1e+1
1e+2
1e+3
1e+4
[B] x M

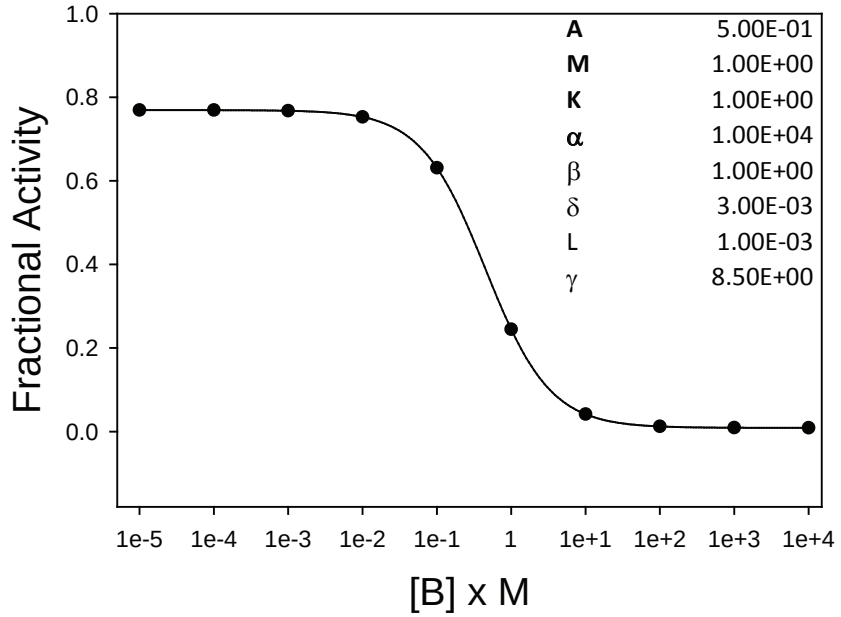
Fractional Activity
1.0
0.8
0.6
0.4
0.2
0.0
A 5.00E-01
M 1.00E+00
K 1.00E+00
α 1.00E+04
β 1.00E+00
δ 3.00E-03
L 1.00E-03
γ 8.50E+00
1e-5
1e-4
1e-3
1e-2
1e-1
1
1e+1
1e+2
1e+3
1e+4
[B] x M

Figure A1.4. Simulations of the effect of allosteric modulator Org 27569 on orthosteric ligand CP 55940 ([A]) affinity (left) and efficacy (right) as a function of Org 27569 ([B]). Simulations were calculated using equation (A.3) and (A.4) shown in Figure 3. Parameters were defined such that the allosteric ligand enhanced orthosteric agonist binding and inhibited orthosteric efficacy. The parameter was set to $\gamma > 1$ indicative of positive binding cooperativity and $\delta < 1$ indicative of negative activation cooperativity. The parameters used were K = M = 1, L = 0.001, α = 10,000, β = 1, γ = 8.5 and δ = 0.03. The concentration of A was 0.5.

Figure A1.5

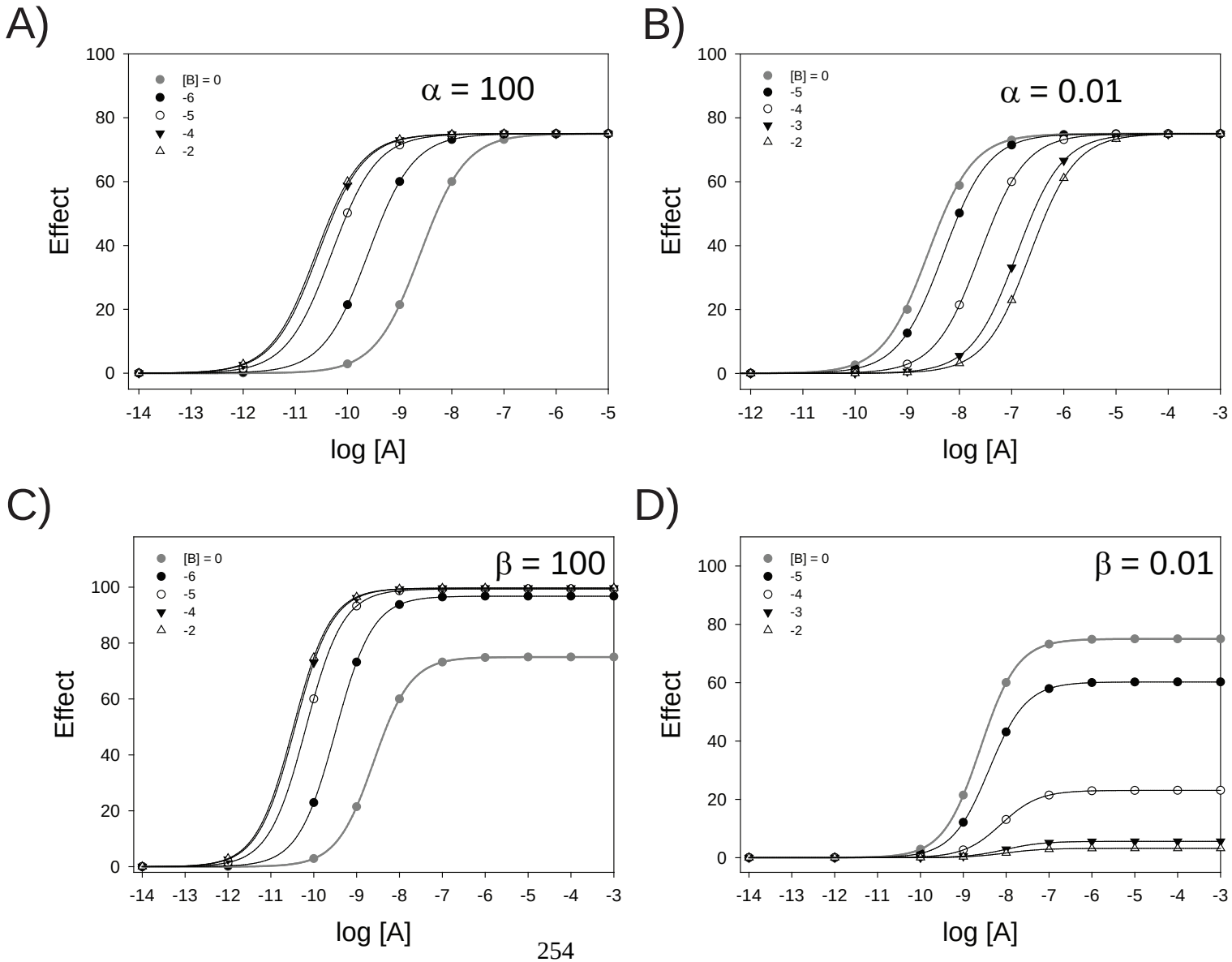
A)
α = 100
[B] = 0
-6
-5
-4
-2
Effect
log [A]
B)
α = 0.01
[B] = 0
-5
-4
-3
-2
Effect
log [A]
C)
β = 100
[B] = 0
-6
-5
-4
-2
Effect
log [A]
D)
β = 0.01
[B] = 0
-5
-4
-3
-2
Effect
log [A]

Figure A1.5. The effect of a positive (A) or negative (B) allosteric modulator with respect to affinity, and the effect of a positive (C) or negative (D) modulation with respect to efficacy. Simulations were calculated using equation A1.5 [E_{max} = 100, τ = 3, n = 1, K_A = 10 nM, K_B = 10 μM]. The α and β values were set to either 100 or 0.01 for values greater than one and less than one. Concentrations of allosteric ligand B are as indicated (inset).

Figure A1.6

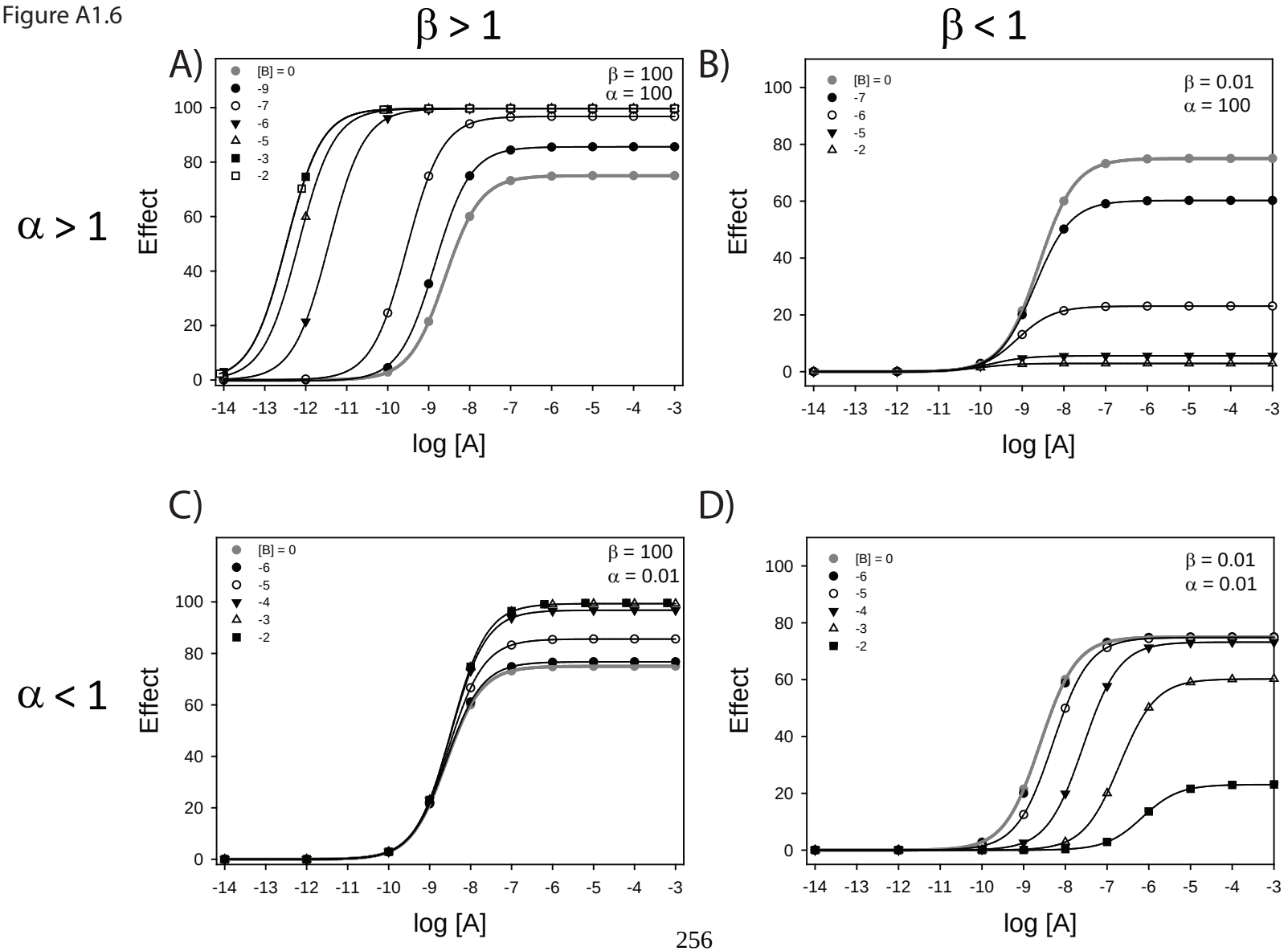
β > 1
β < 1
α > 1
α < 1
A)
B)
C)
D)
[B] = 0
β = 100
α = 100
β = 0.01
α = 100
β = 100
α = 0.01
β = 0.01
α = 0.01
Effect
log [A]

Figure A1.6. The effect of a positive (A & B) or negative (C & D) allosteric modulator with respect to affinity, and the effect of a positive (A & C) or negative (B & D) with respect to efficacy. Simulations were calculated using equation A1.5. [E_{max} = 100, τ = 3, n = 1, K_A = 10 nM, K_B = 10 μM]. The values of α and β are as denoted in the figure. Concentrations of allosteric ligand B are as indicated inset.

Figure A1.7

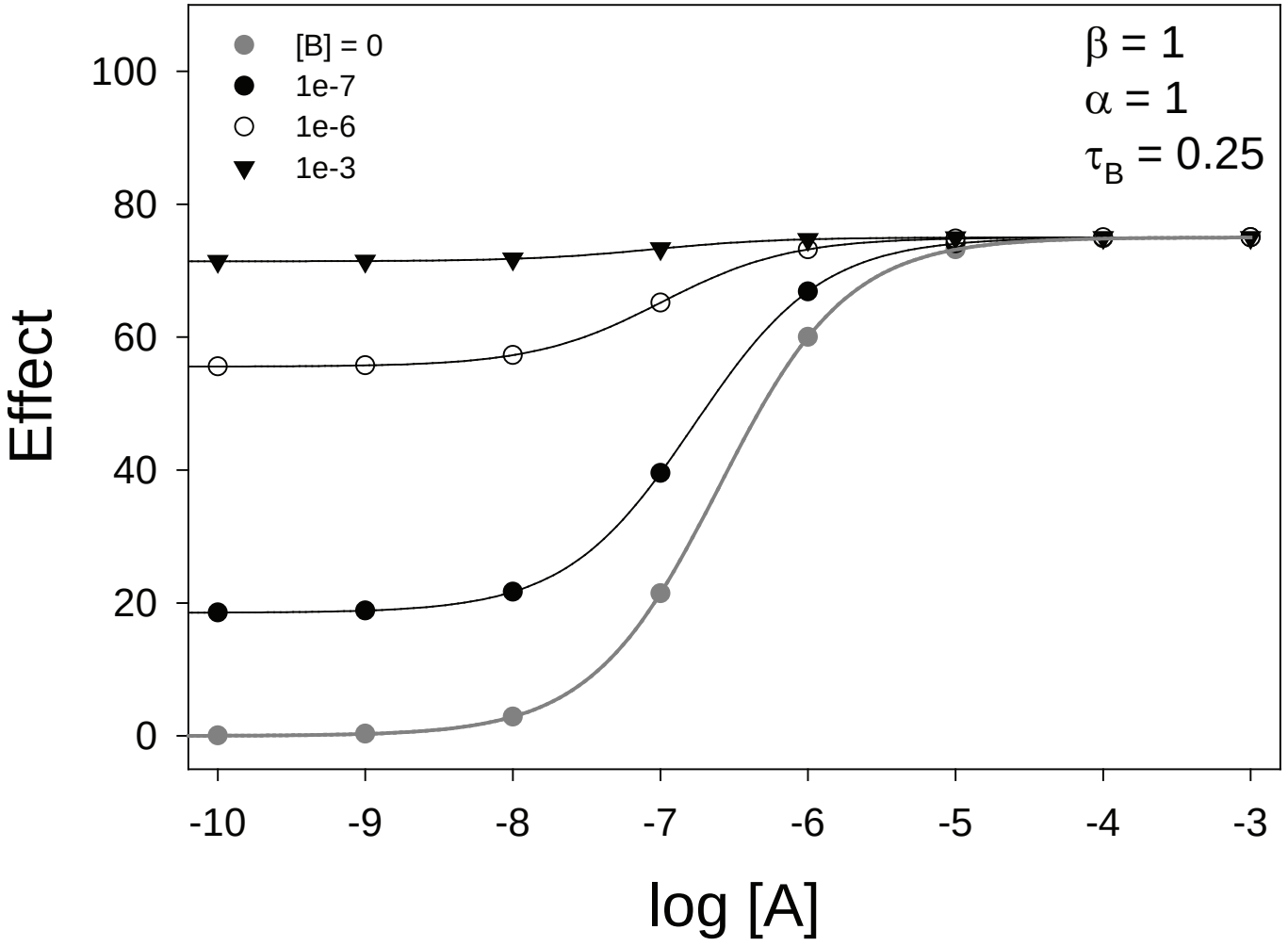
[B] = 0
1e-7
1e-6
1e-3
β = 1
α = 1
τB = 0.25
Effect
100
80
60
40
20
0
-10
-9
-8
-7
-6
-5
-4
-3
log [A]

Figure A1.7. The effect of an ago-allosteric modulator (modulators with direct agonist activity). Simulations were calculated with equation A1.6 [E_{max} = 100, *n* = 1, K_A = 10 μM, KB = 10 nM, τ_A = 3, τ_B = 0.25, α = 1, β =1]. Concentrations of allosteric ligand B are as indicated (inset).

A1.6 References

1. Ehlert, F. J. (1988) *Mol Pharmacol* **33**, 187-194
2. Hall, D. A. (2000) *Mol Pharmacol* **58**, 1412-1423
3. Black, J. W., and Leff, P. (1983) *Proc R Soc Lond B Biol Sci* **220**, 141-162
4. Price, M. R., Baillie, G. L., Thomas, A., Stevenson, L. A., Easson, M., Goodwin, R., McLean, A., McIntosh, L., Goodwin, G., Walker, G., Westwood, P., Marrs, J., Thomson, F., Cowley, P., Christopoulos, A., Pertwee, R. G., and Ross, R. A. (2005) *Mol Pharmacol* **68**, 1484-1495
5. Kenakin, T. (2005) *Nat Rev Drug Discov* **4**, 919-927
6. Leach, K., Sexton, P. M., and Christopoulos, A. (2007) *Trends Pharmacol Sci* **28**, 382-389
7. Kenakin, T. (2004) *Trends Pharmacol Sci* **25**, 186-192
8. Kenakin, T. (2007) *Trends Pharmacol Sci* **28**, 407-415
9. Kenakin, T. P. (2012) *Br J Pharmacol* **165**, 1659-1669
10. Gregory, K. J., Sexton, P. M., and Christopoulos, A. (2010) *Curr Protoc Pharmacol* **Chapter 1**, Unit 1 21
11. Kenakin, T. (2002) *Annu Rev Pharmacol Toxicol* **42**, 349-379
12. Kenakin, T., and Miller, L. J. (2010) *Pharmacol Rev* **62**, 265-304
13. Keov, P., Sexton, P. M., and Christopoulos, A. (2011) *Neuropharmacology* **60**, 24-35
14. Christopoulos, A. (2002) *Nat Rev Drug Discov* **1**, 198-210
15. Christopoulos, A., and Kenakin, T. (2002) *Pharmacol Rev* **54**, 323-374
16. Luttrell, L. M., and Kenakin, T. P. (2011) *Methods Mol Biol* **756**, 3-35
17. May, L. T., Leach, K., Sexton, P. M., and Christopoulos, A. (2007) *Annu Rev Pharmacol Toxicol* **47**, 1-51

Appendix 2

Crystallogenesis of CB_1

A2.1: SUMMARY

In this appendix I will briefly summarize the progress I have made in initial screening of conditions that are amenable to crystalneogensis of CB_1. I created and purified all the constructs and proteins herein. Dr. Penmatsa, from the Gouaux lab was extremely helpful in assisting with the initial screening and instruction in the practical techniques of membrane protein crystallography.

A2.2: Construction and Characterization of crystallization candidate

Since GPCR-T4L fusion constructs have been successfully employed for a number of GPCRs, we began with a similar strategy. For our final crystallization candidate, I engineered 'cys-less' T4L into the Nt2/C2 construct (described in Chapter 4). This was ultimately chosen due to its more compact structure, as indicated by SDS PAGE analysis (see Chapter 4). T4L gene was codon optimized and purchased from GenScript then sub cloned into our Nt2/C2 construct, replacing parts of intracellular loop 3. Moreover, residue C355 was mutated back to a cysteine in this construct, as it is a highly conserved cysteine residue in GPCRs, and our previous findings indicate that the presence of this cysteine enhanced expression (1). Interestingly, this mutant did not appear to be amenable to labeling (data not shown). A 2D model of this construct is illustrated in Figure A2.1.

Next, I confirmed that this construct retained the ability bind radiolabled antagonist (Figure A2.2A). I then made a fusion protein of this construct with GFP, and

screened a number of detergents. We found that we retained the most ideal FSEC profile in our CCD detergent cocktail (Figure 2B). Ultimately, this construct could be immuno-purified and yielded highly pure CB_1 at ~18 μg/15 cm plate (Figure A2.2C).

Over 1000 crystal conditions were screened using a variety of techniques used to crystallize membrane proteins. Shown in Figure A2.3A is a custom screen I developed, based on crystallization conditions of other T4L fusion GPCRs of known structure at the time. Two very promising "hits" were collected from this screen using a bicelle method (2); the conditions are indicated as a red box with an asterisk and shown below in Figure A2.3B & 3C. Importantly, buffer subjected to identical conditions did not produce crystal formation. As a result, the crystals shown in Figure A2.3B & 3C were looped and cryogenically preserved however diffraction data was of extremely poor quality. Future directions include perusing this in more detail.

A2.2.1: Experimental procedures

Purifications were performed essentially as previously described (see Chapter 1). Briefly, 100, 15 cm plates containing COS-1 cells expressing iCB_1-T4L grown in the presence of 100 nM SR141716A were solublized in 0.6/0.1/0.1% CHAPS/DM/CHS and 2 μM SR147161A supplemented purification buffer for 2-3 hours at ~10 mLs/ gram of wet cell pellet. Clarified supernatants were applied to 5 mLs of 1D4 beads (1:1 slurry) and allowed to incubate for 3-5 hours (in batch). Settled beads were washed 10 column volumes of solubilization buffer, then another 10 column volumes of 2XFSEC buffer containing 1 μM SR141716A (via drip). Purified receptor was eluted using 7 mLs of

Elution buffer containing 200 μM 9mer and 1 μM SR141716A (in batch) then concentrated to ~130 μL using an amicon 100k centrifugal filter. Sample was then spiked with 0.5 mM SR141716A and then subjected to a high-speed centrifugation (100,000 x g) to remove precipitated protein. Protein concentration was estimated via lowery and found to be ~6-10 mg/mL. For the data presented in Figure A2.3, 110 μL of concentrated sample was added to 22 μL of 35% DMPC/CHAPSO (2.8:1) (5.8% final bicelle concentration) and screens were set up using the hanging drop method (with about 0.1 μl of mother liquor and 0.1 μL of CB_1 receptor bicell mixture) using the mosquito crystallization robot (ttplabtech).

A2.3 References

1. Fay, J. F., Dunham, T. D., and Farrens, D. L. (2005) *Biochemistry* **44**, 8757-8769
2. Faham, S., Ujwal, R., Abramson, J., and Bowie, J. U. (2009) Chapter 5 Practical Aspects of Membrane Proteins Crystallization in Bicelles. in *Current Topics in Membranes* (Larry, D. ed.), Academic Press. pp 109-125

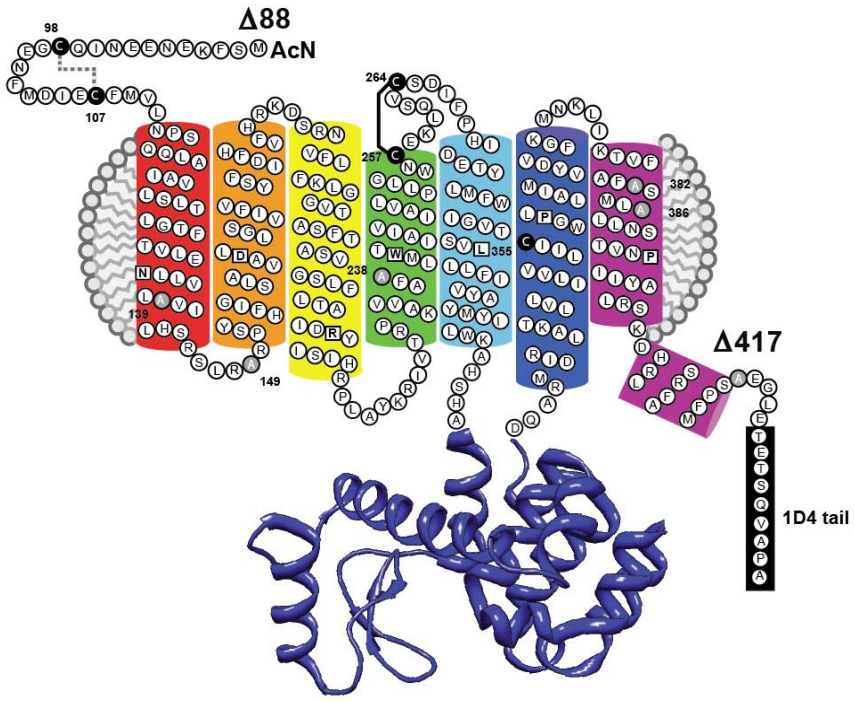

Figure A2.1. 2D cartoon diagram of CB_1-T4L fusion crystallization candidate. Note this construct has an N-terminal Δ88 truncation, C-terminal Δ417 truncation, cysteine residues 98,107,257,264 and 355, T4L replacing IL3, and the 9 amino acid 1D4 motif tag.

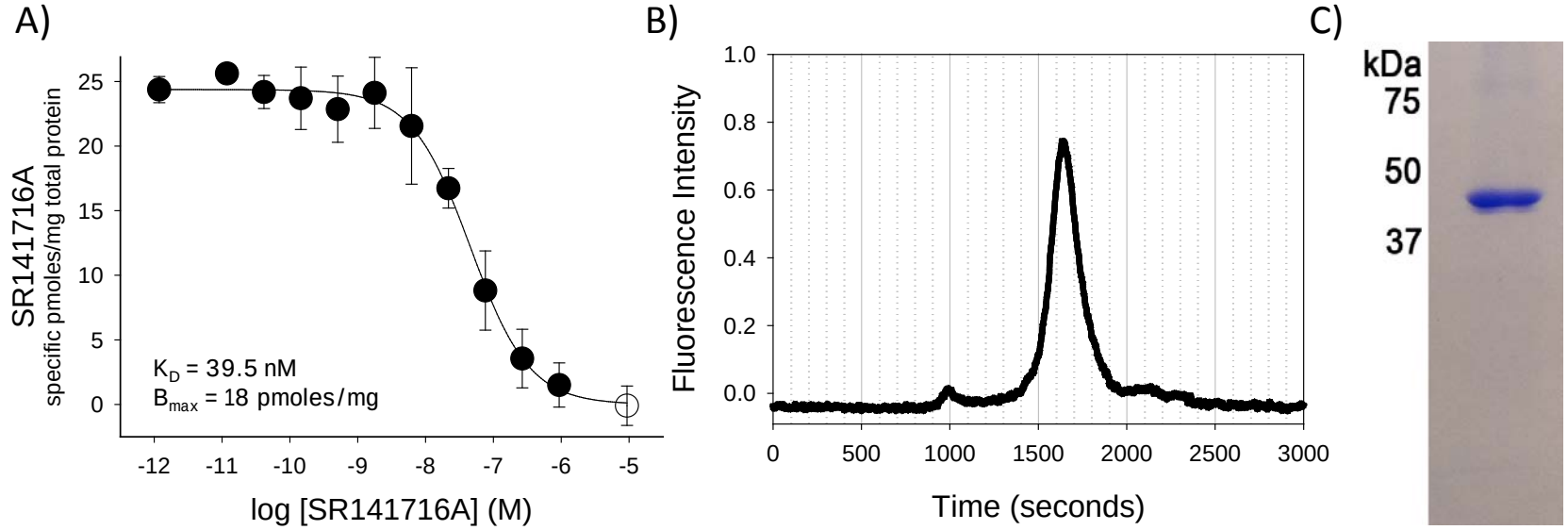

Figure A2.2. Initial characterization of CB_1-T4L fusion crystallization candidate. A) Homologous radiolabeled antagonist binding assay of CB_1-T4L fusion crystallization candidate. Values for K_D and B_{max} values are shown in the figure inset. B) An FSEC of crude solubilized CB_1-T4L-GFP fusion construct showing a very monodisperse symmetrical peak. C) Coomassie stained SDS-PAGE showing high purity of immunoaffinity purified CB_1-T4L crystallization candidate construct.

.

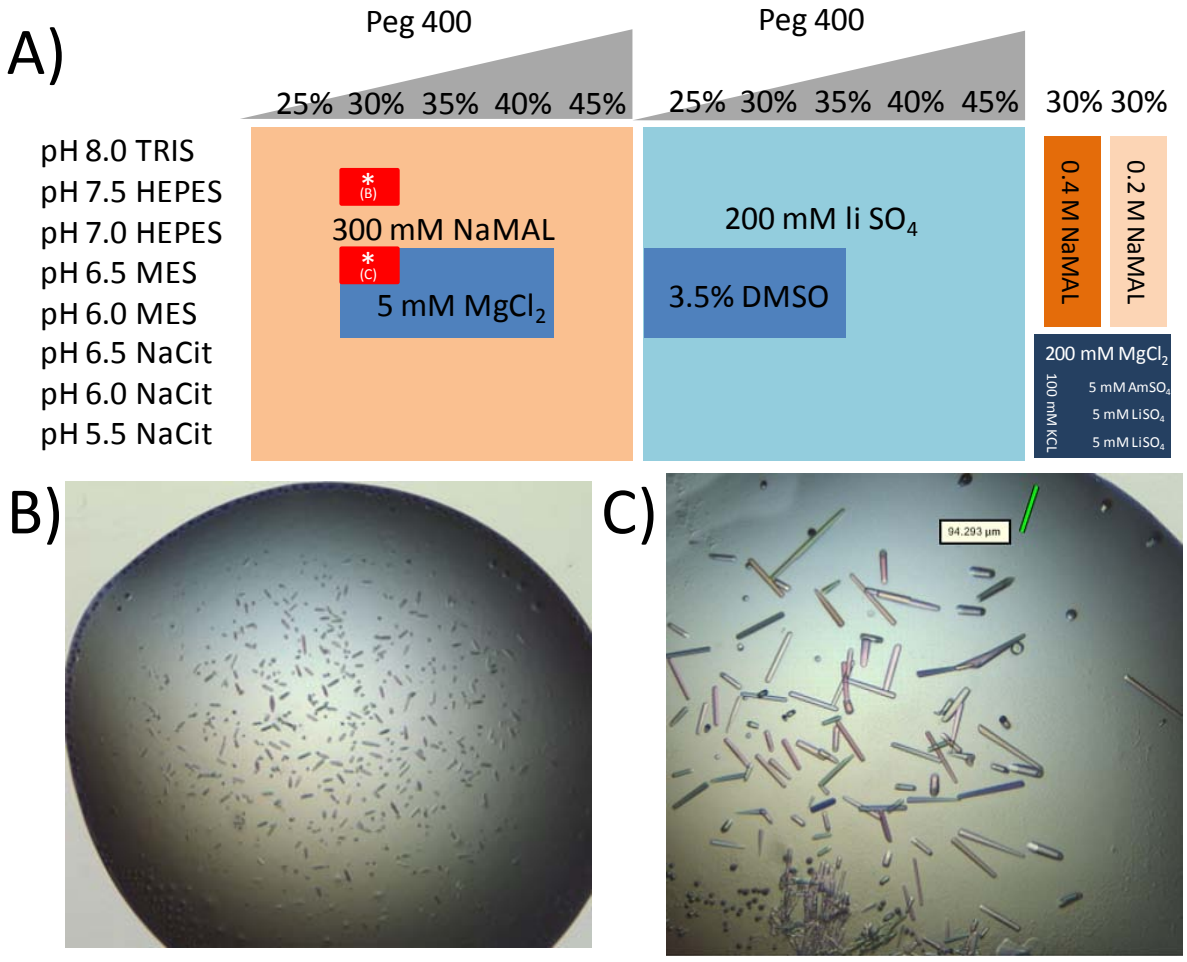

Figure A2.3. Crystallogenesis of CB_1-T4L fusion crystallization candidate. In A) custom screen based on previous GPCR-T4L fusion constructs. Red boxes with white asterisk represent conditions amenable to crystal formation as shown in (B) and (C) respectively. It should be noted, the looped crystals grew to a size larger than what is represented above, as these images were taken a few days prior to looping .

Appendix 3

(An Incomplete) List of GPCRs of Known Structure

(Rhod)opsin

Structure Notes	PDB	Resolution [A]	Reference
first experimental GPCR structures	1F88, 1HZX	2.8	Palczewski K, Kumasaka T, Hori T, Behnke CA, Motoshima H, Fox BA, Le Trong I, Teller DC, Okada T, Stenkamp RE, Yamamoto M, Miyano M. Science. 2000 Aug Crystal structure of rhodopsin: A G protein-coupled receptor. 4;289(5480):739-45. Teller DC, Okada T, Behnke CA, Palczewski K, Stenkamp RE. Advances in determination of a high-resolution three-dimensional structure of rhodopsin, a model of G-protein-coupled receptors (GPCRs). Biochemistry. 2001 Jul 3;40(26):7761-72.
shows functional water molecules	1L9H	2.6	Okada T, Fujiyoshi Y, Silow M, Navarro J, Landau EM, Shichida Y. Functional role of internal water molecules in rhodopsin revealed by X-ray crystallography. Proc Natl Acad Sci U S A. 2002 Apr 30;99(9):5982-7. 2002 Apr 23.
	1GZM	2.65	Li, J., Edwards, P., Burghammer, M., Villa, C., Schertler, G.F.X., Structure of bovine rhodopsin in a trigonal crystal form. Journal: (2004) J.Mol.Biol. 343: 1409
focus on retinal conformation	1U19	2.2	Okada T, Sugihara M, Bondar AN, Elstner M, Entel P, Buss V. The retinal conformation and its environment in rhodopsin in light of a new 2.2 A crystal structure. J Mol Biol. 2004 Sep 10;342(2):571-83.
Thermostable N2C/D282C mutant heterologously expressed in COS cells	2J4Y	3.4	Standfuss J, Xie G, Edwards PC, Burghammer M, Oprian DD, Schertler GF. Crystal structure of a thermally stable rhodopsin mutant. J Mol Biol. 2007 Oct 5;372(5):1179-88. Epub 2007 Mar 12.
photoactivated and ground state	2I35, 2I36, 2I37	3.8, 4.1, 4.15	Salom D, Lodowski DT, Stenkamp RE, Le Trong I, Golczak M, Jastrzebska B, Harris T, Ballesteros JA, Palczewski K. Crystal structure of a photoactivated deprotonated intermediate of rhodopsin. Proc Natl Acad Sci U S A. 2006 Oct 31;103(44):16123-8. Epub 2006 Oct 23
Retinal removed: Opsin	3CAP	2.9	Park JH, Scheerer P, Hofmann KP, Choe HW, Ernst OP. Nature. 2008 Jul 10;454(7201):183-7. Epub 2008 Jun 18. Crystal structure of the ligand-free G-protein-coupled receptor opsin.
activated form of Ops*-GalphaCT peptide complex	3DQB	3.2	Scheerer P, Park JH, Hildebrand PW, Kim YJ, Krauss N, Choe HW, Hofmann KP, Ernst OP. Crystal structure of opsin in its G-protein-interacting conformation. Nature. 2008 Sep 25;455(7212):497-502.
Squid Rhodopsin	2Z73	2.5	Murakami M, Kouyama T. Crystal structure of squid rhodopsin. Nature. 2008 May 15;453(7193):363-7.
squid rhodopsin	2ZIY	3.7	Shimamura, T., Hiraki, K., Takahashi, N., Hori, T., Ago, H., Masuda, K., Takio, K., Ishiguro, M., Miyano, M., Crystal structure of squid rhodopsin with intracellularly extended cytoplasmic region. (2008) J.Biol.Chem. 283: 17753-17756
lumirhodopsin	2HPY	2.8	Nakamichi, H., Okada, T., Local peptide movement in the photoreaction intermediate of rhodopsin. (2006) Proc.Natl.Acad.Sci.Usa 103: 12729-12734
bathorhodopsin	2G87	2.6	Nakamichi, H., Okada, T., Crystallographic model of bathorhodopsin (2006) Angew.Chem.Int.Ed.Engl. 45: 4270-4273
9-cis-rhodopsin	2PED	2.95	Nakamichi, H., Buss, V., Okada, T., Photoisomerization mechanism of rhodopsin and 9-cis-rhodopsin revealed by x-ray crystallography. (2007) Biophys.J. 92: L106-L108
Alternative models for: 1GZM and 2J4Y	3C9L 3C9M	2.65 3.40	Stenkamp, R.E., Alternative models for two crystal structures of bovine rhodopsin.(2008) Acta Crystallogr.,Sect.D 64: 902-9
All-trans retinal soaked into preformed opsin crystals	3PQR 3PXO	2.85 3.00	Choe, H.W., Kim, Y.J., Park, J.H., Morizumi, T., Pai, E.F., Krauss, N., Hofmann, K.P., Scheerer, P., Ernst, O.P., Crystal structure of metarhodopsin II.(2011) Nature 471: 651-655
Thermostable N2C/D282C	4A4M	3.30	Deupi, X., Edwards, P., Singhal, A., Nickle, B., Oprian, D., Schertler,

CAM - M257Y			G., Standfuss, J., Stabilized G protein binding site in the structure of constitutively active metarhodopsin-II.(2012) Proc.Natl.Acad.Sci.USA 109: 119
Thermostable N2C/D282C CAM - E113Q	2X72	3.00	Standfuss, J., Edwards, P.C., Dantona, A., Fransen, M., Xie, G., Oprian, D.D., Schertler, G.F.X., The structural basis of agonist-induced activation in constitutively active rhodopsin. (2011) Nature 471: 656-660

CXCR4 Chemokine Receptor

Structure Notes	PDB	Resolution [A]	Reference
complex with small molecule antagonist IT1t and cyclic peptide antagonist CVX15, T4 lysozyme insertion in 3rd intracellular loop, stabilizing mutations, crystallized in LCP (Cholesterol additive)	3ODU,3OE0,3OE8,3OE9,3OE6	2.5 A, 2.9 A, 3.1 A, 3.1 A, 3.2 A	Wu, B. et al., Structures of the CXCR4 Chemokine GPCR with Small-Molecule and Cyclic Peptide Antagonists. Science 7 Oct 2010

Adenosine Receptor

Structure Notes	PDB	Resolution [A]	Reference
Bound antagonist ZM241385	3EML	2.6	Jaakola VP, Griffith MT, Hanson MA, Cherezov V, Chien EY, Lane JR, Ijzerman AP, Stevens RC. The 2.6 angstrom crystal structure of a human A2A adenosine receptor bound to an antagonist. Science. 2008 Nov 21;322(5905):1211-7. Epub 2008 Oct 2.
Bound agonist UK-432097	3QAK	2.7	Structure of an Agonist-Bound Human A2A Adenosine Receptor Xu, F., Wu, H., Katritch, V., Han, G.W., Jacobson, K.A., Gao, Z-D., Cherezov, V., Stevens, R.C. Science
Bound to agonists adenosine and NECA	2YDO 2YDV	3.0 & 2.6	G. Lebon, T. Warne, P. C. Edwards, K. Bennett, C. J. Langmead, A. G. W. Leslie & C. G. Tate Agonist-bound adenosine A(2A) receptor structures reveal common features of GPCR activation Nature 474, 521–525 (23 June 2011)
A2A adrenergic receptor bound to Fab2839	3VG9 3VGA	3.1 & 2.7	Hino, T., Arakawa, T., Iwanari, H., Yurugi-Kobayashi, T., Ikeda-Suno, C., Nakada-Nakura, Y., Kusano-Arai, O., Weyand, S., Shimamura, T., Nomura, N., Cameron, A., Kobayashi, T., Hamakubo, T., Iwata, S., & Murata, T. (2012).G-protein-coupled receptor inactivation by an allosteric inverse-agonist antibody

β2 Adrenergic Receptor

Structure Notes	PDB	Resolution [A]	Reference
b2AR365-Fab5 complex	2R4S, 2R4R	3.4 / 3.4	Rasmussen SG, Choi HJ, Rosenbaum DM, Kobilka TS, Thian FS, Edwards PC, Burghammer M, Ratnala VR, Sanishvili R, Fischetti RF, Schertler GF, Weis WI, & Kobilka BK (2007). Crystal structure of the human β2 adrenergic G-protein-coupled receptor. Nature 450:383-387.
Complex with Carazolol ligand and bound Cholesterol; T4 lysozyme fusion in 3rd intracellular loop	2RH1	2.4	Cherezov et al. (2007). High-resolution crystal structure of an engineered human β2-adrenergic G protein-coupled receptor. Science 318:1258-1265

T4 lysozyme fusion in 3rd intracellular loop, bound cholesterol	3D4S	2.8	Hanson et al., (2008) A specific cholesterol binding site is established by the 2.8 A structure of the human beta2-adrenergic receptor. Structure 16: 897-905
methylated receptor	3KJ6	3.4	Bokoch et al., Ligand-specific regulation of the extracellular surface of a G-protein-coupled receptor. (2010) Nature 463: 108-112
T4 lysozyme fusion in 3rd intracellular loop, bound cholesterol, mutations: E122W, N187E, C1054T, C1097A; inverse agonist ICI 118,551	3NY8 3NY9 3NYA	2.84 2.48 3.16	Wacker, D., Fenalti, G., Brown, M.A., Katritch, V., Abagyan, R., Cherezov, V., Stevens, R.C., Conserved binding mode of human beta2 adrenergic receptor inverse agonists and antagonist revealed by X-ray crystallography.(2010) J.Am.Chem.Soc. 132: 11443-11445
covalently tethered agonist	3PDS	3.5	Rosenbaum, D.M.,Zhang, C, et al. Structure and function of an irreversible agonist-beta(2) adrenoceptor complex (2011) Nature 469: 236-240.
NB80 bound	3P0G	3.5	Rasmussen et al. Structure of a nanobody-stabilized active state of the beta2 adrenoceptor Nature (2011)
agonist-occupied β2 adrenergic receptor (active) in complex with the (nucleotide free) Gs heterotrimer	3SN6	3.2	Rasmussen et al. Crystal structure of the β2 adrenergic receptor–Gs protein complex Nature (2011)

β1 Adrenergic Receptor

Structure Notes	PDB	Resolution [A]	Reference
Dobutamin bound beta 1 adrenergic receptor (turkey)	2Y01	2.6	Warne, A. et al. (2011) TURKEY BETA1 ADRENERGIC RECEPTOR WITH STABILISING MUTATIONS AND BOUND PARTIAL AGONIST DOBUTAMINE (CRYSTAL DOB102) Nature 469: 241
Thermostabilized turkey receptor	2VT4	2.7	Warne T. et al., (2008) Structure of a beta1-adrenergic G-protein-coupled receptor Nature 454, 486-491
Thermostabilized turkey receptor	2YCW 2YCX 2YCY 2YCZ	3.0 3.25 3.15 3.65	Moukhametzianov, R., Warne, T., Edwards, P.C., Serrano-Vega, M.J., Leslie, A.G., Tate, C.G., Schertler, G.F., Two distinct conformations of helix 6 observed in antagonist-bound structures of abeta1-adrenergic receptor. (2011) Proc.Natl.Acad.Sci.USA 108: 8228

Histamine H1 Receptor

Structure Notes	PDB	Resolution [A]	Reference
H1R with bound drug molecule doxepin	3RZE	3.1	T.Shimamura, M. Shiroishi, S. Weyand, H.Tsujimoto, G. Winter, V. Katritch, R. Abagyan, V. Cherezov, W. Liu, G.W. Han, T. Kobayashi, R.C. Stevens & So Iwata Structure of the human histamine H1 receptor complex with doxepin Nature (2011

Sphingosine 1-phosphate Receptor

Structure Notes	PDB	Resolution [A]	Reference
sphingosine 1-phosphate receptor 1 (S1P1-T4L) with a bound sphingolipid mimic (antagonist)	3V2W 3V2Y	3.35 2.8	Crystal Structure of a Lipid G Protein–Coupled Receptor Michael A. Hanson, Christopher B. Roth, Euijung Jo,Mark T. Griffith, Fiona L. Scott, Greg Reinhart, Hans Desale, Bryan Clemons, Stuart M. Cahalan, Stephan C. Schuerer, M. Germana Sanna, Gye Won Han, Peter Kuhn, Hugh Rosen, Raymond C. Stevens Science Vol. 335 no. 6070 pp. 851-855; 2012

Dopamine D3 Receptor

Structure Notes	PDB	Resolution [A]	Reference
D(3) dopamine receptor, T4 lysozyme insertion in 3rd intracellular loop, in complex with Eticlopride, crystallized in LCP (Cholesterol additive)	3PBL	2.9 A	PDB authors: Chien, E.Y.T., Liu, W., Han, G.W., Katritch, V., Zhao, Q., Cherezov, V., Stevens, R.C., Accelerated Technologies Center for Gene to 3D Structure (ATCG3D)

Opioid Receptors

Structure Notes	PDB	Resolution [A]	Reference
κ-opioid	4DJH	2.9	Wu H, Wacker D, Mileni M, Katritch V, Han GW, Vardy E, Liu W, Thompson AA, Huang XP, Carroll FI, Mascarella SW, Westkaemper RB, Mosier PD, Roth BL, Cherezov V, Stevens RC.Structure of the human κ-opioid receptor in complex with JDTic. Nature. 2012 Mar 21;485(7398):327-32
δ-opioid	4EJ4	3.4	Granier S, Manglik A, Kruse AC, Kobilka TS, Thian FS, Weis WI, Kobilka BK. Structure of the δ-opioid receptor bound to naltrindole. Nature 2012 May 16;485(7398):400-4
μ-opioid	4DKL	2.8	Manglik A, Kruse AC, Kobilka TS, Thian FS, Mathiesen JM, Sunahara RK, Pardo L, Weis WI, Kobilka BK, Granier S. Crystal structure of the μ-opioid receptor bound to a morphinan antagonist.N ature. 2012 Mar 21;485(7398):321-6
NOP or ORL-1 Bound UFP-101	4EA3	3.0	Thompson AA, Liu W, Chun E, Katritch V, Wu H, Vardy E, Huang XP, Trapella C, Guerrini R, Calo G, Roth BL, Cherezov V, Stevens RC. Structure of the nociceptin/orphanin FQ receptor in complex with a peptide mimetic. Nature. 2012 May 16;485(7398):395-9

Muscarinic acetylcholine Receptors

Structure Notes	PDB	Resolution [A]	Reference
M2	3UON	3.0	Haga, K., Kruse, A.C., Asada, H., Yurugi-Kobayashi, T., Shiroishi, M., Zhang, C., Weis, W.I., Okada, T., Kobilka, B.K., Haga, T., Kobayashi, T., Structure of the human M2 muscarinic acetylcholine receptor bound to an antagonist. (2012) Nature 482: 547-551
M3	4DAJ	3.4	Kruse, A.C., Hu, J., Pan, A.C., Arlow, D.H., Rosenbaum, D.M., Rosemond, E., Green, H.F., Liu, T., Chae, P.S., Dror, R.O., Shaw, D.E., Weis, W.I., Wess, J., Kobilka, B. Structure and dynamics of the M3 muscarinic acetylcholine receptor. (2012) Nature 482: 552-556

Appendix 4

Fitting and simulating of models

.

A4.1 Allosteric ternary complex (Ehlert 1988)

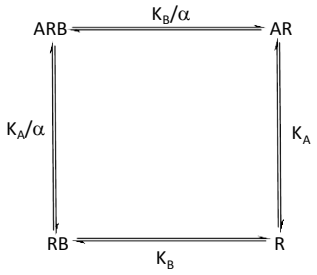

The allosteric ternary complex model was entered into an equation editor in MS Word:

$$Y = \frac{[A]}{[A] + \frac{K_A\left(1 + \frac{[B]}{K_B}\right)}{\left(1 + \frac{\alpha[B]}{K_B}\right)}}$$

Next, I linearized the equation by right clicking the above equation and using the linear feature to provide. :

$$Y = [A]/([A] + (K\_A\ (1 + [B]/K\_B\ ))/((1 + \alpha[B]/K\_B\ )\ ))$$

Then, I manually changed the variables to the following:

$$Y=A/(A+(Ka\ (1+B/Kb\ ))/((1+aB/Kb\ )\ ))$$

This was used as a function equation in Sigma Plot, such that a model could be used to fit the data.

As shown in the screen shot below.

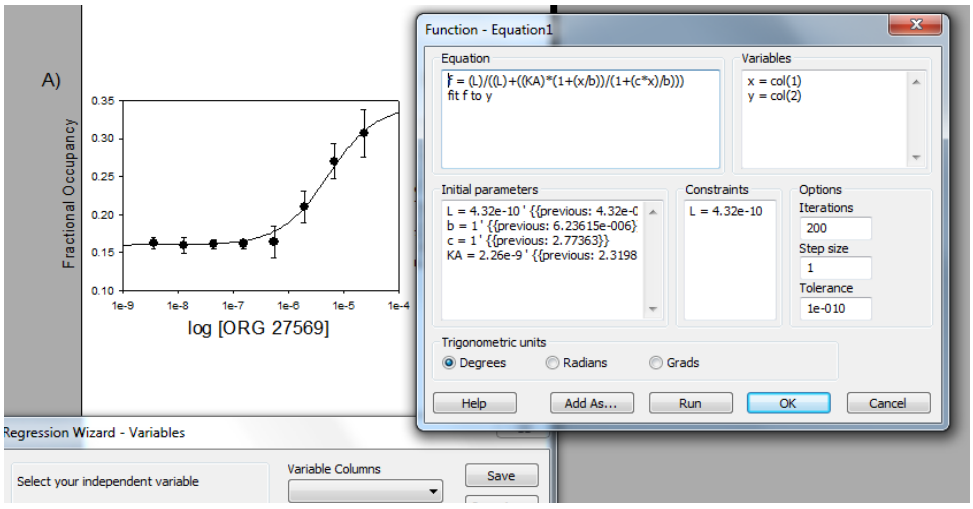

Simulations were performed using Excel, where the variables were redefined as the following cells:

B	M1
A	M2
KB	M3
KA	M4
alpha	M5

Then the following formulas were generated and copied for a series of points and the drug concentration was selected, right clicked, and the 'Name of the Range' changed to A or B respectively.

As a function of A:
"=A/(A+(M4*(1+M1/M3))/((1+(M5*M1)/M3)))"

As a function of B:
"=M2/(M2+(M4*(1+B/M3))/((1+(M5*B)/M3)))"

A4.2 Competitive binding (not allosteric)

$$BR \underset{}{\overset{K_B}{\rightleftharpoons}} R \overset{K_A}{\rightleftharpoons} AR$$

$$\text{Fractional Occupancy } = \frac{[A]}{[A] + K_A(1 + \frac{[B]}{K_B})}$$

Simulations were performed using Excel, where the variables were redefined as the following cells:

B	M1
A	M2
KB	M3
KA	M4

Then the following formulas were generated and copied for a series of points and the drug as described above.

Y = (A)/(A+KA(1+(B/KB)))
Y = (M2)/(M2+M4(1+(M1/M3)))

Note: Alternatively, you can use the Allosteric ternary complex (*vide supra*) and set alpha (M5) to 0.

A4.3 **Operational Model of allostery** (Price, Baillie et al. 2005)

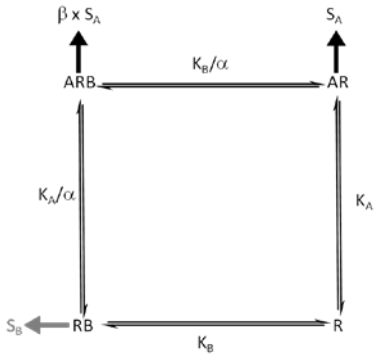

The a Operational Model of allostery was entered into an equation editor in Microsoft word:

$$E = \frac{E_{max}\tau^n[A]^n\left(1+\frac{\alpha\beta[B]}{K_B}\right)^n}{\left[[A]\left(1+\frac{a[B]}{K_B}\right)+K_A\left(1+\frac{[B]}{K_B}\right)\right]^n+\tau^n[A]^n\left(1+\frac{\alpha\beta[B]}{K_B}\right)^n}$$

f=((Em*T*A)*(1+((a*b*B)/KB)))/((A*(1+((a*B)/KB))+(KA*(1+B/KB)))+((T*A)*(1+((a*b*B)/KB))))

This above equation was used as a function equation in Sigma Plot, such that a model could be used to fit the data.

Shown in the screen shot below:

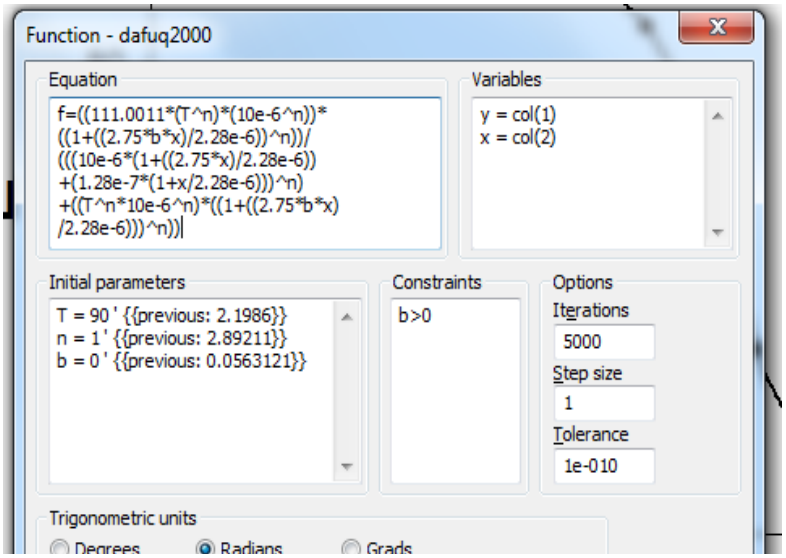

Simulations were performed using Excel, where the variables were redefined as the following cells:

B	M1
A	M2
KA	M3
KB	M4
alpha	M5
Em	M6
T	M7
n	M8
beta	M9

Then, the following formulas were generated and copied for a series of points and the drug concentration was selected, right clicked, and the 'Name of the Range' changed to A or B respectively.

As a function of A:
=((M6*M7*A)*(1+((M5*M9*M1)/M4)))/((A*(1+((M5*M1)/M4))+(M3*(1+M1/M4)))+((M7*A)*(1+((M5*M9*M1)/M4))))

As a function of B:
=((M6*(M7^n)*(M2^n))*((1+((M5*M9*B)/M4))^n))/(((M2*(1+((M5*B)/M4))+(M3*(1+B/M4)))^n)+((M7^n*M2^n)*((1+((M5*M9*B)/M4)))^n))

A4.4 **Allosteric two-state model** (Hall 2000)

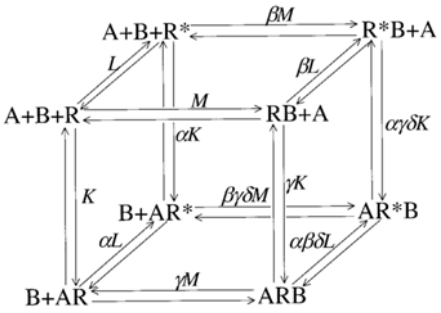

$$\frac{[A]_{Bound}}{[R]_{Total}} = \frac{K[A] + \gamma KM[A][B] + \alpha KL[A] + \alpha\beta\gamma\delta KLM[A][B]}{1 + L + M[B](1 + \beta L) + K[A]\left(1 + \alpha L + \gamma M[B](1 + \alpha\beta\delta L)\right)}$$

f= (KA+gKMAB+aKLA+abgdKLMAB)/(1+L+MB(1+bL)+KA(1+αL+gMB(1+abgdL)))

Then the following formulas were generated and copied for a series of points and the drug as described above.

f=
(M4*M2*+M9*M4*M3*M2*B+M5*M4*M8*M2*+M5*M6*M9*M7*M4*M8*M3*M2*B)/(1+M8+M3*B*(1+M6*M8)+M4*M2*(1+M5*M8+M9*M3*B*(1+M5*M6*M9*M7*M9*M8)))

Simulations were performed using Excel, where the variables were redefined as the following cells:

B = M1 or B
A = M2 or A
M = M3
K =M4
a = M5
b =M6
d = M7
L = M8
y = M9

$$\frac{[A]_{Active}}{[R]_{Total}} = \frac{L(1 + \alpha K[A] + \beta M[B](1 + \alpha\gamma d\delta[A]))}{1 + L + M[B](1 + \beta L) + K[A]\left(1 + \alpha L + \gamma M[B](1 + \alpha\beta\delta L)\right)}$$

Then the following formulas were generated and copied for a series of points and the drug as described above.

M8*(1+M5*M4*M2+M6*M3*B*(1+M5*M9*M7*M4*M2)
f= (L(1+aKA+bMB(1+agdKA))/(1+L+MB(1+bL)+KA(1+αL+gMB(1+abgdL)))
f= (M8*(1+M5*M4*M2+M6*M3*B*(1+M5*M9*M7*M4*M2))/(1+M8+M3*B*(1+M6*M8)+M4*M2*(1+M5*M8+M9*M3*B*(1+M5*M6*M9*M7*M9*M8)))

A4.5 Operational model of allostery (*with intrinsic efficacy*) (Leach, Sexton et al. 2007)

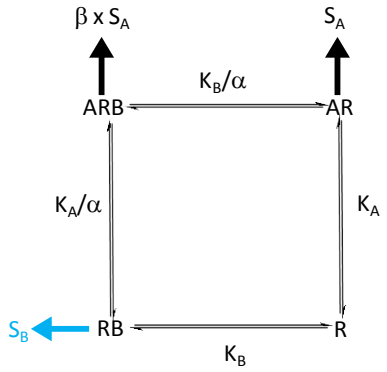

$$E = \frac{E_{max}(\tau_A[A](K_B + \alpha\beta[B]) + \tau_B[B]K_A)^n}{([A]K_B + K_AK_B + K_B[B] + \alpha[A][B])^n + (\tau_A[A](K_B + \alpha\beta[B]) + \tau_B[B]K_A)^n}$$

E= (Em (ta [A](KB+ab[B])+(tb* [B]*KA))^n)/((([A]*KB+KA*KB+KB*[B]+a*[A]*[B])^n)+(ta*[A]*(KB+a*b*[B])+(tb* [B]*KA))^n)

Then the following formulas were generated and copied for a series of points and the drug as described above.

E= (M6 *(M7 *A*(M4+M5*M9*M1)+(M10* M1*M3))^M8)/((A* M4+M3*M4+M4*M1+M5*A*M1)^M8+(M7*A*(M4+M5*M9*M1)+(M10* M1*M3))^M8)

E= (M6*(M7 *M2*(M4+M5*M9*B)+(M10* B*M3))^M8)/((M2* M4+M3*M4+M4*B+M5*M2*B)^M8+(M7*M2*(M4+M5*M9*B)+(M10* B*M3))^M8)

Simulations were performed using Excel, where the variables were redefined as the following cells:

B	
A	M2
KA	M3
KB	M4
alpha	M5
Em	M6
Ta	M7
n	M8

beta	M9
Tb	M10

A4.6 **Allosteric two-site ternary complex model** (Christopoulos and Kenakin 2002)

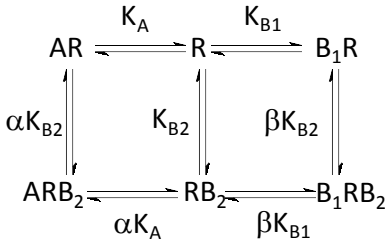

$$Fraction\ Bound = \frac{[A]\left(1+\frac{\alpha[B]}{K_{B2}}\right)}{[A]\left(1+\frac{\alpha[B]}{K_{B2}}\right)+K_A\left(1+\frac{[B]}{K_{B1}}+\frac{[B]}{K_{B2}}\left(1+\frac{\beta[B]}{K_{B1}}\right)\right)}$$

Y = A*(1+a*x*/KB2)/(A*(1+((a*x)/KB2))+KA ((1+x/KB1)+ (x/KB2)* (1+(b*x)/KB1)))

Y = (A*(1+a*x*/g))/(A*(1+((a*x)/g))+KA (1+x/F + ((x/g)* (1+(b*x)/F))))

The equation below was used as a function equation in Sigma Plot, such that a model could be used to fit the data.

f=(L*(1+((A*x)/G)))/(L*(1+((A*x)/G))+(E*(1+(x/h)+((x/(G)*(1+((b*x)/h)))))))

Shown in the screen shot below:

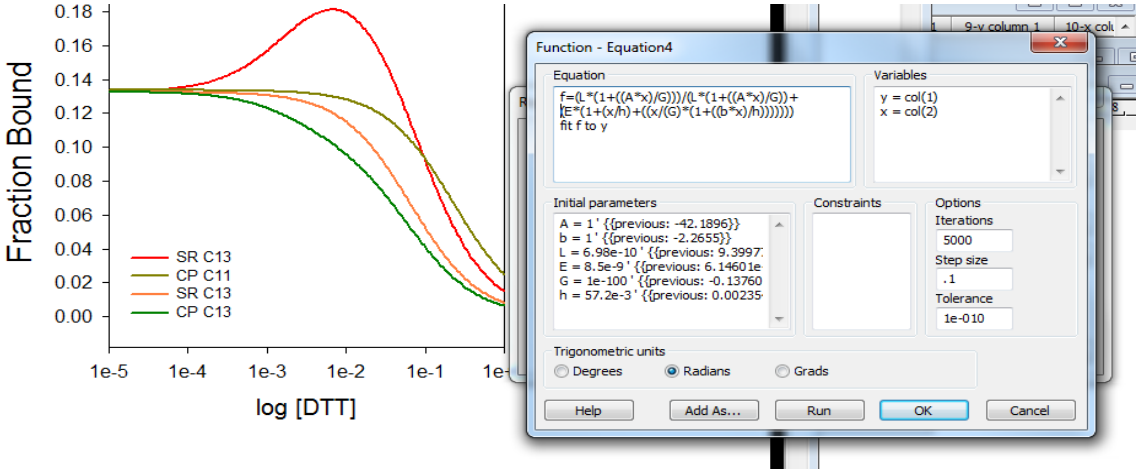

Simulations were performed using Excel, where the variables were redefined as the following cells:

A (L)	M2
KA (e)	M3
KB1(h)	M4
KB2 (g)	M5
alpha	M6
beta	M7

Then the following formulas were generated and copied for a series of points and the drug as described above.

Y
=(M2*(1+((M6*B)/M5)))/(M2*(1+((M6*B)/M5))+(M3*(1+(B/M4)+((B/(M5)*(1+((M7
*B)/M4)))))))

A4.7 Swillens approximation (to account for ligand depletion). (Swillens 1995)

The code below was used as a function equation in Sigma Plot, such that a model could be used to fit the data.

```
conc =7.97
cpm = 53172.67
a = (1+ alpha)*(1 +x/conc);
b = rt*conc/cpm - conc - x + kd*(1 + alpha);
c = -conc*kd;
ls = (-b + sqrt(b*b - 4*a*c))/(2*a);
I = ls*x/conc;
yth = rt*ls/(kd +ls + I) +
alpha*ls*cpm/conc;
fit yth to y with weight w
```

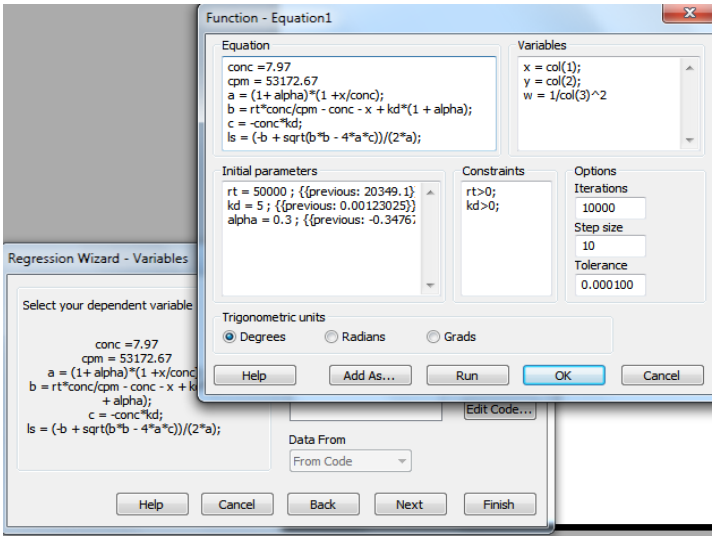

rt = 50000 ; {{previous: 20349.1}}
kd = 5 ; {{previous: 0.00123025}}
alpha = 0.3 ; {{previous: -0.347677}}

Shown in the screen shot right:

A4.8 References

Christopoulos, A. and T. Kenakin (2002). "G protein-coupled receptor allosterism and complexing." Pharmacol Rev **54**(2): 323-374.

Ehlert, F. J. (1988). "Estimation of the affinities of allosteric ligands using radioligand binding and pharmacological null methods." Mol Pharmacol **33**(2): 187-194.

Hall, D. A. (2000). "Modeling the functional effects of allosteric modulators at pharmacological receptors: an extension of the two-state model of receptor activation." Mol Pharmacol **58**(6): 1412-1423.

Leach, K., P. M. Sexton, et al. (2007). "Allosteric GPCR modulators: taking advantage of permissive receptor pharmacology." Trends Pharmacol Sci **28**(8): 382-389.

Price, M. R., G. L. Baillie, et al. (2005). "Allosteric modulation of the cannabinoid CB1 receptor." Mol Pharmacol **68**(5): 1484-1495.

Swillens, S. (1995). "Interpretation of binding curves obtained with high receptor concentrations: practical aid for computer analysis." Mol Pharmacol **47**(6): 1197-1203.